Alejandro Da Silva

Intertwining Cell Adhesion, Gene Expression, and Stress

Åbo Akademi University

Alejandro Da Silva

Alejandro Da Silva received his M.Sc. degree from Simon Bolivar University in 2014, and has since then been working as a Ph.D student in the laboratory of Professor Lea Sistonen at the Faculty of Science and Engineering, Cell Biology at Åbo Akademi University.

Intertwining cell adhesion, gene expression, and stress

Alejandro Da Silva

Cell Biology
Faculty of Science and Engineering
Turku Doctoral Network in Molecular Biosciences
Åbo Akademi University
Turku Bioscience
University of Turku and Åbo Akademi University
Turku, Finland
2023

From the Faculty of Science and Engineering, Cell, Biology, Turku Doctoral Network
In Molecular Bioscience, Åbo Akademi University
Turku Bioscience Center, University of Turku and Åbo Akademi University

Supervised by

Professor Lea Sistonen, PhD and University Lecturer Eva Henriksson, PhD
Faculty of Science and Engineering, Åbo Akademi University
Turku Bioscience Center, University of Turku and Åbo Akademi University,
Turku, Finland

Reviewed by

Docent Emilia Peuhu, PhD
Intitute of Biomedicine, University of Turku, Turku, Finland

and

Docent Pieta Mattila PhD
Intitute of Biomedicine, University of Turku, Turku, Finland

Opponent

Research Director Maria Vartiainen, PhD,
Institute of Biotechnology, University of Helsinki, Helsinki, Finland

ISBN 978-952-12-4287-8 (Printed)
ISBN 978-952-12-4288-5 (Digital)
Painosalama, Turku, Finland 2023

To mother Mary

Table of Contents

Abstract

Cells within an organism are constantly exposed to environmental insults that challenge the homeostasis of their proteome by causing protein misfolding. To survive these adverse situations, cells are equipped with a stress-responsive family of transcription factors called heat shock factors (HSFs). Upon exposure to stress, the HSFs are activated and induce the expression of molecular chaperones, known as heat shock proteins, which in turn aid misfolded proteins to regain their native conformation. HSF1 and HSF2 are the most studied members of the HSFs family, and HSF1 has been considered the master regulator of the proteotoxic stress response. However, despite years of HSFs research, several questions remain unanswered, including: Is there an HSF2-dependent gene expression profile associated with proteotoxic stress? Do HSF1 and HSF2 drive distinct transcriptional programs depending on the type of stress? What are the proteins that interact with HSF2?

The first study of this thesis shows that HSF2 is a prominent transcriptional regulator of the cadherin superfamily of adhesion proteins, and impaired cell-cell adhesion predisposes cells to sustained proteotoxic stress. The second study demonstrates that HSF1 and HSF2 are multi-stress-responsive transcription factors, that trigger distinct transcriptional programs depending on the type of stress. The third study characterizes the protein interactome of HSF2 in a tissue-relevant context and establishes TLN1 as the first adhesion-related HSF2 interacting partner. Lastly, the fourth study in this thesis shows that TLN1 is also present in the nucleus where it strongly binds to chromatin, accumulates in the nucleolus, and regulates gene expression.

Sammanfattning (Swedish Abstract)

Celler i en organism utsätts ständigt för miljöförolämpningar som utmanar deras proteoms homeostas genom att orsaka felveckning av proteiner. För att överleva dessa negativa situationer är cellerna utrustade med en stressresponsiv familj av transkriptionsfaktorer som kallas värmechockfaktorer (HSF:er). Vid exponering för stress aktiveras HSF:erna och inducerar uttrycket av molekylära chaperoner, kända som värmechockproteiner, som i sin tur hjälper felveckade proteiner att återfå sin ursprungliga konformation. HSF1 och HSF2 är de mest studerade medlemmarna i HSF-familjen, och HSF1 har ansetts vara huvudregulatorn för proteotoxisk stressrespons. Men trots år av HSF-forskning förblir flera frågor obesvarade, inklusive: Finns det en HSF2-beroende genuttrycksprofil associerad med proteotoxisk stress? Driver HSF1 och HSF2 distinkta transkriptionsprogram beroende på stresstyp? Vilka är proteinerna som interagerar med HSF2?

Den första studien av denna avhandling visar att HSF2 är en framträdande transkriptionsregulator av kadherin-superfamiljen av adhesionsproteiner, och att nedsatt cell-celladhesion predisponerar celler för ihållande proteotoxisk stress. Den andra studien visar att HSF1 och HSF2 är multistressresponsiva transkriptionsfaktorer, som utlöser distinkta transkriptionsprogram beroende på stresstyp. Den tredje studien karakteriserar proteininteraktomet för HSF2 i ett vävnadsrelevant sammanhang och etablerar TLN1 som den första adhesionsrelaterade HSF2-interagerande partnern. Slutligen visar den fjärde studien i denna avhandling att TLN1 också finns i cellkärnan där det starkt binder till kromatin, ackumuleras i nukleolen och reglerar genuttryck.

List of Original Publications

This thesis work comprises the following original publications and two manuscripts indicated with Roman numerals.

I. Jenny Joutsen*, **Alejandro J. Da Silva***, Jens C. Luoto, Aurelie de Thonel, Jean-Paul Concordet, Valérie Mezger, Délara Sabéran-Djoneidi, Eva Henriksson, Lea Sistonen. (2020). HSF2 protects human osteosarcoma U2OS cells against proteotoxicity by maintaining cell-cell adhesion. *Cell Reports*, 30(2), 583-597. doi: 10.1016/j.celrep.2019.12.037).

II. Samu V Himanen , Mikael C Puustinen , **Alejandro J. Da Silva** , Anniina Vihervaara , Lea Sistonen. (2022). HSFs drive the transcription of distinct genes and enhancers during oxidative stress and heat shock. *Nucleic Acids Research*. 50(11), 6102–6115. doi:10.1093/nar/gkac493.

III. **Alejandro J. Da Silva**, Jens C. Luoto, Hendrick S. E. Hästbacka, Leila S. Colho-Rato, Benjamin T. Goult, Susumu Y. Imanishi, Lea Sistonen, Eva Henriksson. HSF2 interactome in mouse testes reveals a direct interaction between HSF2 and the focal adhesion adaptor protein TLN1. Manuscript.

IV. **Alejandro J. Da Silva**, Hendrik S. E. Hästbacka, Mikael C. Puustinen, Jenny C. Pessa, Benjamin T. Goult, Guillaume Jacquemet, Eva Henriksson, Lea Sistonen. A subpopulation of Talin1 resides in the nucleus and regulates gene expression. BioRxiv doi:https://doi.org/10.1101/2022.03.15.484419. Manuscript.

*Equal contribution

Author Contribution

I. The author contributed in designing part of the research, performing experiments, analyzing results, and writing the manuscript. The author performed the following experiments: immunofluorescence staining, inspection of cell morphology with microscopy, cell viability with calcein and CellTiter-Glo, analysis of PARP-1 and caspase 3 cleavage by immunoblotting, cell aggregation assays and flow cytometry. J.J and L.S wrote the first draft of the manuscript and the revised version upon comments from the rest of the authors.

II. The author contributed in performing experiments, analyzing results, and writing the manuscript. The author performed and analyzed the immunofluorescence staining. S.H and L.S wrote the manuscript and the revised version upon comments from the rest of the authors.

III. The author contributed in designing the research, performing experiments, analyzing results, and writing the manuscript. The author performed the following experiments: LC-MS/MS sample preparation, validation of HSF2-interacting partners through co-immunoprecipitation, GO term analysis, and immunofluorescence staining (experiments and analysis). Author, E.H, and L.S wrote the manuscript and the revised version upon comments from the rest of the authors.

IV. The author contributed in designing the research, performing experiments, analyzing results, and writing the manuscript. The author performed the following experiments: GO term analysis, subcellular fractionations, differential salt gradients, immunofluorescence staining, RNA-seq sample preparation, and analysis of qRT-PCR. Author, E.H, and L.S wrote the manuscript and the revised version upon comments from the rest of the authors.

Abbreviations

ABS	Actin-binding site
BTZ	Bortezomib
CAF	Cancer associated fibroblasts
CAM assay	Chicken chorioallantoic membrane assay
CAM	Cell adhesion molecule
CDH	Cadherin
ChIP-seq	Chromatin immunoprecipitation sequencing
Co-IP	Co-immunoprecipitation
CTCF	CCCTC-binding factor
Dsc	Desmocolin
Dsg	Desmoglein
DBD	DNA-binding domain
ECM	Extracellular matrix
EMT	Epithelial-to-mesenchymal transition
FA	Focal adhesion
FAK	Focal adhesion kinase
HR-A/B/C	Heptad repeat domain
HSE	Heat shock element
HSF	Heat shock factor
HSF1-CaSig	HSF1 cancer signature
HSP	Heat shock protein
HSR	Heat shock response
IgSF	Immunoglobulin superfamily
KO	Knockout

LC-MS/MS	Liquid chromatography-tandem mass spectrometry
LINC	Linker of nucleoskeleton and cytoskeleton
MEF	Mouse embryonic fibroblast
NLC	Nucleolin
PCDH	Protocadherin
Pg	Plakoglobin
PIP2	Phosphatidylinositol 4,5, biphosphate
PIPKIγ661	Phosphatidylinositol phosphate kinase
Pkp	Plakophilin
PLA	Proximity ligation assay
PRO-seq	Precision run-on sequencing
Pol II	RNA polymerase II
PTM	Post-translational modification
RD	Regulatory domain
RIAM	Rap1-interacting-adaptor-molecule
siRNA	Small interfering RNA
SYCP1	Synaptonemal complex protein 1
TAD	Transactivation domain
TLN	Talin
WT	Wildtype

Introduction

Cell adhesion is a fundamental process for every stage in the life of a multicellular organism. On one hand, during embryogenesis cells must adhere to their neighbor cells and substrates to form boundaries and determine the shape of the organism. On the other hand, fully developed organisms rely on cell adhesion to maintain the integrity and functionality of tissues. Indeed, the cells that form part of a tissue, work in synergy partly because the physical connections between them mediate the transmission of information. This mechanosensitive property of cells implies that there is a mechanical homeostasis within tissues, which is constantly surveilled by the proteins mediating cell adhesion. For instance, cells within a wounded tissue, respond to disruptions in cell adhesion by activating the expression of specific genes, which in turn control proliferation, differentiation, and migration. The process through which genes are activated is called transcription, and it is orchestrated by proteins known as transcription factors. HSF1 and HSF2 are stress-responsive transcription factors that react to protein damaging stress, a type of stress that causes proteins to unfold, and their misfunction is linked to pathologies such as neurodegenerative diseases, developmental alterations, and cancer.

This thesis work establishes a connection between cell adhesion and the role of HSF1 and HSF2 in specific types of proteotoxic stress responses. Our data showed that HSF2 is an indispensable transcription factor under chronic proteotoxic stress, a condition in which the prominent HSF2-dependent regulation of cell-cell adhesion is required for cell survival. Although HSF1 and HSF2 were discovered in the context of stress, the transcriptional programs that these HSFs regulate under different types of stress conditions had not been compared before. Therefore, we also compared the role of HSF1 and HSF2 in heat shock and oxidative stress, and our results revealed that these transcription factors regulate different sets of genes depending on the stress condition. Moreover, we characterized the HSF2 interactome in a tissue context and discovered TLN1 as the first adhesion-related HSF2-interacting partner. Lastly, we uncover the nuclear localization of TLN1 and explore its functional impact on gene expression.

Review of the Literature

1 Cell adhesion as a cornerstone of multicellular organisms

All multicellular organisms develop from a single cell that gives rise to a whole individual. Carefully regulated serial divisions of the founder cell, also known as the zygote, generates different cell types with unique properties. Within the multicellular organism, a subset of cell types are organized into tissues and organs, where each cell functions in synergy with the other cells to ensure the optimal fulfillment of vital functions (dos Santos & Liberali, 2019). To ensure proper tissue organization and architecture, multicellular organisms contain a matrix of macromolecules surrounding their cells, which is known as the extracellular matrix (ECM). The ECM is the non-cellular component of tissues and organs, which is composed of proteins and polysaccharides. The ECM has a particular structure and composition in every tissue and organ to provide proper mechanical support and mediate signal transduction in specific conditions (Frantz et al., 2010).

The assembly of single cells into three-dimensional tissues is mediated by the process of cell adhesion. This process can be divided into cell-cell adhesion, referring to the interaction between cells, and cell-matrix adhesion, referring to the interaction between cells and their surrounding ECM. The proteins involved in cell adhesion are generally composed of three major classes: ECM proteins, cell adhesion molecules (CAM)/adhesion receptors, and cytoplasmic adaptor/peripheral membrane proteins (Gumbiner, 1996). The ECM proteins are mostly fibril-forming proteins, like collagens, fibronectins, and laminins, that act as ligands for CAMs (Theocharis et al., 2016). The CAM proteins are generally transmembrane glycoproteins that mediate cell-cell or cell-matrix adhesion through the interaction of their extracellular segments with specific ligands. There are four major groups of CAMs: integrins, selectins, cadherins, and the immunoglobulin superfamily (IgSF). However, some CAM proteins are not included in these major groups, such as non-classical CAMs, e.g. claudins and occludin (Hintermann & Christen, 2019). At the intracellular side of the plasma membrane, CAMs interact with

cytoplasmic adaptor or peripheral membrane proteins. The function of cytoplasmic adaptor proteins (e.g. α-catenin, β-catenin, catenin delta 1 (CTNND1), desmoplakin, talin1) is to connect the adhesion molecules to the cytoskeleton and to transduce signals initiated at the cell surface when CAMs bind their ligands (Gumbiner, 1996).

The shape and organization of tissues are maintained by cytoskeletal components (such as actin filaments, intermediate filaments, and microtubules) and the activity of myosin type II proteins, both of which function in concert with cell-cell and cell-matrix adhesion complexes (Gilbert & Weaver, 2017). Myosin II proteins act as molecular motors that move along actin filaments exerting tension on the cytoskeleton (Shutova & Svitkina, 2018). CAMs, in turn, mediate force transmission along tissues, providing a structural platform to propagate mechanical inputs from the extracellular space. Different stimuli affect the intracellular tension of cells within tissues, causing changes in gene expression, differentiation, cell size, and morphology (Heisenberg & Bellaïche, 2013). For example, stem cells can differentiate into different lineages upon changes in substrate stiffness, and this process is completely abolished in the absence of myosin II (Engler et al., 2006). This cellular response to mechanical cues is particularly important to maintain tissue self-organization and homeostasis.

When a tissue is injured, stem cells must divide and differentiate in a controlled manner to replace the lost cells without producing an overcrowded tissue (da Silveira dos Santos & Liberali, 2019). In this context, mechanical stimuli are critical to regulate tissue regeneration, since signaling pathways that sense plasma membrane tension stop cell proliferation and differentiation once tissue integrity is restored (Elbediwy & Thompson, 2018; Piddini, 2017). In addition to cell division and differentiation, cells must also migrate to repair injuries within tissues. This process is evident in epithelial tissues, due to their role in establishing boundaries within different areas of an organism. When an epithelial tissue is damaged, the epithelial cells acquire a quasi-mesenchymal state through a reversible gene expression program called epithelial-to-mesenchymal transition (EMT) (Dongre & Weinberg, 2019). Cells that undergo EMT are characterized by altered cell-cell contacts and cell polarity, enhanced capacity to degrade the

surrounding ECM, and reorganization of their actin cytoskeleton to cope with the mechanical strain produced during cell migration (Dongre & Weinberg, 2019).

Sustained exposure to mechanical stimuli of high intensity (e.g. pressure, stretching, and shear forces), is known as mechanical stress (Collier & Benesch, 2020). While almost all cells of an organism are susceptible to experience mechanical stress, there are particular cell types, including bone and muscle cells, that are constantly exposed to it (King, 2012). From a structural point of view, cells exposed to mechanical stress need to strengthen their cytoskeleton and reinforce their attachment sites to preserve their integrity and protect their nucleus and genome (Collier & Benesch, 2020) (Figure 1). However, mechanical stress also causes protein damage, promoting the toxic accumulation of proteins that have lost their conformation and function (King, 2012). This condition is known as proteotoxicity, and it will be presented in more detail in section 2. Here, it suffices to say that cells are equipped with a group of proteins, which are known as molecular chaperones, that assist protein folding or degradation under stress conditions to avoid the fatal effects of proteotoxicity (Lindquist, 1986). Molecular chaperones can recognize damaged proteins and selectively mediate their degradation in lysosomes, a process known as chaperone-mediated autophagy (Kaushik & Cuervo, 2018). Interestingly, a similar process, which is known as chaperone-assisted selective autophagy, is essential for the maintenance of skeletal muscle during mechanical stress (Arndt et al., 2010). For instance, the chaperones involved in chaperone-assisted selective autophagy monitor the mechanical unfolding of an actin-crosslinker protein called filamin, targeting it for lysosomal degradation during mechanical stress conditions (Ulbricht et al., 2013). Accordingly, molecular chaperones are highly expressed in organs exposed to mechanical stress (e.g. skeletal muscle, heart, diaphragm), indicating that they are needed to preserve protein homeostasis in these locations (Collier & Benesch, 2020).

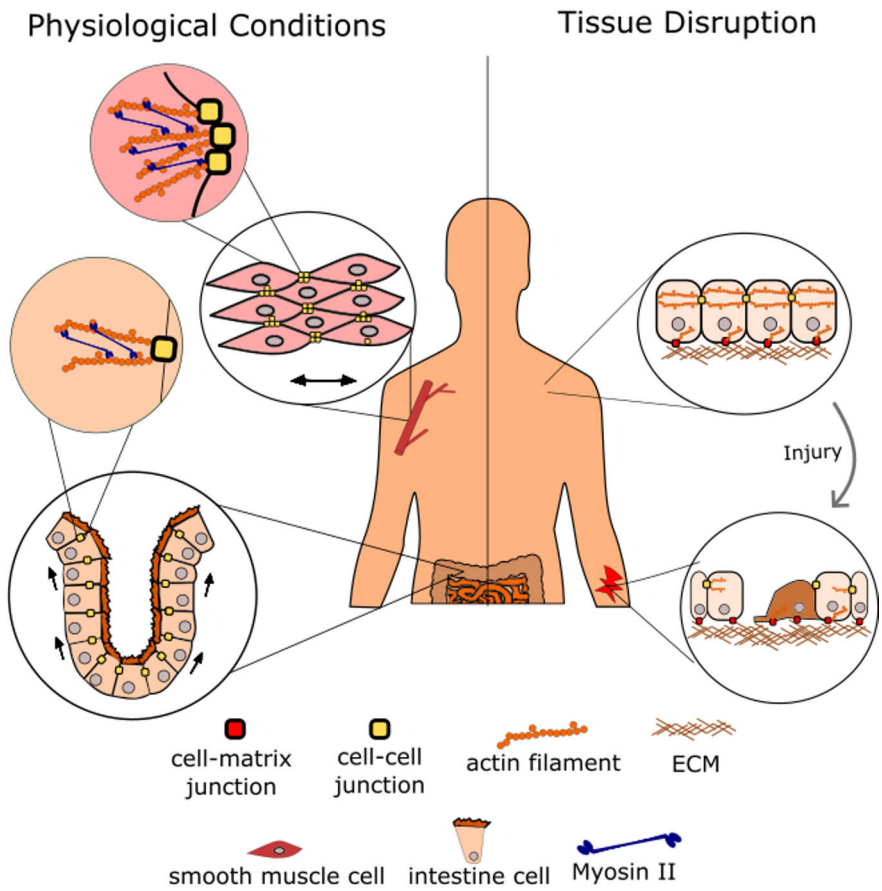

Figure 1. Cell adhesion and tissue homeostasis. In physiological conditions, tissues within an organism are exposed to different intensities of mechanical stimuli. For example, vascular smooth muscle cells bear a great amount of mechanical force, and therefore present more stable cell-cell junctions that are linked to the cytoskeleton to mediate myosin II-dependent intracellular tension. In contrast, intestinal cells are exposed to lower amounts of mechanical force and they possess less stable cell-cell junctions (Friedl & Mayor, 2017). Black arrows indicate the direction of mechanical forces. In stress conditions, cell adhesion is required to preserve intracellular tension and tissue integrity. When a tissue is injured, the cells within it react to regenerate the disruption of cell adhesion and intracellular tension. A wound in the skin is depicted to exemplify tissue injury.

Taken together, cell adhesion is a complex process that is required for the preservation of tissue integrity. The cell's capability to adhere is required to maintain intracellular tension, and therefore carefully regulated cell adhesion is fundamental to preserve tissue homeostasis in physiological conditions and mechanical stress. Importantly, adhesion proteins show extraordinary diversity, and they function in a context-specific manner.

1.1 Cell-cell adhesion

The term cell-cell adhesion includes many different types of intercellular adhesion events, which involve a myriad of adhesion molecules. Direct contacts between cells are mediated by intercellular junctional complexes, which are composed of different adhesion molecules that interact with the cytoskeleton. These junctions are the basis of all types of animal tissues, and many of them are used in parallel by the same cell types (Friedl & Mayor, 2017). The major junctional complexes are tight junctions, adherens junctions, desmosomes, and gap junctions (Figure 2). In epithelial tissues, the tight junctions are composed of the transmembrane proteins claudins and occludin, which act as molecular gates to restrict the diffusion of molecules and connect the actin cytoskeletons of adjacent cells (Zihni et al., 2016). Adherens junctions, in turn, are protein complexes that connect the actin cytoskeleton of adjacent cells through classical cadherins (see section 1.1.1.1), and they are considered a universal adhesion machinery for multicellular organisms since they are found across the metazoan phyla (Oda & Takeichi, 2011). In contrast, desmosomes are important junctional complexes to support mechanically challenged tissues by connecting the intermediate filaments of adjacent cells through demosomal cadherins (see section 1.1.1.2) (Hatzfeld et al., 2017). Gap junctions are intercellular channels composed of transmembrane proteins called connexins that link the actin cytoskeletons of adjacent cells and facilitate the exchange of ions and small molecules among cells within tissues (Beyer & Berthoud, 2018).

The junctional complexes were observed for the first time in epithelial tissues by Marylin Farquhar and George Palade in 1963 (Farquhar & Palade, 1963; Horwitz, 2012). The work of Farquhar and Palade set the physiological context where the molecules

underlining cell-cell adhesion operate. Although the existence of CAMs was already hypothesized by Paul Weiss in 1947, the first adhesion molecules were not discovered until the late 1970s (Horwitz, 2012; Takeichi, 1977; Weiss, 1947). Among the pioneers participating in the quest for CAMs, Masatoshi Takeichi made a remarkable contribution by discovering the process of calcium-mediated cell-cell adhesion and the first set of proteins involved therein (Horwitz, 2012; Takeichi, 1977). Indeed, these proteins were members of a protein superfamily that we now know as cadherins for their important role in calcium-dependent cell-cell adhesion.

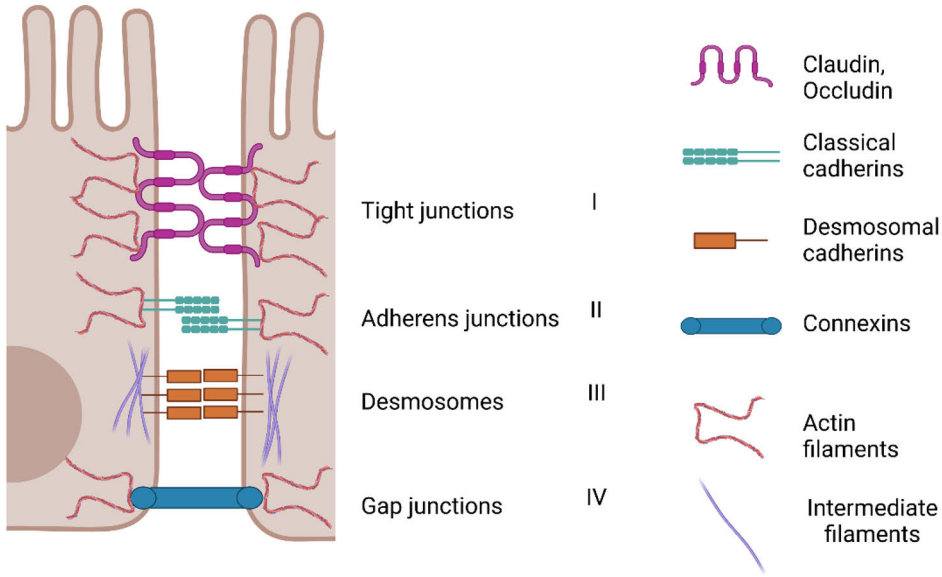

Figure 2. Junctional complexes in epithelial cells. (I) Tight junctions are in the most apical part of the cell-cell contacts in epithelial cells where they build a seal. These junctions are composed of claudins and occludin, which interact with actin filaments. (II) Adherens junctions are adhesion machineries that link actin filaments of adjacent cells and they are composed of cadherins. (III) Desmosomes are hyperadhesive junctions that preserve the structure of mechanically challenged tissues. They are composed of desmosomal cadherins, which link intermediate filaments of adjacent cells together. (IV) Gap junctions are intercellular channels that connect the cytoplasm of adjacent cells. They are composed of connexins, which interact with actin filaments. Modified from Schnell et al., 2013.

1.1.1 Cadherin-mediated cell-cell adhesion

Cadherins constitute a superfamily of transmembrane proteins that were initially discovered as mediators of calcium-dependent cell-cell adhesion (Takeichi, 1988). All cadherins have two or more primary sequences termed the extracellular cadherin (EC) domain, which is known as the hallmark of the cadherin superfamily (Gul et al., 2017; Sotomayor et al., 2014). Several repeats of the EC domain are arranged along the extracellular region of cadherin proteins and conserved calcium-binding sites are alternated in between each repeat of the EC domain (Hirano & Takeichi, 2012) (Figure 3). Upon calcium-binding, the cadherin EC domain rigidifies, becoming more stable to mediate cell-cell adhesion (Sotomayor et al., 2014). The EC domain is crucial for the interaction between cadherins located in neighboring cells, a process known as *trans* interaction, and cadherins located on the same cell membrane, a process known as *cis* interaction (Hirano & Takeichi, 2012). A specific cadherin usually shows homophilic interaction with identical proteins in *cis* or *trans*, but certain subtypes can also interact heterophilically (Takeichi, 2007).

Despite sharing the EC domain, the cadherin superfamily members have a remarkable diversity in structure and function (Hirano & Takeichi, 2012). Therefore, it has been challenging to establish a consistent classification for the families inside this superfamily (Sotomayor et al., 2014). Here, the cadherin superfamily will be classified into two groups: classical cadherins, which were the first group of cadherins to be discovered, and non-classical cadherins. Of the non-classical cadherins, desmosomal cadherins and protocadherins will be described below, since they are among the best-characterized cadherin families (Hirano & Takeichi, 2012). While classical cadherins have a well-defined structure, non-classical cadherins vary drastically in the number of EC domains, length of the transmembrane domain, and composition of the cytoplasmic domain (Sotomayor et al., 2014) (Figure 3). For example, the CELSR family of cadherins and its ortholog the Flamingo cadherins, which belong to the non-classical cadherins, are characterized by the presence of seven transmembrane segments and so-called “variable” domains in addition to the conventional EC domain repeats in their extracellular region

(Goffinet & Tissir, 2017). Other non-classical cadherins, such as the Fat & Dachsous cadherins, have a much higher amount of EC domains than the classical cadherins (Brasch et al., 2012). Protocadherins and desmosomal cadherins, in turn, generally resemble the structure of the classical cadherins, bearing most of the differences in their cytoplasmic regions (Sotomayor et al., 2014) (Figure 3).

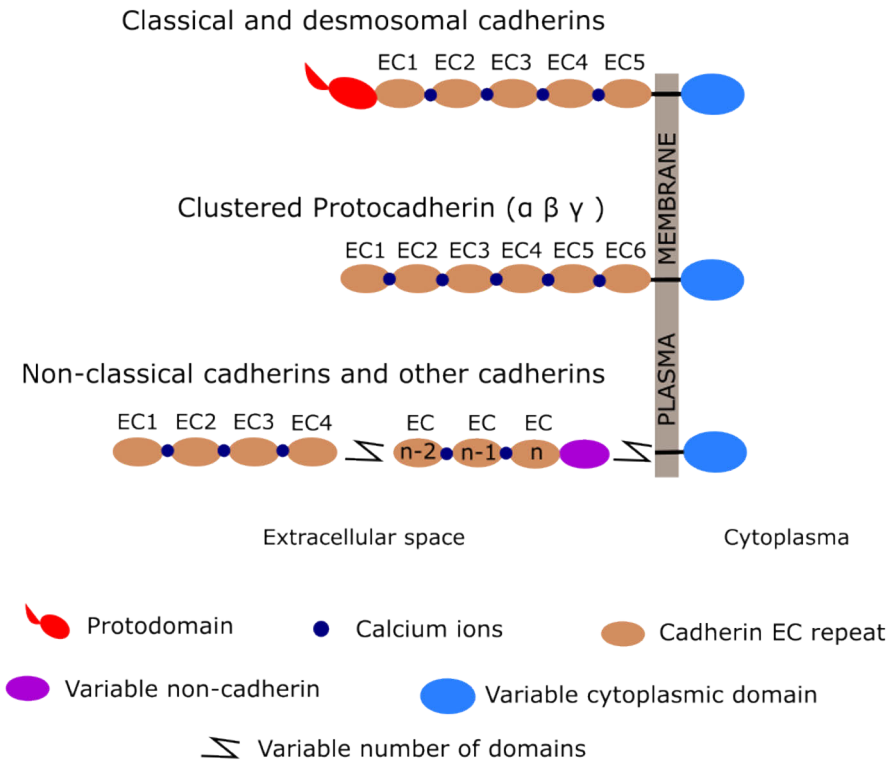

Figure 3. Schematic representation of cadherin superfamily members. Classical and desmosomal cadherins share an identical domain structure, except for the variable cytoplasmic domain. Clustered protocadherins (α,β,γ) have six EC domains and a variable cytoplasmic domain. Non-classical cadherins and other cadherins possess between two and 34 EC domains, variable non-cadherin domains, different amounts of transmembrane segments, and variable cytoplasmic domains. Figure adapted from Sotomayor et al., 2014.

1.1.1.1 Classical cadherins

The classical cadherins are characterized by five EC domains (1-5 EC) in their extracellular region, a single-pass transmembrane domain, and a well conserved cytoplasmic domain (Paulson et al., 2014; Takeichi, 2007) (Figure 3). In mammals, the classical cadherins are divided into type I and type II cadherins, according to the sequence similarity of their cytoplasmic domain (Table 1). Overall, classical cadherins require the cleavage of an N-terminal protodomain to acquire adhesive capability, which in most of the cases takes place as homophilic adhesive interactions mediated by the EC1 domain (Sotomayor et al., 2014). However, heterophilic adhesive interactions can also occur between the different proteins of this family (Paulson et al., 2014) (Table 1).

Table 1. Types of classical cadherins and their interaction partners. Table modified from Paulson et al., 2014. NA: Not applicable.

Type I cadherins	Heterophilic interaction for type I	Type II cadherins	Heterophilic interaction for type II
For E-cadherin (CDH1)	N-cadherin (CDH2)	**VE-cadherin (CDH5)**	NA
N-cadherin (CDH2)	E-cadherin (CDH1) R-cadherin (CDH4)	**K-cadherin (CDH6/6B)**	CDH7, T1-cadherin (CDH9)
P-cadherin (CDH3)	NA	**CDH7**	K-cadherin (CDH6B)
R-cadherin (CDH4)	CDH2	**CDH8**	OB-Cadherin (CDH11)
M-cadherin (CDH15)	NA	**T1-cadherin (CDH9)**	K-cadherin (CDH6B), T2-cadherin (CDH10)
		T2-cadherin (CDH10)	T1-cadherin (CDH9)
		OB-Cadherin (CDH11)	CDH8
		N-cadherin 2 (CDH12)	NA
		CDH18	NA

		CDH19	NA
		MN-cadherin (CDH20)	NA
		PB-cadherin (CDH22)	NA
		CDH24	NA

The classical cadherins are important components of the adherens junctions, where they provide crucial physical support for tissue integrity (Meng & Takeichi, 2009; Najor, 2018; Oda & Takeichi, 2011). Apart from providing physical support, the classical cadherins also mediate the transmission of extracellular stimuli to the actin cytoskeleton through their interaction with cytoplasmic adaptor proteins called catenins (Meng & Takeichi, 2009; Oda & Takeichi, 2011). According to our current understanding, the core cadherin/catenin complex is formed in sequential steps. Initially, CTNND1 and β-catenin interact with the cytoplasmic domain of classical cadherins within the endoplasmic reticulum (ER) (Ladoux et al., 2015). Once the classical cadherins are transported in vesicles from the ER to the membrane, β-catenin interacts with α-catenin and CTNND1 catenin stabilizes this newly formed protein complex (Ladoux et al., 2015). Upon mechanical stimuli, α-catenin undergoes a force-dependent conformational change that is required for its interaction with actin filaments (Ishiyama et al., 2018) (Figure 4A). This connection between the cadherin/catenin complex and filamentous actin allows actomyosin-dependent contractile forces to produce tension across neighboring cells (Teo et al., 2019). In addition, actin-binding proteins that control the stabilization and *de novo* assembly of actin filaments, such as α-actinin-4 and ARP2/3, respectively, are located at the cadherin-enriched junctions, facilitating the recruitment of different signaling molecules (Tang & Brieher, 2012).

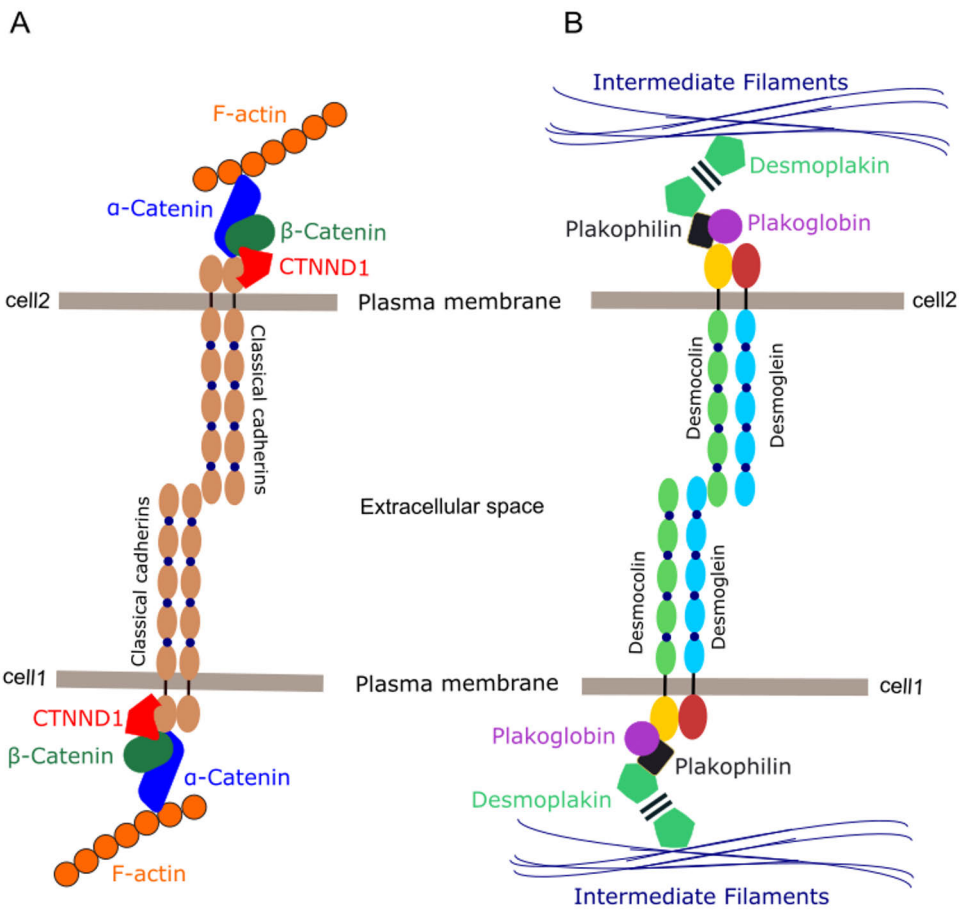

Figure 4. Schematic representation of classical and desmosomal cadherins mediating cell-cell adhesion. A) Classical cadherins form *cis*-dimers that interact in *trans* with other classical cadherins to mediate cell-cell adhesion. Intracellularly, the cytoplasmic domain of classical cadherins forms a protein complex with catenin delta 1 (CTNND1), β-catenin, and α-catenin, which in turn couples the cadherins with filamentous actin. B) According to current knowledge, dimers of desmosomal cadherins interact in *trans* with other desmosomal cadherins to mediate cell-cell adhesion (here a heterodimer is depicted). The cytoplasmic tails of desmosomal cadherins, in turn, interact with plakoglobin and plakophilin, which are coupled to intermediate filaments through desmoplakin. Modified from Angst et al., 2001; Ladoux et al., 2015; Najor, 2018.

The cell-cell adhesion sites in which classical cadherins participate are also important signaling hubs that communicate with molecular pathways involved in cell growth and differentiation, e.g. the Wnt and Hippo pathways (Juliano, 2002). For instance, β-catenin is a fundamental protein in both the classical cadherin-mediated cell-cell adhesion and the Wnt signaling pathway. There are three pools of β-catenin in the cell: a nuclear pool, a cytoplasmic pool, and a membrane-associated pool. The activation of the Wnt signaling pathway promotes the translocation of β-catenin from the cytoplasm to the nucleus, where it associates with the transcription factor T-cell factor/lymphoid enhancer-binding factor and regulates gene expression (Juliano, 2002; Nelson & Nusse, 2004). However, the association of β-catenin to the classical cadherins prevents this translocation, repressing the Wnt pathway signaling (Yulis et al., 2018). Ultimately, classical cadherins control different cellular processes, such as proliferation, apoptosis, differentiation, and metabolism (Takeichi, 2007; Yulis et al., 2018).

Interestingly, the expression of specific members within the classical cadherin subfamily is tightly regulated by members of the SoxB1 and PAX families of transcription factors during development (Paulson et al., 2014). Whereas epigenetic mechanism such as gene promoter methylation plays a fundamental role in regulating cadherin expression in the context of malignancies. However, holistic studies addressing the transcriptional regulation of classical cadherins in different contexts are needed.

1.1.1.2 Non-classical cadherins

The non-classical cadherins are a group of cadherins that share the EC domain of the classical cadherins, but present considerable differences in their cytoplasmic and transmembrane domains. Desmosomal cadherins and protocadherins are among the most studied non-classical cadherins (Meng & Takeichi, 2009).

Desmosomal cadherins

Among the non-classical cadherins, the desmosomal cadherins are the most similar to the classical cadherins in sequence identity, and they form part of the specialized

junctions commonly known as desmosomes (Meng & Takeichi, 2009). The desmosomal cadherins family can be divided into two subfamilies, desmocolins (Dsc1-3) and desmogleins (Dsg1-4), in which each member is generated by alternative splicing in a tissue-dependent manner (Garrod & Chidgey, 2008). Different isoforms of desmocolins and desmogleins bind to each other in *trans* as dimers, of which heterodimers mediate stronger cell-cell adhesion interactions when compared to homodimers (Hatzfeld et al., 2017). The cytoplasmic domain of the desmosomal cadherins differs substantially from the one found in classical cadherins since it contains binding sites for plakoglobin (Pg) and plakophilin (Pkp1-3) (Berika & Garrod, 2014). Plakoglobin and plakophilins, are β-catenin-related proteins that connect the desmosomal cadherins with the intermediate filament cytoskeleton through their interaction with desmoplakin (Hatzfeld et al., 2017) (Figure 4B).

In humans, desmosomes are found in many different tissues, but they are prominent in tissues that are exposed to mechanical stress. Importantly, the intermediate filaments and some of the components of the desmosomes (e.g. the desmosomal cadherin isoforms) vary among tissues, which causes a specialization of this cell-cell adhesion apparatus (Najor, 2018). Contrary to classical cadherins, desmosomal cadherin can switch between a calcium-dependent and a calcium-independent adhesion mode. The calcium-independent mode mediates a hyper-adhesion state that locks cells in epithelia together, whereas the calcium-dependent mode mediates a weaker adhesion that is required during regeneration and wound healing (Berika & Garrod, 2014).

Protocadherins

Protocadherins (PCDH) are the largest family within the cadherin superfamily consisting of two subfamilies: clustered and non-clustered protocadherins (Gul et al., 2017). These subfamilies receive their names according to their location in the genome. While the clustered protocadherins are located in three consecutive gene clusters (Pcdhα, Pcdhβ, Pcdhγ), the non-clustered protocadherins are scattered across the genome (Hirano & Takeichi, 2012). The gene clusters Pcdhα, Pcdhβ, and Pcdhγ are organized in a very

complex manner and they code for a total of 52 proteins in humans (15 Pcdhα, 15 Pcdhβ, 22 Pcdhγ) (Mountoufaris et al., 2018) (Figure 5). The Pcdhα and Pcdhγ clusters are characterized by the presence of so-called variable and constant exons. After transcription, the mRNA of a particular variable exon associates, through alternative splicing, with the mRNAs of all the constant exons within the corresponding gene cluster to produce different isoforms with identical cytoplasmic tails. The Pcdhβ cluster, in contrast, does not contain constant exons, and therefore the protein isoforms encoded by this cluster do not have identical intracellular domains (Hirayama & Yagi, 2017) (Figure 5). All variable exons in the three protocadherin gene clusters have their promoters, allowing different protocadherin isoforms to be expressed in a cell-type and tissue-specific manner (Hirayama & Yagi, 2017). Interestingly, most of the variable exons are expressed stochastically and from individual alleles with the exception of the c-type exons located at the end of the Pcdhα and Pcdhβ clusters (Mountoufaris et al., 2018) (Figure 5).

The abundance of promoters in the Pcdhα, Pcdhβ, and Pcdhγ gene clusters raises an important question: What determines the promoter selectivity between protocadherin isoforms? Even though this question remains enigmatic at the organismal level, important insights have been obtained from experiments conducted in the nervous system. Protocadherins are expressed in different subsets of neurons to increase surface variability and establish a unique protein "barcode" that is fundamental for cell-cell interaction and communication (Canzio & Maniatis, 2019). The best-characterized regulatory mechanism controlling the expression of protocadherins in neurons is mediated by the CCCTC-binding factor (CTCF) (Chen & Maniatis, 2013). CTCF is a highly conserved zinc finger protein that binds to CG-rich consensus sequences when they are unmethylated. After binding to its consensus sequences, CTCF forms chromatin loops that produce local clusters of genes, mediates communication between enhancers and promoters, and defines the boundaries of chromatin compartments. Importantly, CTCF also recruits other proteins, such as RAD21, a subunit of a protein complex known as cohesin, to stabilize the chromatin looping (Kim et al., 2015).

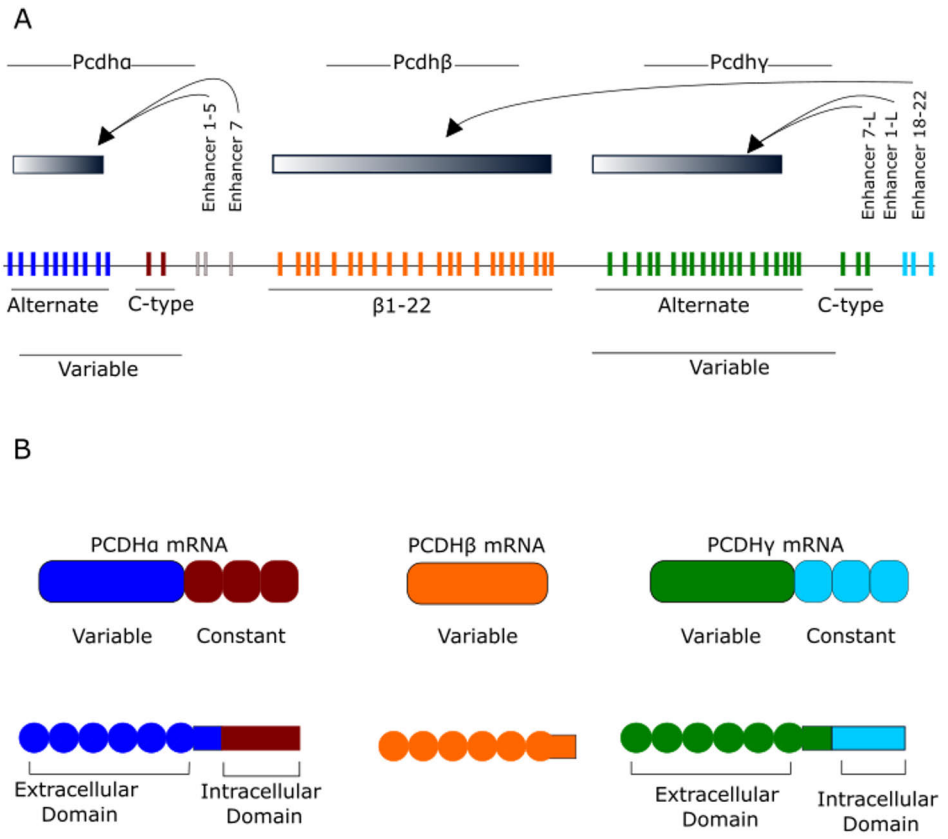

Figure 5: Genomic organization and gene expression scheme of murine clustered protocadherins. A) Schematic representation of Pcdhα, Pcdhβ, and Pcdhγ gene clusters. The exons of the three gene clusters are divided into variable exons (depicted in blue, orange, and green) and constant exons (depicted in brown for Pcdhα and light blue for Pcdhγ). Variable exons can be either alternate, which are stochastically expressed, or C-type exons, which are regulated independently. Pcdhβ does not contain constant exons or C-type exons. Enhancers are shown and arrows indicate which protocadherin cluster they regulate. The black and white gradient bars indicate the strength of functional interaction between individual promoters (not shown) and the enhancers. B) Alternative splicing joins the mRNA from each variable exon with the corresponding constant exon. Each variable exon encodes the whole extracellular domain, transmembrane domain, and the proximal intracellular domain, whereas the constant exons encode the distal intracellular domain (parallel lines indicate the plasma membrane). Modified from Mountoufaris et al., 2018.

Each protocadherin promoter is influenced by one or more enhancers, which were identified by DNase 1 hypersensitivity assays, and therefore are commonly denoted as hypersensitive regions (Mountoufaris et al., 2018) (Figure 5). The CTCF-Cohesin complex draws enhancers near to their corresponding promoters, through chromatin looping, to increase the expression of protocadherin isoforms (Mountoufaris et al., 2018). As mentioned above, DNA methylation inhibits the binding of the CTCF-Cohesin complex to its target sequences, thereby regulating chromatin looping. Even though it is not completely understood how the methylation status of protocadherin promoters and their enhancer sequences is regulated, recent studies conducted in olfactory sensory neurons have shed some light on this topic. In this cell type, promoters within the Pcdhα cluster are by default methylated, and the stochastic transcription of antisense long non-coding RNAs leads to their demethylation (Canzio & Maniatis, 2019). The methylation status of the protocadherin promoters also depends on the activity of the methyltransferase Dnmt3b, which shows a stage-specific pattern of expression during neuronal development (Mountoufaris et al., 2018). Taken together, our current knowledge of the expression of clustered protocadherins is centered on changes in the chromatin landscape, but the identity of other key players in this process, e.g. transcription factors, remains unknown.

Similar to other members of the cadherin superfamily, protocadherins bind to each other in a calcium-dependent manner through their extracellular domain. However, they assemble strictly homophilically in *cis* and/or *trans* (Canzio & Maniatis, 2019). The protocadherin isoforms that originate from the three gene clusters are located at the site of synapsis and they can also be detected throughout the neuronal soma, dendrites, and axons (Chen & Maniatis, 2013). Phenotypic characterization of single, double, and full protocadherin gene cluster knockouts in olfactory sensory neurons has shown a functional synergism among these clusters (Mountoufaris et al., 2018). The axons of olfactory sensory neurons concentrate in specialized structures called glomeruli, which are considered as functional units of olfactory sensory processing (Zou et al., 2009). While the absence of single gene clusters (Pcdhα, Pcdhβ, or Pcdhγ) produces mild

alterations in the structure of olfactory glomeruli, the absence of two (Pcdhαβ $^{-/-}$) or all the gene clusters (Pcdhαβγ $^{-/-}$) causes a profound alteration in the glomeruli structure (Mountoufaris et al., 2017; Mountoufaris et al., 2018). However, recent studies have revealed that the functional impact of protocadherins is not only due to their synergistic activity, since specific protocadherin clusters and even protocadherin isoforms can affect unique processes of brain development. For example, the Pcdhγ cluster is required for dendritic self-avoidance of retinal neurons, and the C-type isoforms from the Pcdhα cluster (Pcdhα*c1* and Pcdhα*c2*) are fundamental for the proper spread of axons belonging to serotonergic neurons through the brain (Chen et al., 2017; Lefebvre et al., 2012; Mountoufaris et al., 2018). In summary, cell-cell adhesion is a complex process mediated by a wide variety of proteins, whose expression and localization needs to be carefully regulated.

1.2 Cell-matrix adhesion

The term cell-matrix adhesion refers to the interaction between cell adhesion receptors and protein components of the ECM (e.g. collagens, fibronectin, laminin). Interestingly, the ECM not only contains ligands that trigger a chemical response within cells, but it also provides positioning and structural information about the surrounding environment (Wickström & Niessen, 2018). Indeed, in most cases, cells can respond to different mechanical signals, because they are able to sense ECM stretching, its topography, and rigidity (Geiger et al., 2009). Cells exposed to mechanical stimuli adapt their shape and cytoskeleton organization, which activates different signaling pathways that control proliferation and differentiation (Orré et al., 2019). Among the adhesion receptors that mediate cell-matrix adhesion, the integrins are the most prominent (Gumbiner, 1996). In contrast to other cell adhesion receptors, the integrin-mediated adhesion can remodel the configuration of the ECM, and they are particularly important for cell migration (Wickström & Niessen, 2018).

According to the classical model, cell migration is a three-step process which includes extension of the leading edge of the cell as a protrusion called lamellipodium, attachment

of the lamellipodium to the substrate (e.g. ECM), and contraction at the posterior part of the cell (Paluch et al., 2016). The formation of the lamellipodium requires dynamic polymerization and depolymerization of actin filaments, which produces an actin treadmilling effect that facilitates the retrograde flow of molecules. Additionally, myosin II-mediated actomyosin contraction generates complementary pulling forces to facilitate cell motility (Gilbert & Weaver, 2017). These intracellular pulling forces are coupled to the substrate through integrins. However, the coupling is not mediated by a direct interaction between the integrins and the actin cytoskeleton. Instead, there are layers of so-called "clutch" proteins that are horizontally stratified (Paluch et al., 2016).

Cells assemble different types of integrin-mediated adhesions, which are classified according to their stability, localization, and protein composition. The earliest microscopically visible adhesion sites are called nascent adhesions, since they are small, dot-like, and transient structures formed at the lamellipodium (Geiger et al., 2009). The nascent adhesions can mature into focal complexes. Although the molecular components of the focal complexes are similar to the nascent adhesions, focal complexes are bigger in size and depend on the force generated by non-muscle myosin II for their formation (Vicente-Manzanares & Horwitz, 2011). Due to the effect of traction forces applied continuously by the activity of non-muscle myosin II A, the focal complexes mature into focal adhesions. Focal adhesions are stable structures characterized by a wide variety of adaptor proteins that crosslink the actin filaments to integrins and transduce the actomyosin-dependent traction forces to the ECM (Case & Waterman, 2015; Geiger et al., 2009). Then, fibrillar adhesions are the endpoint in the adhesion maturation, being characterized by the presence of tensin, a lifetime of several hours, and their association with fibronectin fibers in the ECM (Vicente-Manzanares & Horwitz, 2011).

1.2.1 Integrins as mediators of cell-matrix adhesion

In the 1980s, affinity chromatography with ECM components and monoclonal antibodies were used to identify the cell-matrix adhesion receptors. Initially, several independent studies, using monoclonal antibodies that were known to inhibit cell

adhesion in cultured cells, led to the discovery of a group of glycoproteins with a molecular weight of 140 kDa (Brown & Juliano, 1985; Knudsen, 1985; Wylie et al., 1979). Protein complexes formed by these glycoproteins were suspected to be the transmembrane receptors that would mediate cell adhesion to the ECM, since they were known to interact with ECM components and their solubility properties were similar to integral membrane proteins (Brown & Juliano, 1985; Horwitz, 2012; Tamkun et al., 1986). Tamkun and co-workers reported the characterization of the cDNA sequence corresponding to a subunit of the glycoprotein complex and called it "integrin" due to its important role in connecting the cytoskeleton and the ECM (Tamkun et al., 1986). Characterization of the first integrin subunit, which would be known later as the β1 integrin, marked the starting point of the integrin field facilitating the identification of other members of this protein family (Horwitz, 2012).

Integrins are a family of transmembrane receptors, composed of 18 α subunits and eight β subunits in mammals (Moreno-layseca et al., 2019; Takada et al., 2007). They are organized in heterodimers, which include 24 different permutations among the multiple α and β subunits (Michael & Parsons, 2020). As the predominant cellular receptors for the ECM, integrin heterodimers show selective affinity for particular components of the ECM (Theocharis et al., 2016). Many integrins bind to the Arg-Gly-Asp motif in their protein ligands, such as fibronectin, vitronectin, and fibrinogen (Theocharis et al., 2016). Upon ligand-binding, integrins acquire an active conformation by going through a process known as "outside-in" activation, which is followed by the recruitment of signaling proteins to their cytoplasmic tails. Integrins can also be activated from signals within the cell, a process known as "inside-out" activation (Hamidi & Ivaska, 2018). In this process, intracellular activators bind to the cytoplasmic tail of the β integrin subunit, which in turn undergoes a conformational change that increases ligand-binding affinity (Shattil et al., 2010). Therefore, integrins are considered bidirectional signaling machineries. Once integrins are activated and bind to their substrate, kinase signaling pathways and mechanotranduction events take place to regulate proliferation, differentiation, and survival (Cooper & Giancotti, 2019; Isomursu et al., 2019). One of

the fundamental integrin signaling proteins is the focal adhesion kinase (FAK), which upon integrin activation associates with members of the Scr-family of protein kinases to phosphorylate a wide variety of downstream effectors that regulate cell survival (Cooper & Giancotti, 2019). However, many more signaling proteins localize to the cell-matrix adhesion complexes in which integrins participate.

The network of proteins that is recruited to the cytoplasmic tails of active integrins is known as the integrin adhesome. To identify the members of this protein network, Horton and co-workers analyzed seven mass spectrometry datasets that were performed by different laboratories in distinct cell lines, including human malignant melanoma cells, human foreskin fibroblasts, human chronic myelogenous leukemia cells, mouse kidney fibroblasts, and mouse embryonic fibroblasts (Horton et al., 2015). Each of these mass spectrometry datasets were generated from isolated integrin-associated protein complexes from the plasma membrane. After the analysis, 60 proteins were identified as the core components of integrin-associated complexes, and they were defined as the "consensus" adhesome. The functional categories with the highest coverage among the proteins in the consensus adhesome were protein adaptors, actin regulators, and molecular chaperones. In addition, GTPases, kinases, and phosphatases were also found in the protein network (Horton et al., 2015). Importantly, a wide variety of signaling proteins are involved in the adhesome, and they mediate the signal transduction that controls cell proliferation, differentiation, and motility (Hastings et al., 2019). Protein-protein interaction maps within the consensus adhesome indicate that there are key proteins forming a structural connection between the integrins and the actin cytoskeleton. Among these proteins, talins are particularly important because of their mechanosensory properties and their fundamental function in adhesion maturation (Horton et al., 2016).

1.2.2 Talins as integrin activators and intracellular mechanosensors

Vertebrates have two talin genes, talin 1 (TLN1) and talin 2 (TLN2), which encode proteins that share an identical domain structure and 76% protein sequence identity (Goult et al., 2018). TLN1 has attained the main focus of the field, because of the drastic

phenotypic difference between *tln1*$^{-/-}$ and *tln2*$^{-/-}$ mice. While *tln1*$^{-/-}$ mice die during embryonic development due to arrested gastrulation, *tln2*$^{-/-}$ mice are viable and only show a reduced number of pups that can reach adulthood (Gough & Goult, 2018). TLN2 also shows a tissue-specific pattern of expression, as opposed to the ubiquitous expression of TLN1, which suggests that TLN2's function is confined to specific contexts (Gough & Goult, 2018). However, the ECM-integrin-cytoskeleton link is abolished only when TLN1 and TLN2 are simultaneously depleted in cells, showing some degree of functional redundancy of the isoforms (Zhang et al., 2008).

To date, TLN1 is better characterized than TLN2. TLN1 is a 270 kilodalton protein composed of 18 domains that are grouped into an N-terminal head domain (~400 amino acids) and a C-terminal rod domain (~2000 amino acids) (Klapholz & Brown, 2017) (Figure 6). The head domain belongs to the family of FERM domains and contains four subdomains (F0-F3), which mediate the association of TLN1 with the plasma membrane. F1-F3 bind directly to phosphatidylinositol 4,5, biphosphate (PIP2) lipids, and F3 interacts with β integrin subunits (Gough & Goult, 2018; Klapholz & Brown, 2017). A flexible linker of 82 amino acids connects the head domain to the rod domain. The rod domain is composed of 13 subdomains (R1-13) that participate in force transmission and sense mechanical stimuli (Goult et al., 2018). At the end of the rod domain, there is a dimerization domain (DD), which mediates the formation of anti-parallel TLN1 homodimers (Gough & Goult, 2018).

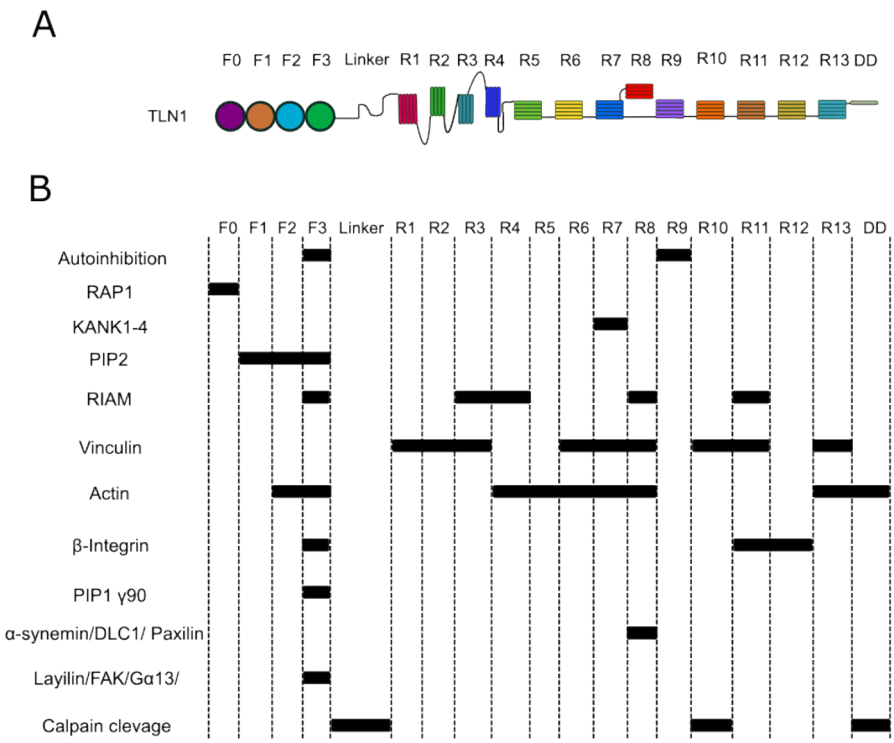

Figure 6. Schematic representation of TLN1 domains and binding sites for interacting partners. A) TLN1 is composed of 18 domains, which are divided into a head domain (F0-F3) and a rod domain (R1-DD). The head and the rod domains are connected by a flexible linker region. B) Several interacting partners bind across TLN1 and the binding site of selected partners are depicted. Modified from Gough & Goult, 2018.

1.2.2.1 Mechanosensitive properties of TLN1

To function as mechanosensors, each subdomain of the TLN1 rod domain can be unfolded upon a different level of tension. This mechanoreactive property is based on the helical structure of each rod subdomain, which gives them a reversible switch-like behavior resembling a spring (Goult et al., 2018). The helical structure of R1, R5-R7, and R9-R12 is particularly interesting since it contains a talin-specific five-helix bundle fold that increases the resistance to tension-dependent unfolding (Gough & Goult, 2018).

Once specific rod subdomains are unfolded, binding sites for interacting partners that are required for adhesion maturation become available (Klapholz & Brown, 2017) (Figure 7). Therefore, it is thought that TLN1 is constantly subjected to cycles of extension and relaxation in which interacting partners are bound and released from it, depending on the intensity of the applied tension (Goult et al., 2018).

There are three different actin-binding sites (ABS) in TLN1, of which ABS1 is located in the head domain (F2-F3) and the other two in the rod domain (ABS2 spanning R4-R8 and ABS3 in R13-DD) (Goult et al., 2018). According to the current model, once TLN1 engages an active integrin β subunit, ABS3 is the first site to interact with actin filaments (Klapholz & Brown, 2017). Subsequently, the rearwards flow of actin that is associated with the integrin-mediated adhesion sites increases tension on the rod domain, causing the unfolding of the R3 subdomain, which is the most mechanosensitive subdomain of TLN1 (Goult et al., 2018). When R3 unfolds, vinculin is recruited to it, stabilizing the stretched subdomain and facilitating the unfolding of ABS2. Vinculin is a key protein for the maturation of adhesion sites since it crosslinks TLN1 with the actin cytoskeleton allowing adhesion reinforcement. Finally, the binding of ABS2 to actin filaments permits the further stretching of TLN1 and consequently the eventual maturation of the adhesion site (Klapholz & Brown, 2017) (Figure 7).

Even though vinculin is the only protein known to have binding sites in the unfolded rod subdomains of TLN1, it is expected that many other unidentified interactors behave in a similar way. This hypothesis is based on current understanding of vinculin and the notion that most of the rod subdomains of TLN1 are constantly unfolded *in vivo*, exposing a considerable amount of the protein surface (Gough & Goult, 2018). There are 11 vinculin-binding sites along the rod domain of TLN1 and all of them need to be revealed by tension (Klapholz & Brown, 2017). Consequently, vinculin molecules bind progressively to TLN1 conforming the rod domain unfolds to promote focal adhesion maturation (Goult et al., 2018).

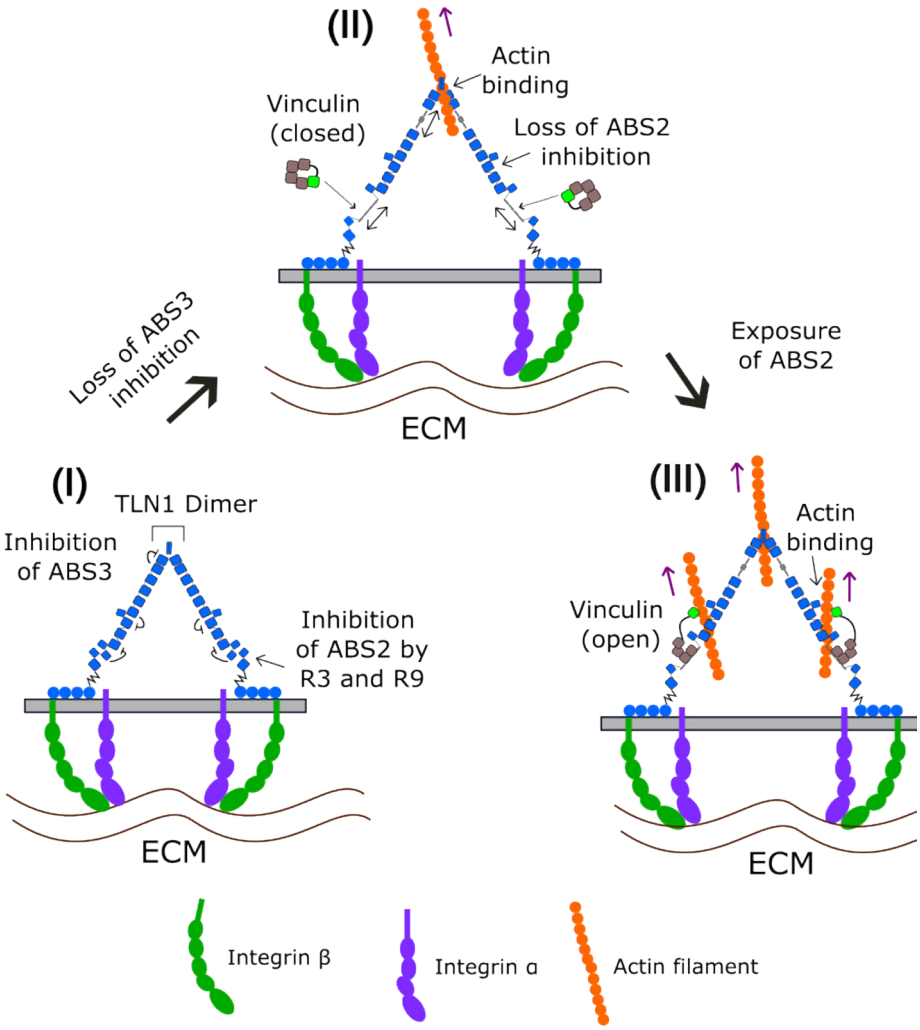

Figure 7. Mechanosensitive properties of the TLN1 rod domain. (I) The actin-binding sites (ABS) of the TLN1 rod domain are inhibited by adjacent domains. When the ABS3 is activated by a yet unknown mechanism, it binds to filamentous actin (orange circles). (II) The rearwards flow of actin (purple arrows), which is caused by actin polymerization and myosin contraction, increases tension in the rod domain causing the unfolding of R3 and exposing a vinculin-binding site. The unfolding of R3, and eventually R9, due to the increase in tension, alleviates the repression of the ABS2 and permits its binding to filamentous actin. (III) Vinculin also changes from a close conformation to an open conformation, in which the vinculin tail (grey) binds to talin and the vinculin head (light green) binds to filamentous actin. Modified from Klapholz & Brown, 2017.

1.2.2.2 Regulation of TLN1

The majority of the known TLN1 interactors bind to folded TLN1 subdomains, and they are released upon stretching. Among these interacting partners, PIP2, the small GTPase Rap1, the Rap1-interacting-adaptor-molecule (RIAM), and the heterotrimeric G protein Gα13 are important for the activation of TLN1 (Klapholz & Brown, 2017). These four proteins interact with the F3 subdomain and release TLN1 from an autoinhibitory state, which, in turn, is mediated by the binding of the TLN1 head domain to the rod domain (Goult et al., 2018). Once TLN1 is out of the autoinhibitory state, it is recruited to the plasma membrane by Rap1/RIAM where the presence of PIP2 lipids provides favorable electrostatic interactions that facilitate the binding of TLN1 to the β integrin subunit (Haining et al., 2016).

TLN1 is also regulated by post-translational modifications (PTMs), including protein cleavage by the protease calpain 2. There are at least three cleavage sites in TLN1: the first is in the linker region between the head domain and the rod domain, the second is located in the R10 subdomain, and the third is preceding the DD domain (Gough & Goult, 2018) (Figure 6B). When TLN1 is cleaved in the linker region, the head domain (~47 kDa) and the rod domain (~190 kDa) are separated (Yan et al., 2001). Interestingly, both fragments of the cleaved TLN1 seem to have independent roles as separate molecules. On one hand, the separated TLN1 head has been shown to interact with phosphatidylinositol phosphate kinase (PIPKIγ661), suggesting that it can affect the synthesis of PIP2 (Franco et al., 2004). On the other hand, the separated rod domain alone can restore cell cycle progression in *tln1*$^{-/-}$ cells that have stopped proliferating (Wang et al., 2011). The cleavage of TLN1 in the linker region also serves as a mechanism of focal adhesion turnover, since it mediates the rapid disassembly of TLN1 from the adhesion site and the consequent loss of tension (Franco et al., 2004). Similarly, loss of the cleavage site preceding the DD domain increases the number of matured adhesions delaying focal adhesion turnover (Bate et al., 2012). In contrast to the cleavage sites already mentioned, the cleavage in the R10 domain is required for proper cell-cell adhesion. Upon tension-dependent unfolding of the R10, calpain 2 cleaves TLN1

producing a ~70 kDa fragment, which contains the dimerization domain and some vinculin- and actin-binding sites. This fragment localizes to cell-cell adhesion sites where it is required for the formation of cadherin-containing plaques, partly by favoring actin polymerization and connecting cytoplasmic adhesion molecules at the adhesion site (Zhang et al., 2012).

Phosphorylation of three particular residues in the TLN1 head domain (T144, T150, and S446) has been shown to regulate the calpain-2-dependent cleavage of TLN1 in the linker region. While site-directed mutagenesis of T144 and T150 into alanine residues mimics the phenotype corresponding to calpain-2-mediated cleavage of TLN1, the substitution of S446 for an alanine residue inhibits TLN1 cleavage, delaying focal adhesion turnover (Li et al., 2016). In addition, phosphorylation of S425 by CDK5 has been shown to mediate β1 integrin activation and consequently cell migration (Jin et al., 2015). Apart from protein cleavage and phosphorylation, there are other PTMs in TLN1, and the functional impact of many of them needs to be elucidated (Table 2).

Table 2. TLN1 PTMs. Adapted from Gough & Goult, 2018.

TLN1 domain	Phosphorylation	Glycosylation	Methylation	Acetylation
Head	S5, Y26, Y70, T78, T96, T114, S1021, Y127, S128, T144, T150, S1225, T167, T190, S311			K1544, K2031, K2115
Linker	S405, S425, S429/T430, Y436, S446, S455/S458, S467			
Rod	S677, S815, S729, S979/S981, S940, S1201, Y1116, T1142, T1263, S1323, S1508, S1641, S1684, S1849, T1855, S1878, S2040, S2127, S2338, y2530, S2535	T1487, T1890	K2454	T1487

1.2.2.3 Diseases associated with TLN1

Mutations and dysregulation of TLN1 have been associated with cancer, hematologic pathologies, and cardiomyopathies (Chen et al., 2020; Haining et al., 2016). Overexpression of TLN1 is common in metastatic cancers, where it is associated with integrin activation and enhanced cell motility (Haining et al., 2016). TLN1 also plays an important role in cancer survival by inducing pro-survival signaling pathways through adhesion-independent activation of protein kinases, such as FAK (Sakamoto et al., 2010). The role of TLN1 in cancer is also evidenced by the effects of TLN1 levels on the efficacy of anti-cancer drugs (Haining et al., 2016). For example, RNAi-mediated downregulation of TLN1 in different breast cancer cells shows increased chemosensitivity to docetaxel, a common chemotherapy drug (Singel et al., 2013).

The effect of TLN1 in hematologic pathologies is evidenced by the phenotype of mice with TLN1-deficient platelets, which are characterized by their inability to halt bleeding upon vessel injury (Nieswandt et al., 2007). These defects in platelet aggregation are thought to arise from defective TLN1-dependent conformational change in the αIIbβ3 integrin pair, which otherwise enhances platelet adhesion to blood vessels (Provasi et al., 2014). In addition, the TLN1-mediated connection between integrins and the actin cytoskeleton is also required for the progressive shrinkage of blood clots during the reparation of the vessel wall (Haling et al., 2011). The levels of TLN1 have also been shown to increase in the cardiomyocytes of failing human hearts, and mice with TLN1-deficient cardiomyocytes exhibit increased hypertrophy and reduced fibrosis upon exposure to pressure overload (Manso et al., 2013). Interestingly, missense mutations in TLN1 are also associated with spontaneous coronary artery injury, showing that the function of TLN1 is also important for the cardiovascular system of humans (Turley et al., 2019). Taken together, TLN1 is associated with different human pathologies that involve misregulation of cell adhesion, migration, and response to mechanical stress.

2 How do cells respond to proteotoxic stress?

All cells are constantly exposed to environmental insults that challenge the homeostasis of their proteome. These adverse situations cause protein damage and eventually lead to cell death unless it is mitigated in time (Lindquist, 1986). Damaged proteins lose their native conformation and solubility, exposing their hydrophobic residues and forming protein aggregates. In order to return to their fully functional native state, the misfolded proteins must be assisted by molecular chaperones (Balchin et al., 2016). The cellular response that involves the induction of molecular chaperones under stress conditions can be classified in two major terms, depending on the subcellular localization where protein damage occurs. If the protein damage accumulates in the endoplasmic reticulum or mitochondria, the molecular response is defined as the unfolded protein response. If damaged proteins accumulate in the cytoplasm, the molecular response is defined as the heat shock response (HSR) (Morimoto & Cuervo, 2014). Importantly, these responses are regulated by different mechanisms. This thesis will be focused on the HSR, which is characterized by the rapid upregulation of conserved stress-responsive molecular chaperones known as heat shock proteins (HSPs) (Lindquist, 1986).

2.1 The heat shock response

The research field of the HSR began in the early 1960's when Ferruccio Ritossa observed a puffing pattern in the *Drosophila busckii* salivary gland polytene chromosomes, which was induced by heat, dinitrophenol or sodium salicylate (Lindquist, 1986; Ritossa, 1962). At that time, it was known that puffs in the *Drosophila* polytene chromosomes were sites of active gene transcription, which raised the question: What were the proteins encoded by those heat-responsive genes? Tissières and co-workers isolated this new set of proteins that were rapidly synthesized upon stress and coincided with the induction of puffs in the polytene chromosomes of *Drosophila* salivary glands (Lindquist, 1986; Tissiéres et al., 1974). Since this stress response was very prominent it became a model system to study gene expression. Indeed, the genes of *Drosophila hsps* were among the first eukaryotic genes to be cloned and characterized in terms of structure and regulation.

After the characterization of the *hsps* in *Drosophila,* it became evident that almost every known organism is equipped with a set of genes coding for this type of molecular chaperones, which gives a universal dimension to the HSR (Lindquist, 1986). Hence, without knowing it himself, Ritossa started a field of research that is relevant to the majority of known organisms. Quoting his own words while he was describing the initial interpretation of his finding "it did not matter if this interpretation was true or false; it was a working link between imagination and reality, like love" (Ritossa, 1996).

2.2 Heat shock proteins

The term heat shock protein (HSP) originated from the prototypical stimulus, namely heat shock, in which the pathway was discovered. However, most HSPs are expressed under physiological conditions, where their function is fundamental for cell viability (Kampinga & Bergink, 2016). The human HSP families include HSPH (Hsp110), HSPC (Hsp90), HSPA (Hsp70), DNAJ (Hsp40), HSPB (small Hsps), and chaperonins including HSPD/E (HSP60/HSP10) and CCT (TRiC) (Kampinga et al., 2009). Under physiological conditions, HSPs from all these families are constitutively expressed to assist newly synthesized proteins to fold, mature, localize to their proper subcellular compartment, and associate with protein assemblies (Gidalevitz et al., 2011). In contrast, under proteotoxic conditions, the stress-inducible members of these families are expressed to degrade proteins or restore the native state of misfolded proteins (Mogk et al., 2018). The function of distinct HSPs is mediated by different molecular mechanisms, of which the activation cycle of HSPAs is among the best understood (Balchin et al., 2016). HSPAs have an N-terminal nucleotide-binding domain, which interacts with ATP, and a C-terminal binding domain that recognizes short hydrophobic-rich amino acid sequences of their targets. DNAJs are co-chaperones that recognize and present the substrate to the ATP-bound HSPAs, which in turn mediate the proper folding of the substrate upon DNAJ-mediated ATP hydrolysis. Once the substrate is folded, a nucleotide exchange factor binds to HSPAs to facilitate the exchange of ADP for ATP and the release of the folded substrate (Balchin et al., 2016). Other HSPs share common features with HSPAs, such as ATP hydrolysis and the recognition of hydrophobic

residues, but the detailed molecular mechanism operating behind their activation cycle is not yet fully understood in many HSP families (Balchin et al., 2016; Kampinga et al., 2009).

Since the activity of HSPs is fundamental for cell viability, it is not surprising that their dysregulation is involved in different diseases. For example, the upregulation of chaperones enables cancer cells to cope with intrinsic proteotoxic stress, and different HSP inhibitors have been developed for therapeutic purposes (Chatterjee & Burns, 2017). Additionally, a vast majority of age-specific neurodegenerative diseases present protein aggregates, which can be disaggregated by the activity of specific HSPs (Mogk et al., 2018). Therefore, HSPs are promising drug targets to treat different diseases, and knowing the molecular mechanisms that regulate their activity is fundamental to design therapeutic strategies.

2.3 Heat shock factors

In the late 1970's, *Drosophila hsps* genes were introduced into different cell types to perform deletion experiments, which aimed to determine the common promoter element regulating the induction of HSPs under stress conditions (Nover, 1987). Already in the early 1980's, the first proposal of a consensus sequence for this gene regulatory element, named the heat shock element (HSE), was made (Mirault et al., 1982; Pelham, 1982). Eventually the HSE consensus sequence was defined as inverted repeats of the pentameric sequence nGAAn (Amin et al., 1988). Importantly, the discovery of the HSE was essential for the isolation of a transcription factor that induced the expression of HSPs under stress condition (Wu, 1995). Crude extracts from heat-shocked *Drosophila* cells were used for footprint analysis to isolate the transcription factor that bound to the HSE and promoted the transcription of a *Drosophila hspa (hsp70)* gene *in vitro* (Parker & Topol, 1984; Wu, 1995). After the isolation of the *Drosophila* HSF, homologs of this transcription factor were found in yeast (Sorger & Pelham, 1987; Wiederrecht et al., 1987), tomato (Scharf et al., 1990), mouse (Sarge et al., 1991), and human (Rabindran et al., 1991; Schuetz et al., 1991).

Currently, HSFs are defined as a versatile family of transcription factors that are well conserved from fungi to humans. While invertebrates exhibit a single HSF, multiple HSFs are present in vertebrates (Roos-Mattjus & Sistonen, 2022). There are seven HSFs in mammals: HSF1, HSF2, HSF3, HSF4, HSF5, HSFX, and HSFY, of which HSF1 and HSF2 are the most studied ones (Joutsen & Sistonen, 2019). HSF1 is considered the functional counterpart of the single HSF in yeast, nematodes, and flies since other HSFs fail to induce the expression of HSPs during stress (Roos-Mattjus & Sistonen, 2022). In contrast, HSF2 is targeted for degradation during acute stress, and its role has been described in the context of development, cell differentiation, cell division, and cancer invasion (Joutsen & Sistonen, 2019).

HSF4 has been intensively studied during the last two decades due to its function in the crystalline lens of the eye. Initially, Bu and co-workers found four missense mutations in the DNA-binding domain of human HSF4 that were linked to autosomal dominant lamellar and Marner cataracts (Bu et al., 2002). Subsequently, Fujimoto and co-workers described the phenotype of *hsf4*$^{-/-}$ mice, which displayed abnormal differentiation of lens epithelial cells and cataract development (Fujimoto et al., 2004). More recently, the number of human HSF4 mutations linked to eye pathologies have increased significantly, reinforcing the idea that HSF4 is fundamental for eye development (Anand et al., 2018; Cao et al., 2018). According to the current model, mutations in HSF4 cause cataracts by impairing the expression of the lens chaperone γ-crystalline and the DNase DLAD (Cui et al., 2013; Fujimoto et al., 2004; Shi et al., 2009).

HSF3 and HSF5 have been only observed in a few organisms, and little is known about their function. HSF3 was initially found in chicken, where it plays a major role in the HSR mimicking the function of mammalian HSF1 (Kawazoe et al., 1999). More than ten years later, HSF3 was also found in mouse where under heat shock conditions, it translocates to the nucleus to induce the expression of non-classical heat shock genes (Fujimoto et al., 2010). Although high protein levels of HSF5 were initially observed in rat and mouse testes, the function of HSF5 in these organisms remains enigmatic (Chalmel et al., 2012). Indeed, the function of HSF5 has been mostly studied in zebrafish,

where it is also highly expressed in testes (Saju et al., 2018). Interestingly, depletion of HSF5 results in male infertility due to drastically reduced sperm count and defects in sperm morphology, which were attributed to transcriptional deregulation of genes related to cell cycle and apoptosis (Saju et al., 2018). Lastly, much less is known about HSFY and HSFX in comparison to other HSFs. HSFY is located in the Y chromosome as palindromic sequences that are mostly expressed in testes, where it is thought to participate in spermatogenesis (Tessari et al., 2004). HSFX is located in the X chromosome and its function has not yet been described (Gomez-Pastor et al., 2018).

2.3.1 Domain structure of HSFs

The hallmark of the HSF family members is the winged helix-turn-helix DNA-binding domain (DBD), which is well conserved in all eukaryotic HSFs (Wu, 1995) (Figure 8). The HSFs DBD is composed of an antiparallel β-sheet with four strands that confines the hydrophobic core of a three-α-helix bundle (Harrison et al., 1994). The crystal structures of human HSF1 and HSF2 DBDs in complex with DNA were recently resolved. Both crystal structures provided evidence for a model in which HSF1 and HSF2 embrace the HSE in the DNA double helix, causing the rest of the protein to be opposite to the DNA-bound DBD. This position exposes distinct surfaces of both HSFs, including the DBD, to different protein-interacting partners (Jaeger et al., 2016; Neudegger et al., 2016).

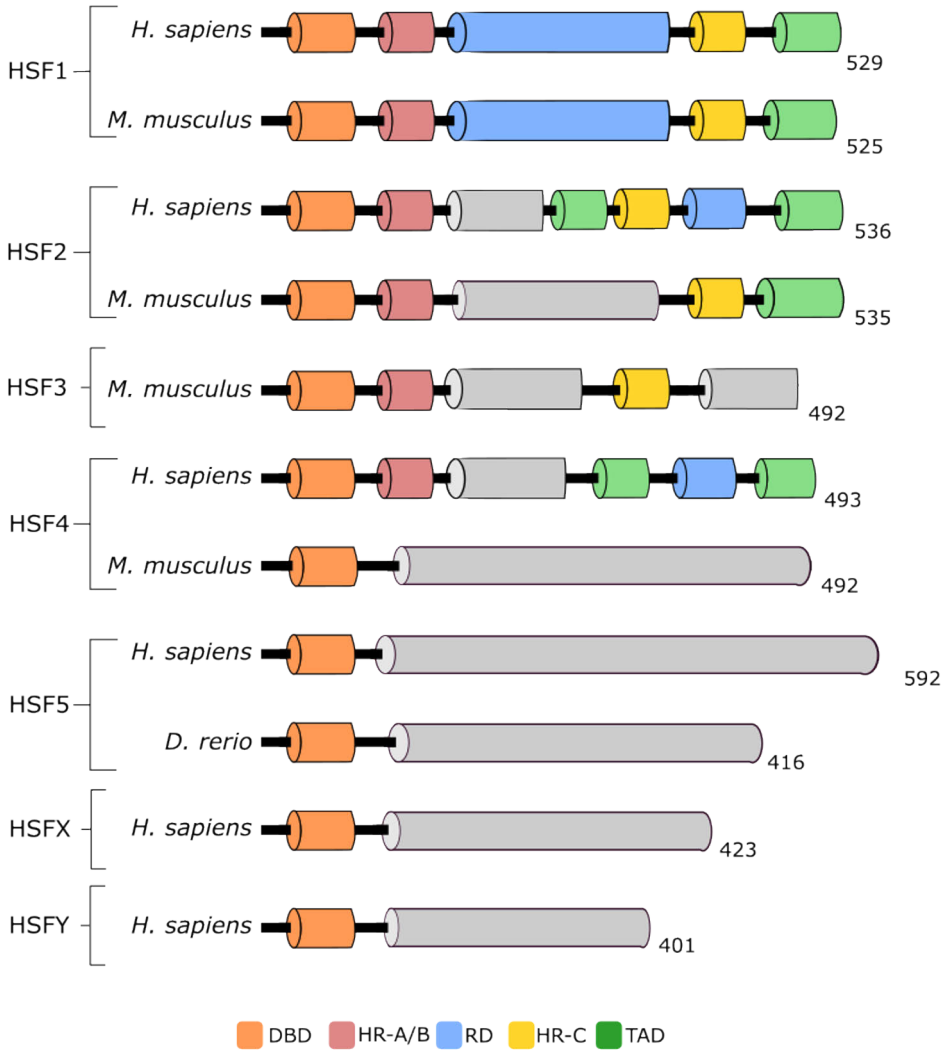

Figure 8. Domain organization across the heat shock factor family. The mammalian genome contains seven HSFs (HSF1-5, HSFX, HSFY), which are composed of different domains. The HSF5 protein has been detected in zebrafish (*Danio rerio)*, rat (*Rattus norvegicus*), and human (*Homo sapiens*). The HSF5 domain structure is compared between the fish and human paralogs. HSF3 has only been observed in chicken (*Gallus gallus*) and mouse (*Mus musculus*). DNA-binding domain (DBD), heptad repeat domains (HR-A/B/C), regulatory domain (RD), and a transactivation domain (TAD). The numbers indicate amino acids. Modified from Joutsen & Sistonen, 2019.

A prerequisite for most HSFs to function as transcription factors is their assembly into oligomers (Gomez-Pastor et al., 2018; Wu, 1995). For this purpose, the majority of HSFs are equipped with conserved hydrophobic leucine-zipper-like heptad repeats (HR-A/B), which are positioned immediately after the DBD (Joutsen & Sistonen, 2019) (Figure 8). In some HSFs, the HR-A/B-mediated oligomerization is inhibited by another heptad repeat that is located in the C-terminus of the protein (HR-C), which mediates intracellular autoinhibition (Gomez-Pastor et al., 2018). Most HSFs also possess a C-terminal transactivation domain (TAD) that controls their activity (Joutsen & Sistonen, 2019). In comparison to other domains of the HSFs, TADs are not well conserved or structured (Westerheide et al., 2012). In fact, most of the current knowledge of this domain comes from investigations focused on HSF1, which provides a limited view considering the individual variability of HSFs (Gomez-Pastor et al., 2018). The HSF1 TAD consists of two modules, AD1 and AD2, which are modified by different PTMs and bound by chromatin remodelers (Corey et al., 2003; Sullivan et al., 2001). These domains are normally repressed in the absence of heat stress by a regulatory domain (RD) located between the HR-A/B and the TADs (Green et al., 1995).

2.3.2 HSF1

Among the mammalian HSFs, HSF1 is essential for the induction of HSPs upon proteotoxic stress, and therefore it is considered the master regulator of the HSR (Himanen et al., 2022; Joutsen & Sistonen, 2019; Mahat et al., 2016; McMillan et al., 1998). Due to the fundamental role of HSF1 in the HSR, the activation and attenuation cycle of this transcription factor is regulated by distinct mechanisms (Joutsen & Sistonen, 2019) (Figure 9). According to the current model, in the absence of stress monomeric HSF1 shuttles between the nucleus and the cytoplasm and it interacts with a repressive multi-chaperone complex (e.g. HSPC, HSPA, DNAJ, and TRiC) (Gomez-Pastor et al., 2018; Kmiecik & Mayer, 2022). Under a wide repertoire of proteotoxic conditions, the chaperones in the repressive complex interact with misfolded proteins and leave HSF1 free to trimerize, translocate to the nucleus, and activate gene expression (Joutsen & Sistonen, 2019). The progressive alleviation of proteotoxic stress is

accompanied by a gradual reduction of HSF1 activity, which is achieved by an HSP-mediated negative feedback loop and PTMs. Essentially, once misfolded proteins are restored or degraded, the molecular chaperones are available to repress HSF1 (Anckar & Sistonen, 2011). Different chaperones seem to operate through distinct molecular mechanisms to inhibit HSF1. For example, the HSPC-FKBP2-p23 complex is required to dissociate HSF1 from the DNA (Guo et al., 2001). HSPA and DNAJ, in turn, interact with the TAD domain of HSF1 and repress its transactivating capacity, but they are unable to dissociate HSF1 from the DNA (Shi et al., 1998). Recently, Kmiecik and co-workers elegantly showed that HSPA8 (HSC70), which is a constitutively expressed member of the HSPA family, removes HSF1 from the DNA in a concentration-dependent manner (Kmiecik et al., 2020). Moreover, this *in vitro* study revealed that DNA-bound HSF1 trimers are monomerized through an unzipping mechanism driven by the entropic pulling of HSPA8 (HSC70), which presumably allows HSF1 monomers to be efficiently recycled (Kmiecik et al., 2020) (Figure 9). Then, Kourtis and co-workers showed that the ubiquitin ligase FBXW7α ubiquitinates HSF1, targeting it for proteasomal degradation upon heat stress, and lack of FBXW7α produces a defective attenuation of the HSR (Kourtis et al., 2015).

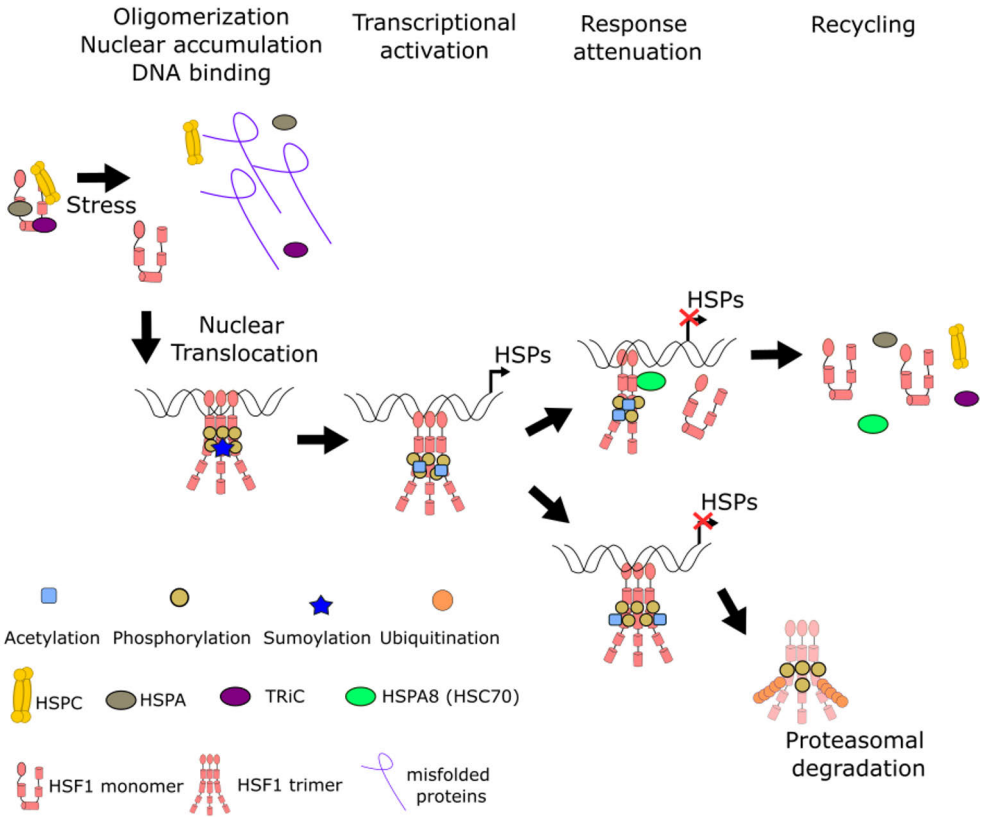

Figure 9. Mechanisms of activation and attenuation of HSF1. Under physiological conditions, monomeric HSF1 interacts with a repressive multi-chaperone complex. Upon a wide variety of proteotoxic stresses, HSF1 is released from the multi-chaperone complex, oligomerizes, translocates to the nucleus, and promotes gene expression. Simultaneously, HSF1 is modified with different PTMs. Phosphorylation and acetylation of particular residues correlate with the transactivating capacity of HSF1, and the induction of HSPs. During the attenuation phase, trimeric HSF1 is dissociated from the DNA by acetylation of its DBD and targeted for ubiquitination-dependent proteasomal degradation. Additionally, HSC70 disassembles DNA-bound HSF1 trimers into monomers, which can be recycled.

Interestingly, HSF1 presents an intrinsic capability to sense stress, since it trimerizes and acquires DNA-binding capacity upon increased temperatures and treatments with sodium salicylate (Hentze et al., 2016; Jurivich et al., 1992). A study conducted by Hentze and co-workers, showed that the HR-C domain of HSF1 unfolds upon temperature elevation, leaving the HR-A/B free to oligomerize, and this phenomenon

occurs in an HSF1 concentration-dependent manner (Hentze et al., 2016). This intrinsic property of HSF1 activation is thought to act in synergy with the chaperone-repressive complex to regulate the activity of HSF1 upon stress (Kmiecik & Mayer, 2022). Additionally, HSF1 also trimerizes and binds to DNA in cells treated with sodium salicylate, but it cannot induce the expression of HSPA, showing that apart from trimerization and DNA-binding capacity HSF1 has other requirements, such as PTMs, to induce target gene expression (Jurivich et al., 1992).

2.3.2.1 Post-translational modifications of HSF1

As illustrated in the HSFs, the function of a protein does not merely depend on its amino acid sequences and structural features. Indeed, after synthesis, functional groups can be covalently linked to proteins that determine protein activity, localization, association with protein assembly, trafficking, and degradation (Wang et al., 2022). Therefore, PTMs, constitute a fundamental regulatory layer of the proteome, which allows protein networks to function in harmony. Not surprisingly, PTMs are tightly involved in the regulation of HSF1, and multiple types of PTMs have been described to modify it (Gomez-Pastor et al., 2018) (Figures 9 and 10). The first notion of PTMs on HSF1 came from studies in yeast that identified the stress-inducible hyperphosphorylation of the single HSF in this organism (Sorger et al., 1987). Since the publication of this seminal study, it was considered that the phosphorylation of key residues in HSF1 was a prerequisite for its transactivating capacity. However, subsequent studies have shown that phosphorylation is dispensable for the transactivating capacity of HSF1. Instead, phosphorylation appears to modulate the activity of HSF1 according to the intensity of the stress (Budzyński et al., 2015; Zheng et al., 2016). There are 23 phosphorylation sites in HSF1, most of which are located in the RD domain (Gomez-Pastor et al., 2018; Joutsen & Sistonen, 2019). Among these sites, S303 and S307 are particularly interesting, since they function as priming sites for other PTMs. The S303 forms part of a phosphorylation-dependent sumoylation motif, which consists of a consensus sumoylation site adjacent to a proline-directed phosphorylation site (Anckar & Sistonen, 2011). Once S303 is phosphorylated, sumoylation of K298 takes place in HSF1 to

repress its transactivating capacity (Hietakangas et al., 2006). In addition, phosphorylation of S303 and S307 is required for the interaction between HSF1 and the ubiquitin ligase FBXW7α, and therefore necessary for the proteasome-mediated degradation of HSF1 (Kourtis et al., 2015). Interestingly, due to the activity of different kinases, the proteasomal degradation of HSF1 is dysregulated in cancer and Huntington's disease, leading to an abnormal accumulation or depletion of HSF1 protein levels, respectively (Gomez-Pastor et al., 2018).

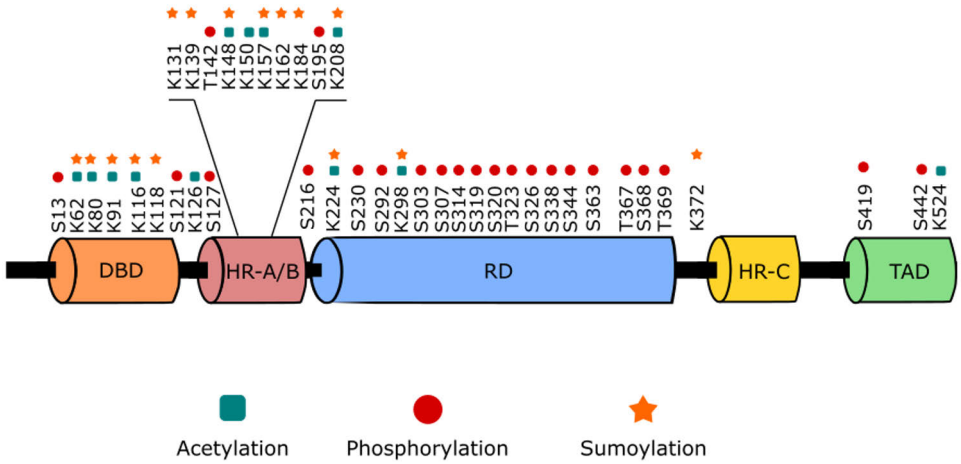

Figure 10. Schematic representation of human HSF1 post-translational modifications. HSF1 is phosphorylated in 23 residues, most of which are located in the regulatory domain (RD) domain. The majority of acetylation and sumoylation sites reside in the DNA-binding domain (DBD) and oligomerization domains (HR-A/B). The carboxy-terminal heptad repeat (HR-C) and the transactivation domain (TAD) are also shown. Modified from Joutsen & Sistonen, 2019.

Apart from the K298 in the phosphorylation-dependent sumoylation motif, HSF1 has 14 sumoylation sites that mostly reside in the DBD and HRA/B (Hendriks et al., 2017). However, the function of these sites has not yet been characterized. Acetylation has been shown to regulate HSF1 activity both under physiological conditions and stress. In the absence of stress, acetylation of HSF1 in K208 and K298, by the histone

acetyltransferase EP300, prevents HSF1 proteasomal degradation (Raychaudhuri et al., 2014, de Thonel et al., 2022). Upon stress, EP300 acetylates HSF1 in K80, which resides in the DBD, promoting the dissociation of HSF1 from the DNA (Westerheide et al., 2009).

Taken together, different PTMs regulate HSF1 during its activation cycle. Under control conditions, phosphorylation keeps HSF1 inactive, while acetylation stabilizes it (Hietakangas et al., 2006, Raychaudhuri et al., 2014). During the outset of stress, the phosphorylation signature of HSF1 is modified to avoid repression and enhance its transactivating capacity (Budzyński et al., 2015; Zheng et al., 2016). When the stress conditions decline, HSF1 undergoes an attenuation cycle in which acetylation and ubiquitination take place. Considering the mechanisms regulating the activity of HSF1, it is tempting to speculate that PTMs direct HSF1 to different genomic loci in different conditions, but this possibility remains to be investigated.

2.3.2.2 Roles of HSF1 in health and disease

Development

Within the first decade after its discovery, HSF1 was mostly considered as a stress-induced transcription factor that controlled the expression of HSPs. However, this view changed with the identification of HSF1-target genes during development (Barna et al., 2018). Early studies in *Drosophila* revealed that the single HSF in this model organism regulates also other genes than the *hsps*, which are required for oogenesis and larval development (Jedlicka et al., 1997). More recent work in *C. elegans* has also shown that there is an HSF-dependent transcriptional profile, which is distinct from the HSR and is required for nematode development (Brunquell et al., 2016).

In mice, HSF1 acts as a maternal factor that is required for gametogenesis and the development of the sensory epithelium (Christians et al., 2000; Metchat et al., 2009; Takaki et al., 2006). The *hsf1*$^{-/-}$ female mice are infertile since their fertilized oocytes are unable to progress beyond the zygote state (Bierkamp et al., 2010). In contrast, male

hsf1$^{-/-}$ mice are fertile, despite showing a reduced number of germ cells and morphological defects in their sperm (Åkerfelt et al., 2010). There are other phenotypes associated with both female and male *hsf1*$^{-/-}$ mice. For example, loss of HSF1 causes reduced organ and body size (Xiao et al., 1999). This phenotype has been recently linked to the activity of the serine-threonine kinase mTOR. mTOR is the catalytic subunit of the protein complexes mTORC1 and mTORC2, which regulate cell growth, proliferation, and survival (Laplante & Sabatini, 2009). With an elegant experimental setup, Su and co-workers showed that HSF1 promotes the activity of the mTORC1 complex by inhibiting the c-Jun N-terminal kinase, which in turn phosphorylates mTORC1 promoting its disassembly (Su et al., 2016). HSF1 is also required for brain development, since *hsf1*$^{-/-}$ mice show brain morphological alterations, such as lateral ventricles enlargement, loss of white matter, progressive myelin loss, and increased levels of ubiquitinated proteins (Homma et al., 2007; Santos & Saraiva, 2004).

Aging and metabolism

In *C. elegans* the HSR undergoes an abrupt decline in early adulthood, correlating with the onset of reproductive maturity. This decline is mediated by an increase in the histone mark H3K27me3 within *hsps* promoters due to reduced activity of the histone demethylase jmjd3.1, which hinders the binding of the single HSF in *C. elegans* (HSF-1 hereafter). The decline of the HSR leads to a reduced lifespan of the organism, and it has been suggested that this is a programmed event to favor progeny fitness (Labbadia & Morimoto, 2015). Apart from the age-dependent deregulation of the HSR, deficiency of HSF-1 reduces the lifespan of *C. elegans* through its cooperation with the transcription factor DAF-16 (FOXO in mammals). Upon activation of the insulin-like growth factor receptor DAF-2 (IGFR in mammals), DAF-16 is phosphorylated and retained in the cytoplasm. In turn, the absence of insulin or upon disruption of DAF-2, DAF-16 and HSF-1 translocate together to the nucleus where they activate anti-aging target genes, which include the HSPs (Hsu et al., 2003). Interestingly, mammals also present an age-dependent decline of HSF1 DNA-binding and induction of the HSR (Fawcett et al., 1994). However, this decline is reversed by caloric restriction, indicating that

proteostasis is regulated by a common mechanism controlling aging and metabolism (Anckar & Sistonen, 2011).

The, mammalian HSF1 is considered as a metabolic sensor, since it is regulated by signaling molecules that monitor energy and nutrient availability, like the protein kinase AMPK and mTORC1. AMPK monitors the equilibrium of the intracellular AMP: ATP ratio, while the mTORC1 complex senses the availability of nutrients, such as amino acids (Su & Dai, 2016). As mentioned above, HSF1 promotes the activity of mTORC1 *via* inhibition of c-Jun N-terminal kinase, which is a mechanism to control organ and body size (Su et al., 2016). In addition, HSF1 and AMPK constitute a mutually repressive complex. On one hand, when the cell is exposed to an accumulation of metabolites that cannot be processed further due to low levels of energy, a condition known as metabolic stress, AMPK phosphorylates HSF1 in serine 121 preventing its translocation to the nucleus (Dai et al., 2015). On the other hand, HSF1 inhibits AMPK activity upon direct interaction, which promotes lipogenesis and protein cholesteroylation (Su et al., 2019). AMPK also regulates HSF1 indirectly by activating the PGC-1α (Li et al., 2017). PGC-1α is a transcriptional co-activator that regulates the expression of genes involved in different metabolic processes, including mitochondria biogenesis and gluconeogenesis. Interestingly, PGC-1α can modulate the activity of HSF1 in a context-dependent manner (Joutsen & Sistonen, 2019). In mouse liver, fasting promotes the activation of PGC-1α, which in turn interacts with HSF1 and represses its transactivating capacity (Minsky & Roeder, 2015). However, in the context of heat shock, PGC-1α interacts with HSF1 and promotes the expression of HSPs (Xu et al., 2016). Taken together, HSF1 is a metabolic sensor that integrates signaling inputs from different energy- and nutrient-sensing pathways.

Neurodegeneration

The age-dependent decay in HSF1 activity is tightly linked to age-related pathologies, including neurodegenerative diseases, which are characterized by abnormal protein misfolding and aggregation that causes high levels of proteotoxicity. Among these

diseases, HSF1 has been shown to present similar disfunctions in the context of Huntington's, Parkinson's, and Alzheimer's diseases (Gomez-Pastor et al., 2018).

Huntington's disease is characterized by the accumulation and aggregation of mutant huntingtin, which is a protein that can accumulate a variable number of polyglutamine repeats. In a Huntington's mouse model (R6/2), deficiency of HSF1 exacerbates the aggregation of mutant huntingtin. The HSF1-mediated suppression of polyglutamine-huntingtin aggregation involves the expression of the transcription factor NFATc2, indicating that the role of HSF1 is not restricted to the induction of HSPs in this disease (Hayashida et al., 2010). Congruently, the expression of constitutively active HSF1 in cultured cells suppresses polyglutamine aggregation more efficiently than the combined expression of HSPAs and DNJs, and the constitutively active HSF1 alleviates the phenotype of R6/2 mice (Fujimoto et al., 2005). In support of the protective role of HSF1 in Huntington's disease, brain samples from human patients present remarkably low levels of HSF1, due to its enhanced proteasomal degradation. Indeed, mutant huntingtin increases the levels of the protein kinase CK2a' and the E3 ligase FBXW7, promoting the phosphorylation and proteasomal degradation of HSF1 (Gomez-Pastor et al., 2017).

A hallmark of Parkinson's disease is the aggregation of α-synuclein and the loss of dopaminergic neurons. In a similar way as in Huntington's disease, the overexpression of α-synuclein promotes the proteasomal degradation of HSF1. This aberrant degradation depends on the ubiquitin ligase NEDD4 and requires the deacetylation of HSF1 by SIRT1 (Kim et al., 2016). Moreover, when HSF1 is overexpressed in cells modeling Parkinson's disease, α-synuclein aggregates are dramatically reduced presumably through the strong induction of HSPA1A (Liangliang et al., 2010).

Among different hypotheses, Alzheimer's disease is thought to be caused by the accumulation of amyloid-β toxic peptide that is generated when a precursor protein is cleaved. The toxic peptides aggregate and cause neuronal loss in the hippocampus and cerebellum, where the number of Purkinje cells are particularly reduced (Gomez-Pastor

et al., 2018). Following the patterns described before for Huntington's and Parkinson's diseases, HSF1 overexpression in an Alzheimer's rat model restores the levels of Purkinje cells in the cerebellum and this effect correlates with increased levels of HSPs (Zou et al., 1998). However, the molecular mechanism of HSF1 downregulation in Alzheimer's disease remains enigmatic. Taken together, the current evidence supports the hypothesis that HSF1 is a protective factor against proteotoxicity in the context of neurodegeneration.

Cancer

Even though signaling cascades that enhance the activity and protein stability of HSF1 constitute promising therapeutic targets to treat devastating neurodegenerative diseases, activating HSF1 is a "double edge sword" due to the prominent role of HSF1 in cancer. Indeed, a wide variety of malignancies show HSF1 addiction, since they depend on the activity of HSF1 to progress. Cancer cells exploit the role of HSF1 as a *primus motor* of the *hsps* genes to alleviate the proteotoxic effects of genomic instability and abnormal rates of cell division. However, the role of HSF1 in cancer goes beyond the induction of HSPs (Dong et al., 2019). Mendillo and co-workers identified a set of genes specifically regulated by HSF1 in the context of cancer, named the HSF1 cancer signature (HSF1-CaSig), which is distinct from the set of genes that are regulated upon heat shock, including genes involved in cell-cycle regulation, metabolism, cell adhesion, and translation (Mendillo et al., 2012). Importantly, the HSF1 cancer signature correlates with poor patient outcome in different types of cancers (e.g. lung, skin, pancreas, and liver tumors), and it can be used to predict cancer severity (Dong et al., 2019). In addition to driving a specific set of genes in cancer cells, HSF1 also supports tumorigenesis by activating a complementary transcriptional profile in cancer-associated fibroblasts. After cancer cells, cancer-associated fibroblasts are the most abundant cell type in the tumor microenvironment, and they are recruited by cancer cells to produce cytokines and growth factors that support tumor growth. Using an elegant experimental setup, Scherz-Shouval and co-workers showed that HSF1 is required for the expression of transforming growth factor beta and the chemokine stromal cell-derived factor 1 by cancer-associated

fibroblasts (CAFs). The subsequent secretion of these signaling molecules, in turn, functions as an autocrine and paracrine signal to promote growth and invasion in the tumor microenvironment (Scherz-Shouval et al., 2014). Since this seminal study, HSF1 has been shown to be upregulated in CAFs of colon and gastric cancers, where it regulates ECM proteins to enhance cancer progression (Grunberg et al., 2021; Levi-galibov et al., 2020).

Due to its important role in cancer, HSF1 inhibitors have a promising therapeutic potential, and many small molecules have been reported in the literature as inhibitors of HSF1 (Dong et al., 2019). However, the majority of these inhibitors have been found by monitoring transcription in gene reporter-based high-throughput screens using the HSE, which is a method that is vulnerable to off-target effects. Moreover, the molecular mechanisms through which these inhibitors function are largely unknown, and evidence for direct interaction with HSF1 is lacking in many cases (Dong et al., 2019). Therefore, future studies are needed to characterize how these small molecules inhibit the transactivating capacity of HSF1.

2.3.3 HSF2

HSF2 was cloned from mouse and human cells in the early 1990's, and two isoforms, HSF2-α and HSF2-β, were found to be expressed in a tissue-dependent manner (Goodson et al., 1995; Sarge et al., 1991; Schuetz et al., 1991). In contrast to HSF1, HSF2 was observed to bind DNA in the absence of heat stress, and its DNA-binding capability was shown to decrease upon heat shock (Sarge et al., 1991). These observations indicated that HSF2 was not a potent inducer of the HSPs upon elevated temperatures. Due to the high homology between the oligomerization domains of both HSFs, however, it was suggested that HSF2 could cooperate with HSF1 to regulate gene expression through the formation of heterooligomers (Schuetz et al., 1991). This suggestion was confirmed by later investigations which characterized the interplay between HSF1 and HSF2 (He et al., 2003; Lecomte et al., 2010; Östling et al., 2007; Sandqvist et al., 2009; Vihervaara et al., 2013). He and co-workers, showed that HSF1

and HSF2 are physically associated and the overexpression of the HSF2-α isoform enhances the induction of HSP70 upon heat shock (He et al., 2003). Subsequently, it was found that HSF2 modulates HSF1-mediated expression of *hsp* genes and the HSF1-HSF2 heterooligomers regulate transcription (Östling et al., 2007; Sandqvist et al., 2009). Chromatin immunoprecipitation coupled with DNA sequencing (ChIP-seq) revealed that HSF1 and HSF2 share most of their target sequences upon heat shock in mouse and human cells (Himanen et al., 2022; Vihervaara et al., 2013). Taken together, these studies provide evidence for a role of HSF2 in the HSR through its interplay with HSF1.

The activity of HSF2 is mainly regulated through its protein levels. Mathew and collaborators demonstrated that HSF2 acquires DNA-binding competence during proteasome inhibition (Mathew et al., 1998). Since the protein levels of HSF2 are crucial for its activity, it is not surprising to find context-dependent regulatory mechanisms that control HSF2 expression. On one hand, during heat shock HSF2 is ubiquitinated and targeted to proteasomal degradation by the E3 ubiquitin ligase anaphase/cyclosome protein complex, resulting in the clearance of HSF2 from the promoter of HSPA1A (Ahlskog et al., 2010). On the other hand, the expression of HSF2 in testes is regulated in a cell-type-specific manner by miR-18, which is a microRNA that targets the mRNA of HSF2 for degradation when it binds to its 3'-UTR (Björk et al., 2010).

2.3.3.1 Post-translational modifications of HSF2

Similarly to HSF1, HSF2 can also be modified by ubiquitination, sumoylation, and acetylation (de Thonel et al., 2020; Joutsen & Sistonen, 2019) (Figure 11). Although HSF2 is ubiquitinated by the E3 ubiquitin ligase anaphase/cyclosome protein complex, these ubiquitination sites have not been confirmed experimentally. Interestingly, two independent mass spectrometry data sets performed in human cells indicate that there are five ubiquitination sites in HSF2 (Kim et al., 2011; Wagner et al., 2011). HSF2 sumoylation was first described by Goodson and co-workers, who identified lysine 82 (K82) as a target for sumoylation. In this first publication, sumoylation was reported to

be required for HSF2 DNA-binding activity (Goodson et al., 2001). However, subsequent studies showed that the sumoylation of K82 inhibits the DNA-binding capability of HSF2, and this is the current view in the field (Anckar et al., 2006; Jaeger et al., 2016; Tateishi et al., 2009). Apart from K82, a proteome-wide analysis performed in human cells, revealed 20 sumoylation sites across the HSF2 DBD and HR-A/B, expanding the range of possible HSF2 modifications (Hendriks et al., 2017). It was also found that HSF2 can be acetylated in eight key lysine residues (K82, K128, K135, K197, K209, K210, K395, and K401), of which at least three (K128, K135, and K197) are acetylated by the acetyl transferases CBP and EP300 to inhibit HSF2's proteasomal degradation (de Thonel et al., 2022). Importantly, the simultaneous mutation of these three lysine residues to glutamines, which mimic HSF2 acetylation, decreases HSF2 poly-ubiquitination, suggesting a crosstalk between acetylation and ubiquitination (de Thonel et al., 2022).

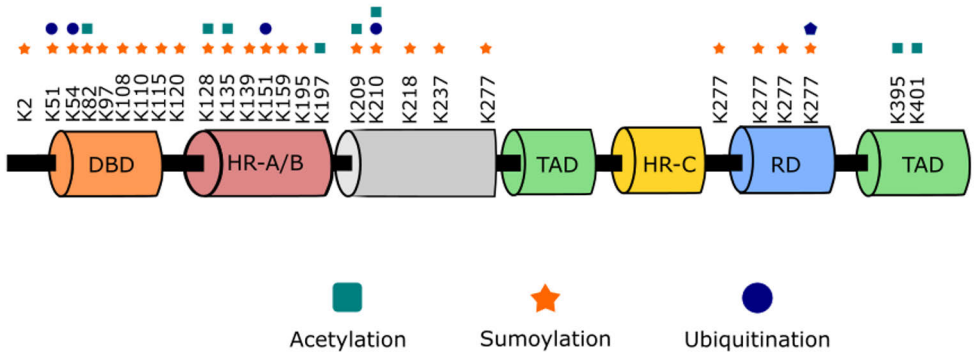

Figure 11. Schematic representation of human HSF2 post-translational modifications. HSF2 contains 24 sumoylation sites, of which the majority reside in the DNA-binding domain (DBD) and the oligomerization domains (HR-A/B). Additionally, five ubiquitination sites have been reported. The carboxy-terminal heptad repeat (HR-C), the transactivation domain (TAD), and the regulatory domain (RD) are also shown. Modified from Joutsen & Sistonen, 2019.

2.3.3.2 HSF2 in health and disease

Soon after its discovery, HSF2 was suggested to act as a developmental and differentiation factor. Sistonen and co-workers reported that the expression of HSF2 increased during hemin-induced erythroid differentiation of human K562 leukemia cells (Sistonen et al., 1992). Moreover, studies in mouse embryonal carcinoma cells, F9 cells, demonstrated that HSF2 constitutively binds to HSE sequences during early stages of mouse embryogenesis (Mezger et al., 1994). Contrary to the ubiquitous expression of HSF1, the expression of HSF2 was also observed to be specific for tissues and cell types (Fiorenza et al., 1995). However, the pivotal evidence that demonstrated the role of HSF2 in development came from the generation of *hsf2*$^{-/-}$ mice by three independent laboratories. Curiously, while two of these mouse models showed similar phenotypes (Kallio et al., 2002; Wang et al., 2003), the third mouse model did not report clear phenotypic changes (McMillan et al., 1998). These differences might be rooted in the different strategies used to generate the mouse models. The mouse models showing an HSF2-associated phenotype were characterized by brain abnormalities, embryonic lethality, reduced female fertility, and a remarkable reduction in testes size. After these physiological disparities were identified in *hsf2*$^{-/-}$ mice, the role of HSF2 has been extensively studied in brain development and spermatogenesis.

Spermatogenesis

Since soon after its discovery HSF2 was thought to be a differentiation factor, its expression pattern was studied in mouse spermatogenesis (Sarge et al., 1994). The process of mammalian spermatogenesis involves continuous waves of cell differentiation that included numerous cell divisions through mitosis and meiosis to finally produce haploid sperm (Kotaja, 2014). In this context, cell differentiation occurs in specialized structures called seminiferous tubules, which form part of the testes (Jan et al., 2012). The seminiferous tubules contain the following cell types in order of differentiation: spermatogonia stem cells, spermatocytes, post-meiotic round spermatids, and spermatozoa (Kotaja, 2014). Among these cell types, meiosis takes place in the

spermatocytes, and they are classified into the following types: preleptotene, leptotene, zygotene, pachytene, and diplotene spermatocytes (Jan et al., 2012). Originally, Sarge and collaborators observed that HSF2 is highly expressed in a stage-specific manner in the nuclei of pachytene spermatocytes and round spermatids, where it exhibits a constitutively DNA-binding state (Sarge et al., 1994). In agreement with these observations, the *hsf2*$^{-/-}$ mice show morphological abnormalities in seminiferous tubules and reduced amount of differentiating spermatids due to increased apoptosis of the pachytene spermatocytes (Kallio et al., 2002). Intriguingly, the interplay between HSF1 and HSF2 is vital for the process of spermatogenesis, since HSF1 and HSF2 double knockout mice are infertile since they exhibit stalling of spermatogenesis in the pachytene state and male infertility (Wang et al., 2004).

How does disruption of HSF2 affect spermatogenesis? To answer this question, Åkerfelt and co-workers performed high-resolution chromatin immunoprecipitation on microarray in mouse testes (Åkerfelt et al., 2008). They found that HSF2 directly occupies the Y chromosome, and lack of HSF2 impairs the expression of Y chromosome multicopy genes that are required for proper sperm morphology (Åkerfelt et al., 2008). The repertoire of HSF2-binding sites during spermatogenesis was recently expanded by Korfanty and co-workers, who performed ChIP-seq in isolated mouse spermatocytes. In this study, HSF2 was found to bind to 1282 sites on the chromatin including promoters, inter-genic, and intra-genic areas. Importantly, HSF1 was observed to co-occupy some areas of the chromatin with HSF2, suggesting that HSF1 and HSF2 cooperate during spermatogenesis (Korfanty et al., 2014). Interestingly, HSF1 and HSF2 interact in mouse testes by forming heterotrimers (Sandqvist et al., 2009).

Corticogenesis

During the second half of mouse gestation, the expression of HSF2 is predominant in the central nervous system, indicating strong HSF2 activity (Rallu et al., 1997). The *hsf2*$^{-/-}$ mouse model presents brain abnormalities, such as reduction of the hippocampus, enlargement of the lateral and third ventricles, and defective formation of the cerebral

cortex, i.e. corticogenesis (Chang et al., 2006; Kallio et al., 2002). During corticogenesis, the migration of neurons in the cerebral cortex is directed by two specific cell types: radial glia and Cajal-Retzius cells. Importantly, *hsf2*$^{-/-}$ mice display a reduced number of both cell types, which affects the signaling pathways governing neuron positioning. Moreover, lack of HSF2 also promotes impaired expression of p35 and p39, proteins that activate the CDK5, which in turn phosphorylates a wide variety of substrates involved in cell migration and cytoskeletal dynamics (Chang et al., 2006). Importantly, HSF2 is a direct transcriptional regulator of p35 during corticogenesis, and impaired binding of HSF2 to the promoter of p35 during fetal alcohol exposure leads to defective corticogenesis (Chang et al., 2006; El Fatimy et al., 2014).

Cancer

Although HSF1 has been widely studied in the context of cancer for approximately 15 years, the role of HSF2 in cancer was only recently characterized. Contrary to the HSF1-CaSig that is required for cancer cells to progress, HSF2 seems to play context-specific roles in different malignancies. HSF2 protein levels are downregulated in epithelial cancers, such as prostate and breast cancers, whereas low-grade gliomas, lung cancer tissues, and esophageal squamous cell carcinoma display high levels of HSF2 (Puustinen & Sistonen, 2020). Moreover, the molecular mechanism through which HSF2 is linked to cancer progression also varies among different cancer types. For example, in breast cancer, HSF2 cooperates with the transcription factor ZEB1 to regulate the expression of a cluster of microRNAs that, in turn, promote cancer cell migration and proliferation (Li et al., 2014). In hepatocellular cancer cells, HSF2 has been shown to alter metabolism through epigenetic regulation of gene expression. Interestingly, HSF2 interacts with the methyl transferase EHMT2 to epigenetically silence the gene encoding for the enzyme FBP1, which is a tumor suppressor gene that hinders cancer cell proliferation by inhibiting aerobic glycolysis (Yang et al., 2019). In prostate cancer, HSF2 functions as a tumor suppressor, where low levels of HSF2 correlate with poor prognosis and high Gleason score, a standard score for assessing cancer patient prognosis and treatment (Björk et al., 2016). Even though the molecular mechanism behind the tumor suppressive

role of HSF2 is not known, a gene expression profile in prostate cancer cells suggested that HSF2 regulates cell-cell adhesion, cytoskeletal dynamics, and extracellular matrix components (Björk et al., 2016). Interestingly, it has been shown that HSF2 cooperates with HSF1 across different types of cancer to regulate the expression of HSPs and non-canonical targets to support malignancy (Smith et al., 2022). Taken together, HSF2 has a context-dependent role in cancer progression, which might involve different gene expression signatures that are regulated in cooperation with HSF1.

Aims of the Study

When I joined Lea Sistonen's laboratory, the role of HSF2 during chronic proteotoxic stress conditions was poorly understood. Therefore, in the first study of this thesis work, we determined the gene expression profile associated with HSF2 upon prolonged treatments with the clinically approved proteasome inhibitor bortezomib (BTZ). In addition, the transcriptional programs of HSF1 and HSF2 under different stress conditions had not been compared before. Consequently, the second study of this thesis work compared HSF1- and HSF2-driven nascent transcriptional programs between oxidative stress and heat shock. Apart from its function in stress conditions, HSF2 has been shown to play important roles in developmental processes, such as spermatogenesis and corticogenesis, but the protein networks that interact with HSF2 in a tissue context had remained enigmatic. Thus, in the third study, we identified the HSF2 interactome in mouse testes, and characterized TLN1 as the first cell adhesion-related HSF2-interacting partner. Curiously, we found that HSF2 and TLN1 interacted predominantly in the nucleus, which prompted us, to investigate the nuclear localization of TLN1 in the fourth study.

The specific aims of this thesis were to:

- Elucidate the HSF2-dependent gene expression profile under prolonged proteotoxic stress
- Compare the HSF1- and HSF2- dependent transcriptional programs in oxidative stress and heat shock
- Determine the HSF2 interactome in mouse testes
- Characterize the function of the peripheral membrane protein talin1 (TLN1) in the nucleus

Experimental Procedures

The corresponding methods, cell lines, and antibodies used in this thesis can be found in the original publications (I-IV). Here an index is presented.

Table 3. Methods used in this thesis

Method	Study
Cell culture	I, II, III, IV
Cell viability assay with calcein and CellTiter-Glo	I
Chicken chorioallantonic membrane (CAM) assay	I
Chromatin immunoprecipitation sequencing (ChIP-seq)	IV
Co-immunoprecipitation	II
CRISPR-Cas9	I
Differential salt fractionation	III
3D organotypic cultures	I
Flow Cytometry	I
Immunoblotting	I, II, III, IV
LC-MS/MS	II
Plasmid construction	III
PRO-seq	IV
Proximity ligation assay	II
Quantitative RT-PCR (qRT-PCR)	I, III, IV
RNA-sequencing	I
Subcellular fractionations	I, III
Transient Transfections	I, III, IV

Table 4. Cell lines used in this thesis

Cell line	Type	Study
HS578T	Human breast carcinoma	III
MCF10A	Human breast epithelial	III
MDA-MB-231	Human breast carcinoma	III
MEFs WT	Mouse embryonic fibroblast	I, IV
MEFs HSF1 knockout	Mouse embryonic fibroblast	I, IV
MEFs HSF2 knockout	Mouse embryonic fibroblast	I, IV
PC-3	Human prostate carcinoma	II, III
RWPE-1	Human prostate epithelial	II
U2OS WT	Human osteosarcoma	I, II
U2OS HSF2 knockout	Human osteosarcoma	I, II

Table 5. Antibodies used in this thesis. ChIP-seq: chromatin immunoprecipitation sequencing, Co-IP: co-immunoprecipitation, IF: immunofluorescence, PLA: proximity ligation assay, WB: western blot.

Antigen	Antibody	Manufacturer	Application	Study
GAPDH	ab9485	Abcam	WB	I
GFP	ab1218, A-11122	Abcam, Thermo Scientific	PLA	II
H4	05-858	Millipore	WB	III
Hsc70	SPA-815	Stressgen	WB	III
HSF1	ADI-SPA-901, AB4	Stressgen, Thermo Scientific	ChIP-seq, WB, co-IP	I, III, IV
HSF2	HPA031455	Sigma-Aldrich	WB, IF	I
HSF2	3E2	Millipore	WB, co-IP	I, II, IV
HSF2	Östling et al., 2008	Sistonen's laboratory	ChIP-seq, WB, co-IP	II, IV
β_1 integrin	610468	BD Biosciences	WB	III
Lamin A/C	ab26300	Abcam	WB	III
Nucleolin	39-6400	Thermo Scientific	IF	III
PARP-1	sc-8007	Santa Cruz Biotechnology	WB	I
TLN1	T3287	Sigma-Aldrich	IF, WB, co-IP	II, III
TLN1	HPA004748	Sigma-Aldrich	IF	III
TLN1	ab78291	Sigma-Aldrich	IF, WB, co-IP	II, III
β-tubulin	T8328, ab6046	Sigma-Aldrich, Abcam	WB	I, IV
α-tubulin	AB 1157911	Hybridoma Bank	WB	III

Results and Discussion

1 HSF2 as a regulator of cell-cell adhesion: implications in the proteotoxic stress response (I)

While heat shock factor 1 (HSF1) is the master regulator of the protein quality-control machinery upon acute stress, the role of HSF2 during stress is not conclusively understood (Gomez-Pastor et al., 2018). Interestingly, HSF2 is required for the survival of cells exposed to prolonged heat shock within a febrile range (Shinkawa et al., 2011). Early experiments in the field of HSFs research have also shown that proteasome inhibition induced by different compounds, such as MG132 and Lactacystin, promotes HSF2 upregulationat the protein level and activates its DNA-binding capability (Kawazoe et al., 1998; Mathew et al., 1998). These observations suggest that HSF2 can respond to disruptions in cellular proteostasis depending on the duration and type of stress.

Under physiological conditions, most proteins are degraded by the 26S proteasome machinery, which recognizes ubiquitinated proteins (Budenholzer et al., 2017). Indeed, the function of the ubiquitin-proteasome system is so fundamental for maintaining cellular proteostasis that a great number of malignancies show high dependency on this system for their cell survival (Manasanch & Orlowski, 2017). Therefore, many proteasome inhibitors such as bortezomib (BTZ), have been generated for therapeutic purposes (Chen et al., 2017). BTZ is a dipeptide boronic acid derivative that partially inhibits the chymotrypsin-like activity of the proteasome, causing prolonged proteotoxic stress (Robak & Robak, 2019). Like other compounds that inhibit the proteasome, BTZ causes an increase in the protein and mRNA levels of HSF2 (Rossi et al., 2014). Upon BTZ treatment both HSF1 and HSF2 occupy the promoter region of different stress-responsive genes (e.g. HSPA), but only HSF1 is required for their expression during stress (Rossi et al., 2014). Moreover, lack of HSF2 has been associated with sensitivity to proteasome inhibition, but the molecular mechanism behind this phenomenon was not known (Lecomte et al., 2010; Rossi et al., 2014). Therefore, we determined the gene

expression profile associated with HSF2 upon prolonged proteotoxic stress caused by proteasomal inhibition with BTZ.

1.1 HSF2 is required for cell survival upon prolonged proteotoxic stress

We first determined the protein levels and subcellular localization of HSF2 in human osteosarcoma U2OS cells exposed to prolonged BTZ treatments. U2OS cells were treated with different concentrations of BTZ (0-100 nM) for either 6 h or 22 h, and the samples were analyzed by immunoblotting (Figure 1A in I). Our results showed that the protein levels of HSF2 increase in a dose and time-dependent manner. Indirect immunofluorescence and subcellular fractionations revealed that, during control conditions, HSF2 is predominantly nuclear in U2OS cells, and this pattern of localization is maintained upon BTZ treatment (Figure 1B and C in I). These results are in agreement with previous studies where HSF2 has been shown to respond in a similar way to proteasome inhibition (Kawazoe et al., 1998; Mathew et al., 1998; Rossi et al., 2014).

To study the role of HSF2 in prolonged proteotoxic stress, we engineered an HSF2 knockout U2OS cell line (referred as 2KO hereafter), by mutating the first exon of *hsf2* using the CRISPR-Cas9 genome editing system. Immunoblotting of 2KO cells showed that HSF2 was successfully abolished, while the levels of HSF1 remained unchanged (Figure 2A and Figure Supplement 1I in I). After validating the 2KO cells, we investigated their viability upon prolonged BTZ treatment. For this purpose, we examined the morphology of WT and 2KO cells upon BTZ treatment (0-50 nM) for 22h. At concentrations of 25 nM and 50 nM BTZ, 2KO cells showed a clear morphological change in comparison to WT cells, indicating cell death (Figure 2B in I). This observation was confirmed when the same experimental setup was used in a Calcein AM assay to quantify the number of living cells, and in a PARP-1 immunoblot, which was used to evaluate the accumulation of cleaved PARP-1 as an indicator of apoptosis (Figure 2C-D in I). To verify that our results are not restricted to BTZ treatment, we repeated these experiments using two HSP90 inhibitors (Geldanamycin and 17AAG), the amino acid analog L-Canavanine, and the proteasome inhibitor MG231 to induce proteotoxic

stress (Figure 2H-I and Figure Supplement 1D-H in I). Indeed, we found that 2KO cells were more sensitive to all the above-mentioned treatments in comparison to WT cells, showing that HSF2 is required for cell survival upon progressive accumulation of damaged proteins during extended periods of time.

We next confirmed that the reduced viability of 2KO cells was not due to Cas9-mediated off-target effects by evaluating the response of another HSF2 knockout U2OS cell line (2KO#2 hereafter) to BTZ treatment (Figure Supplement 1A in I). As expected, 2KO#2 cells recapitulated the accumulation of cleaved PARP-1 when compared to their WT counterparts upon BTZ treatment (Figure Supplement 1A in I). Furthermore, shRNA-mediated downregulation of HSF2 was sufficient to sensitize WT U2OS cells to prolonged BTZ treatment (Figure 2E-F in I), and re-introduction of HSF2 in 2KO cells resulted in significantly less cleavage of PARP-1 compared to Mock-transfected cells (Figure 2G in I). Since all the previously described experiments were conducted in U2OS cells, we also used mouse embryonic fibroblasts (MEFs) to examine whether our results were cell-type specific. MEFs showed BTZ-dependent HSF2 upregulation, indicating that HSF2 also responds to prolonged proteotoxic stress in these cell lines (Figure Supplement 1B in I). WT and *Hsf2*$^{-/-}$ MEFs were treated with BTZ and the accumulation of cleaved Caspase-3, a well-known marker for apoptosis, was examined with immunoblotting. Like 2KO and 2KO#2 cells, *Hsf2*$^{-/-}$ MEFs were more sensitive to BTZ treatments compared to WT MEFs (Figure Supplement 1B-C in I). Therefore, we concluded that our observations were not restricted to the intrinsic characteristics of a particular cell line.

Our findings highlight the importance of the type and duration of stress as determinant factors for the function of HSFs. Previous studies had characterized the role of HSF2 as cooperative and dispensable under acute heat shock conditions, since HSF1 and HSF2 co-localize to the same genomic sites and HSF1 is a more prominent *trans*-activator than HSF2 (Mahat et al., 2016; Östling et al., 2007; Vihervaara et al., 2013). However, HSF2 is required for cell survival under prolonged heat shock treatments in the febrile range of temperatures, indicating that the role of HSF2 is reserved for the accumulation of

misfolded proteins under milder stress conditions (Shinkawa et al., 2011). In this study, we show that HSF2 is indispensable for cell survival under prolonged treatments with proteotoxic agents such as proteasome inhibitors, amino acid analogs, and HSP90 inhibitors. Therefore, we expand the repertoire of stress conditions in which HSF2 is required for cell survival, which emphasizes the importance of this transcription factor in stress responses.

1.2 HSF2 regulates cell adhesion-associated genes

To determine the HSF2-dependent gene expression profile upon prolonged proteotoxic stress, we performed a whole genome transcriptome analysis with RNA-seq. Our RNA-seq setup was composed of WT and 2KO cells treated with 25 nM BTZ for 6 h or 10 h (Figure 3A in I). These conditions were sublethal as shown by bright field microscopy images of the cell morphology (Figure Supplement 2A in I). Furthermore, the protein levels of HSF1 and HSF2 were also verified by immunoblotting to confirm the quality of our samples and the efficacy of the BTZ treatment before performing the RNA-seq screen (Figure Supplement 2B in I). The differentially expressed genes were determined based on a fold change ≥ 3 and a false discovery rate < 0.001. Our analysis had four biological replicas that showed a high correlation according to Spearman's test (Figure Supplement 2C in I). Both WT and 2KO cells presented hundreds of genes upregulated and downregulated upon BTZ treatment, showing that a transcriptional program must be activated in response to BTZ-induced prolonged proteotoxic stress (Figure 3B in I).

The induction of HSPs is a fundamental survival mechanism upon proteotoxic stress, and HSF2 has been shown to regulate the induction of HSPs in an HSF1-dependent manner (Joutsen & Sistonen, 2019; Östling et al., 2007). Therefore, we examined the expression patterns of all human HSPs (Kampinga et al., 2009) in WT and 2KO cells. Surprisingly, the expression patterns of HSPs were extremely similar between both cell lines, with a few exceptions (HSPB2, DNAJC12, and DNAJC18) (Figure 3C in I). Since HSF2 also localizes to the promoters of HSP90 co-chaperones and polyubiquitin genes, we also examined the expression patterns of PTGES3 and AHSA1 (two HSP90

cochaperones) and UBB and UBC (two polyubiquitin genes) (Vihervaara et al., 2013). As in the case of the HSPs, the expression profiles of these genes were not significantly different (Figure 3D in I). In the light of these results, we conclude that 2KO cells are capable of triggering an HSR, but the induction of the HSR is not sufficient to protect these cells from prolonged proteotoxic stress.

Next, we investigated what other genes than HSR related were differentially expressed between WT and 2KO cells. The RNA-seq results identified hundreds of genes that were differentially expressed in 2KO cells compared to the WT cells, already under control conditions and during the BTZ treatments (Figure 4A-B in I). Surprisingly, when we performed a gene ontology (GO) term analysis of the differentially expressed genes in control conditions, cell adhesion and cell-cell adhesion *via* plasma membrane adhesion molecules were enriched terms. Similar GO terms were also observed among the different comparison pairs from our experimental setup (Figure 4A and C in I), revealing that the lack of HSF2 produces an abnormal expression of cell adhesion-associated genes in control and stress conditions. The gene set overlaps between our comparison pairs (Figure 4A in I) were analyzed by Venn diagrams to determine the adhesion molecules that were abnormally expressed in 2KO cells. A total of 114 and 227 genes were upregulated and downregulated, respectively (Figure 4D in I). These genes were then used as input for a functional cluster analysis performed by the DAVID analysis tool (Figure 4E in I). Interestingly, both upregulated and downregulated genes showed a strong association with cell adhesion. While the upregulated genes included collagens (COL16A1 and COL18A1) and laminins (LAMB1 and LAMA5), the downregulated genes mostly included members of the cadherin superfamily of cell-cell adhesion receptors, such as protocadherins, desmosomal cadherins, and Fat-Dachsous cadherins.

1.3 Disruption of HSF2 causes abnormal cadherin expression and impaired cell-cell adhesion

After identifying some members of the cadherin superfamily as HSF2-dependent genes, we investigated the expression profile of all cadherin superfamily members in 2KO cells.

Upon comparison of WT vs 2KO cells in control and BTZ treatment, we detected a prominent downregulation of at least one member of each cadherin subfamily in 2KO cells (Figure 5A in I). Interestingly, among the different cadherin subfamilies, clustered protocadherins showed the most drastic downregulation. To verify that the reduction of cadherin mRNA levels also affected the levels of these proteins, we determined the protein levels of classical cadherins (Pan-Cadherin), N-cadherin (CDH2), and clustered g-protocadherins (Pan-PCDHgA) by immunoblotting. Our results showed that the protein levels of the classical cadherins, specifically N-cadherin, and γ-protocadherins were significantly downregulated in control conditions (Figure 5B in I) and throughout BTZ treatment (Figure Supplement 4A in I). This result is very exciting because it uncovers the role of HSF2 as a key regulator of the cadherin superfamily of cell-cell adhesion receptors already in control conditions. Additionally, although different cadherin genes are affected by a wide variety of signals and transcription factors, a single transcription factor that affects the expression of at least one member from each cadherin subfamily has not been previously identified (Paulson et al., 2014).

To determine the functional impact of impaired cadherin expression in 2KO cells, we performed an aggregation assay. WT and 2KO cells were suspended in a cell aggregation buffer and allowed to form cell-cell contacts in the presence of $CaCl_2$ or the Ca^{2+}-chelating agent EDTA. Congruently with a deficient expression of cadherins, 2KO cells were unable to agglomerate in cell aggregates in the presence of Ca^{2+}, while WT cells formed large cell aggregates (Figure 5C in I). These results were recapitulated when WT and 2KO cells were grown in ultra-low attachment round bottom plates, 3D extracellular matrix (ECM), and the *in vivo* tumor growth with chicken chorioallantoic membrane (CAM) assay (Figure 5D-E and Figure Supplement S4D). Next, we explored the connection between impaired cell-cell adhesion and proteotoxic stress by re-introducing cadherins back into 2KO cells (Figure 6A in I). Since N-cadherin was the most prominently expressed cadherin superfamily member in WT U2OS cells according to our RNA-seq screen, this cadherin was chosen. After verifying the restoration of the N-cadherin protein levels, we also verified that the re-introduction of N-cadherin was

sufficient to restore the cell-cell adhesion properties of 2KO cells (Figure 6B in I). Excitingly, when 2KO cells transfected with N-cadherin were exposed to BTZ treatments, they exhibited less cleaved PARP-1 in comparison to their Mock counterparts (Figure 6C-E in I). These results demonstrate that impaired cell-cell adhesion is a factor that predisposes cells to sustained proteotoxic stress.

Future investigations are required to determine how HSF2 regulates the expression of different cadherins. The HSF2-dependent effect on the expression of clustered protocadherins is particularly puzzling since these cadherins exhibit a complex genomic architecture. The clustered protocadherin genes are composed of many promoters that control the expression of constant and variable exons to produce unique protocadherin variants (Hirayama & Yagi, 2017).

Indeed, one of the best-characterized regulators of the expression of protocadherins, is the zinc finger transcription factor CTCF. CTCF associates with the cohesin complex to form chromatin loops that bring enhancer sequences close to specific protocadherin promoters (Guo et al., 2015). Interestingly, a recent study showed that CTCF directly interacts with the DBD of HSF1 and co-localize with HSF1 in genomic loci (Burchfiel et al., 2021). Since HSF1 and HSF2 share high sequence similarity in their DBD, it is tempting to hypothesize that HSF2 could also interact with CTCF and control the expression of protocadherins through chromatin looping. In addition, ChIP-seq studies in mouse spermatocytes show that HSF2 occupies cadherin genes such as CDH15, CDH5, CDH18, CDH13, FAT1, PCDH9, PCDH17, and PCDHA1 under physiological conditions, suggesting that HSF2 could also regulate their expression directly (Korfanty et al., 2014).

In the light of these results, it is interesting to consider how the misregulation of cadherins could be linked to the *Hsf2*$^{-/-}$ mice phenotype. Members of the cadherin superfamily have been shown to affect neuronal migration (Chang et al., 2006; Hirano & Takeichi, 2012; Kallio et al., 2002), which could explain the brain abnormalities seen in the *Hsf2*$^{-/-}$ mice. The *Hsf2*$^{-/-}$ mice show drastic hippocampus reduction and

mispositioning of neurons in the cerebral cortex (Chang et al., 2006; Kallio et al., 2002). Interestingly, mice lacking N-cadherin and αN-catenin (an adaptor protein that sustains the activity of classical cadherins) also exhibit abnormal cortical architecture and defects in the formation of the hippocampus, respectively (Hirano & Takeichi, 2012). Therefore, the impaired expression of N-cadherin could be a factor of major contribution to the neuronal defects observed in *Hsf2*$^{-/-}$ mice. In support of this idea, a recent study showed that cells derived from patients suffering Rubinstein Taby syndrome, a genetic disorder that is characterized by intellectual disability, exhibit reduced levels of HSF2 and impaired expression of N-cadherin (de Thonel et al., 2022). Taken together, our results reveal that proper cell adhesion is vital under chronic proteotoxic stress and identify HSF2 as a prominent regulator of the cadherin superfamily members.

2 HSF1 and HSF2 as drivers of gene and enhancer expression under different stress conditions (II)

Cells under stress conditions modify their transcriptional programs to survive. Although stress conditions trigger global repression of transcription, selected transcription factors, for example HSFs, are activated to induce the expression of their specific target genes (Himanen & Sistonen, 2019). Previous studies have shown that the activity of HSFs is required for cell survival under different types of stress. However, the transcriptional programs controlled by HSFs in stress conditions, apart from heat shock, remain largely unexplored. Therefore, we investigated the genome-wide transcriptional profile of nascent RNA in WT, HSF1 knockout, and HSF2 knockout MEFs exposed to either heat shock or oxidative stress. Oxidative stress is caused by the abnormal accumulation of reactive oxygen species, which damage proteins, lipids, and nucleic acids by inducing their oxidation (Sies, 2015). Previous studies have shown that heat shock and oxidative stress induce the transcription of enhancers, which are distal regulatory elements that regulate gene expression through chromatin looping (Hou & Kraus, 2021; Nilson et al., 2017). Consequently, we investigated whether HSF1 and HSF2 impact enhancer transcription in these types of stress.

2.1 Oxidative stress and heat shock trigger different transcriptional programs

To investigate the transcriptional profile of nascent RNA under oxidative stress and heat shock, we performed precision run-on sequencing (PRO-seq) in WT, HSF1 knockout, and HSF2 knockout MEFs. PRO-seq was used, since it maps the distribution of transcriptionally active RNA polymerase II in a genome-wide scale with high resolution (Kwak et al., 2013). On one hand oxidative stress was caused by the synthetic quinone menadione (2-methyl-1,4-naphthoquinone), which generates superoxide (O_2^{-}) after its reduced form is oxidized by molecular oxygen (Klotz et al., 2014). On the other hand, heat shock was induced by incubating MEFs at 42 ◦C for 1 h. All samples were normalized using spike-ins, which showed a high correlation (rho > 0.95) among the biological replicas (Figure Supplement 3 in II). Our PRO-seq results revealed that

oxidative stress and heat shock caused pronounced changes in the transcription of genes and enhancers (Figure 1A in II). Curiously, in both types of stress, the downregulated genes were more abundant than the upregulated genes, and an opposite pattern of expression was observed for enhancers (Figure 1A in II). Moreover, we observed that oxidative stress and heat shock caused unique transcriptional changes, indicating that cells mount a stress-specific response upon these cytotoxic insults (Figure 1B in II).

Subsequently, we investigated the transcriptional mechanisms mediating the changes in gene expression under oxidative stress and heat shock. To this end, we analyzed the distribution of Pol II along differentially expressed genes and enhancers under both stress conditions (Figure 1C-E in II). Our analysis revealed that, in the same way as heat shock, oxidative stress triggered upregulation or a downregulation of genes by controlling the release of paused Pol II at the proximity of gene promoters (Figure 1C in II). However, the induction or downregulation of enhancers depended on the recruitment or depletion of Pol II, respectively, in the corresponding enhancer sequences (Figure Supplement 5A in II). These results show that oxidative stress and heat shock trigger transcriptional changes through the comparable transcriptional mechanisms.

Additionally, we examined in detail the position of Pol II within the genes activated by both types of stress. On average, the density of Pol II was higher at the beginning of gene bodies (0–2 kb from the transcription start site) under oxidative stress conditions compared to heat shock. On the contrary, Pol II reached more distal segments of genes under heat shock, exhibiting a more stable density throughout gene bodies (2–4 kb from transcription start site) (Figure 1D in II). Thus, we investigated whether Pol II advances towards the end of oxidative stress-induced genes, by calculating the fold change of engaged Pol II at the start (0.5–2.5 kb relative to transcription start site) and end (-2–0 kb relative to cleavage and polyadenylation site) of these genes. Congruently, oxidative stress only increased the levels of engaged Pol II at the start of the stress-induced genes, whereas upon heat shock the levels of engaged Pol II were increased at both locations (Figure 1E in II). These findings suggest that a substantial amount of the genes affected by oxidative stress present a hindrance in the elongation of Pol II. Since oxidative stress

has been shown to provoke DNA damage, which in turn is known to inhibit the elongation of Pol II (Oh et al., 2020), we measured DNA damage in our experimental conditions. To this end, we investigated the levels of phosphorylated histone H2AX, a well-known marker for DNA damage, with immunofluorescent staining (Rothkamm et al., 2015). Congruently, we found that menadione drastically increased the amount of phosphorylated H2AX as compared to heat shock or control conditions (Figure Supplement 6 in II).

2.2 HSF1 and HSF2 are involved in the oxidative stress response

The role of HSF1 and HSF2 in oxidative stress and the heat shock response was determined by comparing the PRO-seq result of WT MEFs to their HSF1 knockout or HSF2 knockout counterparts. Our analysis revealed that both types of stress induce the upregulation of hundreds of genes and enhancers in an HSF1- and/or HSF2- dependent manner (Figure 2A-B in II). Moreover, MEFs lacking HSF1 or HSF2 exhibited a disrupted transcriptional program when compared to the WT MEFs in the absence of stress (Figure 2C in II). To dissect which genes were directly regulated by HSF1 and HSF2, we performed a ChIP-seq with the same experimental setup as used for PRO-seq. HSF1 presented a strong stress-inducible binding to gene promoters and enhancers in oxidative stress and heat shock (Figure 2D in II). In contrast, HSF2 bound several targets already under control conditions, which has been observed in other cell lines (Murphy et al., 1994; Vihervaara et al., 2013). Interestingly, while the number of HSF2 direct targets did not increase upon heat shock, oxidative stress provoked a prominent binding of HSF2 to promoters and enhancers (Figure 2D in II). We also determined the number of genes and enhancers whose induction upon stress requires the binding of HSF1 or HSF2 to *cis*-acting elements in the genome. In both types of stress, HSF1 was a more prominent *trans*-activator than HSF2, since hundreds of genes and enhancers required HSF1 binding, while only a few targets depended on the binding of HSF2 (Figure 2E in II).

Previous studies have shown that HSF2 primarily acts in cooperation with HSF1 during acute heat shock, but whether HSF1 and HSF2 exhibit a functional interplay under

oxidative stress conditions was not known (Mahat et al., 2016; Östling et al., 2007). Therefore, we examined the proportion of HSF direct targets that were induced in an HSF1- or HSF2- dependent manner upon oxidative stress and heat shock. Our results revealed that in both stress conditions, a great majority of HSF targets were induced in an HSF1-dependent manner, and HSF2 colocalized to the same genomic sites as HSF1 (Figure 3A-C in II). Importantly, we found three genes and ten enhancers whose induction upon oxidative stress was HSF2-dependent, showing that HSF2 can also function as a stress-responsive transcription factor in this context (Figure 3A in II). Therefore, we conclude that similarly to heat shock, HSF2 mostly cooperates with HSF1 to drive the response to oxidative stress.

Since we observed that unique sets of genes and enhancers were regulated by HSF1 and HSF2 in heat shock vs oxidative stress, we asked whether both HSFs bound to stress-specific sites in the chromatin (Figure 3C and Figure Supplement 8 in II). Surprisingly, we found many genes that were occupied and induced by HSF1 and HSF2 only in response to oxidative stress, demonstrating that HSFs show a stress-dependent specificity (Figure 3D in II). Moreover, the HSF1 targets found in heat shock were also bound by HSF1 under oxidative stress, but most of them were not induced (Figure 3E in II). These results suggest that DNA-binding specificity is not the only mechanism regulating the transactivation capacity of HSF1 upon disruption of the redox state.

2.3 HSF1 and HSF2 regulate gene expression through enhancers

Since more than half of the HSF1-dependent genes were not regulated directly by promoter-bound HSF1, we investigated whether these HSF1 targets could be regulated by enhancers (Figure 3E in II). Interestingly, we found that a prominent proportion of these genes were located within 100 kb from enhancer sequences occupied by HSF1 (Figure 4A in II). In contrast, no correlation between HSF1-dependent genes and their distance with HSF1 direct enhancer targets was found under oxidative stress (Figure 4A in II). We also asked whether HSF1 alters different cellular processes through promoters and enhancers. A GO term analysis showed that HSF1 targets containing promoter-

bound HSF1 were related to protein folding and stress responses (Figure 4C-D in II). In contrast, the HSF1-dependent genes residing in the vicinity of direct HSF1 enhancer targets were strongly associated with focal adhesions and transmembrane receptor signaling pathways (Figure 4C-D in II).

Taken together, our study provides a detailed investigation of the transcriptional mechanisms behind the role of HSF1 and HSF2 in two types of cytotoxic stress i.e. oxidative stress and heat shock. We show that HSF1 and HSF2 regulate genes and enhancers under both types of stress. Interestingly, the HSF-dependent transcriptional programs vary depending on the type of stress, which shows, for the first time that HSF1 and HSF2 are multi-stress responsive factors. In the light of these results, it is important to ask how HSF1 and HSF2 find their target genes under different stress conditions. One possibility is that stress-specific protein-interacting partners guide HSF1 and HSF2 to their target genes. Another possibility is that the *trans*-activation capability of both HSFs is inhibited in certain genomic loci by either post-translational modifications or protein-protein interactions under a particular stress condition. Therefore, future studies are needed to determine the mechanisms dictating HSFs specificity.

3 Implications of studies I and II

Studies I and II investigated the role of HSF1 and HSF2 under different stress conditions. In study I we found that the HSF2-dependent regulation of cadherin superfamily genes is indispensable under chronic proteotoxic stress, while study II demonstrated that both HSF1 and HSF2 are multistress-responsive factors, since they drive the transcription of distinct genes and enhancers under oxidative stress and heat shock. Both studies corroborated, in a genome-wide scale, that HSF1 and HSF2 regulate gene expression already under control conditions, which is in line with the role of these transcription factors in development, metabolism, and cell cycle regulation (Joutsen & Sistonen, 2019; Roos-Mattjus & Sistonen, 2022). However, our ChIP-seq experiment in study II showed that HSF1 exhibits a strong stress-inducible binding to promoters and enhancers, whereas HSF2 binds to several promoters and enhancers already prior to stress. These results indicate that the HSF1-dependent genes under control conditions are predominantly regulated in an indirect manner. Curiously, oxidative stress, but not heat shock, induced a prominent binding of HSF2 to promoters and enhancers, which highlights the importance of stress type as a determinant of HSF2's activity. The findings of study I and II rise very important questions, such as: the identity of direct HSF2 targets under chronic proteotoxic stress and whether HSF1 and HSF2 regulate enhancer activation in other types of stress, development, and pathological states.

Future studies should determine the chromatin binding sites of HSF2 upon chronic proteotoxic stress and dissect what genes are direct HSF2 targets. Indeed, since the role of HSF2 under chronic proteotoxic stress is largely unexplored in a genome-wide scale, it is important to compare the HSF2 direct target genes upon proteasomal inhibition as well as treatments with amino acid analogs and chaperone inhibitors. A recent study showed that treatment with gambogic acid, a natural compound that has been proposed to inhibit HSP90, induces the heat shock response and disrupts the protein-protein interaction between HSP90 and HSF2 (Pesonen et al., 2021). Therefore, one can hypothesize that once HSF2 is released from its interaction with HSP90, it will translocate to the nucleus and bind to its target regions in the chromatin.

Another type of chronic stress that has been shown to activate HSF2 is exposure to ethanol (Drissi et al., 2021; El Fatimy et al., 2014). Exposure to ethanol during prenatal development, provokes the binding of HSF2, together with HSF1, to HSP promoters and also disrupts the binding of HSF2 to genes involved in radial neuronal migration (El Fatimy et al., 2014). Moreover, under sustained exposure to ethanol, adult mice lacking HSF2 are unable to trigger changes in synaptic transmission and plasticity in comparison to WT mice (Drissi et al., 2021). Consequently, investigating what genes are under direct regulation of HSF2 upon this type of chronic stress in a genome-wide scale is also an important subject to address in future studies. Indeed, impaired expression of cadherin genes could play a major role in the synaptic defects observed in *hsf2*$^{-/-}$ adult mice under prolonged exposure to ethanol (Drissi et al., 2021). For example, changes in activity and localization of N-cadherin, a gene whose expression has been shown to correlate with the protein levels of HSF2 independently from our study, impair synaptic plasticity processes (Tai et al., 2008; de Thonel et al., 2022). Therefore, it is tempting to speculate that the HSF2-dependent regulation of the cadherin superfamily genes is also involved in the neuronal stress response, which would represent another HSF2-mediated connection between adhesion and stress.

The regulation of enhancers by HSF1 and HSF2 is a groundbreaking finding that provides a new layer of complexity in our functional understanding of both HSFs. Interestingly, among the genes occupied by HSF1 and HSF2 under oxidative stress and heat shock conditions, the majority were co-occupied by these HSFs. This observation suggests that upon disruption of the redox state, HSF2 acts in cooperation with HSF1, which is in agreement with previous studies performed in heat shock and cancer (Mahat et al., 2016; Smith et al., 2022; Vihervaara et al., 2013). However, whether HSF2 could regulate gene expression through a specific set of enhancers under chronic stress or during development needs to be addressed in the future. Taken together, studies I and II expanded the repertoire of stress conditions in which HSF1 and HSF2 function, and unveiled the role of both HSFs in the regulation of cell adhesion and stress-associated enhancers.

4 HSF2 interacts with adhesion-related proteins including TLN1 (III)

HSF1 and HSF2 are versatile transcription factors that play a fundamental role in stress, development, and pathologies (Joutsen & Sistonen, 2019). However, despite years of research, little is known about the protein networks that interact with both transcription factors in different conditions. To fill this gap in knowledge, a recent study conducted by Burchfield and co-workers explored the HSF1 interactome in human cell lines during control conditions, acute proteotoxic stress (heat shock), and chronic proteotoxic stress (Huntington's disease) (Burchfiel et al., 2021). In contrast, only a few HSF2-interacting partners have been validated in the literature, among which HSF1 is the best characterized. HSF1 and HSF2 interact through their leucine zipper-like heptad repeats (HR-A/B) (Figure 8), to form heterotrimers that bind to DNA (Loison et al., 2006; Sandqvist et al., 2009). Indeed, ChIP-seq experiments in the context of stress, development, and cancer have revealed that HSF1 and HSF2 do co-localize in many genomic loci, showing a complex interplay between these transcription factors (Roos-Mattjus & Sistonen, 2022).

Among adult tissues, the levels of HSF2 are exceptionally high in testes, where the process of spermatogenesis occurs inside specialized structures known as seminiferous tubules (Fiorenza et al., 1995; Sarge et al., 1994). Congruently with the high protein levels of HSF2 in testes, the *Hsf2*$^{-/-}$ mice phenotype is characterized by reduced testes size, a disorganized structure of seminiferous tubules, pronounced apoptosis in spermatocytes, and defects in structure and number of spermatozoa (Åkerfelt et al., 2008; Kallio et al., 2002). Therefore, we investigated the HSF2 interactome in mouse testes, a tissue where high levels of HSF2 are required for proper organ development and spermatogenesis.

4.1 HSF2 interacts with cell adhesion-related proteins

HSF2-interacting partners were identified in mouse testes by performing co-immunoprecipitation (co-IP) coupled with liquid chromatography-tandem mass spectrometry (LC-MS/MS) (Figure 1A in III). Immunoblotting of the HSF2 co-IP

sample showed that HSF2 was efficiently enriched as compared to the IgG control and input (Figure 1B in III). Additionally, we corroborated that HSF1 co-precipitated with HSF2, since both proteins have been shown to interact in mouse testes (Sandqvist et al., 2009). After verifying the quality of the co-IP samples, LC-MS/MS analysis was carried out and 464 HSF2-interacting partners were identified (Figure 1C in III). Since 306 of the HSF2-interacting partners were also found in the IgG negative control, we established a cut-off criterion by selecting proteins that exhibited at least two peptide spectrum matches (PSMs) and a ratio of HSF2 PSMs/IgG PSMs > 3. These criteria led to the identification of 105 HSF2-specific partners.

Among the HSF2-interacting partners that met our cut-off criteria, we found proteins involved in biological processes that are disrupted in the absence of HSF2. For example, *hsf2*$^{-/-}$ mice produce spermatozoa with aberrant morphology, and our screen identified two proteins involved in sperm morphogenesis, i.e. MAP7, and NPHP1, as HSF2-interacting partners (Åkerfelt et al., 2008). Mice lacking HSF2 also show a defective axis between the homologous chromosomes of spermatocytes in the pachytene stage of meiosis (Kallio et al., 2002). Interestingly, the HSF2-interactome identified the synaptonemal complex protein 1 (SYCP1), which is fundamental for proper synapsis and recombination of homologous chromosomes during meiosis (de Vries et al., 2005). Therefore, it is tempting to hypothesize that, in addition to changes in gene expression, HSF2 could play an important role in spermatogenesis by promoting or inhibiting the function of its protein-interacting partners.

To gain functional insight into the 105 HSF2-interacting partners, we performed a gene ontology (GO) term analysis (Figure 1D in III). We found that the most enriched GO term within the molecular function ontology was cell adhesion molecule binding. This is particularly interesting because lack of HSF2 has been shown to impair the expression of cell adhesion-related genes, such as cadherin, integrins, and ECM proteins (Björk et al., 2016; Study I) (Table 6).

Table 6. HSF2 regulates the expression of cell adhesion-related genes in human cells. Representative examples of cell adhesion-related genes that are differentially expressed upon decreased HSF2 levels (Björk et al., 2016; Study I).

	ID	Gene Name
Joutsen et al., (2020)	CDH6	Cadherin 6
	CDHR1	Cadherin-Related Family Member 1
	CELSR1	Cadherin Family Member 9
	DSC2	Desmocollin 2
	IGFN1	EEF1A2-Binding Protein 1
	FAT2	FAT Atypical Cadherin 2
	PCDHA7	Protocadherin Alpha 7
	PCDHA10	Protocadherin Alpha 10
	PCDHB4	Protocadherin Beta 4
	PCDHGA7	Protocadherin Gamma Subfamily A, 7
	PCDHGB4	Protocadherin Gamma Subfamily B, 4
	PCDHGC5	Protocadherin Gamma Subfamily C, 5
	PCDH15	Protocadherin Related 15
Björk et al., (2020)	COL13A1	Collagen Type XIII Alpha 1 Chain
	FAT1	FAT Atypical Cadherin 1
	LGALS3	Galectin 3
	ITGA1	Integrin Subunit Alpha 1
	ITGA5	Integrin Subunit Alpha 5
	ITGB2	Integrin Subunit Beta 2
	MCAM	Melanoma Cell Adhesion Molecule
	CDH2	N-Cadherin

Additionally, we also interrogated an HSF2 ChIP-seq dataset from mouse spermatocytes to elucidate whether HSF2 binds to adhesion-related genes (Korfanty et al 2014). Interestingly, we found that HSF2 binds to a wide variety of adhesion-related gene families in spermatocytes, including catenins, protocadherins, cadherins, integrins, claudins, and ADAMSs (Figure 12). In the light of our findings, we studied HSF2-interacting partners related to cell adhesion and we found several adaptor proteins that connect the actin cytoskeleton with transmembrane adhesion receptors. These adaptor proteins were zonula occludens 1 and 2 (ZO1 and ZO2), catenin delta 1 (CTNND1), and

talin1 (TLN1), of which we chose to focus on TLN1 due to its important role in cell-matrix adhesion (Gough & Goult, 2018) (Figure 1E in III).

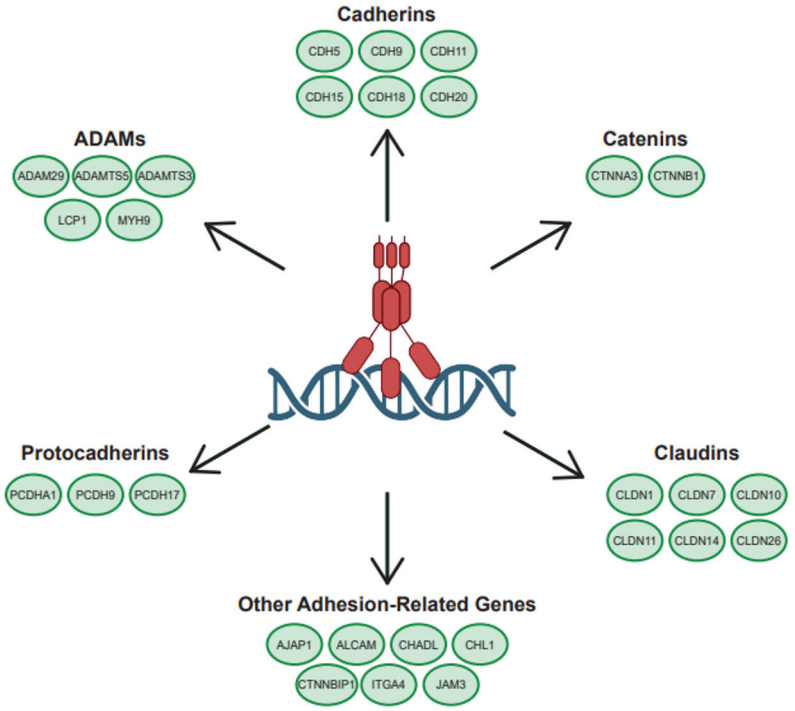

Figure 12. HSF2 occupies genes related to cell adhesion in spermatocytes. Graphical representation of adhesion-related genes whose genomic loci are occupied by HSF2 in mouse spermatocytes (Korfanty et al., 2014).

4.2 HSF2 and TLN1 interact in mouse and human cells

TLN1 is an important adaptor protein in the focal adhesion complexes, where it connects integrin transmembrane receptors to the actin cytoskeleton (Gough & Goult, 2018). We first validated the HSF2-TLN1 interaction in mouse teratocarcinoma F9 cells, where HSF2 is highly abundant and constitutively active (Murphy et al., 1994) (Figure 2A in in III). Once the HSF2-TLN1 interaction was validated in mouse cells, we investigated whether the interaction also occurs in human cell lines, including RWPE-1 (prostate

epithelial), and PC-3 (prostate carcinoma). To this end, we immunoprecipitated HSF2 and performed immunoblotting with antibodies specific for TLN1 and HSF1 (as a positive control). Additionally, we also performed the reciprocal experiment, where TLN1 was immunoprecipitated and the presence of HSF2 and HSF1 was monitored with immunoblotting. Our results revealed that HSF2 and TLN1 interact in both human cell lines, whereas HSF1 did not interact with TLN1 (Figure 2B in III). This finding suggests that the HSF2 molecules that bind to TLN1 are different from HSF2-HSF1 heterotrimers, and also highlights that hetero- and homooligomers of HSF2 exhibit distinct properties.

To complement our biochemical data, we performed immunofluorescent labeling and a proximity ligation assay (PLA). The immunofluorescence labeling revealed that while HSF2 is predominantly nuclear, TLN1 resides in the focal adhesions (FA) near the periphery of the plasma membrane (Figure 2C in III). Moreover, TLN1 also showed a modest nuclear localization, which is in supported by our findings in study IV. Both proteins showed a clear cytoplasmic localization. In addition, the PLA assay indicated that HSF2 and TLN1 are in close proximity (≤40 nm) to each other, implying that both proteins are found in the same complex (Figure 2D in III). To determine the subcellular localization of the HSF2-TLN1 interaction we performed an orthogonal projection of our PLA assay images (Figure 2E in III). Interestingly, we noticed that the majority of the PLA signal was detected in the nucleus, suggesting that HSF2 and TLN1 predominantly interact in this subcellular compartment (Figure 2F in III).

4.3 The C-terminus of HSF2 interacts directly with TLN1

Since HSF1 was not found to interact with TLN1, we examined the similarities and differences between HSF1 and HSF2. These HSFs share similar domains in common, including a DNA binding domain (DBD), an oligomerization domain containing hydrophobic-leucine-zipper-like heptad repeats (HR-A/B), a C-terminal heptad repeat domain (HR-C), regulatory domains (RD), and transactivation domains (AD) (Figure 3A in III). However, their amino acid sequences are considerably different, because beyond the DBD these HSFs share only approximately 35% identity (Roos-Mattjus & Sistonen,

2022). Therefore, we compared the amino acid sequences of HSF1 and HSF2 to determine HSF2-specific sequences that might bind to TLN1 (Figure 3B in III). A sequence alignment of HSF1 and HSF2 in *Homo sapiens*, *Mus musculus*, *Bos taurus*, *Sus scrofa, Gallus gallus,* and *Danio rerio* unveiled that the C-terminus of HSF2 contains the longest conserved HSF2-unique sequence.

Next, we searched for a TLN1-binding motif in the C-terminus of HSF2. TLN1 functions as an adaptor protein that interacts with a wide variety of interacting partners, and therefore specific TLN1-binding motifs have been well described (Gough et al., 2021). Among the best-characterized TLN1-binding motif is the LD motif, a leucine-rich sequence following the consensus LDXLLXXL (Tumbarello et al., 2002). Multiple sequence analyses between the HSF2-specific sequence and the LD motifs of DLC1, RIAM, PXN, KANK1, and KANK2, revealed that the C-terminus of HSF2 indeed contains the distribution of amino acids that corresponds to this type of TLN1-binding motif (Figure 3C in III). Interestingly, we also noticed that all of these TLN1-interacting partners bind to the rod domain of TLN1 in specific subdomains (Figure 3D in III). TLN1 is a 270 kDa adaptor protein composed of an N-terminal head domain with four subdomains (F0-F3), a flexible linker, a C-terminal rod domain with 13 alpha-helical bundles (R1-R13), and a dimerization domain (DD) (Gough & Goult, 2018). Detailed structural work on the interaction between the Rho GAP protein DLC1 and TLN1 has given a mechanistic understanding of how proteins containing an LD domain interact with TLN1 (Zacharchenko et al., 2016). The LD motif of DLC1 forms a helix that docks in between the second and third helices of the R8 helical bundle in the TLN1 rod domain. This type of binding mechanism is known as helix addition, and it requires the presence of key hydrophobic residues in the LD motif (Zacharchenko et al., 2016). Based on the TLN1/DLC1 interaction, the binding of other LD motif-containing proteins, such as the focal adhesion adaptor proteins KANK1, KANK2, and Pax, has been predicted and validated (Bouchet et al., 2016; Zacharchenko et al., 2016). Moreover, the TLN1-binding site of RIAM, a Rap1-GTP interacting protein that activates integrins through TLN1, contains a similar distribution of hydrophobic amino acids as the LD motif. Interestingly,

RIAM binds to the R8 helical bundle of the TLN1 rod domain *via* the same helix addition mechanism as DLC1 and PXN, showing that this specific arrangement of hydrophobic amino acids is indeed recognized by the helical bundles of TLN1 (Lee et al., 2009; (Zacharchenko et al., 2016). Prompted by this finding, we investigated whether the HSF2-specific sequence binds directly to TLN1. To determine if HSF2 and TLN1 interact directly, we performed a fluorescent polarization assay with the LD motif in the HSF2 C-terminal domain and three different regions of TLN1 (R4-R8, R9-R12, R13-DD), using the LD motif of KANK1 as a positive control (Bouchet et al., 2016). Our results showed that the C-terminal domain of HSF2 interacts directly with the folded R4-R8 and R9-R12 regions of TLN1, indicating that HSF2 binds to multiple sites in TLN1 (Figure 3E in III).

The binding of HSF2 to the R4-R8 region of TLN1 is particularly interesting because the unfolding of the R8 domain directly depends on the unfolding of R7 (Yao et al., 2016). Consequently, HSF2 could bind to the folded TLN1 at the FA, and upon stretching the HSF2-TLN1 interaction could be disrupted when a specific threshold of strength is reached. Moreover, HSF2 could be recruited to the plasma membrane by TLN1 as is the case of other TLN1-interacting partners containing LD motifs, such as DLC1, KANK1 and PXN (Li et al., 2011; Zacharchenko et al., 2016; Bouchet et al., 2016). It is also important to consider that our mass spectrometry screen showed that, apart from TLN1, HSF2 interacts with ZO1, ZO2, CTNND1, desmoplakin, and plakoglobin, which are proteins that belong to major cell adhesion protein complexes in the vicinity of the plasma membrane. Firstly, ZO1 and ZO2 belong to the tight junctions, which connect the actin cytoskeleton with the cell-cell adhesion receptors claudins, occludin, and JAMs (Zihni et al., 2016). Secondly, CTNND1 is an important component of the adherens junctions, which connect the actin cytoskeleton with classical cadherins (Oda & Takeichi, 2011). Lastly, desmoplakin and plakoglobin are adaptor proteins that connect desmosomal cadherin with the intermediate filaments network (Garrod & Chidgey, 2008). These results suggest that HSF2 could act as an adhesion surveillance factor in the periphery of the plasma membrane, and upon appropriate stimuli, e.g.

mechanical cues, HSF2 would translocate to the nucleus and regulate the expression of adhesion-related genes (Figure 13).

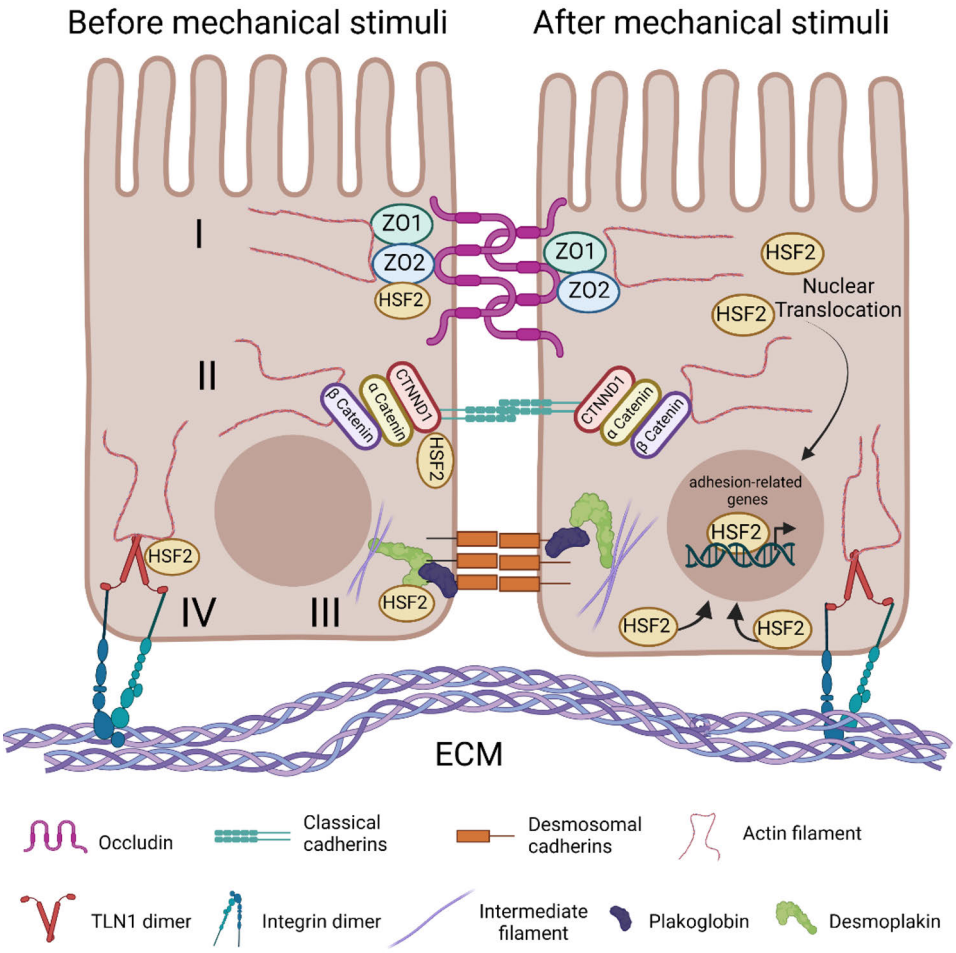

Figure 13. Schematic model of how HSF2 could act as an adhesion surveillance factor. Before mechanical stimuli, HSF2 interacts with adaptor/peripheral membrane proteins in major cell adhesion complexes, including tight junctions (I), adherens junctions (II), desmosomes (III), and focal adhesion (IV). Upon mechanical stimuli, produced by changes in cell-cell or cell-matrix adhesion, HSF2 is released from its interacting partners and translocates to the nucleus to regulate the expression of adhesion-related genes.

5 Nuclear TLN1 as a regulator of gene expression (IV)

Accumulating evidence shows that proteins involved in cell-cell and cell-matrix adhesion are important signaling hubs that transmit signals from the plasma membrane to the nucleus (Zheng & Jiang, 2022). In a recent publication, Byron and co-workers described a subset of adhesion-related proteins that reside in the nucleus, which they named as the nucleo-adhesome, but their function is still unclear (Byron et al., 2022). Therefore, investigating the role of adhesion-related protein in the nucleus is fundamental to know how cells can respond to their environment.

TLN1 is an important mechanosensing protein that connects the integrin adhesion receptors to the actin cytoskeleton in the focal adhesion (FA) protein complexes (Gough & Goult, 2018). Due to the important role of TLN1 in cell-matrix adhesion, diseases such as cancer, cardiovascular malfunction, and hematologic disorders are characterized by dysregulation of the protein levels and function of TLN1 (Azizi et al., 2021; Haining et al., 2016; Y. Li et al., 2021). Curiously, apart from localizing to the FAs, TLN1 is also present in the invadopodia and cytoplasm. In the invadopodia, TLN1 acts as a scaffold to recruit the sodium/hydrogen exchanger 1 protein, whereas in the cytoplasm TLN1 is in an autoinhibited conformational state that is incapable of binding integrins and its function remains unclear (Beaty et al., 2014; Goult et al., 2013; Haage et al., 2018). When we investigated the subcellular localization of TLN1, we were surprised to find TLN1 residing in the nucleus where it interacts with chromatin and regulates gene expression.

5.1 TLN1 resides in the nucleus and interacts strongly with the chromatin

We first examined the cellular component GO terms associated with TLN1-interacting partners that were recently identified by Gough and co-workers (Figure 1A, right panel in IV) (Gough et al., 2021). To discard low-confidence TLN1-interacting partners, we only selected proteins that had a SAINT score ≥ 0.7 for our GO term analysis. Interestingly, among the 72 TLN1-interacting partners that met our cut-off criteria, 37

were nuclear proteins (Figure 1B, right panel in IV). In the light of this result, we performed subcellular fractionations in human non-transformed (MCF10A) and transformed (HS578T, MDA-MB-231, PC3) cells, to determine whether TLN1 exists in the nucleus. The purity of the subcellular fractions was verified by monitoring the enrichment of proteins that primarily reside in one of the following locations: plasma membrane (β1 integrin), cytoplasm (α tubulin), nucleus (lamin A/C), and chromatin (histone H4) (Figure 1C in IV) (Abdrabou et al., 2020; Alanko et al., 2015; Herrmann et al., 2017). Congruently with the localization of the TLN1-interacting partners, the subcellular fractionations revealed that TLN1 was in the nuclear and chromatin fractions of all the cell lines that were tested. Since our chromatin fraction was obtained by treating the final fractionation pellet with micrococcal nucleases to release all proteins associated with DNA, we also determined the strength of the TLN1-chromatin interaction. To this end, we treated the final pellet with a salt gradient of NaCl (0.3, 0.45, 0.6, 0.8, and 1.2 M) to release proteins bound to DNA. With this gradient, proteins weakly bound to DNA (e.g. transcription factors) are soluble in low concentrations of NaCl, while proteins tightly bound to the chromatin (e.g. histones) are displaced with high NaCl concentrations (Herrmann et al., 2017). Interestingly, in MCF10A and MDA-MB-231 cells, TLN1 co-eluted with histone H4 at the highest concentrations of NaCl, whereas in HS578T cells, TLN1 co-eluted with lamin A/C throughout the NaCl gradient (Figure 1D in IV). These results show that TLN1 resides in the nucleus of human cells, where it strongly binds to the chromatin.

5.2 TLN1 concentrates in specific areas within the nucleus

The subnuclear distribution of TLN1 was examined with indirect immunofluorescence staining in HS578T and MDA-MB-231 cells. To circumvent challenges with low antibody specificity, we used three different TLN1 antibodies for our immunofluorescence staining. One of these antibodies recognizes the head domain of TLN1, while the other two recognize the rod domain (Figure 2A in IV). In accordance with the literature, TLN1 could be observed in the FA, at the bottom plane of the cells. However, when we visualized the middle plane of the cell, we noticed a clear nuclear

localization of TLN1 (Figure 2C-E in IV). Curiously, a subpopulation of cells showed a strong foci pattern inside the nucleus. These foci co-localized with the dark areas of the DAPI staining and the nucleolar marker nucleolin (NLC), indicating that TLN1 accumulates in the nucleoli of these cells (Figure 2E in IV) (Jia et al., 2017). These results are in line with our mass spectrometry data analysis, which identified 14 nucleolar proteins as TLN1-interacting partners (Figure 1B, left panel in IV).

5.3 Nuclear TLN1 regulates gene expression

The nuclear localization, strong chromatin interaction, and nucleolar accumulation of TLN1 prompted us to ask whether nuclear TLN1 regulates gene expression. We performed an RNA-seq from HS578T cells transfected with either two small interfering RNAs (siRNA) specific for TLN1 (siTLN1), or a scramble RNA (Scr) as the corresponding negative control (Figure 3A in IV). Since immunoblotting of the siTLN1 transfected cells revealed a prominent reduction of TLN1 protein levels as compared to the Scr control, we investigated the global gene expression profile of these cells (Figure 3A in IV). Depletion of TLN1 caused extensive changes in the gene expression profile of HS578T cells, resulting in the upregulation of 318 genes and the downregulation of 419 genes (Figure 3C in IV). The top 25 upregulated and downregulated differentially expressed genes were used to generate heatmaps from the normalized data (Figure 3D in IV). Due to the fundamental role of TLN1 in cell adhesion, we also explored whether its depletion altered the expression of cell adhesion genes, and we found several examples of such cases (Figure 3E in IV). Moreover, we investigated whether TLN1 depletion altered the expression of proteins with nuclear functions. Interestingly, we identified those encoding nuclear structural proteins (NEMP1, H2BC4), chromatin remodelers (BCL7B, MORF4L1), and transcription factors (NFATC2) (Figure 3F in IV). These results show, for the first time, that there is a gene expression profile associated with TLN1 downregulation.

Since downregulation of TLN1 is likely to affect gene expression *via* loss of FAs, we investigated whether five of the TLN1-dependent genes i.e. SEMA7A, NFATC2,

ACTG1, BCL7B, and SEC23A, changed their expression upon fluctuations in the levels of nuclear TLN1 specifically. To modulate the levels of nuclear TLN1, we constructed a fusion protein consisting of the full-length human TLN1 coupled with GFP and a nuclear localization signal (TLN1-NLS). Confocal microscopy revealed that the TLN1-NLS construct was confined in the nucleus, whereas the corresponding negative control GFP was dispersed in the whole cell (Figure 4A in IV). Once the subcellular localization of the TLN1-NLS and GFP was verified, we measured the mRNA levels of the five TLN1-dependent genes with qPCR (Figure 4B in IV). In accordance with our RNA-seq results, increasing the protein levels of nuclear TLN1 changed the expression of SEMA7A, NFATC2, and ACTG1, in an opposite pattern to that observed upon TLN1-depletion (Figures 3D and 4B in IV). In contrast, the mRNA levels of BCL7B and SEC23A remained unchanged upon the increase of nuclear TLN1, showing that not all TLN1-dependent genes change their expression patterns in function of nuclear TLN1 (Figure 4B in IV). Taken together, these results serve as proof-of-concept to demonstrate the impact of nuclear TLN1 on gene expression.

Our findings raise several questions. For instance, what is the mechanism mediating TLN1 nuclear localization? Nuclear import is usually mediated by nuclear pore complexes that maintain a semipermeable channel through the nuclear envelope (Wente & Rout, 2010). Cargoes smaller than ~40 kDa can diffuse passively through the nuclear pores, whereas bigger cargoes require energy-dependent transport (Terry et al., 2007). Due to the high molecular weight of TLN1 (270 kDa), it is reasonable to infer that active transport is required for its nuclear translocation. However, the capability of the TLN1 to bind phosphatidylinositol-4,5-bisphosphate through its head domain suggests that a phosphoinositide-dependent pathway may also mediate the nuclear localization of the full length TLN1 (Ye et al., 2016). Such a pathway has been previously described for myosin-1C, and it requires the binding of myosin-1C to phospholipids (Nevzorov et al., 2018). Therefore, these possible mechanisms of TLN1 nuclear translocation warrant further investigation.

Another important question is how nuclear TLN1 modulates gene expression. Previous studies have shown that nuclear actin and nuclear myosin-1C, which were initially classified as cytoplasmic proteins, alter chromatin landscape and also cooperate to maintain active RNA polymerase II at gene promoters (Almuzzaini et al., 2015; Klages-Mundt et al., 2018). Our results revealed that TLN1 is tightly associated with the chromatin of transformed and non-transformed human cells (Figure 1C in IV), suggesting that it could function in a similar manner as nuclear actin and/or nuclear myosin-1C. Following this line of reasoning, it is important to consider how nuclear TLN1 can access the chromatin. One possibility is that certain interacting partners mediate the association of TLN1 and the chromatin, since we found many nucleic acids-binding proteins among the TLN1-interacting partners identified by Gough and collaborators (Gough et al., 2021). Another exciting possibility is that TLN1 would bind DNA by electrostatic interactions through its phosphoinositide-binding surfaces, as it has been suggested for myosin-1C (De Lanerolle et al., 2005). Moreover, the presence of TLN1 in the nucleolus opens a new avenue for future studies to investigate the role of TLN1 in gene expression. At this point, it is tempting to speculate that TLN1 plays a role in the processing of rRNA molecules, since several proteins that are involved in this task are found among the nucleolar-associated TLN1-interacting partners. For example, we found proteins that are required for synthesis (e.g. POLR2E, POLR2H, and POLR1C) and maturation (e.g. NIP7 and NOP16) of the polycistronic rRNA precursors (Boisvert et al., 2007; Tafforeau et al., 2013).

Finally, it is important to determine whether nuclear TLN1 responds to mechanical stimuli. A wealth of evidence has shown that a specialized protein complex, known as the linker of nucleoskeleton and cytoskeleton (LINC), transmits mechanical stimuli from the extracellular space to the nucleus (Jahed & Mofrad, 2019). To achieve its function, the LINC complex connects proteins in the inner periphery of the nuclear envelope to the contractile cytoskeleton (Khilan et al., 2021; Miroshnikova et al., 2019). Considering that the 13 α-helical bundles in the rod domain of TLN1 unfold upon mechanical force, it is plausible that nuclear TLN1 is associated with the LINC complex to serve as a

mechanosensitive signaling hub. In support of this view, our mass spectrometry data analysis revealed that TLN1 interacts with nine proteins associated with the nuclear envelope, of which the protein emerin mediates changes in nuclear stiffness upon stimulation of the LINC complex (Janota et al., 2020).

6 Implications of studies III and IV

The study III of this thesis work identified the interactome of HSF2 in a physiologically relevant context and characterized TLN1 as the first adhesion-related HSF2-interacting partner. Since HSF2 and TLN1 were found to interact predominantly in the nucleus, the study IV investigated the nuclear localization and function of TLN1. Our data expands the canonical view of TLN1's subcellular localization and function, which raises several questions: Do HSF2 and TLN1 bind to chromatin as a protein complex? Indeed, HSF2 could mediate the localization of TLN1 at specific genomic loci or *vice-versa*. Future studies should map the chromatin occupancy of HSF2 and TLN1 and test whether the absence of either protein alters the chromatin-binding profile of the other.

Another important subject to be determined is the conformation in which HSF2 and TLN1 interact with each other. Both HSF2 and TLN1 can exist in either an active or an autoinhibited conformation (Gough & Goult, 2018; Joutsen & Sistonen, 2019). Monomeric and/or dimeric HSF2 can be found in an autoinhibited conformation in which its leucine zipper-like heptad repeats, HR-A/B and HR-C, interact intramolecularly. Upon activation, the HR-A/B domain of HSF2 is released from its interaction with the HR-C, allowing HSF2 to oligomerize, translocate to the nucleus, and acquire DNA-binding capacity (Roos-Mattjus & Sistonen, 2022). Additionally, TLN1 exists in an extended conformation, where it binds simultaneously to integrins and the actin cytoskeleton through its head and rod domains, respectively, or an autoinhibited conformation, where dimeric TLN1 forms a so-called donut-shape-structure through the interaction of the head domain with the rod domain (Dedden et al., 2019). Curiously, it has been shown that the autoinhibited form of TLN1 can also interact with the head domain of vinculin, suggesting that this form of TLN1 may also interact with other

proteins and play a role in signal transduction (Dedden et al., 2019). Considering that the HSF2-TLN1 interaction is predominantly nuclear, it is plausible that HSF2 would interact with TLN1 as an oligomer. However, it is important to investigate the conformation of nuclear TLN1 and analyze the structure of the HSF2-TLN1 complex.

The active conformation of TLN1 acts as a mechanosensitive protein that undergoes force-dependent conformational changes in its rod domain (Yao et al., 2016). The rod domain of TLN1 is composed by 13 helical bundles that can stretch and reveal binding sites for TLN1-itneracting partners (Gough & Goult, 2018). Interestingly, our fluorescent polarization assay, showed that the last 16 amino acids of HSF2 bind to two different regions of the TLN1 rod domain, i.e. R4-R8 and R9-R12. This result suggests that force-dependent unfolding of specific TLN1 helical bundles, is not required for the HSF2-TLN1 interaction to take place. However, it is also possible that HFS2 binds to the areas of TLN1 that are buried inside the 13 helical bundles. Taking this idea forward, forthcoming studies should address whether TLN1 can sense mechanical stimuli in the nucleus in a similar manner as it does in the vicinity of the plasma membrane. Could the chromatin-associated TLN1 change conformation and alter the chromatin structure upon mechanical stimuli? Indeed, accumulating evidence shows that the chromatin undergoes extensive remodeling upon mechanical ques, but the mechanisms behind this phenomenon are not yet well understood (Miroshnikova & Wickström, 2022). Taken together, the findings of study III and IV unveil a plethora of new perspectives for the structure, subcellular localization, and function of HSF2 and TLN1.

Concluding Remarks

Among the members of the vertebrate HSF family, HSF1 has been considered as the master regulator of the proteotoxic stress response. Indeed, before this work, an HSF2-dependent gene expression profile under stress conditions was not known. In the first study of this thesis, we identified a set of genes that are regulated by HSF2 upon prolonged proteotoxic stress. On one hand, our groundbreaking results unveiled that HSF2 is a prominent regulator of the cadherin superfamily cell-cell adhesion receptors. On the other hand, we showed that impaired cell-cell adhesion sensitizes cells to prolonged proteotoxic stress. These results open several questions, such as how HSF2 affects gene expression upon prolonged proteotoxic stress and whether HSF2 affects the same set of genes as when proteotoxic stress is caused by chaperone inhibition, proteasome inhibition, and/or exposure to amino acid analogs.

The second study of this thesis work addressed whether HSF1 and HSF2 regulate stress-specific transcriptional programs. To this end, we used oxidative stress and heat shock as distinct stress conditions. We found that these HSFs act as multistress-responsive factors, which reprogram transcription in a stress-specific manner. Moreover, our results revealed that HSF1 and HSF2 regulate gene expression under stress conditions through the induction of enhancers. These results invite us to ask whether the HSFs-mediated regulation of enhancers applies beyond the context of stress.

The third study focused on elucidating the HSF2-interactome in mouse testes, a tissue where HSF2 is required for proper sperm development. Before this work, no studies on the HSF2-interactome had been conducted in the relevant context of tissues. Interestingly, we found that adhesion-related proteins were the most enriched type of HSF2-interacting partners. We also characterized the interaction between HSF2 and the mechanosensitive protein TLN1 in murine and human cell lines. Since many of the HSF2-interacting partners were part of major adhesion complexes at the plasma membrane, our results open exciting possibilities about the function of HSF2. For example, a population of HSF2 in the vicinity of the plasma membrane could respond to

mechanical stimuli, by translocating to the nucleus to regulate cell adhesion-related genes.

Active communication between the plasma membrane and the nucleus is partly mediated by the nuclear translocation of adhesion proteins. Indeed, recent studies have shown that proteins that were initially considered to be strictly cytoplasmic also reside in the nucleus. Since we found that HSF2 interacts with TLN1 predominantly in the nucleus, we investigated the subcellular localization of TLN1 in the fourth study of this thesis. To our surprise, TLN1 indeed is present in the nucleus, where it binds strongly to the chromatin and accumulates in the nucleolus. Moreover, our results demonstrated that changes in the levels of nuclear TLN1 regulate gene expression, which represents a seminal finding. It is for future studies to determine the mechanism mediating TLN1-dependent changes in gene expression and whether HSF2 forms part of such a mechanism.

Taken together, HSFs are versatile transcription factors that operate in a context-dependent manner to orchestrate specific transcriptional programs under stress conditions, development, and disease. Notably, the studies presented in this thesis work not only demonstrated the multifaceted functions of HSFs in different types of stress, but also revealed a prominent connection between HSFs and cell adhesion. This nexus between HSFs and cell adhesion is particularly interesting because dysregulation of HSFs has been previously linked with developmental abnormalities and cancer cell invasion and metastasis. Therefore, the functional impact of HSFs in cell adhesion during development and disease is an exciting subject for future studies.

Acknowledgments

First, I want to thank God, the most important person in my life, for everything. Specially for giving me the gift of doing research in Finland and the opportunity of studying the beauty of life in a cellular level. The work presented in this thesis was conducted in the Faculty of Science and Engineering, Cell Biology, Åbo Akademi University and the Turku Centre for Biotechnology (CBT), University of Turku and Åbo Akademi University. I want to thank John Eriksson, Cecilia Sahlgren, and Annika Meinander for their work as heads of the Cell Biology department. Additionally, I would like to ask all the group leaders in our department particularly John Eriksson, Annika Meinander, Cecilia Sahlgren, Diana Toivola, Kid Törnquist, Malin Åkerfelt and Guillaume Jacquemet and all their past and present group members. Also, the technical staff, especially Thomas Bymark, Gunilla Henriksson, Sten Lindholm, Melissa Haga, and Jari Korhonen are acknowledged for their invaluable assistance in the scientific everyday life. Thank you, Markku Saari, Jouko Sandholm, Jari Korhonen and Pasi Kankanpää for assisting and teaching me how to acquire images. Thank you, Fredrik Karlsson, for helping with the official details regarding my PhD studies and the defense.

I would like to express my deepest gratitude to Lea Sistonen and Eva Henriksson for going beyond the duties of supervising my PhD studies. Lea, thank you for giving me the opportunity to join your group first as a Master's student and then as a PhD candidate. Throughout these years I have always been inspired by your unique ability to have faith (i.e. the realization of what is hoped for and evidence of things not seen) in the midst of uncertainty, your care, your strong dedication and passion for excellence, and your support and help in science and outside science. Eva, thank you for being my first practical supervisor in Åbo Akademi and my PhD thesis co-supervisor, you have always been there to guide me, brainstorm with me, read my drafts, listen to my presentations, and help me in matters outside the lab. I have always admired your heart and how well you take care of those under your supervision.

Thank you, Pieta Mattila and Emilia Peuhu for reviewing my thesis. I deeply appreciate your insightful comments both for my thesis work and manuscripts in preparation!

Professors Nora Kotaja, Ville Hietakangas and Johanna Ivaska are acknowledged for being in my thesis advisory committee and for guiding me during the early phases of this thesis work.

I would like to thank my collaborators for making this work possible and tackling the challenges of research together with me. Aurélie de Thonel, Ben Goult, Délara Sabéran-Djoneidi, Guillaume Jackmet, Hendrik Hästbacka, Jean-Paul Concordet, Jens Luoto, Jenny Joutsen, Leena Laitala, Leila Coelho-Rato, Marek Budzynski, Mikael Puustinen, Samu Himanen, Anniina Virhervaara, Susumu Imanishi, Valérie Mezger, Jenny Pessa,

and Anna Serafia Nylund. Additionally, especial thanks to Pia Roos-Mattjus for her comments and scientific insights along this journey!

Thank you JJ and Marek for your mentorship inside and outside the lab since the beginning of this journey. Thank you, Marek, Jens, Diosangeles, Michael, Leila, Hendrik, Samu for great times inside and outside the lab having lunches, playing games, biking, training calisthenics beyond muscle failure, and many more things. Thank you Hendrik, for always being there to teach me new technology hacks, have great conversations, and always being so willing to help. Thank you JP and Ingrid for your sparks of joy in the lab and your great help in the everyday lab life. Thank you Mikael for your insights about practical life matters in science, finances, and beyond. Thank you Jens for always keeping people together and inviting others to share in the BC community! Thank you Alia for sharing the friendship of a sister with me, for all your support and care. Thank you Arun for always being willing to help inside and outside science! Thank you Anna for high fives in the corridor and always helping everyone around!

I would also like to thank all my friends and family outside science, who also remind me how important is to live life fully in all its dimensions. I want to thank my mother and my father for their deep unconditional love, support, guidance and all the great sacrifices they did to raise and educate me well, I love you. I deeply thank my grandmother Esperanza for her great love, example, wisdom, and her positive influence in my life, together with all my uncles and cousins. I also want to thank all the Catholic community in Finland for being my family in Christ, specially: Fr. Peter, Fr. Stan, all the sisters of St. Birgit in Turku, all my very good friends from the youth group (definitely I can call you my brothers and sisters), and all the families in our parish and in the Stella Maris community. I want to thank specially Kai and Mikaela for your great friendship, example, and guidance in this journey and beyond, thank you for being there for me as family, what I have learned from you and the time we have spent together is unvaluable. Thank you Kalin for your prayers and support in the last steps of this marathon, they made a great difference. Science will never be able to share friendship, love, faith and joy as you all do with me, thank you!

This work has been funded by Turku Doctoral Network in Molecular Biosciences (MolBio), Finnish Cultural Foundation, Åbo Akademi Research Foundation, Otto A. Malm Foundation, Magnus Ehrnrooth Foundation, Mediciniska Understödföreningen Liv och Hälsa, and K. Albin Johansson´s Foundation. I am extremely grateful for all the funding, which simply has made this work possible.

References

& Delwart, E. M. M. E. S. R. (1982). Regulation of heat-shock genes: a DNA sequence upstream of Drosophila hsp70 genes is essential for their induction in monkey cells. *The EMBO Journal*, *1*(10), 1279–1285. https://doi.org/10.1002/j.1460-2075.1982.tb00025.x

Abdrabou, A., Brandwein, D., & Wang, Z. (2020). Differential subcellular distribution and translocation of seven 14-3-3 isoforms in response to EGF and during the cell cycle. *International Journal of Molecular Sciences*, *21*(1), 1–24. https://doi.org/10.3390/ijms21010318

Ahlskog, J. K., Björk, J. K., Elsing, A. N., Aspelin, C., Kallio, M., Roos-Mattjus, P., & Sistonen, L. (2010). Anaphase-Promoting Complex/Cyclosome Participates in the Acute Response to Protein-Damaging Stress. *Molecular and Cellular Biology*, *30*(24), 5608–5620. https://doi.org/10.1128/mcb.01506-09

Åkerfelt, M., Henriksson, E., Laiho, A., Vihervaara, A., Rautoma, K., Kotaja, N., & Sistonen, L. (2008). Promoter ChIP-chip analysis in mouse testis reveals Y chromosome occupancy by HSF2. *Proceedings of the National Academy of Sciences of the United States of America*, *105*(32), 11224–11229. https://doi.org/10.1073/pnas.0800620105

Åkerfelt, M., Morimoto, R. I., & Sistonen, L. (2010). Heat shock factors: integrators of cell stress, development and lifespan. *Nature Reviews Molecular Cell Biology*, *11*(8), 545–555. https://doi.org/10.1038/nrm2938

Alanko, J., Mai, A., Jacquemet, G., Schauer, K., Kaukonen, R., Saari, M., Goud, B., & Ivaska, J. (2015). Integrin endosomal signalling suppresses anoikis. *Nature Cell Biology*, *17*(11), 1412–1421. https://doi.org/10.1038/ncb3250

Almuzzaini, B., Sarshad, A. A., Farrants, A. K. Ö., & Percipalle, P. (2015). Nuclear myosin 1 contributes to a chromatin landscape compatible with RNA polymerase II transcription activation. *BMC Biology*, *13*(1), 1–15. https://doi.org/10.1186/s12915-015-0147-z

Amin, J., Ananthan, J., & Voellmy, R. (1988). *Key Features of Heat Shock Regulatory Elements*. *8*(9), 3761–3769. https://doi.org/https://doi.org/10.1128/mcb.8.9.3761-3769.1989

Anand, D., Agrawal, S. A., Slavotinek, A., & Lachke, S. A. (2018). Mutation update of transcription factor genes FOXE3 , HSF4 , MAF , and PITX3 causing cataracts and other developmental ocular defects. *Human Mutation*, *39*(4), 471–494. https://doi.org/10.1002/humu.23395

Anckar, J., Hietakangas, V., Denessiouk, K., Thiele, D. J., Johnson, M. S., & Sistonen, L. (2006). Inhibition of DNA Binding by Differential Sumoylation of Heat Shock Factors. *Molecular and Cellular Biology*, *26*(3), 955–964. https://doi.org/10.1128/mcb.26.3.955-964.2006

Anckar, J., & Sistonen, L. (2011). Regulation of H SF 1 Function in the Heat Stress Response: Implications in Aging and Disease . *Annual Review of Biochemistry*, *80*(1), 1089–1115. https://doi.org/10.1146/annurev-biochem-060809-095203

Angst, B. D., Marcozzi, C., & Magee, A. I. (2001). The cadherin superfamily: diversity in form and function. *Journal of Cell Science*, *114*(4), 629–641. https://doi.org/10.1242/jcs.114.4.629

Arndt, V., Dick, N., Tawo, R., Dreiseidler, M., Wenzel, D., Hesse, M., Fürst, D. O., Saftig, P., Saint, R., Fleischmann, B. K., Hoch, M., & Höhfeld, J. (2010). Chaperone-Assisted Selective Autophagy Is Essential for Muscle Maintenance. *Current Biology*, *20*(2), 143–148. https://doi.org/10.1016/j.cub.2009.11.022

Azizi, L., Cowell, A. R., Mykuliak, V. V., Goult, B. T., Turkki, P., & Hytönen, V. P. (2021). Cancer associated talin point mutations disorganise cell adhesion and migration. *Scientific Reports*, *11*(1), 1–16. https://doi.org/10.1038/s41598-020-77911-4

Balchin, D., Hayer-Hartl, M., & Hartl, F. U. (2016). In vivo aspects of protein folding and quality control. *Science*, *353*(6294). https://doi.org/10.1126/science.aac4354

Barna, J., Csermely, P., & Vellai, T. (2018). Roles of heat shock factor 1 beyond the heat shock response. *Cellular and Molecular Life Sciences*, *75*(16), 2897–2916. https://doi.org/10.1007/s00018-018-2836-6

Bate, N., Gingras, A. R., Bachir, A., Horwitz, R., Ye, F., Patel, B., Goult, B. T., & Critchley, D. R. (2012). Talin contains a C-terminal calpain2 cleavage site important in focal adhesion dynamics. *PLoS ONE*, *7*(4). https://doi.org/10.1371/journal.pone.0034461

Beaty, B. T., Wang, Y., Bravo-Cordero, J. J., Sharma, V. P., Miskolci, V., Hodgson, L., & Condeelis, J. (2014). Talin regulates moesin-NHE-1 recruitment to invadopodia and promotes mammary tumor metastasis. *Journal of Cell Biology*, *205*(5), 737–751. https://doi.org/10.1083/jcb.201312046

Berika, M., & Garrod, D. (2014). Desmosomal adhesion in vivo. *Cell Communication and Adhesion*, *21*(1), 65–75. https://doi.org/10.3109/15419061.2013.876018

Beyer, E. C., & Berthoud, V. M. (2018). Gap junction gene and protein families: Connexins, innexins, and pannexins. *Biochimica et Biophysica Acta (BBA) - Biomembranes*, *1860*(1), 5–8. https://doi.org/10.1016/j.bbamem.2017.05.016

Bierkamp, C., Luxey, M., Metchat, A., Audouard, C., Dumollard, R., & Christians, E. (2010). Lack of maternal Heat Shock Factor 1 results in multiple cellular and developmental defects, including mitochondrial damage and altered redox homeostasis, and leads to reduced survival of mammalian oocytes and embryos. *Developmental Biology*, *339*(2), 338–353. https://doi.org/10.1016/j.ydbio.2009.12.037

Björk, J. K., Åkerfelt, M., Joutsen, J., Puustinen, M. C., Cheng, F., Sistonen, L., & Nees, M. (2016). Heat-shock factor 2 is a suppressor of prostate cancer invasion. *Oncogene*, *35*(14), 1770–1784. https://doi.org/10.1038/onc.2015.241

Björk, J. K., Sandqvist, A., Elsing, A. N., Kotaja, N., & Sistonen, L. (2010). miR-18, a member of Oncomir-1, targets heat shock transcription factor 2 in spermatogenesis. *Development*, *137*(19), 3177–3184. https://doi.org/10.1242/dev.050955

Boisvert, F. M., Van Koningsbruggen, S., Navascués, J., & Lamond, A. I. (2007). The multifunctional nucleolus. In *Nature Reviews Molecular Cell Biology*. https://doi.org/10.1038/nrm2184

Bouchet, B. P., Gough, R. E., Ammon, Y., van de Willige, D., Post, H., Jacquemet, G., Altelaar, A. M., Heck, A. J., Goult, B. T., & Akhmanova, A. (2016). Talin-KANK1 interaction controls the recruitment of cortical microtubule stabilizing complexes to focal adhesions. *ELife*, *5*, 1–23. https://doi.org/10.7554/eLife.18124

Brasch, J., Harrison, O. J., Honig, B., & Shapiro, L. (2012). Thinking outside the cell: How cadherins drive adhesion. *Trends in Cell Biology*, *22*(6), 299–310. https://doi.org/10.1016/j.tcb.2012.03.004

Brown, P. J., & Juliano, R. L. (1985). Selective inhibition of fibronectin-mediated cell adhesion by monoclonal antibodies to a cell-surface glycoprotein. *Science*, *228*(4706), 1448–1451. https://doi.org/10.1126/science.4012302

Brunquell, J., Morris, S., Lu, Y., Cheng, F., & Westerheide, S. D. (2016). The genome-wide role of HSF-1 in the regulation of gene expression in Caenorhabditis elegans. *BMC Genomics*, *17*(1), 1–18. https://doi.org/10.1186/s12864-016-2837-5

Bu, L., Jin, Y., Shi, Y., Chu, R., Ban, A., Eiberg, H., Andres, L., Zheng, G., Qian, M., Cui, B., Xia, Y., Liu, J., Hu, L., Zhao, G., Hayden, M. R., & Kong, X. (2002). *Mutant DNA-binding domain of HSF4 is associated with autosomal dominant lamellar and Marner cataract*. *31*(4), 276–278. https://doi.org/10.1038/ng921

Budenholzer, L., Cheng, C. L., Li, Y., & Hochstrasser, M. (2017). Proteasome Structure and Assembly. *Journal of Molecular Biology*, *429*(22), 3500–3524. https://doi.org/10.1016/j.jmb.2017.05.027

Budzyński, M. A., Puustinen, M. C., Joutsen, J., & Sistonen, L. (2015). Uncoupling Stress-Inducible Phosphorylation of Heat Shock Factor 1 from Its Activation. *Molecular and Cellular Biology*, *35*(14), 2530–2540. https://doi.org/10.1128/mcb.00816-14

Burchfiel, E. T., Vihervaara, A., Guertin, M. J., Gomez-Pastor, R., & Thiele, D. J. (2021). Comparative interactomes of HSF1 in stress and disease reveal a role for CTCF in HSF1-mediated gene regulation. *Journal of Biological Chemistry*, *296*(34), 100097. https://doi.org/10.1074/jbc.RA120.015452

Byron, A., Griffith, B. G. C., Herrero, A., Loftus, A. E. P., Emma, S., Dawson, J. C., Kogerman, L., Mcgivern, N., Culley, J., & Graeme, R. (2021). *Characterisation of a nucleo-adhesome*. 1–28.

Canzio, D., & Maniatis, T. (2019). The generation of a protocadherin cell-surface recognition code for neural circuit assembly. *Current Opinion in Neurobiology*, *59*(November), 213–220. https://doi.org/10.1016/j.conb.2019.10.001

Cao, Z., Zhu, Y., Liu, L., Wu, S., Liu, B., Zhuang, J., Tong, Y., Chen, X., Xie, Y., Nie, K., Lu, C., Ma, X., & Yang, J. (2018). Novel mutations in HSF4 cause congenital cataracts in Chinese families. *BMC Medical Genetics*, *19*(1), 1–8. https://doi.org/10.1186/s12881-018-0636-3

Case, L. B., & Waterman, C. M. (2015). Integration of actin dynamics and cell adhesion by a three-dimensional, mechanosensitive molecular clutch. *Nature Cell Biology*, *17*(8), 955–963. https://doi.org/10.1038/ncb3191

Chalmel, F., Lardenois, A., Evrard, B., Mathieu, R., Feig, C., Demougin, P., Gattiker, A., Schulze, W., Jégou, B., Kirchhoff, C., & Primig, M. (2012). Global human tissue profiling and protein network analysis reveals distinct levels of transcriptional germline-specificity and identifies target genes for male infertility. *Human Reproduction*, *27*(11), 3233–3248. https://doi.org/10.1093/humrep/des301

Chang, Y., Östling, P., Åkerfelt, M., Trouillet, D., Rallu, M., Gitton, Y., El Fatimy, R., Fardeau, V., Le Crom, S., Morange, M., Sistonen, L., & Mezger, V. (2006). Role of heat-shock factor 2 in cerebral cortex formation and as a regulator of p35 expression. *Genes and Development*, *20*(7), 836–847. https://doi.org/10.1101/gad.366906

Chatterjee, S., & Burns, T. F. (2017). Targeting heat shock proteins in cancer: A promising therapeutic approach. *International Journal of Molecular Sciences*, *18*(9). https://doi.org/10.3390/ijms18091978

Chen, C., Manso, A. M., & Ross, R. S. (2019). Talin and Kindlin as Integrin-Activating Proteins: Focus on the Heart. *Pediatric Cardiology*, *40*(7), 1401–1409. https://doi.org/10.1007/s00246-019-02167-3

Chen, W. V., & Maniatis, T. (2013). Clustered protocadherins. *Development (Cambridge)*, *140*(16), 3297–3302. https://doi.org/10.1242/dev.090621

Chen, W. V., Nwakeze, C. L., Denny, C. A., O'Keeffe, S., Rieger, M. A., Mountoufaris, G., Kirner, A., Dougherty, J. D., Hen, R., Wu, Q., & Maniatis, T. (2017). Pcdhαc2 is required for axonal tiling and assembly of serotonergic circuitries in mice. *Science*, *356*(6336), 406–411. https://doi.org/10.1126/science.aal3231

Chen, Y., Zhang, Y., & Guo, X. (2017). Proteasome dysregulation in human cancer: implications for clinical therapies. *Cancer and Metastasis Reviews*, *36*(4), 703–716. https://doi.org/10.1007/s10555-017-9704-y

Christians, E., Davis, A. A., Thomas, S. D., & Benjamin, I. J. (2000). Maternal effect of Hsf1 on reproductive success. *Nature*, *407*(6805), 693–694. https://doi.org/10.1038/35037669

Collier, M. P., & Benesch, J. L. P. (2020). Small heat-shock proteins and their role in mechanical stress. *Cell Stress and Chaperones*, *25*(4), 601–613. https://doi.org/10.1007/s12192-020-01095-z

Cooper, J., & Giancotti, F. G. (2019). Integrin Signaling in Cancer: Mechanotransduction, Stemness, Epithelial Plasticity, and Therapeutic Resistance. *Cancer Cell*, *35*(3), 347–367. https://doi.org/10.1016/j.ccell.2019.01.007

Corey, L. L., Weirich, C. S., Benjamin, I. J., & Kingston, R. E. (2003). Localized recruitment of a chromatin-remodeling activity by an activator in vivo drives transcriptional elongation. *Genes and Development*, *17*(11), 1392–1401. https://doi.org/10.1101/gad.1071803

Cui, X., Wang, L., Zhang, J., Du, R., Liao, S., Li, D., Li, C., Ke, T., Li, D. W. C., Huang, H., Yin, Z., Tang, Z., & Liu, M. (2013). HSF4 regulates DLAD expression and promotes lens de-nucleation. *Biochimica et Biophysica Acta - Molecular Basis of Disease*, *1832*(8), 1167–1172. https://doi.org/10.1016/j.bbadis.2013.03.007

D. Westerheide, S., Raynes, R., Powell, C., Xue, B., & N. Uversky, V. (2012). HSF Transcription Factor Family, Heat Shock Response, and Protein Intrinsic Disorder. *Current Protein & Peptide Science*, *13*(1), 86–103. https://doi.org/10.2174/138920312799277956

Dai, S., Tang, Z., Cao, J., Zhou, W., Li, H., Sampson, S., & Dai, C. (2015). Suppression of the HSF1-mediated proteotoxic stress response by the metabolic stress sensor AMPK. *The EMBO Journal*, *34*(3), 275–293. https://doi.org/10.15252/embj.201489062

De Lanerolle, P., Johnson, T., & Hofmann, W. A. (2005). Actin and myosin I in the nucleus: What next? *Nature Structural and Molecular Biology*, *12*(9), 742–746. https://doi.org/10.1038/nsmb983

de Thonel, A., Ahlskog, J. K., Daupin, K., Dubreuil, V., Berthelet, J., Chaput, C., Pires, G., Leonetti, C., Abane, R., Barris, L. C., Leray, I., Aalto, A. L., Naceri, S., Cordonnier, M., Benasolo, C., Sanial, M., Duchateau, A., Vihervaara, A., Puustinen, M. C., … Mezger, V. (2022). CBP-HSF2 structural and functional interplay in Rubinstein-Taybi neurodevelopmental disorder. *Nature Communications*, *13*(1), 7002. https://doi.org/10.1038/s41467-022-34476-2

de Vries, F. A. T., de Boer, E., van den Bosch, M., Baarends, W. M., Ooms, M., Yuan, L., Liu, J., van Zeeland, A. A., Heyting, C., & Pastink, A. (2005). Mouse Sycp1 functions in synaptonemal complex assembly, meiotic recombination, and XY body formation. *Genes & Development*, *19*(11), 1376–1389. https://doi.org/10.1101/gad.329705

Dedden, D., Schumacher, S., Kelley, C. F., Zacharias, M., Biertümpfel, C., Fässler, R., & Mizuno, N. (2019). The Architecture of Talin1 Reveals an Autoinhibition Mechanism. *Cell*, *179*(1), 120-131.e13. https://doi.org/10.1016/j.cell.2019.08.034

Dong, B., Jaeger, A. M., & Thiele, D. J. (2019). Inhibiting Heat Shock Factor 1 in Cancer: A Unique Therapeutic Opportunity. *Trends in Pharmacological Sciences*, *40*(12), 986–1005. https://doi.org/10.1016/j.tips.2019.10.008

Dongre, A., & Weinberg, R. A. (2019). New insights into the mechanisms of epithelial–mesenchymal transition and implications for cancer. *Nature Reviews Molecular Cell Biology*, *20*(2), 69–84. https://doi.org/10.1038/s41580-018-0080-4

Drissi, I., Deschamps, C., Alary, R., Robert, A., Dubreuil, V., Le Mouël, A., Mohammed, M., Sabéran-Djoneidi, D., Mezger, V., Naassila, M., & Pierrefiche, O. (2021). Role of heat shock transcription factor 2 in the NMDA-dependent neuroplasticity induced by chronic ethanol intake in mouse hippocampus. *Addiction Biology*, *26*(2), 1–13. https://doi.org/10.1111/adb.12939

El Fatimy, R., Miozzo, F., Mouël, A., Abane, R., Schwendimann, L., Sabéran-Djoneidi, D., Thonel, A., Massaoudi, I., Paslaru, L., Hashimoto-Torii, K., Christians, E., Rakic, P., Gressens, P., & Mezger, V. (2014). Heat shock factor 2 is a stress-responsive mediator of neuronal migration defects in models of fetal alcohol syndrome. *EMBO Molecular Medicine*, *6*(8), 1043–1061. https://doi.org/10.15252/emmm.201303311

Elbediwy, A., & Thompson, B. J. (2018). Evolution of mechanotransduction via YAP/TAZ in animal epithelia. *Current Opinion in Cell Biology*, *51*(February), 117–123. https://doi.org/10.1016/j.ceb.2018.02.003

Engler, A. J., Sen, S., Sweeney, H. L., & Discher, D. E. (2006). Matrix Elasticity Directs Stem Cell Lineage Specification. *Cell*, *126*(4), 677–689. https://doi.org/10.1016/j.cell.2006.06.044

FARQUHAR, M. G., & PALADE, G. E. (1963). Junctional complexes in various epithelia. *The Journal of Cell Biology*, *17*, 375–412. https://doi.org/10.1083/jcb.17.2.375

Fawcett, T. W., Sylvester, S. L., Sarge, K. D., Morimoto, R. I., & Holbrook, N. J. (1994). Effects of neurohormonal stress and aging on the activation of mammalian heat shock factor 1. *Journal of Biological Chemistry*, *269*(51), 32272–32278.

Fiorenza, M. T., Farkas, T., Dissing, M., Kolding, D., & Zimarino, V. (1995). Complex expression of murine heat shock transcription factors. *Nucleic Acids Research*, *23*(3), 467–474. https://doi.org/10.1093/nar/23.3.467

Franco, S. J., Rodgers, M. A., Perrin, B. J., Han, J., Bennin, D. A., Critchley, D. R., & Huttenlocher, A. (2004). Calpain-mediated proteolysis of talin regulates adhesion dynamics. *Nature Cell Biology*, *6*(10), 977–983. https://doi.org/10.1038/ncb1175

Frantz, C., Stewart, K. M., & Weaver, V. M. (2010). The extracellular matrix at a glance. *Journal of Cell Science*, *123*(24), 4195–4200. https://doi.org/10.1242/jcs.023820

Friedl, P., & Mayor, R. (2017). Tuning Collective Cell Migration by Cell–Cell Junction Regulation. *Cold Spring Harbor Perspectives in Biology*, *9*(4), a029199. https://doi.org/10.1101/cshperspect.a029199

Fujimoto, M., Hayashida, N., Katoh, T., Oshima, K., Shinkawa, T., Prakasam, R., Tan, K., Inouye, S., Takii, R., & Nakai, A. (2010). A Novel Mouse HSF3 Has the Potential to Activate Nonclassical Heat-Shock Genes during Heat Shock. *Molecular Biology of the Cell*, *21*(1), 106–116. https://doi.org/10.1091/mbc.e09-07-0639

Fujimoto, M., Izu, H., Seki, K., Fukuda, K., Nishida, T., Yamada, S. I., Kato, K., Yonemura, S., Inouye, S., & Nakai, A. (2004). HSF4 is required for normal cell growth and differentiation during mouse lens development. *EMBO Journal*, *23*(21), 4297–4306. https://doi.org/10.1038/sj.emboj.7600435

Fujimoto, M., Takaki, E., Hayashi, T., Kitaura, Y., Tanaka, Y., Inouye, S., & Nakai, A. (2005). Active HSF1 significantly suppresses polyglutamine aggregate formation in cellular and mouse models. *Journal of Biological Chemistry*, *280*(41), 34908–34916. https://doi.org/10.1074/jbc.M506288200

Garrod, D., & Chidgey, M. (2008). Desmosome structure, composition and function. *Biochimica et Biophysica Acta (BBA) - Biomembranes*, *1778*(3), 572–587. https://doi.org/10.1016/j.bbamem.2007.07.014

Geiger, B., Spatz, J. P., & Bershadsky, A. D. (2009). Environmental sensing through focal adhesions. *Nature Reviews Molecular Cell Biology*, *10*(1), 21–33. https://doi.org/10.1038/nrm2593

Gidalevitz, T., Prahlad, V., & Morimoto, R. I. (2011). The stress of protein misfolding: From single cells to multicellular organisms. *Cold Spring Harbor Perspectives in Biology*, *3*(6), 1–18. https://doi.org/10.1101/cshperspect.a009704

Gilbert, P. M., & Weaver, V. M. (2017). Cellular adaptation to biomechanical stress across length scales in tissue homeostasis and disease. *Seminars in Cell and Developmental Biology*, *67*, 141–152. https://doi.org/10.1016/j.semcdb.2016.09.004

Goffinet, A. M., & Tissir, F. (2017). Seven pass Cadherins CELSR1-3. *Seminars in Cell and Developmental Biology*, *69*, 102–110. https://doi.org/10.1016/j.semcdb.2017.07.014

Gomez-Pastor, R., Burchfiel, E. T., Neef, D. W., Jaeger, A. M., Cabiscol, E., McKinstry, S. U., Doss, A., Aballay, A., Lo, D. C., Akimov, S. S., Ross, C. A., Eroglu, C., & Thiele, D. J. (2017). Abnormal degradation of the neuronal stress-protective transcription factor HSF1 in Huntington's disease. *Nature Communications*, *8*(May 2016), 1–17. https://doi.org/10.1038/ncomms14405

Gomez-Pastor, R., Burchfiel, E. T., & Thiele, D. J. (2018). Regulation of heat shock transcription factors and their roles in physiology and disease. *Nature Reviews Molecular Cell Biology*, *19*(1), 4–19. https://doi.org/10.1038/nrm.2017.73

Goodson, M. L., Hong, Y., Rogers, R., Matunis, M. J., Park-Sargell, O. K., & Sarge, K. D. (2001). SUMO-1 Modification Regulates the DNA Binding Activity of Heat Shock Transcription Factor 2, a Promyelocytic Leukemia Nuclear Body Associated Transcription Factor. *Journal of Biological Chemistry*, *276*(21), 18513–18518. https://doi.org/10.1074/jbc.M008066200

Goodson, M. L., Park-Sarge, O. K., & Sarge, K. D. (1995). Tissue-dependent expression of heat shock factor 2 isoforms with distinct transcriptional activities. *Molecular and Cellular Biology*, *15*(10), 5288–5293. https://doi.org/10.1128/MCB.15.10.5288

Gough, R. E., & Goult, B. T. (2018). The tale of two talins – two isoforms to fine-tune integrin signalling. *FEBS Letters*, *592*(12), 2108–2125. https://doi.org/10.1002/1873-3468.13081

Gough, R. E., Jones, M. C., Zacharchenko, T., Le, S., Yu, M., Jacquemet, G., Muench, S. P., Yan, J., Humphries, J. D., Jørgensen, C., Humphries, M. J., & Goult, B. T. (2021). Talin mechanosensitivity is modulated by a direct interaction with cyclin-dependent kinase-1. *Journal of Biological Chemistry*, *297*(1), 1–18. https://doi.org/10.1016/j.jbc.2021.100837

Goult, B. T., Xu, X. P., Gingras, A. R., Swift, M., Patel, B., Bate, N., Kopp, P. M., Barsukov, I. L., Critchley, D. R., Volkmann, N., & Hanein, D. (2013). Structural studies on full-length talin1 reveal a compact auto-inhibited dimer: Implications for talin activation. *Journal of Structural Biology*, *184*(1), 21–32. https://doi.org/10.1016/j.jsb.2013.05.014

Goult, B. T., Yan, J., & Schwartz, M. A. (2018). Talin as a mechanosensitive signaling hub. *Journal of Cell Biology*, *217*(11), 3776–3784. https://doi.org/10.1083/jcb.201808061

Green, M., Schuetz, T. J., Sullivan, E. K., & Kingston, R. E. (1995). A heat shock-responsive domain of human HSF1 that regulates transcription activation domain function. *Molecular and Cellular Biology*, *15*(6), 3354–3362. https://doi.org/10.1128/mcb.15.6.3354

Grunberg, N., Pevsner-Fischer, M., Goshen-Lago, T., Diment, J., Stein, Y., Lavon, H., Mayer, S., Levi-Galibov, O., Friedman, G., Ofir-Birin, Y., Syu, L.-J., Migliore, C., Shimoni, E., Stemmer, S. M., Brenner, B., Dlugosz, A. A., Lyden, D., Regev-Rudzki, N., Ben-Aharon, I., & Scherz-Shouval, R. (2021). Cancer-Associated Fibroblasts Promote Aggressive Gastric Cancer Phenotypes via Heat Shock Factor 1–Mediated Secretion of Extracellular Vesicles. *Cancer Research*, *81*(7), 1639–1653. https://doi.org/10.1158/0008-5472.CAN-20-2756

Gul, I. S., Hulpiau, P., Saeys, Y., & van Roy, F. (2017). Evolution and diversity of cadherins and catenins. *Experimental Cell Research*, *358*(1), 3–9. https://doi.org/10.1016/j.yexcr.2017.03.001

Gumbiner, B. M. (1996). Cell adhesion: The molecular basis of tissue architecture and morphogenesis. *Cell*, *84*(3), 345–357. https://doi.org/10.1016/S0092-8674(00)81279-9

Guo, Y., Guettouche, T., Fenna, M., Boellmann, F., Pratt, W. B., Toft, D. O., Smith, D. F., & Voellmy, R. (2001). Evidence for a Mechanism of Repression of Heat Shock Factor 1 Transcriptional Activity by a Multichaperone Complex. *Journal of Biological Chemistry*, *276*(49), 45791–45799. https://doi.org/10.1074/jbc.M105931200

Guo, Y., Xu, Q., Canzio, D., Shou, J., Li, J., Gorkin, D. U., Jung, I., Wu, H., Zhai, Y., Tang, Y., Lu, Y., Wu, Y., Jia, Z., Li, W., Zhang, M. Q., Ren, B., Krainer, A. R., Maniatis, T., & Wu, Q. (2015). CRISPR Inversion of CTCF Sites Alters Genome Topology and Enhancer/Promoter Function. *Cell*, *162*(4), 900–910. https://doi.org/10.1016/j.cell.2015.07.038

Haage, A., Goodwin, K., Whitewood, A., Camp, D., Bogutz, A., Turner, C. T., Granville, D. J., Lefebvre, L., Plotnikov, S., Goult, B. T., & Tanentzapf, G. (2018). Talin Autoinhibition Regulates Cell-ECM Adhesion Dynamics and Wound Healing In Vivo. *Cell Reports*, *25*(9), 2401-2416.e5. https://doi.org/10.1016/j.celrep.2018.10.098

Haining, A. W. M., Lieberthal, T. J., & Del Río Hernández, A. (2016). Talin: A mechanosensitive molecule in health and disease. *FASEB Journal*, *30*(6), 2073–2085. https://doi.org/10.1096/fj.201500080R

Haling, J. R., Monkley, S. J., Critchley, D. R., & Petrich, B. G. (2011). Talin-dependent integrin activation is required for fibrin clot retraction by platelets. *Blood*, *117*(5), 1719–1722. https://doi.org/10.1182/blood-2010-09-305433

Hamidi, H., & Ivaska, J. (2018). Every step of the way: integrins in cancer progression and metastasis. *Nature Reviews Cancer*, *18*(9), 533–548. https://doi.org/10.1038/s41568-018-0038-z

Harrison, C. J., Bohm, A. A., & Nelson, H. C. M. (1994). Crystal structure of the DNA binding domain of the heat shock transcription factor. *Science*, *263*(5144), 224–227. https://doi.org/10.1126/science.8284672

Hastings, J. F., Skhinas, J. N., Fey, D., Croucher, D. R., & Cox, T. R. (2019). The extracellular matrix as a key regulator of intracellular signalling networks. *British Journal of Pharmacology*, *176*(1), 82–92. https://doi.org/10.1111/bph.14195

Hatzfeld, M., Keil, R., & Magin, T. M. (2017). Desmosomes and intermediate filaments: Their consequences for tissue mechanics. *Cold Spring Harbor Perspectives in Biology*, *9*(6). https://doi.org/10.1101/cshperspect.a029157

Hayashida, N., Fujimoto, M., Tan, K., Prakasam, R., Shinkawa, T., Li, L., Ichikawa, H., Takii, R., & Nakai, A. (2010). Heat shock factor 1 ameliorates proteotoxicity in cooperation with the transcription factor NFAT. *EMBO Journal*, *29*(20), 3459–3469. https://doi.org/10.1038/emboj.2010.225

He, H., Soncin, F., Grammatikakis, N., Li, Y., Siganou, A., Gong, J., Brown, S. A., Kingston, R. E., & Calderwood, S. K. (2003). Elevated Expression of Heat Shock Factor (HSF) 2A Stimulates HSF1-induced Transcription during Stress *. *Journal of Biological Chemistry*, *278*(37), 35465–35475. https://doi.org/10.1074/jbc.M304663200

Heisenberg, C. P., & Bellaïche, Y. (2013). XForces in tissue morphogenesis and patterning. *Cell*, *153*(5), 948. https://doi.org/10.1016/j.cell.2013.05.008

Hendriks, I. A., Lyon, D., Young, C., Jensen, L. J., Vertegaal, A. C. O., & Nielsen, M. L. (2017). Site-specific mapping of the human SUMO proteome reveals co-modification with phosphorylation. *Nature Structural and Molecular Biology*, *24*(3), 325–336. https://doi.org/10.1007/s00246-019-02167-3

Hentze, N., Le Breton, L., Wiesner, J., Kempf, G., & Mayer, M. P. (2016). Molecular mechanism of thermosensory function of human heat shock transcription factor Hsf1. *ELife*, *5*(1), 1–24. https://doi.org/10.7554/elife.11576

Herrmann, C., Avgousti, D., & Weitzman, M. (2017). Differential Salt Fractionation of Nuclei to Analyze Chromatin-associated Proteins from Cultured Mammalian Cells. *Bio-Protocol*, *7*(6), 1–13. https://doi.org/10.21769/bioprotoc.2175

Hietakangas, V., Anckar, J., Blomster, H. A., Fujimoto, M., Palvimo, J. J., Nakai, A., & Sistonen, L. (2006). PDSM, a motif for phosphorylation-dependent SUMO modification. *Proceedings of the National Academy of Sciences of the United States of America*, *103*(1), 45–50. https://doi.org/10.1073/pnas.0503698102

Himanen, S. V, Puustinen, M. C., Da Silva, A. J., Vihervaara, A., & Sistonen, L. (2022). HSFs drive transcription of distinct genes and enhancers during oxidative stress and heat shock. *Nucleic Acids Research*, *50*(11), 6102–6115. https://doi.org/10.1093/nar/gkac493

Himanen, S. V, & Sistonen, L. (2019). New insights into transcriptional reprogramming during cellular stress. *Journal of Cell Science*, *132*(21). https://doi.org/10.1242/jcs.238402

Hintermann, & Christen. (2019). The Many Roles of Cell Adhesion Molecules in Hepatic Fibrosis. *Cells*, *8*(12), 1503. https://doi.org/10.3390/cells8121503

Hirano, S., & Takeichi, M. (2012). Cadherins in brain morphogenesis and wiring. *Physiological Reviews*, *92*(2), 597–634. https://doi.org/10.1152/physrev.00014.2011

Hirayama, T., & Yagi, T. (2017). Regulation of clustered protocadherin genes in individual neurons. *Seminars in Cell and Developmental Biology*, *69*, 122–130. https://doi.org/10.1016/j.semcdb.2017.05.026

Homma, S., Jin, X., Wang, G., Tu, N., Min, J., Yanasak, N., & Mivechi, N. F. (2007). Demyelination, astrogliosis, and accumulation of ubiquitinated proteins, hallmarks of CNS disease in hsf1-deficient mice. *Journal of Neuroscience*, *27*(30), 7974–7986. https://doi.org/10.1523/JNEUROSCI.0006-07.2007

Horton, E. R., Byron, A., Askari, J. A., Ng, D. H. J., Millon-Frémillon, A., Robertson, J., Koper, E. J., Paul, N. R., Warwood, S., Knight, D., Humphries, J. D., & Humphries, M. J. (2015). Definition of a consensus integrin adhesome and its dynamics during adhesion complex assembly and disassembly. *Nature Cell Biology*, *17*(12), 1577–1587. https://doi.org/10.1038/ncb3257

Horton, E. R., Humphries, J. D., James, J., Jones, M. C., Askari, J. A., & Humphries, M. J. (2016). The integrin adhesome network at a glance. *Journal of Cell Science*, 4159–4163. https://doi.org/10.1242/jcs.192054

Horwitz, A. R. (2012). The origins of the molecular era of adhesion research. *Nature Reviews Molecular Cell Biology*, *13*(12), 805–811. https://doi.org/10.1038/nrm3473

Hou, T. Y., & Kraus, W. L. (2021). Spirits in the Material World: Enhancer RNAs in Transcriptional Regulation. *Trends in Biochemical Sciences*, *46*(2), 138–153. https://doi.org/10.1016/j.tibs.2020.08.007

Hsu, A. L., Murphy, C. T., & Kenyon, C. (2003). Regulation of aging and age-related disease by DAF-16 and heat-shock factor. *Science*, *300*(5622), 1142–1145. https://doi.org/10.1126/science.1083701

Ishiyama, N., Sarpal, R., Wood, M. N., Barrick, S. K., Nishikawa, T., Hayashi, H., Kobb, A. B., Flozak, A. S., Yemelyanov, A., Fernandez-Gonzalez, R., Yonemura, S., Leckband, D. E., Gottardi, C. J., Tepass, U., & Ikura, M. (2018). Force-dependent allostery of the α-catenin actin-binding domain controls adherens junction dynamics and functions. *Nature Communications*, *9*(1), 1–17. https://doi.org/10.1038/s41467-018-07481-7

Isomursu, A., Lerche, M., Taskinen, M. E., Ivaska, J., & Peuhu, E. (2019). Integrin signaling and mechanotransduction in regulation of somatic stem cells. *Experimental Cell Research*, *378*(2), 217–225. https://doi.org/10.1016/j.yexcr.2019.01.027

Jaeger, A. M., Pemble, C. W., Sistonen, L., & Thiele, D. J. (2016). Structures of HSF2 reveal mechanisms for differential regulation of human heat-shock factors. *Nature Structural & Molecular Biology*, *23*(2), 147–154. https://doi.org/10.1038/nsmb.3150

Jahed, Z., & Mofrad, M. R. (2019). The nucleus feels the force, LINCed in or not! *Current Opinion in Cell Biology*, *58*(June), 114–119. https://doi.org/10.1016/j.ceb.2019.02.012

Jan, S. Z., Hamer, G., Repping, S., de Rooij, D. G., Van Pelt, A. M. M., & Vormer, T. L. (2012). Molecular control of rodent spermatogenesis. *Biochimica et Biophysica Acta - Molecular Basis of Disease*, *1822*(12), 1838–1850. https://doi.org/10.1016/j.bbadis.2012.02.008

Janota, C. S., Calero-Cuenca, F. J., & Gomes, E. R. (2020). The role of the cell nucleus in mechanotransduction. *Current Opinion in Cell Biology*, *63*, 204–211. https://doi.org/10.1016/j.ceb.2020.03.001

Jedlicka, P., Mortin, M. A., & Wu, C. (1997). Multiple functions of Drosophila heat shock transcription factor in vivo. *EMBO Journal*, *16*(9), 2452–2462. https://doi.org/10.1093/emboj/16.9.2452

Jia, W., Yao, Z., Zhao, J., Guan, Q., & Gao, L. (2017). New perspectives of physiological and pathological functions of nucleolin (NCL). *Life Sciences*, *186*(May), 1–10. https://doi.org/10.1016/j.lfs.2017.07.025

Jin, J.-K., Tien, P.-C., Cheng, C.-J., Song, J. H., Huang, C., Lin, S.-H., & Gallick, G. E. (2015). Talin1 phosphorylation activates β1 integrins: a novel mechanism to promote prostate cancer bone metastasis. *Oncogene*, *34*(14), 1811–1821. https://doi.org/10.1038/onc.2014.116

Joutsen, J., Da Silva, A. J., Luoto, J. C., Budzynski, M. A., Nylund, A. S., de Thonel, A., Concordet, J. P., Mezger, V., Sabéran-Djoneidi, D., Henriksson, E., & Sistonen, L. (2020). Heat Shock Factor 2 Protects against Proteotoxicity by Maintaining Cell-Cell Adhesion. *Cell Reports*. https://doi.org/10.1016/j.celrep.2019.12.037

Joutsen, J., & Sistonen, L. (2019). Tailoring of proteostasis networks with heat shock factors. *Cold Spring Harbor Perspectives in Biology*, *11*(4), 1–18. https://doi.org/10.1101/cshperspect.a034066

Juliano, R. L. (2002). Signal Transduction by Cell Adhesion Receptors and the Cytoskeleton: Functions of Integrins, Cadherins, Selectins, and Immunoglobulin-Superfamily Members. *Annual Review of Pharmacology and Toxicology*, *42*(1), 283–323. https://doi.org/10.1146/annurev.pharmtox.42.090401.151133

Jurivich, D., Sistonen, L., Kroes, R., & Morimoto, R. (1992). Effect of sodium salicylate on the human heat shock response. *Science*, *255*(5049), 1243–1245. https://doi.org/10.1126/science.1546322

Kallio, M., Chang, Y., Manuel, M., Alastalo, T. P., Rallu, M., Gitton, Y., Pirkkala, L., Loones, M. T., Paslaru, L., Larney, S., Hiard, S., Morange, M., Sistonen, L., & Mezger, V. (2002). Brain abnormalities, defective meiotic chromosome synapsis and female subfertility in HSF2 null mice. *EMBO Journal*, *21*(11), 2591–2601. https://doi.org/10.1093/emboj/21.11.2591

Kampinga, H. H., & Bergink, S. (2016). Heat shock proteins as potential targets for protective strategies in neurodegeneration. *The Lancet Neurology*, *15*(7), 748–759. https://doi.org/10.1016/S1474-4422(16)00099-5

Kampinga, H. H., Hageman, J., Vos, M. J., Kubota, H., Tanguay, R. M., Bruford, E. A., Cheetham, M. E., Chen, B., & Hightower, L. E. (2009). Guidelines for the nomenclature of the human heat shock proteins. *Cell Stress and Chaperones*, *14*(1), 105–111. https://doi.org/10.1007/s12192-008-0068-7

Kaushik, S., & Cuervo, A. M. (2018). The coming of age of chaperone-mediated autophagy. *Nature Reviews Molecular Cell Biology*, *19*(6), 365–381. https://doi.org/10.1038/s41580-018-0001-6

Kawazoe, Y., Nakai, A., Tanabe, M., & Nagata, K. (1998). Proteasome inhibition leads to the activation of all members of the heat-shock-factor family. *European Journal of Biochemistry*, *255*(2), 356–362. https://doi.org/10.1046/j.1432-1327.1998.2550356.x

Kawazoe, Y., Tanabe, M., Sasai, N., Nagata, K., & Nakai, A. (1999). HSF3 is a major heat shock responsive factor duringchicken embryonic development. *European Journal of Biochemistry*, *265*(2), 688–697. https://doi.org/10.1046/j.1432-1327.1999.00762.x

Khilan, A. A., Al-Maslamani, N. A., & Horn, H. F. (2021). Cell stretchers and the LINC complex in mechanotransduction. *Archives of Biochemistry and Biophysics*, *702*(February), 108829. https://doi.org/10.1016/j.abb.2021.108829

Kim, E., Wang, B., Sastry, N., Masliah, E., Nelson, P. T., Cai, H., & Liao, F. F. (2016). NEDD4-mediated HSF1 degradation underlies α-synucleinopathy. *Human Molecular Genetics*, *25*(2), 211–222. https://doi.org/10.1093/hmg/ddv445

Kim, S., Yu, N.-K., & Kaang, B.-K. (2015). CTCF as a multifunctional protein in genome regulation and gene expression. *Experimental & Molecular Medicine*, *47*(6), e166–e166. https://doi.org/10.1038/emm.2015.33

Kim, W., Bennett, E. J., Huttlin, E. L., Guo, A., Li, J., Possemato, A., Sowa, M. E., Rad, R., Rush, J., Comb, M. J., Harper, J. W., & Gygi, S. P. (2011). Systematic and Quantitative Assessment of the Ubiquitin-Modified Proteome. *Molecular Cell*, *44*(2), 325–340. https://doi.org/10.1016/j.molcel.2011.08.025

King, J. S. (2012). Mechanical stress meets autophagy: Potential implications for physiology and pathology. *Trends in Molecular Medicine*, *18*(10), 583–588. https://doi.org/10.1016/j.molmed.2012.08.002

Klages-Mundt, N. L., Kumar, A., Zhang, Y., Kapoor, P., & Shen, X. (2018). The Nature of Actin-Family Proteins in Chromatin-Modifying Complexes. *Frontiers in Genetics*, *9*(September), 1–16. https://doi.org/10.3389/fgene.2018.00398

Klapholz, B., & Brown, N. H. (2017a). Talin – the master of integrin adhesions. *Journal of Cell Science*, jcs.190991. https://doi.org/10.1242/jcs.190991

Klapholz, B., & Brown, N. H. (2017b). Talin – the master of integrin adhesions. *Journal of Cell Science*, *130*(15), 2435–2446. https://doi.org/10.1242/jcs.190991

Klotz, L. O., Hou, X., & Jacob, C. (2014). 1,4-naphthoquinones: From oxidative damage to cellular and inter-cellular signaling. *Molecules*, *19*(9), 14902–14918. https://doi.org/10.3390/molecules190914902

Kmiecik, S. W., Le Breton, L., & Mayer, M. P. (2020). Feedback regulation of heat shock factor 1 (Hsf1) activity by Hsp70-mediated trimer unzipping and dissociation from <scp>DNA</scp>. *The EMBO Journal*, *39*(14), 1–22. https://doi.org/10.15252/embj.2019104096

Kmiecik, S. W., & Mayer, M. P. (2022). Molecular mechanisms of heat shock factor 1 regulation. *Trends in Biochemical Sciences*, *47*(3), 218–234. https://doi.org/10.1016/j.tibs.2021.10.004

Knudsen, K. A. (1985). The calcium-dependent myoblast adhesion that precedes cell fusion is mediated by glycoproteins. *Journal of Cell Biology*, *101*(3), 891–897. https://doi.org/10.1083/jcb.101.3.891

Korfanty, J., Stokowy, T., Widlak, P., Gogler-Piglowska, A., Handschuh, L., Podkowiński, J., Vydra, N., Naumowicz, A., Toma-Jonik, A., & Widlak, W. (2014). Crosstalk between HSF1 and HSF2 during the heat shock response in mouse testes. *International Journal of Biochemistry and Cell Biology*, *57*, 76–83. https://doi.org/10.1016/j.biocel.2014.10.006

Kotaja, N. (2014). MicroRNAs and spermatogenesis. *Fertility and Sterility*, *101*(6), 1552–1562. https://doi.org/10.1016/j.fertnstert.2014.04.025

Kourtis, N., Moubarak, R. S., Aranda-Orgilles, B., Lui, K., Aydin, I. T., Trimarchi, T., Darvishian, F., Salvaggio, C., Zhong, J., Bhatt, K., Chen, E. I., Celebi, J. T., Lazaris, C., Tsirigos, A., Osman, I., Hernando, E., & Aifantis, I. (2015). FBXW7 modulates cellular stress response and metastatic potential through HSF1 post-translational modification. *Nature Cell Biology*, *17*(3), 322–332. https://doi.org/10.1038/ncb3121

Kwak, H., Fuda, N. J., Core, L. J., & Lis, J. T. (2013). Precise Maps of RNA Polymerase Reveal How Promoters Direct Initiation and Pausing. *Science*, *339*(6122), 950–953. https://doi.org/10.1126/science.1229386

Labbadia, J., & Morimoto, R. I. (2015). Repression of the Heat Shock Response Is a Programmed Event at the Onset of Reproduction. *Molecular Cell*, *59*(4), 639–650. https://doi.org/10.1016/j.molcel.2015.06.027

Ladoux, B., Nelson, W. J., Yan, J., & Mège, R. M. (2015). The mechanotransduction machinery at work at adherens junctions. *Integrative Biology (United Kingdom)*, *7*(10), 1109–1119. https://doi.org/10.1039/c5ib00070j

Laplante, M., & Sabatini, D. M. (2009). mTOR signaling at a glance. *Journal of Cell Science*, *122*(20), 3589–3594. https://doi.org/10.1242/jcs.051011

Lecomte, S., Desmots, F., Le Masson, F., Le Goff, P., Michel, D., Christians, E. S., & Le Dréan, Y. (2010). Roles of heat shock factor 1 and 2 in response to proteasome inhibition: Consequence on p53 stability. *Oncogene*, *29*(29), 4216–4224. https://doi.org/10.1038/onc.2010.171

Lee, H. S., Lim, C. J., Puzon-McLaughlin, W., Shattil, S. J., & Ginsberg, M. H. (2009). RIAM activates integrins by linking talin to Ras GTPase membrane-targeting sequences. *Journal of Biological Chemistry*, *284*(8), 5119–5122. https://doi.org/10.1074/jbc.M807117200

Lefebvre, J. L., Kostadinov, D., Chen, W. V., Maniatis, T., & Sanes, J. R. (2012). Protocadherins mediate dendritic self-avoidance in the mammalian nervous system. *Nature*, *488*(7412), 517–521. https://doi.org/10.1038/nature11305

Levi-galibov, O., Lavon, H., Wassermann-dozorets, R., Pevsner-fischer, M., Mayer, S., Wershof, E., Stein, Y., Brown, L. E., Zhang, W., Friedman, G., Nevo, R., Golani, O., Katz, L. H., Yaeger, R., Laish, I., Porco, J. A., Sahai, E., Shouval, D. S., Kelsen, D., & Scherz-shouval, R. (2020). Heat Shock Factor 1-dependent extracellular matrix remodeling mediates the transition from chronic intestinal inflammation to colon cancer. *Nature Communications*, 1–19. https://doi.org/10.1038/s41467-020-20054

Li, J., Labbadia, J., & Morimoto, R. I. (2017). Rethinking HSF1 in Stress, Development, and Organismal Health. *Trends in Cell Biology*, *27*(12), 895–905. https://doi.org/10.1016/j.tcb.2017.08.002

Li, P., Sheng, C., Huang, L., Zhang, H., Huang, L., Cheng, Z., & Zhu, Q. (2014). MiR-183/-96/-182 cluster is up-regulated in most breast cancers and increases cell proliferation and migration. *Breast Cancer Research*, *16*(1), 1–17. https://doi.org/10.1186/s13058-014-0473-z

Li, Y., Gao, S., Han, Y., Song, L., Kong, Y., Jiao, Y., Huang, S., Du, J., & Li, Y. (2021). Variants of Focal Adhesion Scaffold Genes Cause Thoracic Aortic Aneurysm. *Circulation Research*, 8–23. https://doi.org/10.1161/CIRCRESAHA.120.317361

Li, Y., Luo, X., Sun, Y., Cui, Z., Liu, Y., Liu, R., & Guo, X. (2016). High stoichiometry phosphorylation of talin at T144/T150 or S446 produces contrasting effects on calpain-mediated talin cleavage and cell migration. *Journal of Cancer*, *7*(12), 1645–1652. https://doi.org/10.7150/jca.14192

Liangliang, X., Yonghui, H., Shunmei, E., Shoufang, G., Wei, Z., & Jiangying, Z. (2010). Dominant-positive HSF1 decreases alpha-synuclein level and alpha-synuclein-induced toxicity. *Molecular Biology Reports*, *37*(4), 1875–1881. https://doi.org/10.1007/s11033-009-9623-2

Lindquist, S. (1986). The Heat-Shock Response. *Annual Review of Biochemistry*, *55*(1), 1151–1191. https://doi.org/10.1146/annurev.bi.55.070186.005443

Loison, F., Debure, L., Nizard, P., Le Goff, P., Michel, D., & Le Dréan, Y. (2006). Up-regulation of the clusterin gene after proteotoxic stress: Implication of HSF1-HSF2 heterocomplexes. *Biochemical Journal*, *395*(1), 223–231. https://doi.org/10.1042/BJ20051190

Mahat, D. B., Salamanca, H. H., Duarte, F. M., Danko, C. G., & Lis, J. T. (2016). Mammalian Heat Shock Response and Mechanisms Underlying Its Genome-wide Transcriptional Regulation. *Molecular Cell*, *62*(1), 63–78. https://doi.org/10.1016/j.molcel.2016.02.025

Manasanch, E. E., & Orlowski, R. Z. (2017). Proteasome inhibitors in cancer therapy. *Nature Reviews Clinical Oncology*, *14*(7), 417–433. https://doi.org/10.1038/nrclinonc.2016.206

Manso, A. M., Li, R., Monkley, S. J., Cruz, N. M., Ong, S., Lao, D. H., Koshman, Y. E., Gu, Y., Peterson, K. L., Chen, J., Abel, E. D., Samarel, A. M., Critchley, D. R., & Ross, R. S. (2013). Talin1 Has Unique Expression versus Talin 2 in the Heart and Modifies the Hypertrophic Response to Pressure Overload. *Journal of Biological Chemistry*, *288*(6), 4252–4264. https://doi.org/10.1074/jbc.M112.427484

Mathew, A., Mathur, S. K., & Morimoto, R. I. (1998). Heat Shock Response and Protein Degradation: Regulation of HSF2 by the Ubiquitin-Proteasome Pathway. *Molecular and Cellular Biology*, *18*(9), 5091–5098. https://doi.org/10.1128/mcb.18.9.5091

McMillan, D. R., Xiao, X., Shao, L., Graves, K., & Benjamin, I. J. (1998). Targeted disruption of heat shock transcription factor 1 abolishes thermotolerance and protection against heat-inducible apoptosis. *Journal of Biological Chemistry*, *273*(13), 7523–7528. https://doi.org/10.1074/jbc.273.13.7523

Mendillo, M. L., Santagata, S., Koeva, M., Bell, G. W., Hu, R., Tamimi, R. M., Fraenkel, E., Ince, T. A., Whitesell, L., & Lindquist, S. (2012). HSF1 drives a transcriptional program distinct from heat shock to support highly malignant human cancers. *Cell*, *150*(3), 549–562. https://doi.org/10.1016/j.cell.2012.06.031

Meng, W., & Takeichi, M. (2009). Adherens Junction: Molecular Architecture and Regulation. *Cold Spring Harbor Perspectives in Biology*, *1*(6), a002899–a002899. https://doi.org/10.1101/cshperspect.a002899

Metchat, A., Åkerfelt, M., Bierkamp, C., Delsinne, V., Sistonen, L., Alexandre, H., & Christians, E. S. (2009). Mammalian Heat Shock Factor 1 Is Essential for Oocyte Meiosis and Directly Regulates Hsp90α Expression. *Journal of Biological Chemistry*, *284*(14), 9521–9528. https://doi.org/10.1074/jbc.M808819200

Mezger, V., Rallu, M., Morimoto, R. I., Morange, M., & Renard, J.-P. (1994). Heat Shock Factor 2-like Activity in Mouse Blastocysts. *Developmental Biology*, *166*(2), 819–822. https://doi.org/10.1006/dbio.1994.1361

Michael, M., & Parsons, M. (2020). New perspectives on integrin-dependent adhesions. *Current Opinion in Cell Biology*, *63*, 31–37. https://doi.org/10.1016/j.ceb.2019.12.008

Minsky, N., & Roeder, R. G. (2015). Direct link between metabolic regulation and the heat-shock response through the transcriptional regulator PGC-1α. *Proceedings of the National Academy of Sciences of the United States of America*, *112*(42), E5669–E5678. https://doi.org/10.1073/pnas.1516219112

Miroshnikova, Y. A., Cohen, I., Ezhkova, E., & Wickström, S. A. (2019). Epigenetic gene regulation, chromatin structure, and force-induced chromatin remodelling in epidermal development and homeostasis. *Current Opinion in Genetics and Development*, *55*, 46–51. https://doi.org/10.1016/j.gde.2019.04.014

Miroshnikova, Y. A., & Wickström, S. A. (2022). Mechanical Forces in Nuclear Organization. *Cold Spring Harbor Perspectives in Medicine*, *14*(1). https://doi.org/10.1101/cshperspect.a039685

Mogk, A., Bukau, B., & Kampinga, H. H. (2018). Cellular Handling of Protein Aggregates by Disaggregation Machines. *Molecular Cell*, *69*(2), 214–226. https://doi.org/10.1016/j.molcel.2018.01.004

Moreno-layseca, P., Icha, J., Hamidi, H., & Ivaska, J. (2019). Europe PMC Funders Group Integrin trafficking in cells and tissues. *Nat Cell Biol.*, *21*(2), 122–132. https://doi.org/10.1038/s41556-018-0223-z.Integrin

Morimoto, R. I., & Cuervo, A. M. (2014). Proteostasis and the aging proteome in health and disease. *Journals of Gerontology - Series A Biological Sciences and Medical Sciences*, *69*, S33–S38. https://doi.org/10.1093/gerona/glu049

Mountoufaris, G., Canzio, D., Nwakeze, C. L., Chen, W. V., & Maniatis, T. (2018). Writing, Reading, and Translating the Clustered Protocadherin Cell Surface Recognition Code for Neural Circuit Assembly. *Annual Review of Cell and Developmental Biology*, *34*(1), 471–493. https://doi.org/10.1146/annurev-cellbio-100616-060701

Mountoufaris, G., Chen, W. V., Hirabayashi, Y., O'Keeffe, S., Chevee, M., Nwakeze, C. L., Polleux, F., & Maniatis, T. (2017). Multicluster Pcdh diversity is required for mouse olfactory neural circuit assembly. *Science*, *356*(6336), 411–414. https://doi.org/10.1126/science.aai8801

Murphy, S. P., Gorzowski, J. J., Sarge, K. D., & Phillips, B. (1994). Characterization of constitutive HSF2 DNA-binding activity in mouse embryonal carcinoma cells. *Molecular and Cellular Biology*, *14*(8), 5309–5317. https://doi.org/10.1128/mcb.14.8.5309-5317.1994

Najor, N. A. (2018a). Desmosomes in Human Disease. *Annual Review of Pathology: Mechanisms of Disease*, *13*(1), 51–70. https://doi.org/10.1146/annurev-pathol-020117-044030

Najor, N. A. (2018b). Desmosomes in Human Disease. *Annual Review of Pathology: Mechanisms of Disease*, *13*(1), 51–70. https://doi.org/10.1146/annurev-pathol-020117-044030

Nelson, W. J., & Nusse, R. (2004). Convergence of Wnt, β-Catenin, and Cadherin pathways. *Science*, *303*(5663), 1483–1487. https://doi.org/10.1126/science.1094291

Neudegger, T., Verghese, J., Hayer-Hartl, M., Hartl, F. U., & Bracher, A. (2016). Structure of human heat-shock transcription factor 1 in complex with DNA. *Nature Structural and Molecular Biology*, *23*(2), 140–146. https://doi.org/10.1038/nsmb.3149

Nevzorov, I., Sidorenko, E., Wang, W., Zhao, H., & Vartiainen, M. K. (2018). Myosin-1C uses a novel phosphoinositide-dependent pathway for nuclear localization. *EMBO Reports*, *19*(2), 290–304. https://doi.org/10.15252/embr.201744296

Nieswandt, B., Moser, M., Pleines, I., Varga-Szabo, D., Monkley, S., Critchley, D., & Fässler, R. (2007). Loss of talin1 in platelets abrogates integrin activation, platelet aggregation, and thrombus formation in vitro and in vivo. *Journal of Experimental Medicine*, *204*(13), 3113–3118. https://doi.org/10.1084/jem.20071827

Nilson, K. A., Lawson, C. K., Mullen, N. J., Ball, C. B., Spector, B. M., Meier, J. L., & Price, D. H. (2017). Oxidative stress rapidly stabilizes promoter-proximal paused Pol II across the human genome. *Nucleic Acids Research*, *45*(19), 11088–11105. https://doi.org/10.1093/nar/gkx724

Nover, L. (1987). Expression of heat shock genes in homologous and heterologous systems. *Enzyme and Microbial Technology*, *9*(3), 130–144. https://doi.org/10.1016/0141-0229(87)90066-4

Oda, H., & Takeichi, M. (2011). Structural and functional diversity of cadherin at the adherens junction. *Journal of Cell Biology*, *193*(7), 1137–1146. https://doi.org/10.1083/jcb.201008173

Oh, J., Fleming, A. M., Xu, J., Chong, J., Burrows, C. J., & Wang, D. (2020). RNA polymerase II stalls on oxidative DNA damage via a torsion-latch mechanism involving lone pair–π and CH–π interactions. *Proceedings of the National Academy of Sciences*, *117*(17), 9338–9348. https://doi.org/10.1073/pnas.1919904117

Orré, T., Rossier, O., & Giannone, G. (2019). The inner life of integrin adhesion sites: From single molecules to functional macromolecular complexes. *Experimental Cell Research*, *379*(2), 235–244. https://doi.org/10.1016/j.yexcr.2019.03.036

Östling, P., Björk, J. K., Roos-Mattjus, P., Mezger, V., & Sistonen, L. (2007). Heat Shock Factor 2 (HSF2) contributes to inducible expression of hsp genes through interplay with HSF1. *Journal of Biological Chemistry*, *282*(10), 7077–7086. https://doi.org/10.1074/jbc.M607556200

Paluch, E. K., Aspalter, I. M., & Sixt, M. (2016). Focal Adhesion–Independent Cell Migration. *Annual Review of Cell and Developmental Biology*, *32*(1), 469–490. https://doi.org/10.1146/annurev-cellbio-111315-125341

Parker, C. S., & Topol, J. (1984). A drosophila RNA polymerase II transcription factor binds to the regulatory site of an hsp 70 gene. *Cell*, *37*(1), 273–283. https://doi.org/10.1016/0092-8674(84)90323-4

Paulson, A. F., Prasad, M. S., Thuringer, A. H., & Manzerra, P. (2014a). Regulation of cadherin expression in nervous system development. *Cell Adhesion and Migration*, *8*(1), 19–28. https://doi.org/10.4161/cam.27839

Paulson, A. F., Prasad, M. S., Thuringer, A. H., & Manzerra, P. (2014b). Regulation of cadherin expression in nervous system development. *Cell Adhesion and Migration*, *8*(1), 19–28. https://doi.org/10.4161/cam.27839

Pelham, H. R. B. (1982). A regulatory upstream promoter element in the Drosophila Hsp 70 heat-shock gene. *Cell*, *30*(2), 517–528. https://doi.org/10.1016/0092-8674(82)90249-5

Pesonen, L., Svartsjö, S., Bäck, V., de Thonel, A., Mezger, V., Sabéran-Djoneidi, D., & Roos-Mattjus, P. (2021). Gambogic acid and gambogenic acid induce a thiol-dependent heat shock response and disrupt the interaction between HSP90 and HSF1 or HSF2. *Cell Stress and Chaperones*, *26*(5), 819–833. https://doi.org/10.1007/s12192-021-01222-4

Piddini, E. (2017). Epithelial Homeostasis: A Piezo of the Puzzle. *Current Biology*, *27*(6), R232–R234. https://doi.org/10.1016/j.cub.2017.02.002

Provasi, D., Negri, A., Coller, B. S., & Filizola, M. (2014). Talin-driven inside-out activation mechanism of platelet αIIbβ3 integrin probed by multimicrosecond, all-atom molecular dynamics simulations. *Proteins: Structure, Function, and Bioinformatics*, *82*(12), 3231–3240. https://doi.org/10.1002/prot.24540

Puustinen, M. C., & Sistonen, L. (2020). Molecular Mechanisms of Heat Shock Factors in Cancer. *Cells*, *9*(5), 1202. https://doi.org/10.3390/cells9051202

Rabindran, S. K., Giorgi, G., Clos, J., & Wu, C. (1991). Molecular cloning and expression of a human heat shock factor, HSF1. *Proceedings of the National Academy of Sciences*, *88*(16), 6906–6910. https://doi.org/10.1073/pnas.88.16.6906

Rallu, M., Loones, M. T., Lallemand, Y., Morimoto, R., Morange, M., & Mezger, V. (1997). Function and regulation of heat shock factor 2 during mouse embryogenesis. *Proceedings of the National Academy of Sciences of the United States of America*, *94*(6), 2392–2397. https://doi.org/10.1073/pnas.94.6.2392

Ritossa, F. (1962). A new puffing pattern induced by temperature shock and DNP in drosophila. *Experientia*, *18*(12), 571–573. https://doi.org/10.1007/BF02172188

Ritossa, F. (1996). Discovery of the heat shock response. *Cell Stress & Chaperones*, *1*(2), 97. https://doi.org/10.1379/1466-1268(1996)001<0097:DOTHSR>2.3.CO;2

Robak, P., & Robak, T. (2019). Bortezomib for the Treatment of Hematologic Malignancies: 15 Years Later. *Drugs in R and D*, *19*(2), 73–92. https://doi.org/10.1007/s40268-019-0269-9

Roos-Mattjus, P., & Sistonen, L. (2021). Interplay between mammalian heat shock factors 1 and 2 in physiology and pathology. *FEBS Journal*, *289*, 7710–7725. https://doi.org/10.1111/febs.16178

Rossi, A., Riccio, A., Coccia, M., Trotta, E., La Frazia, S., & Santoro, M. G. (2014). The proteasome inhibitor bortezomib is a potent inducer of zinc finger an1-type domain 2A gene expression: Roleofheatshockfactor 1 (HSF1)- heatshockfactor 2 (HSF2) heterocomplexes. *Journal of Biological Chemistry*, *289*(18), 12705–12715. https://doi.org/10.1074/jbc.M113.513242

Rothkamm, K., Barnard, S., Moquet, J., Ellender, M., Rana, Z., & Burdak-Rothkamm, S. (2015). DNA damage foci: Meaning and significance. *Environmental and Molecular Mutagenesis*, *56*(6), 491–504. https://doi.org/10.1002/em.21944

Saju, J. M., Hossain, M. S., Liew, W. C., Pradhan, A., Thevasagayam, N. M., Tan, L. S. E., Anand, A., Olsson, P. E., & Orbán, L. (2018). Heat Shock Factor 5 Is Essential for Spermatogenesis in Zebrafish. *Cell Reports*, *25*(12), 3252-3261.e4. https://doi.org/10.1016/j.celrep.2018.11.090

Sandqvist, A., Björk, J. K., Åkerfelt, M., Chitikova, Z., Grichine, A., Vourc'h, C., Jolly, C., Salminen, T. A., Nymalm, Y., & Sistonen, L. (2009). Heterotrimerization of Heat-Shock Factors 1 and 2 Provides a Transcriptional Switch in Response to Distinct Stimuli. *Molecular Biology of the Cell*, *20*(5), 1340–1347. https://doi.org/10.1091/mbc.e08-08-0864

Santos, S. D., & Saraiva, M. J. (2004). Enlarged ventricles, astrogliosis and neurodegeneration in heat shock factor 1 null mouse brain. *Neuroscience*, *126*(3), 657–663. https://doi.org/10.1016/j.neuroscience.2004.03.023

Sarge, K. D., Park-Sarge, O.-K., Kirby, J. D., Mayo, K. E., & Morimoto, R. I. (1994). Expression of Heat Shock Factor 2 in Mouse Testis: Potential Role as a Regulator of Heat-Shock Protein Gene Expression during Spermatogenesis1. *Biology of Reproduction*, *50*(6), 1334–1343. https://doi.org/10.1095/biolreprod50.6.1334

Sarge, K. D., Zimarino, V., Holm, K., Wu, C., & Morimoto, R. I. (1991). Cloning and characterization of two mouse heat shock factors with distinct inducible and constitutive DNA-binding ability. *Genes and Development*, *5*(10), 1902–1911. https://doi.org/10.1101/gad.5.10.1902

Scharf, K. D., Rose, S., Zott, W., Schöffl, F., Nover, L., & Schöff, F. (1990). Three tomato genes code for heat stress transcription factors with a region of remarkable homology to the DNA-binding domain of the yeast HSF. *The EMBO Journal*, *9*(13), 4495–4501. https://doi.org/10.1002/j.1460-2075.1990.tb07900.x

Scherz-Shouval, R., Santagata, S., Mendillo, M. L., Sholl, L. M., Ben-Aharon, I., Beck, A. H., Dias-Santagata, D., Koeva, M., Stemmer, S. M., Whitesell, L., & Lindquist, S. (2014). The Reprogramming of Tumor Stroma by HSF1 Is a Potent Enabler of Malignancy. *Cell*, *158*(3), 564–578. https://doi.org/10.1016/j.cell.2014.05.045

Schnell, U., Cirulli, V., & Giepmans, B. N. G. (2013). EpCAM: Structure and function in health and disease. *Biochimica et Biophysica Acta - Biomembranes*, *1828*(8), 1989–2001. https://doi.org/10.1016/j.bbamem.2013.04.018

Schuetz, T. J., Gallo, G. J., Sheldon, L., Tempst, P., & Kingston, R. E. (1991). Isolation of a cDNA for HSF2: Evidence for two heat shock factor genes in humans. *Proceedings of the National Academy of Sciences of the United States of America*, *88*(16), 6911–6915. https://doi.org/10.1073/pnas.88.16.6911

Shattil, S. J., Kim, C., & Ginsberg, M. H. (2010). The final steps of integrin activation: the end game. *Nature Reviews Molecular Cell Biology*, *11*(4), 288–300. https://doi.org/10.1038/nrm2871

Shi, X., Cui, B., Wang, Z., Weng, L., Xu, Z., Ma, J., Xu, G., Kong, X., & Hu, L. (2009). Removal of Hsf4 leads to cataract development in mice through down-regulation of γS-crystallin and Bfsp expression. *BMC Molecular Biology*, *10*, 1–14. https://doi.org/10.1186/1471-2199-10-10

Shi, Y., Mosser, D. D., & Morimoto, R. I. (1998). Molecular chaperones as HSF1-specific transcriptional repressors. *Genes and Development*, *12*(5), 654–666. https://doi.org/10.1101/gad.12.5.654

Shinkawa, T., Tan, K., Fujimoto, M., Hayashida, N., Yamamoto, K., Takaki, E., Takii, R., Prakasam, R., Inouye, S., Mezger, V., & Nakai, A. (2011). Heat shock factor 2 is required for maintaining proteostasis against febrile-range thermal stress and polyglutamine aggregation. *Molecular Biology of the Cell*, *22*(19), 3571–3583. https://doi.org/10.1091/mbc.E11-04-0330

Shutova, M. S., & Svitkina, T. M. (2018). Mammalian nonmuscle myosin II comes in three flavors. *Biochemical and Biophysical Research Communications*, *506*(2), 394–402. https://doi.org/10.1016/j.bbrc.2018.03.103

Sies, H. (2015). Redox Biology Oxidative stress : a concept in redox biology and medicine. *Redox Biology*, *4*, 180–183. https://doi.org/10.1016/j.redox.2015.01.002

Sistonen, L., Sarge, K. D., Phillips, B., Abravaya, K., & Morimoto, R. I. (1992). Activation of heat shock factor 2 during hemin-induced differentiation of human erythroleukemia cells. *Molecular and Cellular Biology*, *12*(9), 4104–4111. https://doi.org/10.1128/mcb.12.9.4104

Smith, R. S., Takagishi, S. R., Amici, D. R., Metz, K., Gayatri, S., Alasady, M. J., Wu, Y., Brockway, S., Taiberg, S. L., Khalatyan, N., Taipale, M., Santagata, S., Whitesell, L., Lindquist, S., Savas, J. N., & Mendillo, M. L. (2022). HSF2 cooperates with HSF1 to drive a transcriptional program critical for the malignant state. *Science Advances*, *8*(11), 1–15. https://doi.org/10.1126/sciadv.abj6526

Sorger, P. K., Lewis, M. J., & Pelham, H. R. B. (1987). Heat shock factor is regulated differently in yeast and HeLa cells. *Nature*, *329*(6134), 81–84. https://doi.org/10.1038/329081a0

Sorger, P. K., & Pelham, H. R. (1987). Purification and characterization of a heat-shock element binding protein from yeast. *The EMBO Journal*, *6*(10), 3035–3041. https://doi.org/10.1002/j.1460-2075.1987.tb02609.x

Sotomayor, M., Gaudet, R., & Corey, D. P. (2014). Sorting out a promiscuous superfamily: Towards cadherin connectomics. *Trends in Cell Biology*, *24*(9), 524–536. https://doi.org/10.1016/j.tcb.2014.03.007

Su, K.-H., & Dai, C. (2016). Metabolic control of the proteotoxic stress response: implications in diabetes mellitus and neurodegenerative disorders. *Cellular and Molecular Life Sciences*, *73*(22), 4231–4248. https://doi.org/10.1007/s00018-016-2291-1

Su, K., Cao, J., Tang, Z., Dai, S., He, Y., Sampson, S. B., Benjamin, I. J., & Dai, C. (2016). HSF1 critically attunes proteotoxic stress sensing by mTORC1 to combat stress and promote growth. *Nature Cell Biology*, *18*(5), 527–539. https://doi.org/10.1038/ncb3335

Su, K. H., Dai, S., Tang, Z., Xu, M., & Dai, C. (2019). Heat Shock Factor 1 Is a Direct Antagonist of AMP-Activated Protein Kinase. *Molecular Cell*, *76*(4), 546-561.e8. https://doi.org/10.1016/j.molcel.2019.08.021

Sullivan, E. K., Weirich, C. S., Guyon, J. R., Sif, S., & Kingston, R. E. (2001). Transcriptional Activation Domains of Human Heat Shock Factor 1 Recruit Human SWI/SNF. *Molecular and Cellular Biology*, *21*(17), 5826–5837. https://doi.org/10.1128/mcb.21.17.5826-5837.2001

Tafforeau, L., Zorbas, C., Langhendries, J. L., Mullineux, S. T., Stamatopoulou, V., Mullier, R., Wacheul, L., & Lafontaine, D. L. J. (2013). The complexity of human ribosome biogenesis revealed by systematic nucleolar screening of pre-rRNA processing factors. *Molecular Cell*. https://doi.org/10.1016/j.molcel.2013.08.011

Tai, C. Y., Kim, S. A., & Schuman, E. M. (2008). Cadherins and synaptic plasticity. *Current Opinion in Cell Biology*, *20*(5), 567–575. https://doi.org/10.1016/j.ceb.2008.06.003

Takada, Y., Ye, X., & Simon, S. (2007). The integrins. *Genome Biology*, *8*(5). https://doi.org/10.1186/gb-2007-8-5-215

Takaki, E., Fujimoto, M., Sugahara, K., Nakahari, T., Yonemura, S., Tanaka, Y., Hayashida, N., Inouye, S., Takemoto, T., Yamashita, H., & Nakai, A. (2006). Maintenance of Olfactory Neurogenesis Requires HSF1 , a Major Heat Shock Transcription Factor in Mice *. *Journal of Biological Chemistry*, *281*(8), 4931–4937. https://doi.org/10.1074/jbc.M506911200

Takeichi, M. (1977). Functional correlation between cell adhesive properties and some cell surface proteins. *Journal of Cell Biology*, *75*(2), 464–474. https://doi.org/10.1083/jcb.75.2.464

Takeichi, M. (1988). The cadherins: cell-cell adhesion molecules controlling animal morphogenesis. *Development*, *102*(4), 639–655. https://doi.org/10.1242/dev.102.4.639

Takeichi, M. (2007). The cadherin superfamily in neuronal connections and interactions. *Nature Reviews Neuroscience*, *8*(1), 11–20. https://doi.org/10.1038/nrn2043

Tamkun, J. W., DeSimone, D. W., Fonda, D., Patel, R. S., Buck, C., Horwitz, A. F., & Hynes, R. O. (1986). Structure of integrin, a glycoprotein involved in the transmembrane linkage between fibronectin and actin. *Cell*, *46*(2), 271–282. https://doi.org/10.1016/0092-8674(86)90744-0

Tang, V. W., & Brieher, W. M. (2012). α-Actinin-4/FSGS1 is required for Arp2/3-dependent actin assembly at the adherens junction. *Journal of Cell Biology*, *196*(1), 115–130. https://doi.org/10.1083/jcb.201103116

Tateishi, Y., Ariyoshi, M., Igarashi, R., Hara, H., Mizuguchi, K., Seto, A., Nakai, A., Kokubo, T., Tochio, H., & Shirakawa, M. (2009). Molecular basis for SUMOylation-dependent regulation of DNA binding activity of heat shock factor 2. *Journal of Biological Chemistry*, *284*(4), 2435–2447. https://doi.org/10.1074/jbc.M806392200

Teo, J. L., Parton, R. G., & Yap, A. S. (2019). The membrane environment of cadherin adhesion receptors: A working hypothesis. *Biochemical Society Transactions*, *47*(4), 985–995. https://doi.org/10.1042/BST20180012

Terry, L. J., Shows, E. B., & Wente, S. R. (2007). Crossing the nuclear envelope: Hierarchical regulation of nucleocytoplasmic transport. *Science*, *318*(5855), 1412–1416. https://doi.org/10.1126/science.1142204

Tessari, A., Salata, E., Ferlin, A., Bartoloni, L., Slongo, M. L., & Foresta, C. (2004). Characterization of HSFY, a novel AZFb gene on the Y chromosome with a possible role in human spermatogenesis. *Molecular Human Reproduction*, *10*(4), 253–258. https://doi.org/10.1093/molehr/gah036

Theocharis, A. D., Skandalis, S. S., Gialeli, C., & Karamanos, N. K. (2016). Extracellular matrix structure. *Advanced Drug Delivery Reviews*, *97*, 4–27. https://doi.org/10.1016/j.addr.2015.11.001

Tissiéres, A., Mitchell, H. K., & Tracy, U. M. (1974). Protein synthesis in salivary glands of Drosophila melanogaster: Relation to chromosome puffs. *Journal of Molecular Biology*, *84*(3), 389–398. https://doi.org/10.1016/0022-2836(74)90447-1

Tumbarello, D. A., Brown, M. C., & Turner, C. E. (2002). The paxillin LD motifs. *FEBS Letters*, *513*(1), 114–118. https://doi.org/10.1016/S0014-5793(01)03244-6

Turley, T. N., Theis, J. L., Sundsbak, R. S., Evans, J. M., O'Byrne, M. M., Gulati, R., Tweet, M. S., Hayes, S. N., & Olson, T. M. (2019). Rare Missense Variants in TLN1 Are Associated With Familial and Sporadic Spontaneous Coronary Artery Dissection. *Circulation: Genomic and Precision Medicine*, *12*(4), 1–17. https://doi.org/10.1161/CIRCGEN.118.002437

Ulbricht, A., Eppler, F. J., Tapia, V. E., Van Der Ven, P. F. M., Hampe, N., Hersch, N., Vakeel, P., Stadel, D., Haas, A., Saftig, P., Behrends, C., Fürst, D. O., Volkmer, R., Hoffmann, B., Kolanus, W., & Höhfeld, J. (2013). Cellular mechanotransduction relies on tension-induced and chaperone-assisted autophagy. *Current Biology*, *23*(5), 430–435. https://doi.org/10.1016/j.cub.2013.01.064

Vicente-Manzanares, M., & Horwitz, A. R. (2011). Adhesion dynamics at a glance. *Journal of Cell Science*, *124*(23), 3923–3927. https://doi.org/10.1242/jcs.095653

Vihervaara, A., Sergelius, C., Vasara, J., Blom, M. A. H., Elsing, A. N., Roos-Mattjus, P., & Sistonen, L. (2013). Transcriptional response to stress in the dynamic chromatin environment of cycling and mitotic cells. *Proceedings of the National Academy of Sciences of the United States of America*, *110*(36). https://doi.org/10.1073/pnas.1305275110

Wagner, S. A., Beli, P., Weinert, B. T., Nielsen, M. L., Cox, J., Mann, M., & Choudhary, C. (2011). A Proteome-wide, Quantitative Survey of In Vivo Ubiquitylation Sites Reveals Widespread Regulatory Roles. *Molecular & Cellular Proteomics*, *10*(10), M111.013284. https://doi.org/10.1074/mcp.m111.013284

Wang, G., Ying, Z., Jin, X., Tu, N., Zhang, Y., Phillips, M., Moskophidis, D., & Mivechi, N. F. (2004). Essential Requirement for Both hsf1 and hsf2 Transcriptional Activity in Spermatogenesis and Male Fertility. *Genesis*, *38*(2), 66–80. https://doi.org/10.1002/gene.20005

Wang, G., Zhang, J., Moskophidis, D., & Mivechi, N. F. (2003). Targeted disruption of the heat shock transcription factor (hsf)-2 gene results in increased embryonic lethality, neuronal defects, and reduced spermatogenesis. *Genesis*, *36*(1), 48–61. https://doi.org/10.1002/gene.10200

Wang, P., Ballestrem, C., & Streuli, C. H. (2011). The C terminus of talin links integrins to cell cycle progression. *Journal of Cell Biology*, *195*(3), 499–513. https://doi.org/10.1083/jcb.201104128

Wang, S., Osgood, A. O., & Chatterjee, A. (2022). Uncovering post-translational modification-associated protein – protein interactions. *Current Opinion in Structural Biology*, *74*, 102352. https://doi.org/10.1016/j.sbi.2022.102352

WEISS, P. (1947). The problem of specificity in growth and development. *The Yale Journal of Biology and Medicine*, *19*(3), 235–278. https://doi.org/10.1016/b978-1-4832-2919-5.50016-7

Wente, S. R., & Rout, M. P. (2010). The Nuclear Pore Complex and Nuclear Transport. *Cold Spring Harbor Perspectives in Biology*, *2*(10), a000562–a000562. https://doi.org/10.1101/cshperspect.a000562

Westerheide, S. D., Anckar, J., Stevens, S. M., Sistonen, L., & Morimoto, R. I. (2009). Stress-inducible regulation of heat shock factor 1 by the deacetylase SIRT. *Science*, *323*(5917), 1063–1066. https://doi.org/10.1126/science.1165946

Wickström, S. A., & Niessen, C. M. (2018). Cell adhesion and mechanics as drivers of tissue organization and differentiation: local cues for large scale organization. *Current Opinion in Cell Biology*, *54*, 89–97. https://doi.org/10.1016/j.ceb.2018.05.003

Wiederrecht, G., Shuey, D. J., Kibbe, W. A., & Parker, C. S. (1987). The saccharomyces and Drosophila heat shock transcription factors are identical in size and DNA binding properties. *Cell*, *48*(3), 507–515. https://doi.org/10.1016/0092-8674(87)90201-7

Wu, C. (1995). HEAT SHOCK TRANSCRIPTION FACTORS : Structure and Regulation translocation. *Annual Review of Cell and Developmental Biology*, *11*, 441–469.

Wylie, D. E., Damsky, C. H., & Buck, C. A. (1979). Studies on the function of cell surface glycoproteins. I. Use of antisera to surface membranes in the identification of membrane components relevant to cell-substrate adhesion. *The Journal of Cell Biology*, *80*(2), 385–402. https://doi.org/10.1083/jcb.80.2.385

Xavier da Silveira dos Santos, A., & Liberali, P. (2019). From single cells to tissue self-organization. *FEBS Journal*, *286*(8), 1495–1513. https://doi.org/10.1111/febs.14694

Xiao, X. Z., Zuo, X. X., Davis, A. A., McMillan, D. R., Curry, B. B., Richardson, J. A., & Benjamin, I. J. (1999). HSF1 is required for extra-embryonic development, postnatal growth and protection during inflammatory responses in mice. *EMBO Journal*, *18*(21), 5943–5952. https://doi.org/10.1093/emboj/18.21.5943

Xu, L., Ma, X., Bagattin, A., & Mueller, E. (2016). The transcriptional coactivator PGC1α protects against hyperthermic stress via cooperation with the heat shock factor HSF1. *Cell Death and Disease*, *7*(2), 1–9. https://doi.org/10.1038/cddis.2016.22

Yan, B., Calderwood, D. A., Yaspan, B., & Ginsberg, M. H. (2001). Calpain Cleavage Promotes Talin Binding to the β3 Integrin Cytoplasmic Domain. *Journal of Biological Chemistry*, *276*(30), 28164–28170. https://doi.org/10.1074/jbc.M104161200

Yang, L.-N., Ning, Z.-Y., Wang, L., Yan, X., & Meng, Z.-Q. (2019). HSF2 regulates aerobic glycolysis by suppression of FBP1 in hepatocellular carcinoma. *Am J Cancer Res*, *9*(8), 1607–1621. www.ajcr.us/

Yao, M., Goult, B. T., Klapholz, B., Hu, X., Toseland, C. P., Guo, Y., Cong, P., Sheetz, M. P., & Yan, J. (2016). The mechanical response of talin. *Nature Communications*, *May*. https://doi.org/10.1038/ncomms11966

Ye, X., McLean, M. A., & Sligar, S. G. (2016). Phosphatidylinositol 4,5-Bisphosphate Modulates the Affinity of Talin-1 for Phospholipid Bilayers and Activates Its Autoinhibited Form. *Biochemistry*, *55*(36), 5038–5048. https://doi.org/10.1021/acs.biochem.6b00497

Yulis, M., Kusters, D. H. M., & Nusrat, A. (2018). Cadherins: cellular adhesive molecules serving as signalling mediators. *Journal of Physiology*, *596*(17), 3883–3898. https://doi.org/10.1113/JP275328

Zacharchenko, T., Qian, X., Goult, B. T., Jethwa, D., Almeida, T. B., Ballestrem, C., Critchley, D. R., Lowy, D. R., & Barsukov, I. L. (2016). LD Motif Recognition by Talin: Structure of the Talin-DLC1 Complex. *Structure*, *24*(7), 1130–1141. https://doi.org/10.1016/j.str.2016.04.016

Zhang, F., Saha, S., & Kashina, A. (2012). Arginylation-dependent regulation of a proteolytic product of talin is essential for cell-cell adhesion. *Journal of Cell Biology*, *197*(6), 819–836. https://doi.org/10.1083/jcb.201112129

Zhang, X., Jiang, G., Cai, Y., Monkley, S. J., Critchley, D. R., & Sheetz, M. P. (2008). Talin depletion reveals independence of initial cell spreading from integrin activation and traction. *Nature Cell Biology*, *10*(9), 1062–1068. https://doi.org/10.1038/ncb1765

Zheng, H. C., & Jiang, H. M. (2022). Shuttling of cellular proteins between the plasma membrane and nucleus (Review). *Molecular Medicine Reports*, *25*(1), 1–12. https://doi.org/10.3892/mmr.2021.12530

Zheng, X., Krakowiak, J., Patel, N., Beyzavi, A., Ezike, J., Khalil, A. S., & Pincus, D. (2016). Dynamic control of Hsf1 during heat shock by a chaperone switch and phosphorylation. *ELife*, *5*(November), 1–26. https://doi.org/10.7554/eLife.18638

Zihni, C., Mills, C., Matter, K., & Balda, M. S. (2016). Tight junctions: from simple barriers to multifunctional molecular gates. *Nature Reviews Molecular Cell Biology*, *17*(9), 564–580. https://doi.org/10.1038/nrm.2016.80

Zou, D. J., Chesler, A., & Firestein, S. (2009). How the olfactory bulb got its glomeruli: A just so story? *Nature Reviews Neuroscience*, *10*(8), 611–618. https://doi.org/10.1038/nrn2666

Zou, J., Guo, Y., Guettouche, T., Smith, D. F., & Voellmy, R. (1998). Repression of heat shock transcription factor HSF1 activation by HSP90 (HSP90 complex) that forms a stress-sensitive complex with HSF1. *Cell*, *94*(4), 471–480. https://doi.org/10.1016/S0092-8674(00)81588-3

Original Publications and Manuscripts

Article

Cell Reports

Heat Shock Factor 2 Protects against Proteotoxicity by Maintaining Cell-Cell Adhesion

Graphical Abstract

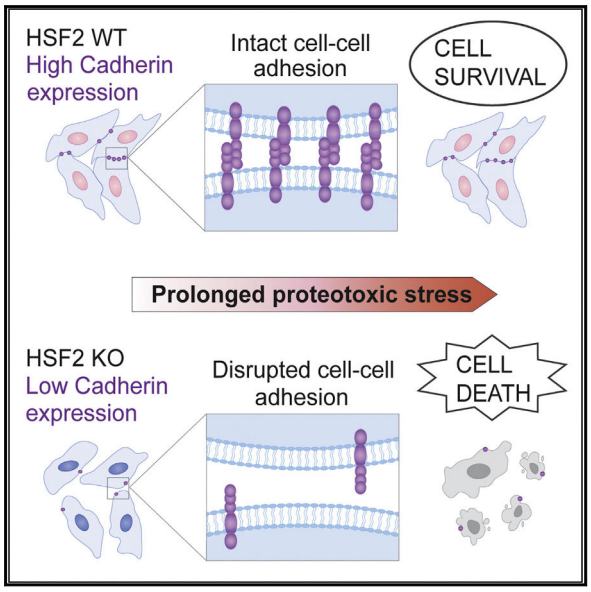

Highlights

- HSF2 is required to maintain cell-cell adhesion
- HSF2 deficiency leads to downregulation of cadherin superfamily genes
- Impaired cell-cell adhesion sensitizes cells to prolonged proteotoxic stress
- Cadherin-mediated cell-cell adhesion is a survival determinant upon proteotoxicity

Authors

Jenny Joutsen, Alejandro Jose Da Silva, Jens Christian Luoto, ..., Délara Sabéran-Djoneidi, Eva Henriksson, Lea Sistonen

Correspondence

lea.sistonen@abo.fi

In Brief

Joutsen et al. show that heat shock factor 2 (HSF2) is essential for cell survival during prolonged proteotoxicity. Lack of HSF2 leads to marked misregulation of cadherin superfamily genes and functional impairment of cell-cell adhesion. Cell-cell adhesion is found to be a key determinant of proteotoxic stress resistance.

Joutsen et al., 2020, Cell Reports *30*, 583–597
January 14, 2020
https://doi.org/10.1016/j.celrep.2019.12.037

CellPress

Cell Reports
Article

OPEN ACCESS
CellPress

Heat Shock Factor 2 Protects against Proteotoxicity by Maintaining Cell-Cell Adhesion

Jenny Joutsen,[1,2,7] Alejandro Jose Da Silva,[1,2,7] Jens Christian Luoto,[1,2] Marek Andrzej Budzynski,[1,2] Anna Serafia Nylund,[1,2] Aurelie de Thonel,[3,4,5] Jean-Paul Concordet,[6] Valérie Mezger,[3,4,5] Délara Sabéran-Djoneidi,[3,4,5] Eva Henriksson,[1,2] and Lea Sistonen[1,2,8,*]

[1]Faculty of Science and Engineering, Cell Biology, Åbo Akademi University, Tykistökatu 6, 20520 Turku, Finland
[2]Turku Bioscience Centre, University of Turku and Åbo Akademi University, Tykistökatu 6, 20520 Turku, Finland
[3]CNRS, UMR 7216 "Epigenetic and Cell Fate," 75250 Paris Cedex 13, France
[4]University of Paris Diderot, Sorbonne Paris Cité, 75250 Paris Cedex 13, France
[5]Département Hospitalo-Universitaire DHU PROTECT, Paris, France
[6]INSERM U1154, CNRS UMR 7196, Muséum National d'Histoire Naturelle, Paris, France
[7]These authors contributed equally
[8]Lead Contact
*Correspondence: lea.sistonen@abo.fi
https://doi.org/10.1016/j.celrep.2019.12.037

SUMMARY

Maintenance of protein homeostasis, through inducible expression of molecular chaperones, is essential for cell survival under protein-damaging conditions. The expression and DNA-binding activity of heat shock factor 2 (HSF2), a member of the heat shock transcription factor family, increase upon exposure to prolonged proteotoxicity. Nevertheless, the specific roles of HSF2 and the global HSF2-dependent gene expression profile during sustained stress have remained unknown. Here, we found that HSF2 is critical for cell survival during prolonged proteotoxicity. Strikingly, our RNA sequencing (RNA-seq) analyses revealed that impaired viability of HSF2-deficient cells is not caused by inadequate induction of molecular chaperones but is due to marked downregulation of cadherin superfamily genes. We demonstrate that HSF2-dependent maintenance of cadherin-mediated cell-cell adhesion is required for protection against stress induced by proteasome inhibition. This study identifies HSF2 as a key regulator of cadherin superfamily genes and defines cell-cell adhesion as a determinant of proteotoxic stress resistance.

INTRODUCTION

The cells in a human body are constantly exposed to environmental stressors, which challenge the maintenance of protein homeostasis, also called proteostasis. To survive insults that disturb proteostasis, cells rely on a selection of protective mechanisms that can be launched upon stress exposures. The heat shock response is a well-conserved stress protective pathway that is induced in response to cytosolic protein damage and mediated by heat shock transcription factors (HSFs; Joutsen and Sistonen, 2019). Upon activation, HSFs oligomerize, accumulate in the nucleus, and bind to their target heat shock elements (HSEs) at multiple genomic loci (Vihervaara et al., 2013, 2017; Mahat et al., 2016). The canonical HSF target genes encode molecular chaperones, such as heat shock proteins (HSPs), which assist in the maintenance of a correct protein folding environment by refolding the misfolded proteins or directing them to protein degradation machineries (Hartl et al., 2011). In addition, HSFs are important in a variety of other physiological and pathological processes and the repertoire of HSF target genes has been shown to extend beyond the HSPs (Hahn et al., 2004; Åkerfelt et al., 2010; Gonsalves et al., 2011; Mendillo et al., 2012; Riva et al., 2012; Björk et al., 2016; Li et al., 2016).

The human genome encodes six HSF family members (HSF1, HSF2, HSF4, HSF5, HSFX, and HSFY), of which HSF1 and HSF2 are the most extensively studied (Joutsen and Sistonen, 2019). Although these factors are homologous in their DNA-binding domains, they share only a few similarities in the tissue expression patterns, regulatory mechanisms, and signals that stimulate their activity (Jaeger et al., 2016; Gomez-Pastor et al., 2018). HSF1 is essential for HSP expression and cell survival under acute stress conditions (Joutsen and Sistonen, 2019). HSF2 is an unstable protein and its expression is highly context dependent, fluctuating in different cell and tissue types (Sarge et al., 1991; Alastalo et al., 1998), developmental stages (Mezger et al., 1994; Rallu et al., 1997), and during the cell cycle (Elsing et al., 2014). Consequently, regulation of HSF2 protein levels has been considered to be the main determinant of its DNA-binding capacity (Mathew et al., 1998; Budzyński and Sistonen, 2017). Interestingly, the DNA-binding activity of HSF2 increases in cells exposed to lactacystin- or MG132-induced proteasome inhibition (Kawazoe et al., 1998; Mathew et al., 1998; Pirkkala et al., 2000), indicating that HSF2 can respond to proteostasis disruption. Nevertheless, the molecular details of the activation mechanisms of HSF2 are currently not conclusively understood.

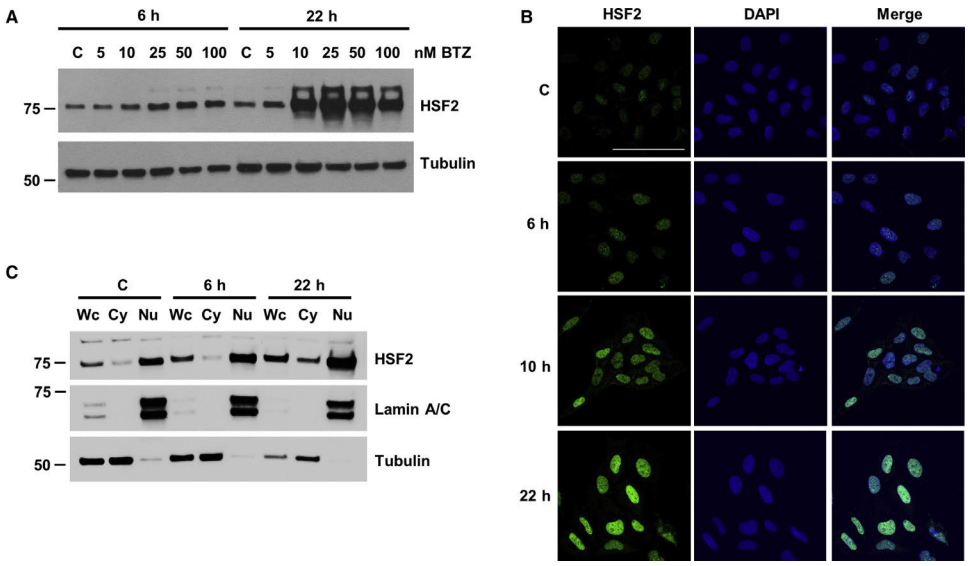

Figure 1. HSF2 Is Upregulated upon Prolonged Bortezomib (BTZ) Treatment

(A) Immunoblot analysis of HSF2 expression. U2OS WT cells were treated with indicated concentrations of BTZ for 6 or 22 h. Control (C) cells were treated with DMSO. Tubulin was used as a loading control.

(B) Confocal microscopy images of HSF2 immunofluorescence staining. U2OS WT cells were plated on coverslips and treated with 25 nM BTZ for 6, 10, or 22 h. Control cells were treated with DMSO. Samples were fixed and stained with anti-HSF2 antibody. DAPI was used for DNA detection. The overlay of HSF2 and DAPI maximum intensity projection signals is shown in merge. Scale bar, 100 μm.

(C) Immunoblot analysis of HSF2 in subcellular fractions. U2OS WT cells were treated with 25 nM BTZ for 6 and 22 h. Control cells were treated with DMSO. Wc, whole cell fraction; Cy, cytoplasmic fraction; and Nu, nuclear fraction. Lamin A/C and Tubulin were used as fractionation controls.

The ubiquitin-proteasome system is one of the main cellular mechanisms regulating protein turnover, thereby affecting multiple aspects of cell physiology, such as signal transduction and apoptosis (Hershko and Ciechanover, 1998; Varshavsky, 2012). Due to the fundamental function in cell physiology, the proteasome complex has emerged as an important target for anti-cancer therapy (Deshaies, 2014). The most common drug to inhibit proteasome function is bortezomib (BTZ; PS-341, VELCADE), which is currently used as a standard treatment in hematological malignancies (Chen et al., 2011). BTZ is a dipeptide boronic acid derivative that targets the chymotrypsin-like activity of the 26S proteasome, causing progressive accumulation of damaged proteins (Kisselev et al., 2006; Chen et al., 2011; Goldberg, 2012). By exposing human blood-derived primary cells to clinically relevant concentrations of BTZ, Rossi and colleagues demonstrated that prolonged proteasome inhibition results in upregulation of HSF2 at both mRNA and protein levels (Rossi et al., 2014). They also showed that HSF2, together with HSF1, localizes to the promoters of *HSP70* and *AIRAP* (zinc finger AN1-type domain 2a) genes (Rossi et al., 2014). In another study, sensitivity to proteasome inhibition was linked to HSF2 deficiency in mouse embryonic fibroblasts (Lecomte et al., 2010), but the mechanisms by which HSF2 promotes cell survival are currently unknown.

In this study, we show that HSF2 is critical for survival of cells during prolonged proteasome inhibition. To our surprise, the genome-wide expression analyses revealed that HSF2 disruption results in a profound downregulation of genes belonging to the cadherin superfamily and subsequent functional impairment of cell-cell adhesion. Furthermore, we show that failure to form adequate cadherin-mediated cell-cell adhesion contacts predisposes cells to proteasome inhibition-induced cell death. These results identify HSF2 as a key regulator of cadherin genes. Taken together, we show that by maintaining cadherin-mediated cell-cell adhesion, HSF2 acts as an important pro-survival factor during sustained proteotoxic stress.

RESULTS

U2OS Cells Lacking HSF2 Are Predisposed to BTZ-Induced Proteotoxicity

To explore the role of HSF2 in prolonged proteotoxic stress, we first examined the expression and cellular localization of HSF2 during BTZ treatment. Human osteosarcoma U2OS cells were treated with different concentrations of BTZ (0–100 nM) for 6 or 22 h and HSF2 protein levels were examined with immunoblotting. The time points were selected to assess both the

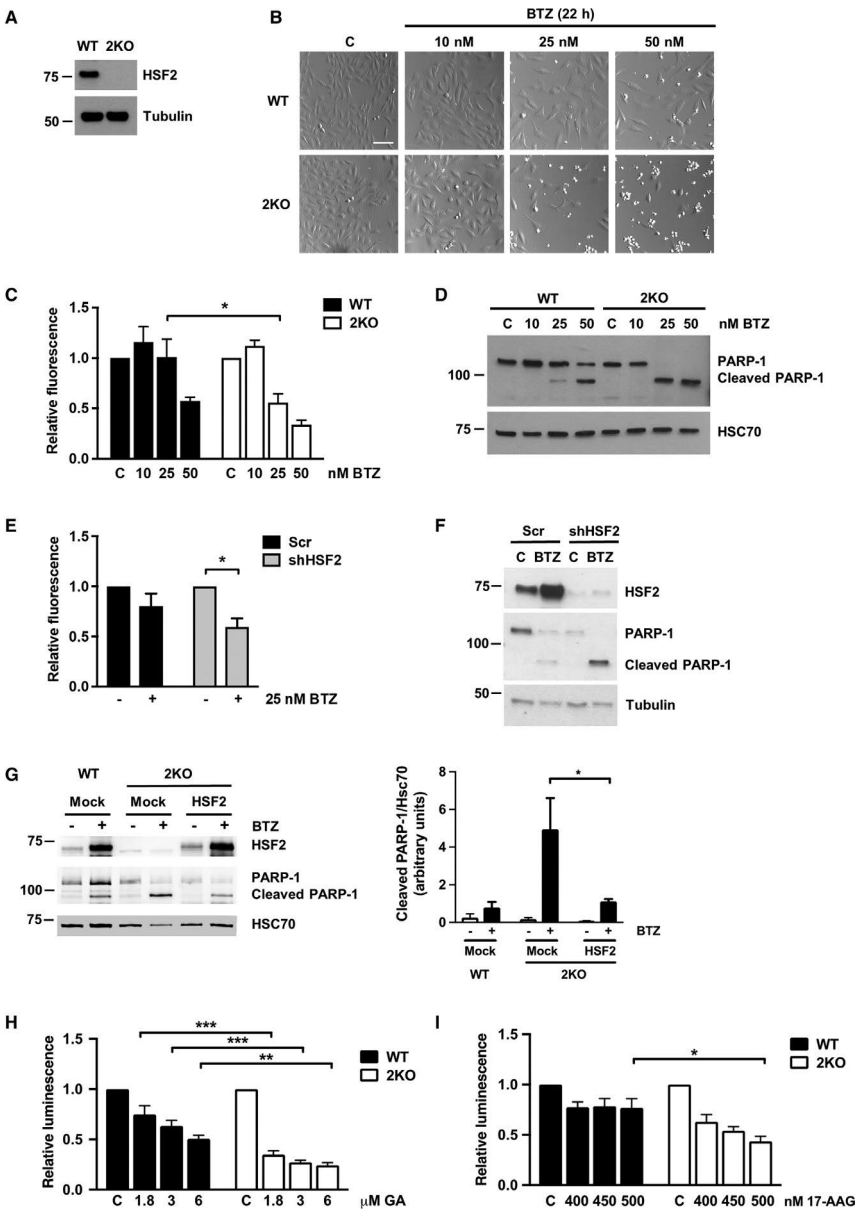

(legend on next page)

short-term and the long-term exposure to BTZ. HSF2 was slightly upregulated already at the 6-h time point and at 22 h its expression was highly elevated (Figure 1A), which is in agreement with a previous report (Rossi et al., 2014). Indirect immunofluorescence and analysis of distinct subcellular fractions revealed that HSF2, which is known to be both cytoplasmic and nuclear (Sheldon and Kingston, 1993; Sistonen et al., 1994), resides predominantly in the nucleus already under control conditions and the nuclear localization is further enhanced during BTZ treatment (Figures 1B and 1C). These results show that cells respond to BTZ treatment with marked increases in HSF2 levels and accumulation in the nucleus.

Next, we asked if HSF2 is required for cell survival under sustained stress conditions. We generated a U2OS *HSF2* knockout cell line (2KO hereafter), where HSF2 expression was abolished by mutating the first exon of the *HSF2* gene using the CRISPR-Cas9 method. In these cells, the protein expression of HSF2 was completely abrogated (Figure 2A). U2OS WT and 2KO cells were treated with indicated concentrations of BTZ for 22 h and examined with microscopy. We observed a dramatic difference in the viability of the wild-type (WT) and 2KO cells, since the cells lacking HSF2 exhibited an apoptotic non-adherent phenotype in concentrations where the WT cells remained adherent (Figure 2B). Quantitative cell viability measurements confirmed that the survival of 2KO cells was significantly impaired upon BTZ treatment (Figure 2C). Furthermore, 2KO cells accumulated more cleaved PARP-1 than WT cells, demonstrating a more pronounced activation of apoptosis (Ling et al., 2002) (Figure 2D). Similar results were obtained with another *HSF2* knockout cell line (2KO#2 hereafter) (Figure S1A) and with *Hsf2*$^{-/-}$ MEFs (mouse embryonic fibroblasts) (Figures S1B and S1C), confirming that the observations are not cell type specific. To verify that the decreased survival of 2KO cells was not caused by off-target effects of the CRISPR-Cas9 gene editing method, we transfected the U2OS WT cells with scramble (Scr) or HSF2-targeting short hairpin RNA (shRNA) plasmids and treated the cells with BTZ for 22 h. In accordance with the results obtained with 2KO cells, transient HSF2 downregulation significantly reduced cell viability upon BTZ treatment and enhanced the progression of apoptosis, which was detected by increased accumulation of cleaved PARP-1 (Figures 2E and 2F). In contrast, re-introduction of HSF2 to the 2KO cells resulted in significantly less cleaved PARP-1 than in the Mock-transfected cells after BTZ treatment (Figure 2G). Hence, we conclude that HSF2 is essential for cell survival upon proteotoxic stress.

In addition to BTZ, treatments with MG132, a well-established proteasome inhibitor, and amino acid analog L-canavanine, which causes protein misfolding when incorporated into nascent peptide chains, clearly reduced the viability of HSF2-deficient cells (Figures S1D–S1H). Importantly, when we exposed the cells to even more extended proteotoxic stress of 46 h, induced by HSP90 inhibitor drugs (Geldanamycin, 17-AAG), the HSF2-deficient cells exhibited reduced survival (Figures 2H and 2I). Altogether these results demonstrate that HSF2 is critical for cell survival upon prolonged accumulation of damaged proteins.

In contrast to HSF2, which has been found to be downregulated in a subset of human cancers (Björk et al., 2016), the expression, nuclear accumulation, and transcriptional activity of HSF1 are increased in a majority of studied cancer types (Björk et al., 2018; Gomez-Pastor et al., 2018). Phosphorylation of serine 326 (pS326) in HSF1 is considered to be a marker for its activation (Guettouche et al., 2005; Mendillo et al., 2012). HSF1 expression and pS326 have been established as requirements for multiple myeloma cell survival during BTZ treatment (Shah et al., 2016). Therefore, we examined whether the decreased survival of 2KO cells was due to impaired HSF1 expression or phosphorylation upon proteasome inhibition. U2OS WT and 2KO cells were treated with BTZ or MG132, and the HSF1 protein levels and S326 phosphorylation status were analyzed with immunoblotting. Importantly, no difference in HSF1 expression or S326 phosphorylation between WT and 2KO cells was observed upon proteasome inhibition (Figure S1I). These results demonstrate that although HSF1 is an essential survival factor during acute stress (Gomez-Pastor et al., 2018), it alone is not sufficient to protect cells against prolonged proteotoxicity.

Figure 2. HSF2 Is Required for Cell Survival upon Prolonged Bortezomib (BTZ) Treatment

(A) Immunoblot analysis of HSF2 expression in U2OS WT and HSF2 KO (2KO) cells. Tubulin was used as a loading control.

(B) Bright-field microscopy images of WT and 2KO cells treated with indicated concentrations of BTZ for 22 h. Control cells were treated with DMSO. Scale bar, 100 μm.

(C) Calcein AM assay of WT and 2KO cells treated as in (B). Relative fluorescence was calculated against each respective control that was set to 1. The data are presented as mean values of at least three independent experiments + SEM; *$p < 0.05$.

(D) Immunoblot analysis of PARP-1. Cells were treated as in (B). HSC70 was used as a loading control.

(E) Calcein AM assay of U2OS WT cells transfected with Scr or HSF2-targeting shRNA constructs (Östling et al., 2007) and treated with 25 nM BTZ for 22 h. Relative fluorescence was calculated against each respective control that was set to 1. The data are presented as mean values of three independent experiments + SEM; *$p < 0.05$.

(F) Immunoblot analysis of HSF2 and PARP-1. Cells were transfected and treated as in (E). Tubulin was used as a loading control.

(G) Immunoblot analysis of HSF2 and PARP-1. HSF2 levels in U2OS 2KO cells were restored to those in WT cells by transiently transfecting the cells with either Mock or HSF2 encoding plasmids. Cells were treated with 25 nM BTZ for 22 h. Control cells were treated with DMSO. HSC70 was used as a loading control. The amount of cleaved PARP-1 relative to HSC70 was quantified with ImageJ. The data are presented as mean values of three independent experiments + SEM; *$p < 0.05$.

(H) CellTiter-Glo assay of U2OS WT and 2KO cells treated with indicated concentrations of Geldanamycin (GA) for 46 h. Control cells were treated with DMSO. Relative luminescence was calculated against each control that was set to 1. The data are presented as mean values of three independent experiments + SEM; **$p < 0.01$ and ***$p < 0.001$.

(I) CellTiter-Glo assay of U2OS WT and 2KO cells treated with indicated concentrations of 17-AAG for 46 h. Control cells were treated with DMSO. Relative luminescence was calculated against each control that was set to 1. The data are presented as mean values of three independent experiments + SEM; *$p < 0.05$. See also Figure S1.

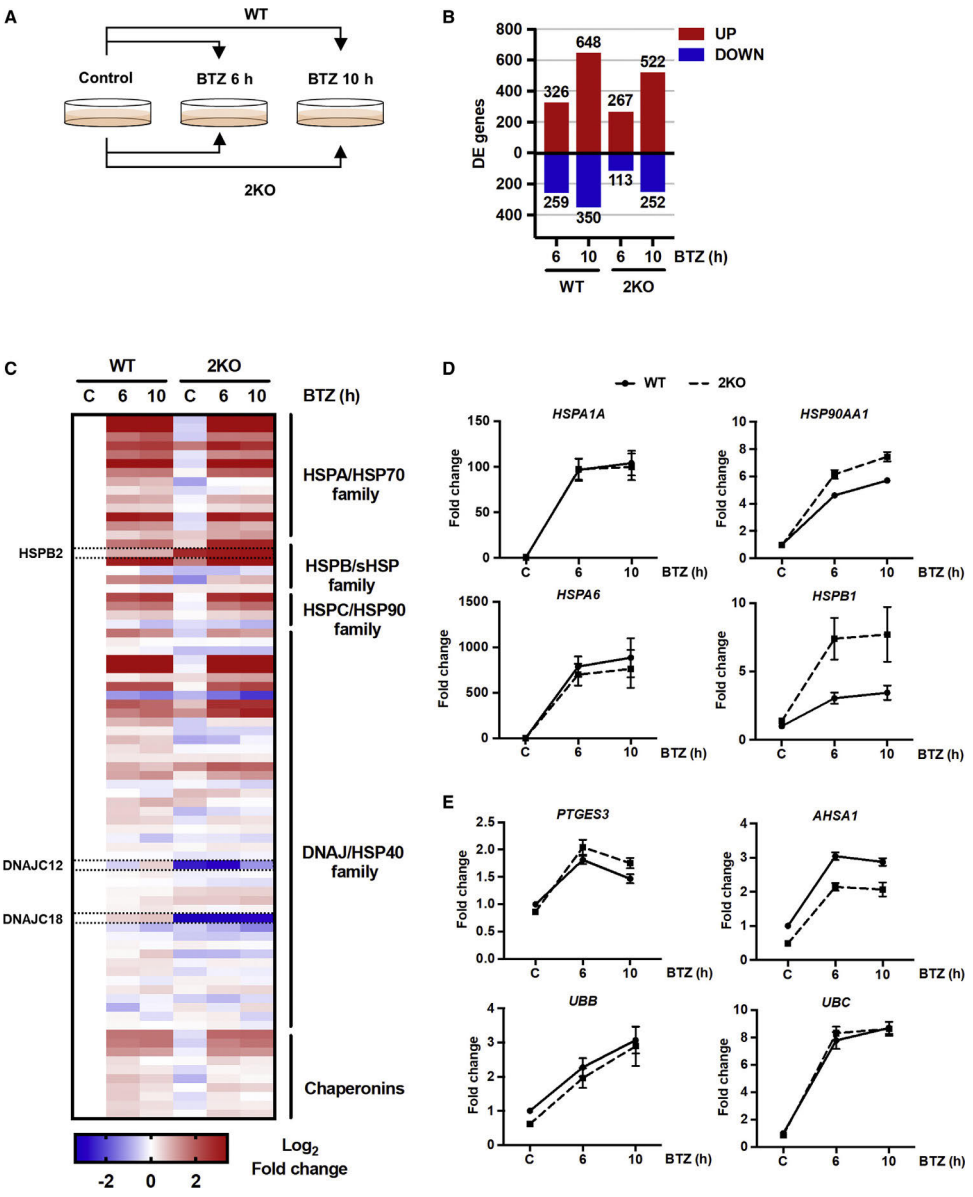

(legend on next page)

Induction of Heat Shock Response Is Not Sufficient to Protect Cells against Proteotoxicity

Similarly to many other surveillance transcription factors, such as p53 (Kubbutat et al., 1997), HIF-1α (Kallio et al., 1999), and Nrf2 (Kobayashi et al., 2004), HSF2 is an unstable protein under normal growth conditions (Ahlskog et al., 2010). HSF2 expression fluctuates in response to stress exposure, tumor progression, and during the cell cycle (Ahlskog et al., 2010: Elsing et al., 2014; Björk et al., 2016), and high expression levels of HSF2 correlate with its increased DNA-binding activity (Mathew et al., 1998; Sarge et al., 1994). Due to the massive increase in nuclear HSF2 levels upon BTZ treatment (Figures 1B and 1C), we investigated if the impaired survival of 2KO cells was caused by misregulation of HSF2 target genes. U2OS WT and 2KO cells were treated with 25 nM BTZ for 6 or 10 h (Figure 3A), and the global gene expression profiles were analyzed with RNA-seq. It is important to note that the selected time points represent sub-lethal proteotoxic stress conditions, at which the cell viability is not yet compromised (Figure S2A). Before mRNA purification, the knockout phenotype was confirmed with immunoblotting (Figure S2B). Stress-inducible hyperphosphorylation of HSF1 (Sarge et al., 1993) and increased HSP70 expression were observed in both WT and 2KO cells (Figure S2B). To identify the HSF2-dependent target genes, we first compared the inducible gene expression profiles between WT and 2KO cells in response to BTZ treatment for 6 and 10 h (Figure 3A). Differentially expressed (DE) genes were determined with the Bioconductor R package Limma (Ritchie et al., 2015), with fold change $\geq$3 and false discovery rate (FDR) <0.001, from quadruplet samples that correlated well to each other (Figure S2C). According to the analysis, BTZ treatment resulted in a significant upregulation and downregulation of genes in WT (>600 and >300, respectively) and 2KO (>500 and >200, respectively) cells (Figure 3B; Table S1). The complete dataset is available at Gene Expression Omnibus under GEO: GSE115973.

The HSF-regulated heat shock response is one of the main cellular survival pathways induced by proteotoxic stress (Joutsen and Sistonen, 2019), and it is characterized by simultaneous upregulation of genes essential for maintaining the correct protein folding environment (Vihervaara et al., 2018). To examine whether the impaired survival of 2KO cells is caused by a compromised heat shock response, we analyzed the inducible expression patterns of all human molecular chaperone genes (Kampinga et al., 2009), in WT and 2KO cells treated with BTZ. Intriguingly, the chaperone expression profiles of WT and 2KO cells were nearly identical, and only *HSPB2*, *DNAJC12*, and *DNAJC18* exhibited distinct expression patterns in 2KO cells (Figure 3C). A closer examination of the RNA-seq data for the expression of selected chaperone genes, i.e., *HSPA1A* (HSP70), *HSP90AA1* (HSP90), *HSPA6* (HSP70B′), and *HSPB1* (HSP27), revealed equal or even higher expression levels in 2KO cells than in WT cells (Figure 3D). In response to proteotoxic stress, HSF2 also localizes to the promoters of genes encoding HSP90 co-chaperones and polyubiquitin (Vihervaara et al., 2013). To study whether the regulation of these genes was disturbed in 2KO cells, HSP90 co-chaperones *PTGES3* (p23) and *AHSA1* (AHA1), as well as the polyubiquitin genes *UBB* and *UBC*, were examined from our RNA-seq data. Since no significant differences were observed in the expression patterns of any of these genes (Figure 3E), we conclude that despite the intact heat shock response, the 2KO cells were not protected against proteotoxic stress. These findings indicate that other determinants, beyond molecular chaperones, govern cell survival during prolonged proteotoxicity.

Disruption of HSF2 Leads to Misregulation of Cell-Adhesion-Associated Genes

To determine the differentially expressed genes between the WT and 2KO cells, we examined the 2KO:WT comparison pair at each experimental time point (0, 6, and 10 h) (Figure 4A). Using the stringent cutoff criteria (fold change [FC] $\geq$ 3; FDR 0.001), 2KO cells were found to display significant misregulation of 819 genes already under normal growth conditions (2KO, C; WT, C), and the proportion of upregulated and downregulated genes remained similar throughout the BTZ treatments (2KO, 6 h; WT, 6 h: 2KO, 10 h; 2KO, 10 h) (Figure 4B; Table S1). Gene Ontology (GO) term analysis of the misregulated genes revealed a specific enrichment of terms related to cell adhesion and cell-cell adhesion via plasma membrane adhesion molecules (Figure 4C; Table S1). Similar GO terms among the comparison pairs implied that the genes misregulated in 2KO cells are tightly linked to cellular adhesion properties both under control and stress conditions (Figure 4C).

To identify the adhesion molecules that are abnormally expressed in 2KO cells under both control and stress conditions, the gene set overlaps were examined with Venn diagrams. Among the comparison pairs, a total of 114 and 277 genes were upregulated and downregulated, respectively (Figure 4D). Functional cluster annotation of the 114 upregulated genes with the DAVID analysis tool (Dennis et al., 2003) confirmed

Figure 3. Induction of the Heat Shock Response Is Not Sufficient to Protect HSF2-Deficient Cells against BTZ-Induced Proteotoxic Stress

(A) A schematic overview of the RNA-seq experiment outline. U2OS WT and 2KO cells were treated with 25 nM BTZ for 6 or 10 h. Control cells were treated with DMSO. After treatments, mRNA was extracted and analyzed by RNA-seq. Experiments were performed in biological quadruplets. The arrows depict comparison pairs.

(B) Differentially expressed (DE) genes in each comparison pair were determined with the Bioconductor R package Limma (Ritchie et al., 2015) (FC $\geq$ 3; FDR < 0.001). The upregulated and downregulated genes in a given comparison pair are indicated with red and blue bars, respectively.

(C) Normalized gene expression data for human heat shock proteins, as defined in Kampinga et al. (2009), was used to calculate the fold change of each gene in relation WT control sample. The data are presented as a heatmap of $\log_2$-transformed values and were generated with GraphPad Prism7. Examples of genes that exhibit a divergent expression pattern are framed.

(D and E) mRNA expression levels of selected heat shock proteins (*HSPA1A*, *HSP90AA1*, *HSPA6*, and *HSPB1)* (D), HSP90 co-chaperones (*PTGES3* and *AHSA1*), and stress-responsive ubiquitin genes (*UBB* and *UBC*) (E) determined with RNA-seq. The data are presented as mean values ± SEM relative to WT control sample that was set to 1.

See also Figure S2 and Table S1.

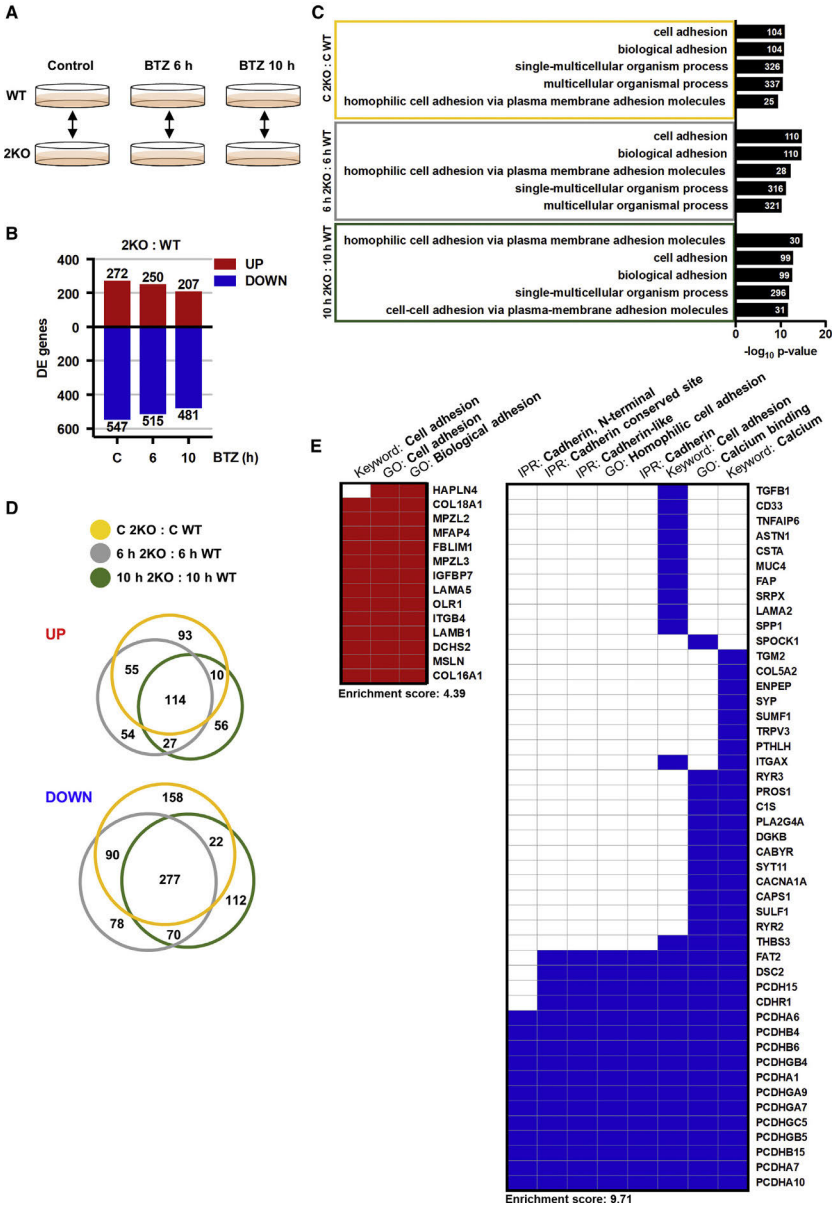

(legend on next page)

the strong association to cell adhesion and an extracellular matrix, including collagens (*COL16A1* and *COL18A1*) and laminins (*LAMB1* and *LAMA5*) (Figure 4E, left panel; Figure S3). Interestingly, the 277 downregulated genes included members from multiple cadherin sub-families, such as protocadherins (*PCDHA1* and *PCDHA7*), desmosomal cadherins (*DSC2*), and Fat-Dachsous cadherins (*FAT2*), suggesting that the cadherin-mediated cell adhesion was extensively misregulated in 2KO cells (Figure 4E, right panel). The most prominent changes were detected in protocadherins, as 13 distinct protocadherin genes were significantly downregulated in 2KO cells both under normal growth conditions and upon exposure to BTZ-induced stress (Figure 4E).

Cells Lacking HSF2 Display Abnormal Cadherin Expression

Cadherins are transmembrane adhesion molecules that mediate Ca^{2+}-dependent cell-cell adhesion via the conserved extracellular cadherin domains (Hirano and Takeichi, 2012). The human genome encodes 110 cadherin genes, which together form the cadherin superfamily consisting of distinct cadherin sub-families (Hirano and Takeichi, 2012). Since the cadherin genes appeared as an HSF2-dependent gene group and showed significant misregulation in multiple sub-family members, we examined the expression profiles of all cadherin superfamily genes in 2KO cells. Normalized gene expression data were used to generate a heatmap encompassing all cadherin genes encoded by the human genome. By comparing the expression profiles of WT and 2KO cells in control and BTZ-induced stress conditions, we observed a prominent downregulation of the entire cadherin superfamily. At least one member from every sub-family was found downregulated in 2KO cells, including classical cadherins (*CDH2* and *CDH6*), desmosomal cadherins (*DSC2* and *DSG2*), CDH23-PCDH15 cadherins (*CDH12*), Fat-Dachsous cadherins (*FAT2* and *FAT4*), Flamingo cadherins (*CELSR1*), and Calsyntenins (*CLSTN2*) (Figure 5A; Table S1). The most striking downregulation was detected in clustered α-, β-, and γ-protocadherins (Peek et al., 2017), of which a majority were found to be abnormally expressed in 2KO cells (Figure 5A). Based on these results, we propose that cadherins are the main adhesion molecules downregulated in HSF2-depleted U2OS cells.

For understanding the biological relevance of the RNA-seq analyses, we determined the protein expression levels of classical cadherins (Pan-Cadherin), N-cadherin (*CDH2*), and clustered γ-protocadherins (Pan-PCDHγA) by immunoblotting. As shown in Figure 5B, classical cadherins, specifically N-cadherin, and γ-protocadherins were significantly downregulated also at the protein level (Figure 5B), and the downregulation was maintained throughout the BTZ treatment (Figure S4A). Since cadherins are essential in mediating Ca^{2+}-dependent cell-cell contacts, we examined the functional impact of our observations using a cell aggregation assay, where single cells were allowed to freely make cell-cell adhesion contacts in suspension. U2OS WT and 2KO cells were suspended in cell aggregation buffer supplemented with either $CaCl_2$ or EDTA. WT cells supplemented with Ca^{2+} formed large cell aggregates, which were completely abolished in Ca^{2+}-chelating conditions (EDTA) (Figures 5C and S4B). In stark contrast, 2KO cells were unable to form cell aggregates even in the presence of Ca^{2+} (Figures 5C and S4B), indicating that HSF2 is required to maintain cadherin-mediated cell-cell contacts.

Loss of distinct cell-cell adhesion molecules has been associated with cellular inability to form three-dimensional (3D) spheroids in ultra-low attachment (ULA) round bottom plates (Stadler et al., 2018). When U2OS WT and 2KO cells were grown on ULA plates, we found that WT cells formed compact spheroids in 48 h. In contrast, 2KO cells were not able to integrate into compact spheres, thereby occupying a significantly larger area of the ULA plates (Figure 5D). Similar spheroid-forming phenotypes were observed when WT and 2KO cells were grown on bacterial plates (Figure S4C). We further explored the spheroid-forming capacity by culturing the cells in a 3D extracellular matrix (ECM) and the *in vivo* tumor growth with chicken chorioallantoic membrane (CAM) assay. As expected, the spheroids and tumors originating from 2KO cells were significantly smaller than the WT counterparts (Figures 5E and S4D), further strengthening the findings of functional impairment of cell-cell adhesion in the absence of HSF2. A profound decline in the expression and function of cadherin superfamily proteins was also observed in 2KO#2 cells (Figures S4E–S4H), demonstrating that the alterations are not specific for a single-clone. Altogether these results show that the lack of HSF2 leads to disrupted cadherin expression at the mRNA and protein levels, thereby resulting in deterioration of cadherin-mediated cell-cell adhesion.

Impaired Cell-Cell Adhesion Sensitizes Cells to Proteotoxic Stress

Although it is well acknowledged that cadherins are essential mediators of tissue integrity and pivotal in regulating the development of multicellular organisms (Hirano and Takeichi, 2012; Peek et al., 2017), their impact on proteotoxic stress resistance

Figure 4. HSF2 Regulates Expression of Genes Associated with Cadherin-Mediated Cell-Cell Adhesion

(A) A schematic overview of the U2OS WT and 2KO comparison pairs.

(B) DE genes in 2KO:WT comparison pairs (control, 6 h, and 10 h) were determined with the Bioconductor R package Limma (Ritchie et al., 2015) (FC $\geq$ 3; FDR < 0.001). The upregulated and downregulated genes are indicated with red and blue bars, respectively.

(C) Gene Ontology (GO) terms were analyzed with topGO and GOstats packages in Bioconductor R. Biological processes from each comparison pair were ranked according to their p values and the five most significantly changed GO terms are shown. The number of genes associated with a given term is indicated.

(D) Venn diagrams presenting the interrelationship of significantly (FC $\geq$ 3; FDR < 0.001) upregulated or downregulated genes in 2KO:WT comparison pairs at control (orange), 6-h (gray), and 10-h (green) time points. Diagrams were generated using the BioVenn web application.

(E) Gene term heatmap generated with DAVID Functional Annotation Clustering Tool based on the 114 upregulated (left panel) and the 277 downregulated (right panel) genes in 2KO cells in all treatment conditions as shown in (D). Red and blue squares denote positive association between the gene and the keyword, GO term, or InterPro (IPR) term. Cluster enrichment score for the upregulated gene cluster is 4.39 and for the downregulated gene cluster it is 9.71.

See also Figure S3 and Table S1.

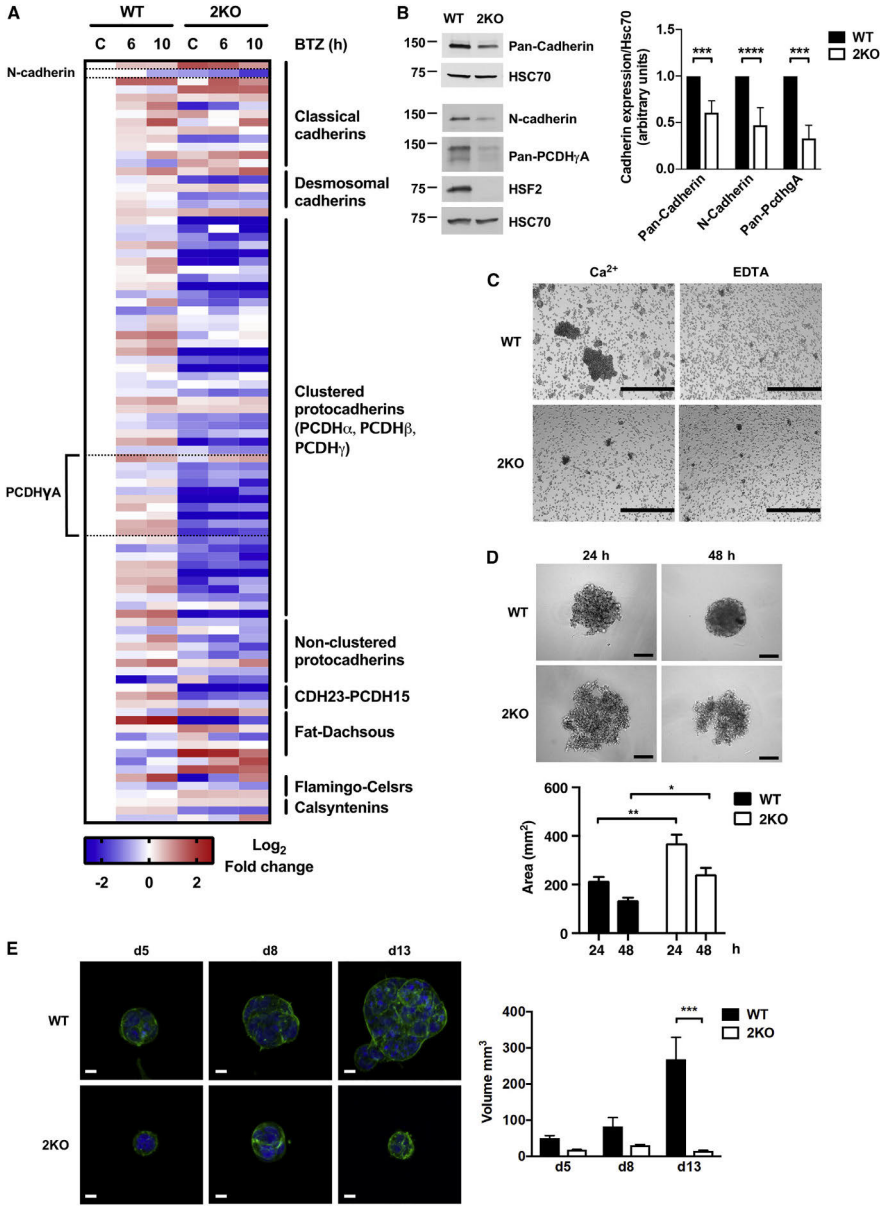

(legend on next page)

has remained unexplored. To examine whether the observed impairment of cell-cell adhesion in 2KO cells also contributes to the susceptibility of the cells to BTZ-induced stress, we restored the cellular adhesion properties by re-introducing N-cadherin to 2KO cells. N-cadherin was selected for these experiments, because it is the most abundantly expressed cadherin superfamily member in WT U2OS cells, according to our RNA-seq data (GEO: GSE115973), and it was found to be downregulated in 2KO cells. WT and 2KO cells were transfected with either Mock or N-cadherin plasmids, and the N-cadherin expression was examined with immunoblotting (Figure 6A). As shown in Figure 6A, we were able to restore the N-cadherin levels in 2KO cells, which resulted in a functional rescue of cell-cell adhesion in 2KO cells (Figure 6B). Importantly, when exposed to BTZ, the 2KO cells expressing exogenous N-cadherin displayed significantly less cleaved PARP-1 than the Mock-transfected cells (Figures 6C, 6D, and S5), suggesting that restoration of cell-cell adhesion can suppress cell death caused by BTZ-induced proteotoxic stress.

All cadherin superfamily proteins are characterized by extracellular cadherin repeat domains, which mediate homophilic adhesion contacts between adjacent cells (Seong et al., 2015). Stabilization of the extracellular domains is regulated by Ca^{2+}, which binds to the interdomain regions of the consecutive cadherin repeats and rigidifies the ectodomain structure. To be able to comprehensively investigate the role of cadherins in the cellular resistance to proteotoxic stress, we first treated WT U2OS cells and MEFs with BTZ for 20 h to induce proteotoxic stress, after which the whole cadherin-mediated cell-cell adhesion program was destabilized by specifically depleting the extracellular Ca^{2+} with EGTA (Figure 6E). Serum-free culture conditions were used for complete depletion of extracellular Ca^{2+}. We observed that Ca^{2+} depletion intensified cell death, which was evidenced by the enhanced PARP-1 and Caspase-3 cleavage in WT U2OS cells and MEFs, respectively, after a combined treatment with both BTZ and EGTA (Figure 6F). Altogether, these results show that cadherin-mediated cell-cell adhesion is a key determinant of cell survival upon BTZ treatment and that destabilization of cadherin contacts predisposes cells to stress-induced proteotoxicity.

DISCUSSION

Maintenance of cellular proteostasis is fundamental for the viability of all cells and organisms (Joutsen and Sistonen, 2019). The heat shock response is critical for promoting proteostasis and it is under strict control of the HSFs, among which HSF1 is considered as the main factor responding to acute stress. Until now, the role of HSF2 in the cellular response to sustained proteotoxicity has remained unknown. We hypothesized that HSF2 is required to protect cells against progressive accumulation of protein damage. To test this hypothesis, we used proteasome inhibitors (BTZ and MG132), L-Canavanine, and HSP90 inhibitors as our experimental tools to induce long-term proteotoxic stress. BTZ treatment has been previously shown to upregulate HSF2 at both mRNA and protein levels in blood-derived human primary cells and to induce HSF2 binding at designated gene loci (Rossi et al., 2014). Our data showed that BTZ treatment also leads to a remarkable increase in HSF2 protein levels in malignant human cells. Moreover, we demonstrate that the amount of nuclear HSF2 is markedly increased in BTZ-treated cells, showing that HSF2 specifically responds to proteasome inhibition. We found that HSF2 is not only activated by BTZ-induced proteotoxicity, but it is absolutely essential for cell survival under these conditions. Based on our results, we conclude that HSF2 is required to protect cells against progressive accumulation of damaged proteins.

Elevated protein levels of HSF1 and its phosphorylation on serine 326 were recently shown to be a prerequisite for multiple myeloma cell survival upon BTZ treatment (Shah et al., 2016; Fok et al., 2018). Therefore, we explored whether HSF2 depletion sensitizes cells to BTZ through misregulated HSF1, specifically, or the heat shock response in general. Neither difference in HSF1 levels nor serine 326 phosphorylation was detected between WT and HSF2-depleted cells treated with proteasome inhibitors. Strikingly, the classical heat shock response, as characterized by the global upregulation of molecular chaperones, HSP90 co-chaperones, and polyubiquitin genes, was not compromised in cells lacking HSF2. These results indicate that HSF2 promotes cell survival independently of HSF1. Thus, we provide evidence that the ability to survive proteotoxic stress does not solely

Figure 5. HSF2 Controls Cellular Adhesion Properties through Cadherin Superfamily Proteins

(A) Normalized gene expression data from the RNA-seq analysis for cadherin superfamily genes, as defined in Hirano and Takeichi (2012), was used to calculate the fold change of each gene in relation to respective expression in the WT control sample. The data are presented as a heatmap of log_2-transformed fold changes and were generated with GraphPad Prism7. N-cadherin and protocadherin gamma subfamily A (PCDHγA) were chosen for further analyses.

(B) Immunoblot analysis of classical cadherins, N-cadherin, and the members of PCDHγA in U2OS WT and 2KO cells. Lack of HSF2 expression in 2KO cells was confirmed and HSC70 was used as a loading control. The amount of cadherins relative to respective HSC70 level was quantified with ImageJ. The data are presented as mean values of three independent experiments + SEM; ***$p < 0.001$ and ****$p < 0.0001$.

(C) Cell aggregation assay of U2OS WT and 2KO cells suspended in cell aggregation buffer supplemented with 3 mM $CaCl_2$ (Ca^{2+}) or 3 mM EDTA. Cells were rotated for 2.5 h at 37°C and visualized with bright-field microscopy. Scale bar, 1 mm.

(D) Bright-field microscopy images of U2OS WT and 2KO cells cultured in ULA plates. Cells were imaged after 24 and 48 h. Scale bar, 200 μm. The size of the spheroid area was quantified with ImageJ. The data are presented as mean values of three independent experiments + SEM. *$p < 0.05$ and **$p < 0.01$.

(E) Confocal microscopy images of U2OS WT and 2KO cells. Cells were cultured in 3D in Matrigel for 5, 8, and 13 days. At the indicated days, spheroids were fixed, and F-actin was stained with Alexa 488-labeled phalloidin (green). DAPI was used to stain the nuclei (blue). *Z* stacks of the spheroids were imaged with a spinning disc confocal microscope. The maximum intensity projection images represent the average spheroid size for each cell line at indicated time points from three biological repeats. Scale bar, 10 μm. The volume of the spheroids was quantified with ImageJ with the 3D Object Counter v2.0 plugin (Bolte and Cordelières, 2006). The data are presented as mean values of three independent experiments + SEM. ***$p < 0.001$.

See also Figure S4.

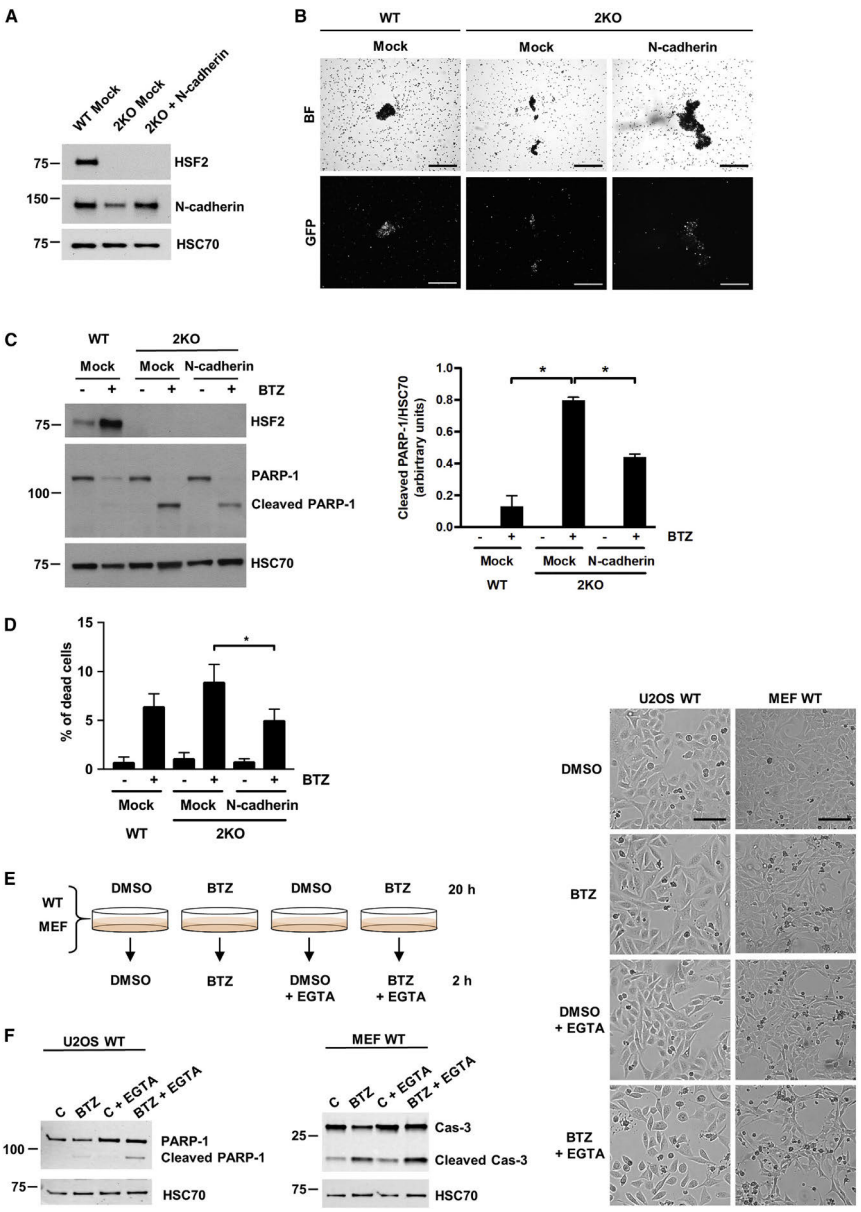

(legend on next page)

depend on the induction of molecular chaperones but engages a larger repertoire of cellular pathways and properties.

To our surprise, despite the stringent cutoff criteria (FC $\geq$ 3; FDR 0.001), we found a considerable number of genes displaying altered expression profiles in cells lacking HSF2. Among the most prominently misregulated genes were those belonging to the cadherin superfamily. Here, we demonstrate that lack of HSF2 leads to a profound downregulation of cadherins both at mRNA and protein levels, identifying HSF2 as a key regulator of cadherin genes. Cadherins are a large group of transmembrane adhesion molecules, which mediate Ca^{2+}-dependent cell-cell adhesion and thereby function as essential mediators of tissue integrity (Hirano and Takeichi, 2012). We found that HSF2-deficient cells display functional impairment of cadherin-mediated cell-cell adhesion already under normal growth conditions. Together with earlier results of HSF2 displaying DNA-binding capacity already in the absence of stress (Sarge et al., 1991; Åkerfelt et al., 2008; Vihervaara et al., 2013), these results suggest that HSF2 has a physiological role in regulating cadherin functions. Excitingly, impaired migration and mispositioning of neurons have been shown to underlie the corticogenesis defects in *Hsf2*$^{-/-}$ mice (Kallio et al., 2002; Chang et al., 2006), and cadherin superfamily proteins are fundamental for correct neuronal migration (Hayashi and Takeichi, 2015). Thus, it is tempting to speculate that the HSF2-dependent disruption of cadherin-mediated cell-cell contacts contributes to the abnormal corticogenesis of *Hsf2*$^{-/-}$ mice.

The downregulation of cadherin gene expression raises important questions about the mechanisms by which HSF2 regulates these genes. Genome-wide mapping of HSF2 binding sites has been previously determined with chromatin immunoprecipitation sequencing (ChIP-seq) in human K562 erythroleukemia cells (Vihervaara et al., 2013) and in mouse testis (Korfanty et al., 2014). Remarkably, both studies identified HSF2 occupancy on multiple cadherin superfamily genes. Since non-adherent K562 cells are deficient of endogenously expressed classical cadherins and distinct protocadherins (Ozawa and Kemler, 1998), it is not surprising that HSF2 was found to occupy only the *CLSTN* gene under control growth conditions (Vihervaara et al., 2013). However, upon acute heat stress, HSF2 binding was observed at classical cadherins (*CDH4*), desmogleins (*DSG2*), Fat-Dachous cadherins (*DCHS2*), Flamingo cadherins (*CELSR2*), and CDH23-PCDH15 cadherins (*CDH23*) (Vihervaara et al., 2013), demonstrating that multiple genes belonging to the cadherin superfamily can be targeted by HSF2 in human cells. In mouse testis, HSF2 was also shown to occupy several cadherin genes, including *CDH15*, *CDH5*, *CDH18*, *CDH13*, *FAT1*, *PCDH9*, *PCDH17*, and *PCDHA1* (Korfanty et al., 2014). Importantly, we now demonstrate the functional relevance of HSF2-mediated cadherin regulation and propose HSF2 as a central regulator of cadherin genes.

Failure in the maintenance of proteostasis is a hallmark of aging and neurodegenerative diseases (Douglas and Dillin, 2010). Intriguingly, in a mouse model of Huntington's disease, lack of HSF2 was shown to predispose mouse brain to poly-Q aggregates and reduce lifespan (Shinkawa et al., 2011), suggesting that HSF2 is required to protect neurons from progressive accumulation of damaged proteins. Cell survival upon proteotoxic stress has been conventionally considered to depend on inducible transcriptional programs, such as the heat shock response or the unfolded protein response (Walter and Ron, 2011; Gomez-Pastor et al., 2018). However, in this study, we show that HSF2-dependent maintenance of cell-cell adhesion is an essential determinant of proteotoxic stress resistance. Our results indicate that misregulation of distinct cellular properties already under normal growth conditions can sensitize cells to proteotoxicity. HSF1 and HSF2 represent the two arms of the cellular resistance toward proteotoxic stress; HSF1 as an acute responder to protein damage and HSF2 as a factor maintaining the long-term stress resistance. Notably, in a meta-analysis of transcriptional changes associated with Alzheimer's disease and aging, HSF2 was identified as a gene commonly downregulated during aging (Ciryam et al., 2016). Therefore, it is possible that the age-associated downregulation of HSF2 and subsequent disruption of cadherin-mediated cell-cell adhesion participates in sensitizing cells, such as neurons, to aggregate mismanagement.

STAR★METHODS

Detailed methods are provided in the online version of this paper and include the following:

- KEY RESOURCES TABLE
- LEAD CONTACT AND MATERIALS AVAILABILITY

Figure 6. Impaired Cell-Cell Contacts Sensitize Cells to BTZ-Induced Proteotoxic Stress

(A–D) N-cadherin levels in U2OS 2KO cells were restored to those in WT cells by transiently transfecting the cells with either Mock or N-cadherin plasmids co-expressing GFP.

(A) Immunoblot analysis of HSF2 and N-cadherin. HSC70 was used as a loading control.

(B) Cell aggregation assay was performed as in Figure 5C. Cell aggregates were imaged with bright-field (BF) and fluorescence filters (GFP). Scale bar, 500 μm.

(C) For immunoblot analysis of HSF2 and PARP-1, cells were treated with 25 nM BTZ for 22 h. Control cells were treated with DMSO. HSC70 was used as a loading control. The amount of cleaved PARP-1 relative to the respective HSC70 level was quantified with ImageJ. The data are presented as mean values of three independent experiments + SEM; *$p < 0.05$.

(D) Flow cytometry analysis of fluorescently labeled cleaved PARP-1 antibody. Cells were treated with 25 nM BTZ for 22 h. Control cells were treated with DMSO. The data are presented as mean values of three independent experiments + SEM; *$p < 0.05$. The statistical analysis was performed with a Student's t test.

(E) A schematic overview of the calcium-depletion experiments.

(F) U2OS WT cells were treated with or without 25 nM BTZ for 20 h in serum-free growth medium after which the extracellular calcium was depleted with 4 mM EGTA and BTZ treatment continued for 2 h. MEFs were treated with 5 or 10 nM BTZ for 20 h in serum-free growth medium after which the extracellular calcium was depleted with 2 mM EGTA and BTZ continued for 2 h. Control cells were treated with DMSO. PARP-1 and Caspase-3 cleavage was assessed with immunoblotting. Cells were imaged with a bright-field microscope. Scale bar, 200 μm.

See also Figure S5.

- EXPERIMENTAL MODEL AND SUBJECT DETAILS
  - Generation of HSF2 knock-out U2OS cells with CRISPR-Cas9
  - Cell culture
  - Chicken chorioallantoic membrane (CAM) assay
- METHOD DETAILS
  - Treatments
  - Transfections
  - Immunoblotting
  - Immunofluorescence
  - Subcellular fractionation
  - Cell viability measurements
  - Cell aggregation assays
  - RNA-sequencing
  - Flow cytometry
  - Quantitative RT-PCR (qRT-PCR)
  - 3D cell culture and immunofluorescence
  - Visualization of the data
- QUANTIFICATION AND STATISTICAL ANALYSIS
  - Bioinformatic analysis of the RNA-seq data
  - Other data analyses
- DATA AND CODE AVAILABILITY

SUPPLEMENTAL INFORMATION

Supplemental Information can be found online at https://doi.org/10.1016/j.celrep.2019.12.037.

ACKNOWLEDGMENTS

We thank Joshua Weiner (University of Iowa, Iowa, US) for helpful discussions and advice and for providing us with the anti-PanPCDHγA antibody. Mikael Puustinen from the Sistonen laboratory is acknowledged for his assistance with the CAM-assay. All members of the Sistonen laboratory and Véronique Dubreuil from the Mezger laboratory are thanked for their valuable comments and critical review of the manuscript. Imaging was performed at the Cell Imaging Core, Turku Bioscience Centre, University of Turku and Åbo Akademi University. The instruments used in this project belong to the infrastructure of Biocenter Finland. We thank Markku Saari and Jouko Sandholm from the Cell Imaging Core of Turku Bioscience Centre for technical assistance and advice. The Bioinformatics unit of Turku Bioscience Centre is acknowledged for their assistance with the RNA-seq data analysis. The Bioinformatics unit is supported by University of Turku, Åbo Akademi University, and Biocenter Finland. This study has been funded by the Academy of Finland (L.S.); Sigrid Juselius Foundation (L.S.); Turku Doctoral Network in Molecular Biosciences (A.J.D.S. and J.C.L.); Finnish Cultural Foundation (J.J.); Cancer Foundation Finland (J.J. and L.S.); Åbo Akademi University Research Foundation (J.J. and M.A.B.); Magnus Ehrnrooth Foundation (A.J.D.S. and L.S.); Tor, Joe and Pentti Borg Memory Foundation (J.J.); Ida Montin's Foundation (J.J.); Otto A. Malm Foundation (J.J. and A.J.D.S.); the Medical Research Foundation Liv och Hälsa (J.J. and L.S.); K. Albin Johansson's Foundation (J.J., A.J.D.S., and E.H.); Agence Nationale Recherche (Program SAMENTA ANR-13-SAMA-0008-01; A.d.T., V.M., and D.S.-D.); Short Researcher Mobility France Embassy/MESRI-Finnish Society of Science and Letters (V.M.); and CNRS/Project International de Coopération Scientifique PICS 2013-2015 (A.d.T., V.M., and D.S.-D.).

AUTHOR CONTRIBUTIONS

J.J., A.J.D.S., and L.S. designed the research; J.J., A.J.D.S., J.C.L., M.A.B., A.S.N., and E.H. performed the experiments; A.d.T., J.-P.C., V.M., and D.S.-D. generated and analyzed the U2OS cell lines; J.J., A.J.D.S., J.C.L., E.H., and L.S. analyzed the data; and J.J., A.J.D.S., and L.S. wrote the manuscript with all authors providing feedback.

DECLARATION OF INTERESTS

The authors declare no competing interests.

Received: June 19, 2019
Revised: October 15, 2019
Accepted: December 12, 2019
Published: January 14, 2020

REFERENCES

Ahlskog, J.K., Björk, J.K., Elsing, A.N., Aspelin, C., Kallio, M., Roos-Mattjus, P., and Sistonen, L. (2010). Anaphase-promoting complex/cyclosome participates in the acute response to protein-damaging stress. Mol. Cell. Biol. *30*, 5608–5620.

Åkerfelt, M., Henriksson, E., Laiho, A., Vihervaara, A., Rautoma, K., Kotaja, N., and Sistonen, L. (2008). Promoter ChIP-chip analysis in mouse testis reveals Y chromosome occupancy by HSF2. Proc. Natl. Acad. Sci. USA *105*, 11224–11229.

Åkerfelt, M., Morimoto, R.I., and Sistonen, L. (2010). Heat shock factors: integrators of cell stress, development and lifespan. Nat. Rev. Mol. Cell Biol. *11*, 545–555.

Alastalo, T.P., Lönnström, M., Leppä, S., Kaarniranta, K., Pelto-Huikko, M., Sistonen, L., and Parvinen, M. (1998). Stage-specific expression and cellular localization of the heat shock factor 2 isoforms in the rat seminiferous epithelium. Exp. Cell Res. *240*, 16–27.

Alexa, A., and Rahnenfuhrer, J. (2019). topGO: Enrichment Analysis for Gene Ontology. R package version 2.37.0. https://bioconductor.org (Bioconductor).

Andrews, S. (2010). FastQC: a quality control tool for high throughput sequence data. Babraham Bioinformatics. www.bioinformatics.babraham.ac.uk/projects/fastqc.

Björk, J.K., Ahonen, I., Mirtti, T., Erickson, A., Rannikko, A., Bützow, A., Nordling, S., Lundin, J., Lundin, M., Sistonen, L., Nees, M., and Åkerfelt, M. (2018). Increased HSF1 expression predicts shorter disease-specific survival of prostate cancer patients following radical prostatectomy. Oncotarget *9*, 31200–31213.

Björk, J.K., Åkerfelt, M., Joutsen, J., Puustinen, M.C., Cheng, F., Sistonen, L., and Nees, M. (2016). Heat-shock factor 2 is a suppressor of prostate cancer invasion. Oncogene *35*, 1770–1784.

Bolte, S., and Cordelières, F.P. (2006). A guided tour into subcellular colocalization analysis in light microscopy. J. Microsc. *224*, 213–232.

Budzyński, M., and Sistonen, L. (2017). Versatile Functions of Heat Shock Factors: It Is Not All about Stress. Curr. Immunol. Rev. *13*, 4–18.

Chang, Y., Östling, P., Åkerfelt, M., Trouillet, D., Rallu, M., Gitton, Y., El Fatimy, R., Fardeau, V., Le Crom, S., Morange, M., et al. (2006). Role of heat-shock factor 2 in cerebral cortex formation and as a regulator of p35 expression. Genes Dev. *20*, 836–847.

Chen, D., Frezza, M., Schmitt, S., Kanwar, J., and Dou, Q.P. (2011). Bortezomib as the first proteasome inhibitor anticancer drug: current status and future perspectives. Curr. Cancer Drug Targets *11*, 239–253.

Ciryam, P., Kundra, R., Freer, R., Morimoto, R.I., and Dobson, C.M. (2016). A transcriptional signature of Alzheimer's disease is associated with a metastable subproteome at risk for aggregation. Proc. Natl. Acad. Sci. USA *113*, 4753–4758.

Dennis, G., Jr., Sherman, B.T., Hosack, D.A., Yang, J., Gao, W., Lane, H.C., and Lempicki, R.A. (2003). DAVID: Database for Annotation, Visualization, and Integrated Discovery. Genome Biol. *4*, 3.

Deshaies, R.J. (2014). Proteotoxic crisis, the ubiquitin-proteasome system, and cancer therapy. BMC Biol. *12*, 94.

Douglas, P.M., and Dillin, A. (2010). Protein homeostasis and aging in neurodegeneration. J. Cell Biol. *190*, 719–729.

Elsing, A.N., Aspelin, C., Björk, J.K., Bergman, H.A., Himanen, S.V., Kallio, M.J., Roos-Mattjus, P., and Sistonen, L. (2014). Expression of HSF2 decreases in mitosis to enable stress-inducible transcription and cell survival. J. Cell Biol. *206*, 735–749.

Falcon, S., and Gentleman, R. (2007). Using GOstats to test gene lists for GO term association. Bioinformatics *23*, 257–258.

Fok, J.H.L., Hedayat, S., Zhang, L., Aronson, L.I., Mirabella, F., Pawlyn, C., Bright, M.D., Wardell, C.P., Keats, J.J., De Billy, E., et al. (2018). HSF1 Is essential for myeloma cell survival and a promising therapeutic target. Clin. Cancer Res. *24*, 2395–2407.

Gentleman, R.C., Carey, V.J., Bates, D.M., Bolstad, B., Dettling, M., Dudoit, S., Ellis, B., Gautier, L., Ge, Y., Gentry, J., et al. (2004). Bioconductor: open software development for computational biology and bioinformatics. Genome Biol. *5*, R80.

Goldberg, A.L. (2012). Development of proteasome inhibitors as research tools and cancer drugs. J. Cell Biol. *199*, 583–588.

Gomez-Pastor, R., Burchfiel, E.T., and Thiele, D.J. (2018). Regulation of heat shock transcription factors and their roles in physiology and disease. Nat. Rev. Mol. Cell Biol. *19*, 4–19.

Gonsalves, S.E., Moses, A.M., Razak, Z., Robert, F., and Westwood, J.T. (2011). Whole-genome analysis reveals that active heat shock factor binding sites are mostly associated with non-heat shock genes in Drosophila melanogaster. PLoS ONE *6*, e15934.

Guettouche, T., Boellmann, F., Lane, W.S., and Voellmy, R. (2005). Analysis of phosphorylation of human heat shock factor 1 in cells experiencing a stress. BMC Biochem. *6*, 4.

Hahn, J.-S., Hu, Z., Thiele, D.J., and Iyer, V.R. (2004). Genome-wide analysis of the biology of stress responses through heat shock transcription factor. Mol. Cell. Biol. *24*, 5249–5256.

Härmä, V., Virtanen, J., Mäkelä, R., Happonen, A., Mpindi, J.P., Knuuttila, M., Kohonen, P., Lötjönen, J., Kallioniemi, O., and Nees, M. (2010). A comprehensive panel of three-dimensional models for studies of prostate cancer growth, invasion and drug responses. PLoS ONE *5*, e10431.

Hartl, F.U., Bracher, A., and Hayer-Hartl, M. (2011). Molecular chaperones in protein folding and proteostasis. Nature *475*, 324–332.

Hayashi, S., and Takeichi, M. (2015). Emerging roles of protocadherins: from self-avoidance to enhancement of motility. J. Cell Sci. *128*, 1455–1464.

Hershko, A., and Ciechanover, A. (1998). The ubiquitin system. Annu. Rev. Biochem. *67*, 425–479.

Hirano, S., and Takeichi, M. (2012). Cadherins in brain morphogenesis and wiring. Physiol. Rev. *92*, 597–634.

Huang, W., Sherman, B.T., and Lempicki, R.A. (2009). Systematic and integrative analysis of large gene lists using DAVID bioinformatics resources. Nat. Protoc. *4*, 44–57.

Hulsen, T., de Vlieg, J., and Alkema, W. (2008). BioVenn - a web application for the comparison and visualization of biological lists using area-proportional Venn diagrams. BMC Genomics *9*, 488.

Jaeger, A.M., Pemble, C.W., 4th, Sistonen, L., and Thiele, D.J. (2016). Structures of HSF2 reveal mechanisms for differential regulation of human heat-shock factors. Nat. Struct. Mol. Biol. *23*, 147–154.

Joutsen, J., and Sistonen, L. (2019). Tailoring of Proteostasis Networks with Heat Shock Factors. Cold Spring Harb. Perspect. Biol. *11*, a034066.

Kallio, P.J., Wilson, W.J., O'Brien, S., Makino, Y., and Poellinger, L. (1999). Regulation of the hypoxia-inducible transcription factor 1α by the ubiquitin-proteasome pathway. J. Biol. Chem. *274*, 6519–6525.

Kallio, M., Chang, Y., Manuel, M., Alastalo, T.P., Rallu, M., Gitton, Y., Pirkkala, L., Loones, M.T., Paslaru, L., Larney, S., et al. (2002). Brain abnormalities, defective meiotic chromosome synapsis and female subfertility in HSF2 null mice. EMBO J. *21*, 2591–2601.

Kampinga, H.H., Hageman, J., Vos, M.J., Kubota, H., Tanguay, R.M., Bruford, E.A., Cheetham, M.E., Chen, B., and Hightower, L.E. (2009). Guidelines for the nomenclature of the human heat shock proteins. Cell Stress Chaperones *14*, 105–111.

Kawazoe, Y., Nakai, A., Tanabe, M., and Nagata, K. (1998). Proteasome inhibition leads to the activation of all members of the heat-shock-factor family. Eur. J. Biochem. *255*, 356–362.

Kim, D., Pertea, G., Trapnell, C., Pimentel, H., Kelley, R., and Salzberg, S.L. (2013). TopHat2: accurate alignment of transcriptomes in the presence of insertions, deletions and gene fusions. Genome Biol. *14*, R36.

Kisselev, A.F., Callard, A., and Goldberg, A.L. (2006). Importance of the different proteolytic sites of the proteasome and the efficacy of inhibitors varies with the protein substrate. J. Biol. Chem. *281*, 8582–8590.

Kobayashi, A., Kang, M.I., Okawa, H., Ohtsuji, M., Zenke, Y., Chiba, T., Igarashi, K., and Yamamoto, M. (2004). Oxidative stress sensor Keap1 functions as an adaptor for Cul3-based E3 ligase to regulate proteasomal degradation of Nrf2. Mol. Cell. Biol. *24*, 7130–7139.

Korfanty, J., Stokowy, T., Widlak, P., Gogler-Piglowska, A., Handschuh, L., Podkowiński, J., Vydra, N., Naumowicz, A., Toma-Jonik, A., and Widlak, W. (2014). Crosstalk between HSF1 and HSF2 during the heat shock response in mouse testes. Int. J. Biochem. Cell Biol. *57*, 76–83.

Kubbutat, M.H., Jones, S.N., and Vousden, K.H. (1997). Regulation of p53 stability by Mdm2. Nature *387*, 299–303.

Lecomte, S., Desmots, F., Le Masson, F., Le Goff, P., Michel, D., Christians, E.S., and Le Dréan, Y. (2010). Roles of heat shock factor 1 and 2 in response to proteasome inhibition: consequence on p53 stability. Oncogene *29*, 4216–4224.

Li, J., Chauve, L., Phelps, G., Brielmann, R.M., and Morimoto, R.I. (2016). E2F coregulates an essential HSF developmental program that is distinct from the heat-shock response. Genes Dev. *30*, 2062–2075.

Liao, Y., Smyth, G.K., and Shi, W. (2013). The Subread aligner: fast, accurate and scalable read mapping by seed-and-vote. Nucleic Acids Res. *41*, e108.

Ling, Y.H., Liebes, L., Ng, B., Buckley, M., Elliott, P.J., Adams, J., Jiang, J.D., Muggia, F.M., and Perez-Soler, R. (2002). PS-341, a novel proteasome inhibitor, induces Bcl-2 phosphorylation and cleavage in association with G2-M phase arrest and apoptosis. Mol. Cancer Ther. *1*, 841–849.

Mahat, D.B., Salamanca, H.H., Duarte, F.M., Danko, C.G., and Lis, J.T. (2016). Mammalian heat shock response and mechanisms underlying its genome-wide transcriptional regulation. Mol. Cell *62*, 63–78.

Mali, P., Yang, L., Esvelt, K.M., Aach, J., Guell, M., DiCarlo, J.E., Norville, J.E., and Church, G.M. (2013). RNA-guided human genome engineering via Cas9. Science *339*, 823–826.

Mathew, A., Mathur, S.K., and Morimoto, R.I. (1998). Heat shock response and protein degradation: regulation of HSF2 by the ubiquitin-proteasome pathway. Mol. Cell. Biol. *18*, 5091–5098.

Mendillo, M.L., Santagata, S., Koeva, M., Bell, G.W., Hu, R., Tamimi, R.M., Fraenkel, E., Ince, T.A., Whitesell, L., and Lindquist, S. (2012). HSF1 drives a transcriptional program distinct from heat shock to support highly malignant human cancers. Cell *150*, 549–562.

Mezger, V., Rallu, M., Morimoto, R.I., Morange, M., and Renard, J.P. (1994). Heat shock factor 2-like activity in mouse blastocysts. Dev. Biol. *166*, 819–822.

Östling, P., Björk, J.K., Roos-Mattjus, P., Mezger, V., and Sistonen, L. (2007). Heat shock factor 2 (HSF2) contributes to inducible expression of hsp genes through interplay with HSF1. J. Biol. Chem. *282*, 7077–7086.

Ozawa, M., and Kemler, R. (1998). Altered cell adhesion activity by pervanadate due to the dissociation of alpha-catenin from the E-cadherin.catenin complex. J. Biol. Chem. *273*, 6166–6170.

Peek, S.L., Mah, K.M., and Weiner, J.A. (2017). Regulation of neural circuit formation by protocadherins. Cell. Mol. Life Sci. *74*, 4133–4157.

Pirkkala, L., Alastalo, T.-P., Zuo, X., Benjamin, I.J., and Sistonen, L. (2000). Disruption of heat shock factor 1 reveals an essential role in the ubiquitin proteolytic pathway. Mol. Cell. Biol. *20*, 2670–2675.

Rallu, M., Loones, M., Lallemand, Y., Morimoto, R., Morange, M., and Mezger, V. (1997). Function and regulation of heat shock factor 2 during mouse embryogenesis. Proc. Natl. Acad. Sci. USA *94*, 2392–2397.

Ritchie, M.E., Phipson, B., Wu, D., Hu, Y., Law, C.W., Shi, W., and Smyth, G.K. (2015). limma powers differential expression analyses for RNA-sequencing and microarray studies. Nucleic Acids Res. *43*, e47.

Riva, L., Koeva, M., Yildirim, F., Pirhaji, L., Dinesh, D., Mazor, T., Duennwald, M.L., and Fraenkel, E. (2012). Poly-glutamine expanded huntingtin dramatically alters the genome wide binding of HSF1. J. Huntingtons Dis. *1*, 33–45.

Robinson, M.D., McCarthy, D.J., and Smyth, G.K. (2010). edgeR: a Bioconductor package for differential expression analysis of digital gene expression data. Bioinformatics *26*, 139–140.

Rossi, A., Riccio, A., Coccia, M., Trotta, E., La Frazia, S., and Santoro, M.G. (2014). The proteasome inhibitor bortezomib is a potent inducer of zinc finger AN1-type domain 2a gene expression: role of heat shock factor 1 (HSF1)-heat shock factor 2 (HSF2) heterocomplexes. J. Biol. Chem. *289*, 12705–12715.

Rueden, C.T., Schindelin, J., Hiner, M.C., DeZonia, B.E., Walter, A.E., Arena, E.T., and Eliceiri, K.W. (2017). ImageJ2: ImageJ for the next generation of scientific image data. BMC Bioinformatics *18*, 529.

Sarge, K.D., Zimarino, V., Holm, K., Wu, C., and Morimoto, R.I. (1991). Cloning and characterization of two mouse heat shock factors with distinct inducible and constitutive DNA-binding ability. Genes Dev. *5*, 1902–1911.

Sarge, K.D., Murphy, S.P., and Morimoto, R.I. (1993). Activation of heat shock gene transcription by heat shock factor 1 involves oligomerization, acquisition of DNA-binding activity, and nuclear localization and can occur in the absence of stress. Mol. Cell. Biol. *13*, 1392–1407.

Sarge, K.D., Park-Sarge, O.K., Kirby, J.D., Mayo, K.E., and Morimoto, R.I. (1994). Expression of heat shock factor 2 in mouse testis: potential role as a regulator of heat-shock protein gene expression during spermatogenesis. Biol. Reprod. *50*, 1334–1343.

Schindelin, J., Arganda-Carreras, I., Frise, E., Kaynig, V., Longair, M., Pietzsch, T., Preibisch, S., Rueden, C., Saalfeld, S., Schmid, B., et al. (2012). Fiji: an open-source platform for biological-image analysis. Nat. Methods *9*, 676–682.

Seong, E., Yuan, L., and Arikkath, J. (2015). Cadherins and catenins in dendrite and synapse morphogenesis. Cell Adhes. Migr. *9*, 202–213.

Shah, S.P., Nooka, A.K., Jaye, D.L., Bahlis, N.J., Lonial, S., and Boise, L.H. (2016). Bortezomib-induced heat shock response protects multiple myeloma cells and is activated by heat shock factor 1 serine 326 phosphorylation. Oncotarget *7*, 59727–59741.

Sheldon, L.A., and Kingston, R.E. (1993). Hydrophobic coiled-coil domains regulate the subcellular localization of human heat shock factor 2. Genes Dev. *7*, 1549–1558.

Shinkawa, T., Tan, K., Fujimoto, M., Hayashida, N., Yamamoto, K., Takaki, E., Takii, R., Prakasam, R., Inouye, S., Mezger, V., and Nakai, A. (2011). Heat shock factor 2 is required for maintaining proteostasis against febrile-range thermal stress and polyglutamine aggregation. Mol. Biol. Cell *22*, 3571–3583.

Sistonen, L., Sarge, K.D., and Morimoto, R.I. (1994). Human heat shock factors 1 and 2 are differentially activated and can synergistically induce hsp70 gene transcription. Mol. Cell. Biol. *14*, 2087–2099.

Stadler, M., Scherzer, M., Walter, S., Holzner, S., Pudelko, K., Riedl, A., Unger, C., Kramer, N., Weil, B., Neesen, J., et al. (2018). Exclusion from spheroid formation identifies loss of essential cell-cell adhesion molecules in colon cancer cells. Sci. Rep. *8*, 1151.

Varshavsky, A. (2012). The ubiquitin system, an immense realm. Annu. Rev. Biochem. *81*, 167–176.

Vihervaara, A., Sergelius, C., Vasara, J., Blom, M.A.H., Elsing, A.N., Roos-Mattjus, P., and Sistonen, L. (2013). Transcriptional response to stress in the dynamic chromatin environment of cycling and mitotic cells. Proc. Natl. Acad. Sci. USA *110*, E3388–E3397.

Vihervaara, A., Duarte, F.M., and Lis, J.T. (2018). Molecular mechanisms driving transcriptional stress responses. Nat. Rev. Genet. *19*, 385–397.

Vihervaara, A., Mahat, D.B., Guertin, M.J., Chu, T., Danko, C.G., Lis, J.T., and Sistonen, L. (2017). Transcriptional response to stress is pre-wired by promoter and enhancer architecture. Nat. Commun. *8*, 255.

Walter, P., and Ron, D. (2011). The unfolded protein response: from stress pathway to homeostatic regulation. Science *334*, 1081–1086.

Zhang, B., Groffen, J., and Heisterkamp, N. (2007). Increased resistance to a farnesyltransferase inhibitor by N-cadherin expression in Bcr/Abl-P190 lymphoblastic leukemia cells. Leukemia *21*, 1189–1197.

STAR★METHODS

KEY RESOURCES TABLE

REAGENT or RESOURCE	SOURCE	IDENTIFIER
Antibodies		
Rabbit polyclonal anti-GAPDH	Abcam	Cat#Ab9485; RRID:AB_307275
Rat monoclonal anti-HSC70	Enzo Life Sciences	Cat#ADI-SPA-815; RRID:AB_10617277
Rabbit polyclonal anti-HSF1	Enzo Life Sciences	Cat#ADI-SPA-901; RRID:AB_10616511
Rabbit polyclonal anti-HSF1 p326	Abcam	Cat#Ab76076; RRID:AB_1310328
Rabbit polyclonal anti-HSF2	Sigma-Aldrich	Cat#HPA031455; RRID:AB_10670702
Mouse anti-HSP70	Enzo Life Sciences	Cat#ADI-SPA-810; RRID:AB_10616513
Rabbit monoclonal anti-N-cadherin	Millipore	Cat#04-1126; RRID:AB_1977064
Rabbit polyclonal anti-N-cadherin	Abcam	Cat#Ab76057; RRID:AB_1310478
Mouse monoclonal anti-PARP-1	Santa Cruz Biotechnology	Cat#Sc-8007; RRID:AB_628105
Rabbit polyclonal anti-cleaved Caspase 3	Abcam	Cat#Ab2302; RRID:AB_302962
Mouse monoclonal anti-Pan-PCDHγA	NeuroMab	Cat#75-178; RRID:AB_2159447
Rabbit polyclonal anti-Pan-Cadherin	Abcam	Cat#Ab6529; RRID:AB_305545
Mouse monoclonal anti-Lamin A/C	Cell Signaling Technology	Cat#4777S; RRID:AB_10545756
Mouse monoclonal anti- β-tubulin	Sigma-Aldrich	Cat#T8328; RRID:AB_1844090
Mouse monoclonal anti-cleaved PARP antibody conjugated to BV421		Cat#564129; RRID:AB_2738611
Goat anti-rabbit Alexa Fluor 488	Invitrogen	Cat# R37116; RRID:AB_2556544
Chemicals, Peptides, and Recombinant Proteins		
Bortezomib	Santa Cruz Biotechnology	Cat#sc-217785
MG132	Peptide Institute Inc.	Cat#317-V
17-AAG	InvivoGen	Cat#anti-agl-5
Geldanamycin	InvivoGen	Cat#anti-gl-5
L-Canavanine sulfate salt	Sigma-Aldrich	Cat#C9758
Alexa Fluor 488 Phalloidin	Thermo Fisher Scientiffic	Cat#A12379; Cat #A22287
Critical Commercial Assays		
CellTiter-Glo reagent	Promega	Cat#G7570
Calcein AM	R&D Systems	Cat#4892-010-K
AllPrep DNA/RNA/miRNA Universal Kit	QIAGEN	Cat#80224
Matrigel	Corning	Cat#356231
RNeasy mini kit	QIAGEN	Cat#74106
iScript cDNA Synthesis Kit	Bio-Rad	Cat#1708891
GenJet	SignaGen Laboratories	Cat#SL100489-OS
Deposited Data		
RNA-seq raw data	This paper	GEO: GSE115973
Experimental Models: Cell Lines		
U2OS wild-type	This paper	N/A
U2OS HSF2 knock out	This paper	N/A
U2OS HSF2 knock out clone 2	This paper	N/A
Mouse embryonic fibroblasts wild-type	Östling et al., 2007	N/A
Mouse embryonic fibroblasts *Hsf2*$^{-/-}$	Östling et al., 2007	N/A
Experimental Models: Organisms/Strains		
Chicken: fertilized white Leghorn chicken eggs	Munax Oy	N/A

(*Continued on next page*)

Continued

REAGENT or RESOURCE	SOURCE	IDENTIFIER
Oligonucleotides		
Primers for generating HSF2 knock-out U2OS cells with CRISPR-Cas9 see Table S2	This paper	N/A
Primer RNA18S5 forward: GCAATTATTCCCCATGAACG	Sigma-Aldrich	N/A
Primer RNA18S5 reverse: GGGACTTAATCAACGCAAGC	Sigma-Aldrich	N/A
Probe RNA18S5: FAM-TTCCCAGTAAGTGCG GGTC-BHQ	Sigma-Aldrich	N/A
Primer DSC2 forward: ATCCATTAGAGGACACACTCTGA	Sigma-Aldrich	N/A
Primer DSC2 reverse: GCCACCGATCCTCTTCCTTC	Sigma-Aldrich	N/A
Primer PCDHA6 forward: TGACTGTTGAATGATGGCGGA	Sigma-Aldrich	N/A
Primer PCDHA6 reverse: TCGGGTACGGAGTAGTGGAG	Sigma-Aldrich	N/A
Primer PCDH10A forward: AGGCATCAGCCAGTTTCTCAA	Sigma-Aldrich	N/A
Primer PCDH10A reverse: GAGAGCAGCAGACACTGGAC	Sigma-Aldrich	N/A
Recombinant DNA		
pMLM3636, Human-gRNA-Expression Vector	Keith Joung laboratory, Addgene	RRID:Addgene_43860
pcDNA3.3-TOPO hCas9	Mali et al., 2013; Addgene	RRID:Addgene_41815
pEGFP-N1	Clontech	N/A
shRNA against HSF2 in pSUPERIOR	Östling et al., 2007	N/A
shRNA scrambled in pSUPERIOR	Östling et al., 2007	N/A
N-Cadherin in pCCL-c-MNDU3c-PGK-EGFP	Zhang et al., 2007; Addgene	RRID:Addgene_38153
Software and Algorithms		
FastQC version 0.20.1	Andrews, 2010; FastQC.	http://www.bioinformatics.babraham.ac.uk/projects/fastqc/
TopHat2 version 2.1.0	Kim et al., 2013	https://ccb.jhu.edu/software/tophat/index.shtml
Subreads version 1.5.0	Liao et al., 2013	
R: A language an Environment for Statistical Computing	R Core Tean	https://www.r-project.org/
Bioconductor	Gentleman et al., 2004	http://www.bioconductor.org/
Bioconductor R package edgeR	Robinson et al., 2010	https://bioconductor.org/packages/release/bioc/html/edgeR.html
Bioconductor R package Limma	Ritchie et al., 2015	https://bioconductor.org/packages/release/bioc/html/limma.html
Bioconductor R package topGO	Alexa and Rahnenfuhrer, 2019	https://bioconductor.org/packages/release/bioc/html/topGO.html
Bioconductor R package GOstats	Falcon and Gentleman, 2007	https://bioconductor.org/packages/release/bioc/html/GOstats.html
ImageJ v1.51n	Rueden et al., 2017	https://imagej.net/Citing
Fiji	Schindelin et al., 2012	https://imagej.net/Citing
3D Object Counter	Bolte and Cordelières, 2006	https://imagej.net/Citing
FlowJo	Version 10	https://www.flowjo.com/
DAVID Bioinformatic Tool	Huang et al., 2009	https://david.ncifcrf.gov/home.jsp
GraphPad Prism Software	Version 7 and 8	https://www.graphpad.com/
BioVenn	Hulsen et al., 2008	http://www.biovenn.nl

LEAD CONTACT AND MATERIALS AVAILABILITY

Further information and requests for resources and reagents should be directed to and will be fulfilled by the Lead Contact, Lea Sistonen (lea.sistonen@abo.fi). The resources are shared for research and educational purposes without restriction.

EXPERIMENTAL MODEL AND SUBJECT DETAILS

Generation of HSF2 knock-out U2OS cells with CRISPR-Cas9

Guide RNAs (gRNA) targeting the exon 1 of *HSF2* were designed using CRISPOR software (http://crispor.tefor.net/) and cloned into pMLM3636 gRNA expression plasmid (a gift from Keith Joung, Addgene plasmid #43860). Human osteosarcoma U2OS cells were transfected with Cas9 and gRNA expression plasmids using Amaxa electroporation as recommended by the manufacturer (Lonza). The hCas9 was a gift from George Church (Addgene plasmid #41815; http://addgene.org/41815; RRID:Addgene_41815). One week after transfections, cells were seeded at single cell density. Clones were genotyped by DNA sequencing of PCR products spanning the targeted region of the *HSF2* gene. The selected U2OS clones presented 3 different outframe mutations on *HSF2* exon 1, each corresponding to a different allele (Table S2). Guide RNA sequence targeting the 1st AUG of the *HSF2* exon 1: 5′-UGCGCCGC GUUAACAAUGAA-3′. Following primers were used for PCR for validation: forward (hHSF2_Cr_ATG_F): 5′-AGTCGGCTCCTGG GATTG-3′ and reverse (hHSF2_Cr_ATG_R): 5′-AGTGAGGAGGCGGTTATTCAG-3′. For the experiments, we utilized HSF2 knock-out cell clone 1 (hereafter 2KO) and HSF2 knock-out cell clone 2 (hereafter 2KO#2).

Cell culture

U2OS cells and mouse embryonic fibroblasts (WT and *Hsf2*$^{-/-}$ MEFs, Östling et al., 2007) were cultured in DMEM (Dulbecco's Modified Eagle's media, D6171, Sigma-Aldrich), supplemented with 10% fetal calf serum, 2 mM L-glutamine and 100 μg/ml penicillin-streptomycin, and grown in 5% CO_2 at 37°C. Culture media for MEFs were also supplemented with 1 X MEM non-essential amino acid solution (M7145, Sigma-Aldrich).

Chicken chorioallantoic membrane (CAM) assay

The CAM-assay was performed as in Björk et al. (2016). Briefly, fertilized white Leghorn chicken eggs were incubated at 37°C under 60% humidity (embryo development day 0, EDD0). Separation of the developing CAM was induced on EDD4. On EDD8, 1 × 10^6 U2OS WT and 2KO cells were mixed with Matrigel in 1:1 ratio and implanted on the CAM. On EDD11, the tumors were photographed *in ovo*. Tumor area was measured in blind using ImageJ.

METHOD DETAILS

Treatments

Proteasome inhibition was induced with Bortezomib (BTZ, sc-217785, Santa Cruz Biotechnology) or MG132 (Z-Leu-Leu-Leu-H, 317-V, Peptide Institute Inc.). For HSP90 inhibition, 17-AAG (anti-agl-5, InvivoGen) and Geldanamycin (anti-gl-5, InvivoGen) were used. All inhibitors were diluted in DMSO (dimethyl sulfoxide, D8418, Sigma-Aldrich) and applied to cells in final concentrations indicated in the figures. Control cells were treated with DMSO only. To induce protein misfolding with amino acid analogs, cells were starved for 17 h in L-arginine free culture medium (A14431-01, GIBCO) supplemented with 10% fetal calf serum, 2 mM L-glutamine and 100 μg/ml penicillin-streptomycin. Following that, L-Canavanine sulfate salt (C9758, Sigma-Aldrich) was applied to the cells in final concentrations indicated in the figure. Cells were treated for 3 or 6 h. After the treatments, cells were visualized with Leica phase contrast microscope, an EVOS FL Cell Imaging System (Thermo Fisher Scientific), or an Axio Vert A1-FL LED microscope (Carl Zeiss) and harvested for further analyses.

Transfections

For transfections, 6 × 10^6 U2OS WT or 2KO cells were suspended in 400 μL of Opti-MEM (11058-021, GIBCO) and subjected to electroporation (230 V, 975 μF) in BTX electroporation cuvettes (45-0126, BTX). To downregulate HSF2 in WT cells, HSF2 targeting shRNA and Scr vectors as previously described (Östling et al., 2007), were used. For restoring the protein levels of HSF2 and N-Cadherin in 2KO cells, HSF2 in pcDNA3.1/myc-His(-)A vector and N-cadherin in pCCL-c-MNDU3c-PGK-EGFP (Zhang et al., 2007) (a gift from Nora Heisterkamp; Addgene plasmid #38153; http://addgene.org/38153; RRID:Addgene_38153) were used. Empty pcDNA3.1/myc-His(-)A vector was used as Mock. One day after transfection, cells were trypsinized, counted, re-plated, and let to recover for 24 h before BTZ treatments.

For cell aggregation assays, cells were transfected with GenJet (#SL100489-OS, SignaGen Laboratories) according to manufacturer's instructions. Briefly, cells were plated 18 to 24 h prior to transfections to ensure 80% confluency, and fresh culture media with supplements was added to the cells before transfections. The N-Cadherin encoding vector (described above) was used for transfections, and pEGFP-N1 (Clontech) was used as a Mock. The plasmids and the GenJet reagent were diluted in serum free media, and applied to the cells in a ratio of 1:2 (DNA:GenJet reagent). Cells were incubated with the DNA:GenJet mixture for 4 h, washed with PBS, and supplemented with complete culture media. Cells were let to recover for 24 h before the cell aggregation experiments.

Immunoblotting

Cells were collected in culture media, washed with PBS (L0615, BioWest) and lysed in lysis buffer [50 mM HEPES, pH 7.4, 150 mM NaCl, 1 mM EDTA, 2 mM $MgCl_2$, 1% Triton X-100, 10% glycerol, 1 x complete Protease Inhibitor Cocktail (04693159001, Roche Diagnostics), 50 mM NaF, 0.2 mM Na_3VO_4]. Protein concentration of the lysates was determined with Bradford assay. Equal amounts

of cell lysates were resolved on 4%–20% or 7.5% Mini-PROTEAN® TGX precast gels (Bio-Rad) and the proteins were transferred to a nitrocellulose membrane. For HSF2 detection, membranes were boiled for 15 min in MQ-H_2O and blocked in 3% milk-PBS-Tween20 solution for 1 h at RT. Primary antibodies were diluted in 0.5% BSA-PBS-0.02% NaN_3 and the membranes were incubated in respective primary antibodies overnight at 4°C. The following antibodies were used: anti-GAPDH (ab9485, Abcam), anti-HSC70 (ADI-SPA-815, Enzo Life Sciences), anti-HSF1 (ADI-SPA-901, Enzo Life Sciences), anti-HSF1 pS326 (ab76076, Abcam), anti-HSF2 (HPA031455, Sigma-Aldrich), anti-HSP70 (ADI-SPA-810, Enzo Life Sciences), N-cadherin (04-1126, Millipore or ab76057, Abcam), anti-PARP-1 (F-2, sc-8007, Santa Cruz Biotechnology), anti-Caspase-3 (ab2302, Abcam), anti-Pan-PCDHγA (75-178, NeuroMab), anti-Pan-Cadherin (ab6529, Abcam), anti-Lamin A/C (4777S, Cell Signaling Technology), and anti-β-Tubulin (T8328, Sigma-Aldrich). Secondary antibodies were HRP-conjugated and purchased from Promega, GE Healthcare or Abcam. All immunoblotting experiments were performed at least three times.

Immunofluorescence

2×10^5 U2OS WT cells were plated on coverslips or MatTek plates (P35GC-.5-14-C, MatTek Corporation) 24 h before treatments. Cells were fixed with 4% paraformaldehyde (PFA) for 15 min, permeabilized in 0.1% Triton X-100 in PBS and washed three times with PBST (PBS-0.5% Tween20). Cells were blocked with 10% FBS in PBS for 1 h at RT and incubated overnight at 4°C with a primary anti-HSF2 antibody (HPA031455, Sigma-Aldrich), which was diluted 1:20 in 10% FBS-PBS. Secondary goat anti-rabbit Alexa Fluor 488 (R37116, Invitrogen) was diluted 1:500 in 10% FBS-PBS and the cells were incubated for 1 h in RT. Cells were washed three times with PBST, incubated with 300 nM DAPI diluted in PBS or mounted in Mowiol-DABCO or VECTASHIELD mounting medium, and imaged with a 3i CSU-W1 spinning disc confocal microscope (Intelligent Imaging Innovations).

Subcellular fractionation

2×10^6 U2OS WT cells were plated and cultured overnight. The following day, cells were treated with 25 nM BTZ for 6 or 22 h. Control cells were treated with DMSO for 22 h. Cells were collected in culture media and washed with PBS. 20% of the suspended cells were collected for preparation of the whole cell lysate and lysed. The remaining 80% were collected for subcellular fractionation. Cytoplasmic and nuclear fractions were prepared using NE-PER Nuclear and Cytoplasmic Extraction Reagents (78833, Thermo Fisher Scientific) according to manufacturer's instructions. Briefly, suspended cells were washed with cold PBS. The cell pellet was suspended in 200 μL of cytoplasmic extraction reagent I. After incubation on ice, 11 μL of cytoplasmic extraction reagent II was added. The suspension was incubated on ice and centrifuged (16 000 g, 5 min). The supernatant was collected and the pellet was resuspended in 100 μL of nuclear extraction reagent, incubated on ice and centrifuged (16 000 g, 10 min). The supernatant (nuclear extract) was collected and the protein concentrations were determined by BCA assay (23225, Thermo Fischer Scientific).

Cell viability measurements

5×10^3 U2OS WT and HSF2 KO cells were cultured in clear bottom 96-well plate (6005181, Perking Elmer) in complete culture media. Cells were treated with indicated concentrations of Bortezomib or MG132 for 22 h. For calcium-depletion, cells were treated with or without 25 nM BTZ (U2OS cells) or 5 and 10 nM BTZ (MEFs) for 20 h in serum free media. The extracellular calcium was depleted with 4 mM EGTA (U2OS cells) and 2 mM EGTA (MEFs) in calcium-free media and the Bortezomib treatment was continued for 2 h. Control cells were treated with DMSO. After treatments cells were washed with PBS and incubated for 30 min at 37°C with Calcein AM (4892-010-K, R&D Systems) diluted 1:1000 in PBS. Fluorescence intensity was measured with Hidex Sense microplate reader (HIDEX Corp) with excitation and emission wavelengths 485 nm and 535 nm, respectively. Alternatively, CellTiter-Glo reagent (G7570, Promega) was added to the wells in 1:1 ratio and the luminescence was measured with Hidex Sense microplate reader. Respective blank values were subtracted from the sample values and the viability of untreated control samples was set to value 1. All measurements were repeated at least three times.

Cell aggregation assays

After trypsinization, 5×10^5 U2OS WT and 2KO cells were suspended in 2 mL of aggregation assay buffer (137 mM NaCl, 5.4 mM KCl, 0.63 mM, Na_2HPO_4, 5.5 mM glucose, and 10 mM HEPES, pH 7.4) supplemented with either 3 mM $CaCl_2$ or 3 mM EDTA. Cells were rotated for 2.5 h in 150 rpm at 37°C, after which the aggregates were imaged with the EVOS FL Cell Imaging System (Thermo Fisher Scientific) or with an Axio Vert A1-FL LED microscope (Carl Zeiss). Cell aggregation assays were performed in biological triplicates. The area of the three biggest aggregates in each sample was measured with ImageJ (U. S. National Institutes of Health, Bethesda, Maryland, USA) for quantification purposes. All cell aggregation experiments were repeated at least three times.

RNA-sequencing

2×10^6 U2OS WT and HSF2 KO cells were plated and cultured overnight. Following day, cells were treated with 25 nM BTZ for 6 or 10 h. Control cells were treated with DMSO. Cells were collected, and total RNA was purified with AllPrep DNA/RNA/miRNA Universal Kit (80224, QIAGEN) according to manufactureŕs instructions. Genomic DNA from mRNA columns was digested with DNase I. The RNA library was prepared according to Illumina TruSeq® Stranded mRNA Sample Preparation Guide (part #15031047). Briefly, poly-A containing mRNA molecules were purified with poly-T oligo magnetic beads and fragmented with divalent cations under elevated temperatures. For first-strand cDNA synthesis, RNA fragments were copied using reverse transcriptase and random

primers. Unique Illumina TrueSeq indexing adapters were ligated to each sample. The quality and concentration of cDNA samples were analyzed with Advanced Analytical Fragment Analyzer and Bioanalyzer 2100 (Agilent, Santa Clara, CA, USA) and Qubit® Fluorometric Quantitation (Life Technologies). Samples were sequenced with Illumina HiSeq 3000 (Illumina). All the experimental steps after the RNA extraction were conducted in the Finnish Microarray and Sequencing Center, Turku, Finland. RNA-sequencing was performed from four independent sample series.

Flow cytometry

0.5×10^6 U2OS WT and 2KO cells were fixed at 4°C with BD Cytofix/Cytoperm (554722, BD Bioscience) and washed with cold BD Perm/Wash (554723, BD Bioscience) solution. Cells were incubated over night at 4°C with anti-cleaved PARP antibody conjugated to BV421 (564129, BD Horizon), which was diluted 1:250 in BD Perm/Wash solution. Fluorescence was analyzed with a BD LSRFortessa flow cytometer (BD Bioscience) using a standard Pacific Blue filter set (450/50 nm). The flow cytometry profiles were analyzed using FlowJo 10 software.

Quantitative RT-PCR (qRT-PCR)

RNA was isolated using a RNeasy mini kit (74106, QIAGEN) according to the manufacturer's instructions and quantified using a NanoDrop ND-1000 spectrophotometer (Thermo Fisher Scientific). Following that, 1 μg of total RNA was reverse transcribed with an iScript cDNA Synthesis Kit (#1708891, Bio-Rad). SensiFAST Probe Lo-ROX and SensiFAST SYBR® Lo-ROX kits (Bioline) were used for qRT-PCRs that were performed with QuantStudio 3 Real-Time PCR system (Applied Biosystems, Thermo Fisher Scientific). All primers and probes were purchased from Sigma Aldrich. The following forward (f) and reverse (r) primers, and probes (pr) were used: fRNA18S5, 5′-GCAATTATTCCCCATGAACG-3′; rRNA18S, 5′- GGGACTTAATCAACGCAAGC-3′; prRNA18S5, 5′-FAM-TTCCCAGTAAGTGCG GGTC-BHQ-3′; fDSC2; 5′-ATCCATTAGAGGACACACTCTGA-3′; rDSC2, 5′- GCCACCGATCCTCTT CCTTC-3′; fPCDHA6, 5′-TGACTGTTGAATGATGGCGGA-3′; rPCDHA6, 5′-TCGGGTACGGAGTAGTGGAG-3′; fPCDHA10, 5′- AGG CATCAGCCAGTTTCTCAA-3′; rPCDHA10, 5′-GAGAGCAGCAGACACTGGAC-3′. The mRNA expression levels were normalized against the respective 18S RNA (*RNA18S5*) expression in a given sample. All reactions were run in triplicate from samples derived from four biological replicates.

3D cell culture and immunofluorescence

5×10^3 U2OS WT and 2KO cells were cultured on Clear Round Bottom Ultra-Low Attachment (ULA) Microplates (#7007, Corning). 1×10^6 cells were used for bacterial plates. After 24 and 48 h, cells were imaged with Axio Vert A1-FL LED microscope (Carl Zeiss). For 3D in Matrigel, cells were embedded in growth factor reduced Matrigel (#356231, Corning) and cultured in Angiogenesis μ-slides (#81501, Ibidi) as described previously (Härmä et al., 2010). Briefly, wells were filled with 10 μl of Matrigel:culture medium (1:1 ratio), which was polymerized at 37°C for 60 min. WT, 2KO, or 2KO#2 cells were seeded on top of the gel at a density of 700 cells per well, let to attach at 37°C for 2 h, and covered with 20 μl of Matrigel:culture medium (1:4 ratio). The upper layer of Matrigel:culture medium was polymerized at 37°C overnight, and appropriate humidity was ensured by adding droplets of MQ-H_2O between the wells. Culture medium was changed every second day, and cell growth was monitored by imaging the cultures with a Zeiss Axio Vert A1-FL LED microscope (Carl Zeiss).

For immunofluorescence, spheroids were washed with 40 μl of PBS and fixed with 25 μl of 4% PFA for 20 min at RT, followed by three washes with 40 μl of PBS. Spheroids were stained with 25 μl of 0.7% Triton X-100, 1:500 Alexa Fluor 488 Phalloidin (#A12379, #A22287, Thermo Fisher Scientific), 300 nM DAPI in PBS at RT for 1 h. The stained spheroids were stored in PBS at 4°C until imaging. The spheroids were imaged as z stacks with a 3i CSU-W1 spinning disc confocal microscope (Intelligent Imaging Innovations) using the same settings between the repeats. Spheroid volume was calculated based on the phalloidin staining using ImageJ v1.51n (Rueden et al., 2017) software with the 3D Object Counter v2.0 (Bolte and Cordelières, 2006) plugin. The threshold for background and object voxels were manually adjusted for each image in order to capture the whole volume of each spheroid.

Visualization of the data

Heatmaps were generated with GraphPad Prism 7 Software (GraphPad Prism Software, La Jolla California USA, https://www.graphpad.com). Venn diagrams were generated with BioVenn web application (http://www.biovenn.nl/). DAVID Bioinformatic Resources 6.7 (https://david-d.ncifcrf.gov/home.jsp) was used for functional annotation clustering.

QUANTIFICATION AND STATISTICAL ANALYSIS

Bioinformatic analysis of the RNA-seq data

The quality of the raw sequencing reads was confirmed with FastQC version 0.20.1 and aligned against the hg38 human genome assembly using TopHat2 version 2.1.0. Subreads version 1.5.0 was used to calculate gene level expression counts according to RefSeq-based gene annotations. The downstream analysis was carried out with R and Bioconductor. The data were normalized with TMM normalization method on the edgeR package. In all sample groups, the Spearman's correlation value was above 0.97, indicating high reproducibility. Statistical testing between the sample groups was carried out using Bioconductor R package Limma (Ritchie et al., 2015) and the differentially expressed genes were filtered using fold change $\geq$ 3 and false discovery rate (FDR) of

0.001 as cutoff. Enrichment analysis for the differentially expressed (DE) filtered genes was performed with topGO and GOstats packages. GO terms in each comparison pair were ranked according to their significance (lowest p value) and the most significantly changed terms were selected for the figures. Additional information regarding the term IDs can be found from http://geneontology.org.

Other data analyses

Statistical analyses were performed with GraphPad Prism 7 and 8 Software (GraphPad Prism Software, La Jolla California USA, https://www.graphpad.com). The statistical significance was analyzed with two-way ANOVA and Holm-Sidak's post hoc test unless indicated differently. For details, see Figures 1, 2, 3, 4, 5, and 6.

DATA AND CODE AVAILABILITY

The original data are available at Gene Expression Omnibus (GEO) database under accession number GSE115973.

Cell Reports, Volume *30*

Supplemental Information

Heat Shock Factor 2 Protects against Proteotoxicity by Maintaining Cell-Cell Adhesion

Jenny Joutsen, Alejandro Jose Da Silva, Jens Christian Luoto, Marek Andrzej Budzynski, Anna Serafia Nylund, Aurelie de Thonel, Jean-Paul Concordet, Valérie Mezger, Délara Sabéran-Djoneidi, Eva Henriksson, and Lea Sistonen

Supplementary Figure 1

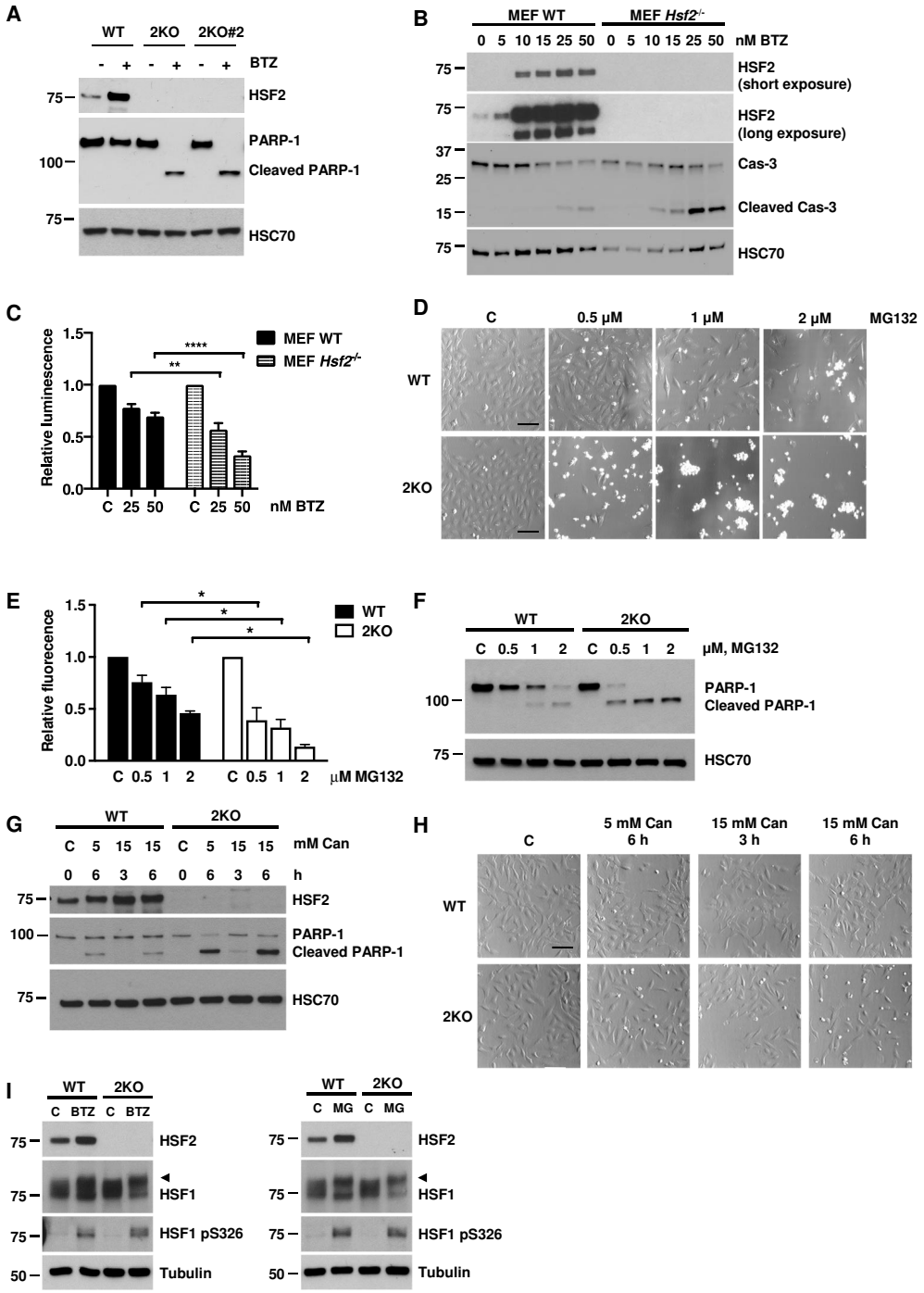

Figure S1. HSF2 depletion sensitizes cells to proteotoxic stress independently of HSF1 phosphorylation on serine 326 (Related to Figure 1). (A) Immunoblot analysis of HSF2 and PARP-1. U2OS WT, 2KO, and HSF2 knock-out clone 2 (2KO#2) cells were treated with 25 nM BTZ for 22 h. Control cells were treated with DMSO. HSC70 was used as a loading control. **(B)** Immunoblot analysis of HSF2 and Caspase-3. WT and $Hsf2^{-/-}$ MEFs were treated with indicated concentrations of BTZ for 22 h. Control cells were treated with DMSO. HSC70 was used as a loading control. **(C)** CellTiter-Glo assay of WT and $Hsf2^{-/-}$ MEFs treated with 25 or 50 nM BTZ for 22 h. Control cells were treated with DMSO. Relative luminescence was calculated against each respective control that was set to 1. The data is presented as mean values of at least three independent experiments + SEM, $^{**}p < 0.01$, $^{****}p < 0.0001$. **(D)** Bright-field microscopy images of U2OS WT and HSF2 KO (2KO) cells treated with indicated concentrations of MG132 for 22 h. Control cells were treated with DMSO. Scale bar 100 µm. **(E)** Calcein AM assay of WT and 2KO cells treated as in D. Relative fluorescence was calculated against each respective control that was set to 1. The data is presented as mean values of at least three independent experiments + SEM, $^{*}p < 0.05$. **(F)** Immunoblot analysis of PARP-1. Cells were treated as in D. HSC70 was used as a loading control. **(G)** Immunoblot analysis of HSF2 and PARP-1. U2OS WT and 2KO cells were starved in L-arginine free growth medium for 17 h after which the medium was supplemented with L-canavanine (Can) in indicated concentrations. Cells were treated in this growth medium for 3 or 6 h. HSC70 was used 32 as a loading control. **(H)** Bright-field microscopy images of U2OS WT and 2KO cells treated as in G. Scale bar 100 µm. **(I)** Immunoblot analysis of HSF2, HSF1 and HSF1 pS326. Cells were treated with either 50 nM BTZ or 10 µM MG132 (MG) for 6 h. Tubulin was used as a loading control. Arrowheads denote hyperphosphorylation of HSF1 (Sarge et al. 1993).

Supplementary Figure 2

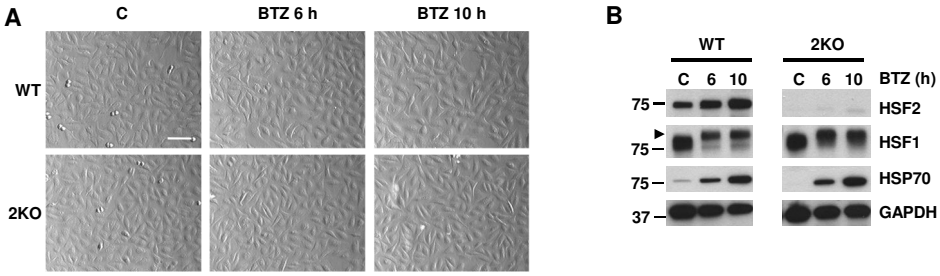

C

Group	Name	minCor	meanCor	medianCor	maxcCor	corSD
1	WT C	0,972	0,975	0,975	0,976	0,002
2	WT 6 h	0,971	0,972	0,972	0,973	0,001
3	WT 10 h	0,972	0,972	0,972	0,973	0,001
4	2KO C	0,973	0,974	0,973	0,975	0,001
5	2KO 6 h	0,972	0,973	0,973	0,974	0,001
6	2KO 10 h	0,972	0,973	0,973	0,974	0,001

Figure S2. RNA-sequencing was performed in WT and HSF2-depleted U2OS cells (Related to Figure 3). (A) Bright-field microscopy images of U2OS WT and HSF2 KO (2KO) cells treated with 25 nM BTZ for 6 or 10 h. Control cells were treated with DMSO. Scale bar 100 µm. (B) Immunoblot analysis of HSF2, HSF1 and HSP70. GAPDH was used as a loading control. Arrowheads denote hyperphosphorylation of HSF1 (Sarge et al. 1993). (C) Spearman's correlation of RNA-seq sample replicates (n = 4).

Supplementary Figure 3

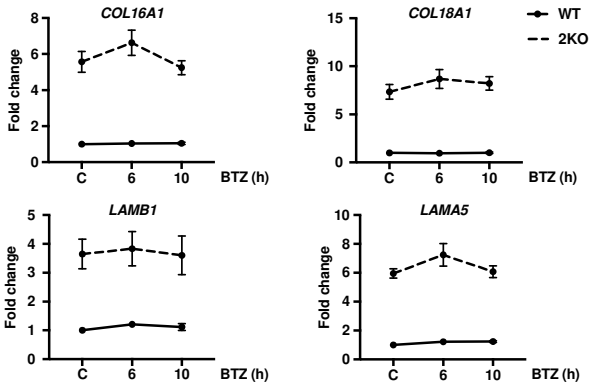

Figure S3. HSF2-dependent genes are linked to cell adhesion (Related to Figure 4.). mRNA expression levels of COL16A1, COL18A1, LAMB1, and LAMA5 in control (C) and BTZ-treated WT and 2KO cells determined with RNA-seq. The data is presented as mean values ± SEM relative to WT control sample that was set to 1.

Supplementary Figure 4

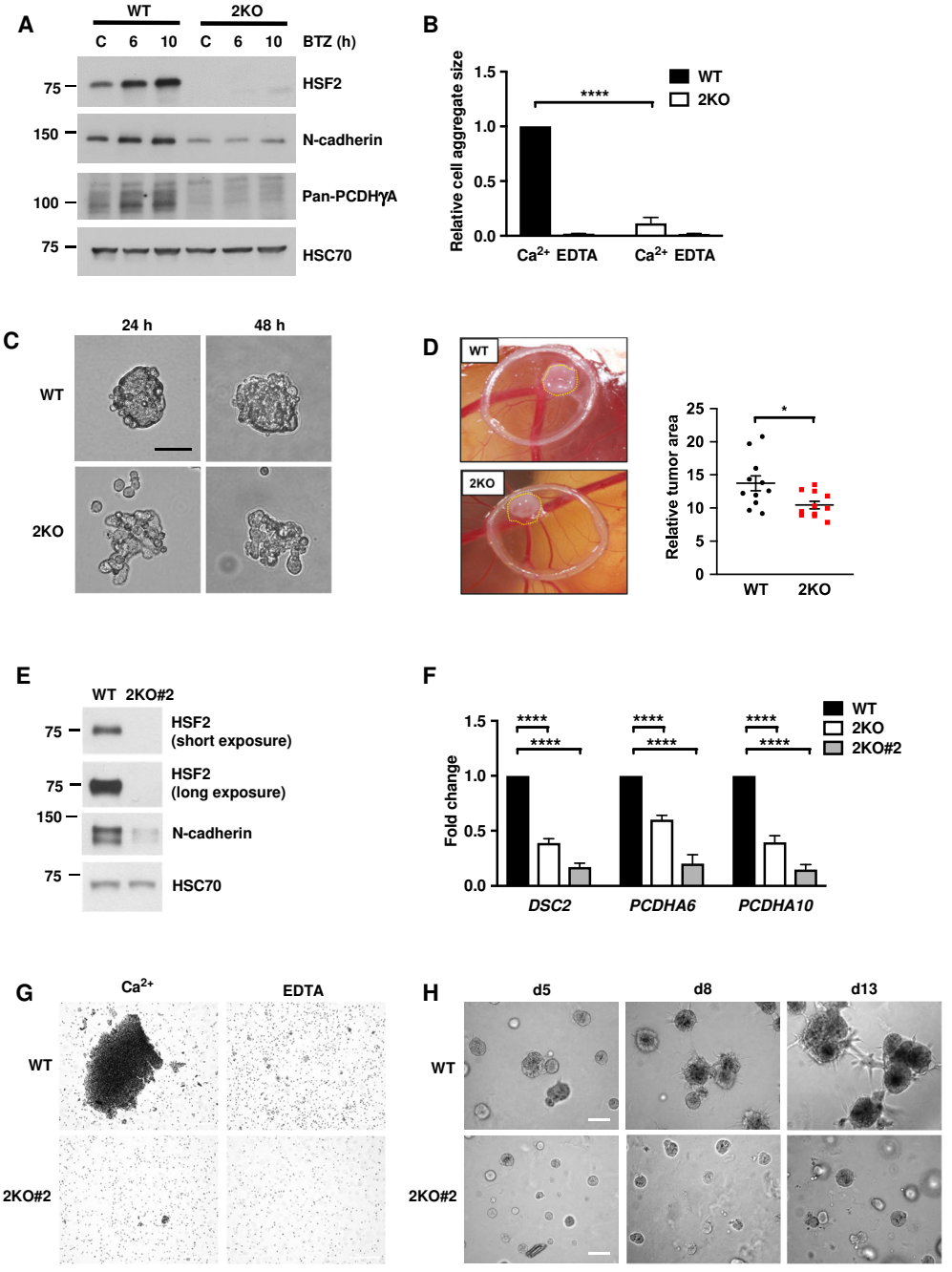

Figure S4. Cadherin misregulation and sensitization to proteotoxicity in the absence of HSF2 (Related to Figure 5). (A) Immunoblot analysis of HSF2, N-cadherin, and the members of PCDHγA (Pan-PCDHγA). U2OS WT and 2KO cells were treated with 25 nM BTZ for 6 or 10 h. HSC70 was used as a loading control. **(B)** The size of the U2OS WT and 2KO cell aggregates was quantified with ImageJ. The data is presented as mean values of three independent experiments + SEM. ****p < 0.0001. **(C)** Bright-field microscopy images of U2OS WT and 2KO cells cultured in bacterial plates. Cells were imaged after 24 and 48 h. Scale bar 200 µm. **(D)** Representative photographs of cells grown on CAM. U2OS WT and 2KO cells were implanted on CAM and the tumor growth was followed for three days. The difference in the area of tumors is visualized by overlaying the area of the WT tumor (dotted yellow line) to the 2KO tumor area. Relative tumor areas were quantified with ImageJ. Statistical analysis was performed with student's t-test. The data is presented as independent data points ± SEM. *p < 0.05. **(E)** Immunoblot analysis of HSF2 and N cadherin in U2OS WT and 2KO#2 cells. HSC70 was used as a loading control. **(F)** mRNA expression of desmocollin 2 (*DSC2*), protocadherin α6 (*PCDHA6*), and protocadherin α10 (*PCDHA10*) of cadherin superfamily in WT, 2KO, and 2KO#2 cells. The mRNA levels were quantified with qRT-PCR. The data is presented as mean values of three independent experiments + SEM, ****p < 0.0001. **(G)** Cell aggregation assay of U2OS WT and 2KO#2 cells suspended in cell aggregation buffer supplemented with 3 mM CaCl2 (Ca^{2+}) or 3 mM EDTA. Cells were rotated for 2.5 h at 37°C and visualized with bright-field microscopy. Scale bar 1 mm. **(H)** Bright-field microscopy images of U2OS WT and 2KO#2 cells cultured in 3D in Matrigel. The spheroids were imaged at days 5, 8, and 13. Scale bar 100 µm.

Supplementary Figure 5

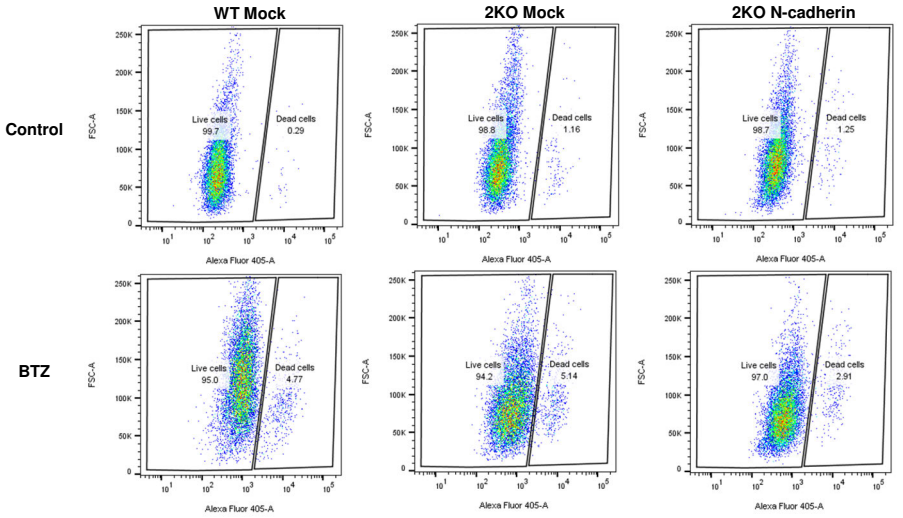

Figure S5. Quantitative analysis of apoptosis (Related to Figure 6). U2OS WT and 2KO cells were transfected and treated as in Figure 6, after which they were stained with anti-cleaved PARP antibody. Fluorescence was analyzed with a flow cytometer using a standard filter set 450/50 nm. The flow cytometry profiles were analyzed using FlowJo 10 software.

6102–6115 *Nucleic Acids Research, 2022, Vol. 50, No. 11* *Published online 10 June 2022*
https://doi.org/10.1093/nar/gkac493

HSFs drive transcription of distinct genes and enhancers during oxidative stress and heat shock

Samu V. Himanen[1,2], Mikael C. Puustinen[1,2], Alejandro J. Da Silva[1,2], Anniina Vihervaara[3] and Lea Sistonen[1,2,*]

[1]Faculty of Science and Engineering, Cell Biology, Åbo Akademi University, 20520 Turku, Finland, [2]Turku Bioscience Centre, University of Turku and Åbo Akademi University, 20520 Turku, Finland and [3]Department of Gene Technology, Science for Life Laboratory, KTH Royal Institute of Technology, 17165 Stockholm, Sweden

Received April 26, 2022; Editorial Decision May 19, 2022; Accepted May 25, 2022

II

ABSTRACT

Reprogramming of transcription is critical for the survival under cellular stress. Heat shock has provided an excellent model to investigate nascent transcription in stressed cells, but the molecular mechanisms orchestrating RNA synthesis during other types of stress are unknown. We utilized PRO-seq and ChIP-seq to study how Heat Shock Factors, HSF1 and HSF2, coordinate transcription at genes and enhancers upon oxidative stress and heat shock. We show that pause-release of RNA polymerase II (Pol II) is a universal mechanism regulating gene transcription in stressed cells, while enhancers are activated at the level of Pol II recruitment. Moreover, besides functioning as conventional promoter-binding transcription factors, HSF1 and HSF2 bind to stress-induced enhancers to trigger Pol II pause-release from poised gene promoters. Importantly, HSFs act at distinct genes and enhancers in a stress type-specific manner. HSF1 binds to many chaperone genes upon oxidative and heat stress but activates them only in heat-shocked cells. Under oxidative stress, HSF1 localizes to a unique set of promoters and enhancers to *trans*-activate oxidative stress-specific genes. Taken together, we show that HSFs function as multi-stress-responsive factors that activate distinct genes and enhancers when encountering changes in temperature and redox state.

GRAPHICAL ABSTRACT

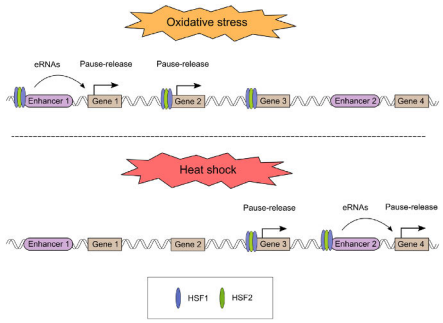

INTRODUCTION

Cells are exposed to various cytotoxic stresses including elevated temperatures and oxidative stress. While increased temperatures lead to protein misfolding, oxidative stress is caused by elevated production of reactive oxygen species (ROS) that oxidize macromolecules (proteins, lipids and nucleic acids) (1,2). Regulation of ROS levels is critical for cell survival and also for normal physiology, since basal levels of ROS activate cellular signaling pathways, while increased production of ROS promotes aging and progression of many diseases, such as cancer (1,3). To combat cytotoxic stresses, cells extensively reprogram their transcription (4). Although genome-wide transcription is repressed upon stress, certain stress-responsive transcription factors can *trans*-activate pro-survival genes, allowing cells to overcome the adverse conditions (4–6). Transcription under oxidative stress is known to be regulated by nuclear factor erythroid 2-related factor 2 (Nrf2) and forkhead box transcription factors (FOXOs), while proteotoxic stress-inducible transcription is driven by a family of heat shock factors (HSFs) (4). In addition to gene activation, cytotoxic con-

*To whom correspondence should be addressed. Tel: +358 2 2153311; Email: lea.sistonen@abo.fi

ditions have been shown to activate transcription at numerous enhancers, which are distal regulatory elements in the DNA that can promote gene expression through loop formation (6–10). Intriguingly, active enhancers produce short and unstable enhancer RNAs (eRNAs) that regulate gene transcription by mechanisms which are not entirely understood (10). The characteristic pattern of eRNA transcription serves as a means to identify active enhancers *de novo* using methods that measure nascent transcription at a nucleotide resolution (11–13).

The master *trans*-activators in stressed cells include the HSFs, which are activated in response to various proteotoxic stresses, e.g. heat shock (14,15). Proteotoxic stress impairs proper protein folding and causes accumulation of unfolded proteins (2). To prevent and mitigate these damages, HSFs rapidly *trans*-activate genes encoding heat shock proteins (HSPs), which, in turn, function as molecular chaperones (4). HSF1 is the master regulator of chaperone expression and the most studied member of the HSF family, whereas HSF2 has been mainly characterized as a developmental transcription factor, particularly in gametogenesis and neurogenesis (15). Intriguingly, exogenous human HSF2, but not HSF1, can substitute for yeast HSF to provide thermotolerance, demonstrating that HSF2 has a capability to act as a stress-responsive transcription factor (16). There is also evidence for a context-dependent interplay between HSF1 and HSF2, either competitive or synergistic, but the functional role of HSF2 in stress-inducible transcription has remained elusive (17,18). Although HSF1 has been identified as the master regulator of the heat shock response and other proteotoxic stresses, it is also activated in response to oxidative stress (19). The biological significance of HSF1 in the regulation of redox status was previously reported in a study, where increased production of cardiac ROS was observed in the absence of HSF1 (20). Nevertheless, how HSF1 and other member of the HSF family contribute to transcriptional reprogramming upon oxidative stress is unknown.

Recently, it was shown that apart from binding promoters, HSF1 is recruited to heat-induced enhancers to activate genes, such as forkhead box O3 (*Foxo3*) and tax1-binding protein 1 (*Tax1bp1*) (6,9,21). The function of the HSF family members in the genome-wide enhancer activation under different stress conditions is, however, not known. In this study, we compared the stress-specific transcription programs by tracking transcription at genes and enhancers in cells exposed to either oxidative stress or heat shock. We used precision run-on sequencing (PRO-seq), which quantifies transcriptionally engaged RNA polymerase II (Pol II) complexes at a single nucleotide resolution across the genome (11). Unlike RNA-seq and other conventional methods that measure steady-state mRNA levels, PRO-seq allows detection of active transcription at promoter-proximal regions, upstream divergent transcripts, gene bodies, termination windows and enhancers (11,12,22). Combining PRO-seq with chromatin immunoprecipitation sequencing (ChIP-seq), we identified HSF1 and HSF2 as new regulators of oxidative stress-inducible transcription. HSF1 and HSF2 were recruited to distinct genomic sites in cells exposed to oxidative stress or heat shock, which triggered the activation of stress-specific transcription programs. Furthermore, besides functioning as conventional promoter-binding transcription factors, HSFs activate several oxidative stress- and heat-inducible enhancers. Finally, we found that in contrast to the promoter-bound HSF1, which drives the classical chaperone genes, binding of HSF1 to enhancers activates genes encoding proteins localized at plasma membrane and cell junctions. Taken together, our results show that HSFs function as multi-stress-responsive transcription factors that orchestrate stress-specific transcription programs through genes and enhancers.

MATERIALS AND METHODS

Cell lines

Wild-type (WT) and HSF1 knock-out (KO) MEFs were derived from mice generated in the laboratory of Ivor J. Benjamin (23). HFS2 KO MEFs were derived from mice generated in the laboratory of Valerie Mezger (24).

Cell culture and treatments

MEFs were grown in Dulbecco's modified Eagle's medium (Sigma) supplemented with 10% fetal bovine serum, 2 mM L-glutamine, 50 μg/ml penicillin/streptomycin, and non-essential amino acids (Gibco). Cells were maintained at 37°C with 5% CO_2. Cells were exposed to heat shock by submerging the cell culture dishes into a 42°C water bath for 1 h. This heat shock condition was used for all the PRO-seq and ChIP-seq analyzes. Oxidative stress was induced by treating the cells with freshly prepared menadione solution at 37°C. For PRO-seq and ChIP-seq, cells were treated with 30 μM menadione for 2 h, whereas for GSH/GSSG assay, cells were treated with 10, 30 and 50 μM menadione for 2 h. DNA damage was induced by exposing cells to 2 mM hydroxyurea for 17 h.

Western blotting

Cells were lysed in Laemmli sample buffer (30% glycerol; 3% SDS; 188 mM Tris–Cl, pH 6.8; 0.015% bromophenol blue; 3% β-mercaptoethanol). Equal volumes of lysates were run on SDS-PAGE, after which proteins were transferred to nitrocellulose membrane. Membranes were blocked with nonfat dried milk diluted in PBS-Tween20 for 1 h at room temperature (RT). Proteins bound to membrane were analyzed using primary antibodies against HSF1 (ADI-SPA-901, Enzo), HSF2 (3E2, EMD Millipore) and β-tubulin (T8328, Merck). Next, the membranes were incubated in secondary HRP-conjugated antibodies, and the proteins were detected with enhanced chemiluminescence.

Immunofluorescence

WT MEFs were plated on MatTek plates (P35GC-1.5-14-C, MatTek Corporation) 48 h before treatments. Cells were fixed with 4% paraformaldehyde (PFA) for 10 min, permeabilized in 0.1% Triton X-100 in PBS and washed three times with PBS. Samples were blocked with 10% FBS in PBS for 1 h at RT and incubated overnight at 4°C with a primary anti-γH2AX antibody (05-636, EMD Millipore,

6104 Nucleic Acids Research, 2022, Vol. 50, No. 11

1:500 in 10% FBS-PBS). Following primary antibody incubations, the samples were washed three times with PBS. Next, samples were incubated in a secondary goat anti-mouse Alexa Fluor488 antibody (A11001, Invitrogen, 1:500 in 10% FBS–PBS) for 1 h at RT. Finally, the samples were washed two times with PBS, incubated with 300 nM DAPI diluted in PBS, and covered with VECTASHIELD mounting medium (H-1000, Vector Laboratories). All images were acquired with a 3i CSU-W1 spinning disc confocal microscope (Intelligent Imaging Innovations).

Measurement of GSH/GSSG ratio

The effect of menadione on the induction of oxidative stress was determined by measuring the ratio between oxidized and reduced glutathione (GSH/GSSG) using a commercial kit by Promega (GSH/GSSG-Glo Assay, V6611).

PRO-seq

PRO-seq was performed from two biological replicates as described previously (11,25). Specifically, PRO-seq was performed in WT, HSF1 KO, and HSF2 KO MEFs that were untreated, exposed to 30 μM menadione for 2 h or heat-shocked at 42°C for 1 h. Nuclei of MEFs were isolated in buffer A (10 mM Tris–HCl pH 7.4, 300 mM sucrose, 3 mM $CaCl_2$, 2 mM $MgCl_2$, 0.1% Triton X-100, 0.5 mM DTT) using a dounce homogenizer. The isolated nuclei were flash-frozen and stored at –80°C in a storage buffer (10 mM Tris–HCl pH 8.0, 25% glycerol, 5 mM $MgCl_2$, 0.1 mM EDTA, 5 mM DTT). Run-on reactions were performed at 37°C for 3 min in the presence of biotinylated nucleotides (5 mM Tris–HCl pH 8.0, 2.5 mM $MgCl_2$, 150 mM KCl, 0.5 mM DTT, 0.5% Sarkosyl, 0.4 u/μl RNase inhibitor, 0.025 mM biotin-ATP/CTP/GTP/UTP [Perkin Elmer]). Equal amounts of nuclei extracted from *Drosophila* S2 cells were used as spike-in material in run-on reactions. Total RNA was isolated with Trizol, precipitated with ethanol and fragmented by base hydrolysis using NaOH. Biotinylated transcripts were isolated with streptavidin-coated magnetic beads (M280, Invitrogen). In the next steps, TruSeq small-RNA adaptors were ligated to the ends of nascent RNAs. Before ligating 5′adaptor, the 5′-cap was removed with RNA 5′ pyrophosphohydrolase (Rpph, NEB), after which 5′end was repaired with T4 polynucleotide kinase (NEB). Nascent RNAs containing the adaptors were converted to cDNA, amplified by PCR and sequenced using NovaSeq 6000. The raw files are available in GEO accession: GSE183245.

ChIP-seq

HSF1- and HSF2-bound DNA fragments were isolated from two biological replicates using ChIP as previously described (26). Specifically, ChIP-seq was performed in WT MEFs that were untreated, exposed to 30 μM menadione for 2 h or heat-shocked at 42°C for 1 h. Cells were crosslinked with 1% paraformaldehyde for 5 min, after which paraformaldehyde was quenched with 125 mM glycine. Cells were lysed and the chromatin was fragmented by sonication with Bioruptor Pico (Diagenode) using seven cycles (30 s on/off). Agarose gel electrophoresis was used to verify that fragment size after sonication was 300–400 bp. The following antibodies were used for immunoprecipitation: HSF1 (ADI-SPA-901, Enzo), HSF2 (26), and normal rabbit IgG (EMD Millipore). Crosslinks were reversed by incubating the samples at 65°C overnight, and the DNA was purified with phenol:chloroform. ChIP-seq libraries were generated using NEXTFLEX ChIP-seq kit and barcodes (Perkin Elmer). NovaSeq 6000 was used to sequence ChIP-seq libraries. The raw files are available in GEO accession: GSE183245.

Mapping of PRO-seq and ChIP-seq data

Adapters were removed from the sequencing reads using cutadapt (27) and the reads were mapped to mouse genome (mm10) using Bowtie 2 (28). PRO-seq reads were mapped in single-end mode with parameters: –sensitive-local. ChIP-seq reads were mapped in paired-end mode with parameters: –sensitive-local –no-mixed –no-discordant –no-unal. The raw data (GSE183245) is available in Gene Expression Omnibus database (https://www.ncbi.nlm.nih.gov/geo/).

Normalization of PRO-seq data

Various strategies are used for the normalization of PRO-seq data, including normalization to spike-ins, read counts in ends of longs genes, and read counts in genes that remain unregulated or inactive across samples (5,7,29–33). Spike-in normalization is highly recommended due to its ability to detect global changes in the level of transcription that would be left undetected with several other methods, such as sequencing depth normalization (29). To utilize spike-ins, we added equal amounts of nuclei from *Drosophila* S2 cells to each run-on reaction in the PRO-seq samples. Since transcripts produced by *Drosophila* S2 nuclei are retained in the samples through every step of PRO-seq, reads mapping to *Drosophila* genome can be used for the normalization of the sample data (9,29,34). Normalization was performed by correcting read counts from spike-in genome to library sizes, followed by calculation of final normalization factors for each sample as described earlier (29).

Normalization of ChIP-seq data

Spike-in normalization was utilized by adding equal amounts of chromatin from heat-shocked human Hs578T cells to each immunoprecipitation reaction. Hs578T cells were exposed to heat shock because it triggers the binding of HSF1 and HSF2 to chromatin, which in turn, allows simultaneous immunoprecipitation of HSF-bound DNA from the sample and spike-in material. We verified that each sample contained equal proportion of spike-in material by mapping the sequencing reads to human genome (hg38).

Quantification of transcription at genes

Actively transcribed genes were identified using discriminative regulatory elements identification from global run-on data (dREG; https://dreg.dnasequence.org) (13), which detects transcription initiation sites at genes and enhancers. Intersecting TSSs of annotated genes with dREG-called initiation sites resulted in a list of 19,350 active genes that were

Nucleic Acids Research, 2022, Vol. 50, No. 11 6105

retained for further analyses. Transcription was quantified from the gene bodies, which were defined as +0.5 kb from TSS to –0.5 kb from CPS. In addition, the maximum length of genes was set to 300 kb, since Pol II can only travel 240 kb during 2 h-treatments at elongation rate of 2 kb/min (35,36).

Identification of transcribed enhancers

Transcribed regulatory regions, including promoters and enhancers, were identified from the PRO-seq data using dREG gateway (https://dreg.dnasequence.org/) (13), as described in previous studies (6,9). The dREG-identified regions of divergent transcription that resided over 1 kb from the TSSs of annotated genes, were defined as transcribed enhancers. To make a unified list of enhancers across the samples, we first identified enhancers individually in each sample and then merged the coordinates of overlapping enhancers using bedtools merge with parameters: d -100 (31). The resulting list contained 44 593 enhancers, whose level of transcription was quantified in each sample from the coordinates detected by dREG. Paused Pol II can be observed at enhancers similarly to promoter-proximal regions, although pausing of Pol II is more evident at promoter-proximal regions (37). Quantification of enhancer transcription from dREG coordinates contains a possible site of Pol II pausing.

Differential expression analysis

Changes in transcription of genes and enhancers were determined using DESeq2 (38). Differential gene expression was measured in gene bodies, whose coordinates were defined as +0.5 kb from TSS to –0.5 kb from CPS. Changes in enhancer transcription were analyzed separately from plus and minus strands using the enhancer coordinates determined with dREG. To call statistically significant changes in transcription of both genes and enhancers, *P*-value threshold was set to 0.05, and fold change threshold to 1.5 for upregulated and to 0.667 for downregulated genes/enhancers.

ChIP-seq peak calling

ChIP-seq peaks were identified from two combined replicates using findPeaks tools included in HOMER program (39). For HSF1 and HSF2 peaks to be called statistically significant, we set the FDR threshold to 0.001 (default value used by HOMER) and required that the fold change over IgG was at least five. For H3K27ac and H3K4me1 peaks to be statistically significant, FDR threshold was set to 0.001 and fold change over input was required to be at least four. HSF1 and HSF2 peaks were called using parameters: -style factor -F 5 -L 7 -localSize 20 000. H3K27ac and H3K4me1 peaks were called using parameters: -region -L 0 -size 250.

GO analysis

Biological processes enriched in distinct groups of HSF target genes were identified using Metascape tool (40) (https://metascape.org/gp/index.html#/main/step1). GO terms were determined for two different heat-inducible gene groups: (i) target genes, whose promoters were bound by HSF1, (ii) target genes devoid of promoter-bound HSF1 that were located within 100 kb of enhancer-bound HSF1. GO terms were ranked in descending order based on the number of genes associated with each term.

Analysis of HSE content

Content of HSE motif in the target genes and enhancers of HSFs was analyzed using findMotifsGenome.pl tool included in HOMER program (39). HSE content was analyzed within 2 kb regions centered around the summits of HSF1 and HSF2 peaks.

Additional datasets used

H3K27ac and H3K4me1 ChIP-seq data is from GEO dataset: GSE99009.

RESULTS

Oxidative stress and heat shock reprogram transcription of distinct genes and enhancers

To examine reprogramming of transcription in response to two different types of cell stress, i.e. oxidative stress and heat shock, we tracked transcription at a nucleotide resolution in mouse embryonic fibroblasts (MEFs) utilizing PRO-seq. For determining the specific roles of HSF1 and HSF2 in orchestrating transcription under these stresses, PRO-seq was performed in HSF1 knock-out (KO) MEFs and HSF2 KO MEFs, in addition to wild-type (WT) MEFs (Supplementary Figure S1A and S1B). Oxidative stress was induced by treating MEFs with different concentrations of a commonly used ROS generator, menadione, for 2 h (41). From the concentrations tested, 30 μM was selected for transcriptional analyses, since it was the lowest concentration that caused oxidative stress, as measured by the decrease in the ratio of reduced and oxidized glutathione (GSG/GSSG) (Supplementary Figure S2). The heat shock response was induced by exposing MEFs to 42°C for 1 h. For accurate analyses of PRO-seq samples between distinct conditions and cell lines, we utilized spike-in normalization, which verified high correlation (rho > 0.95) of the biological replicates (Supplementary Figure S3).

The normalized PRO-seq data was used to investigate the impact of menadione treatment and heat shock on transcription of genes and enhancers. Transcribed regulatory regions were identified using the divergent pattern of transcription that characterizes active promoters and enhancers in mammals (12,13). Enhancers were distinguished from promoters by requiring them to reside over 1 kb from any transcription start site (TSS) of annotated genes. As previously reported (6,13), the active enhancers identified from PRO-seq profiles, contained enhancer-associated histone marks H3K27ac and H3K4me1 (42,43) (Supplementary Figure S4). Both menadione and heat shock caused remarkable changes in transcription of genes and enhancers (Figure 1A). Interestingly, the changes in transcription were more prominent upon oxidative stress than upon heat shock

6106 Nucleic Acids Research, 2022, Vol. 50, No. 11

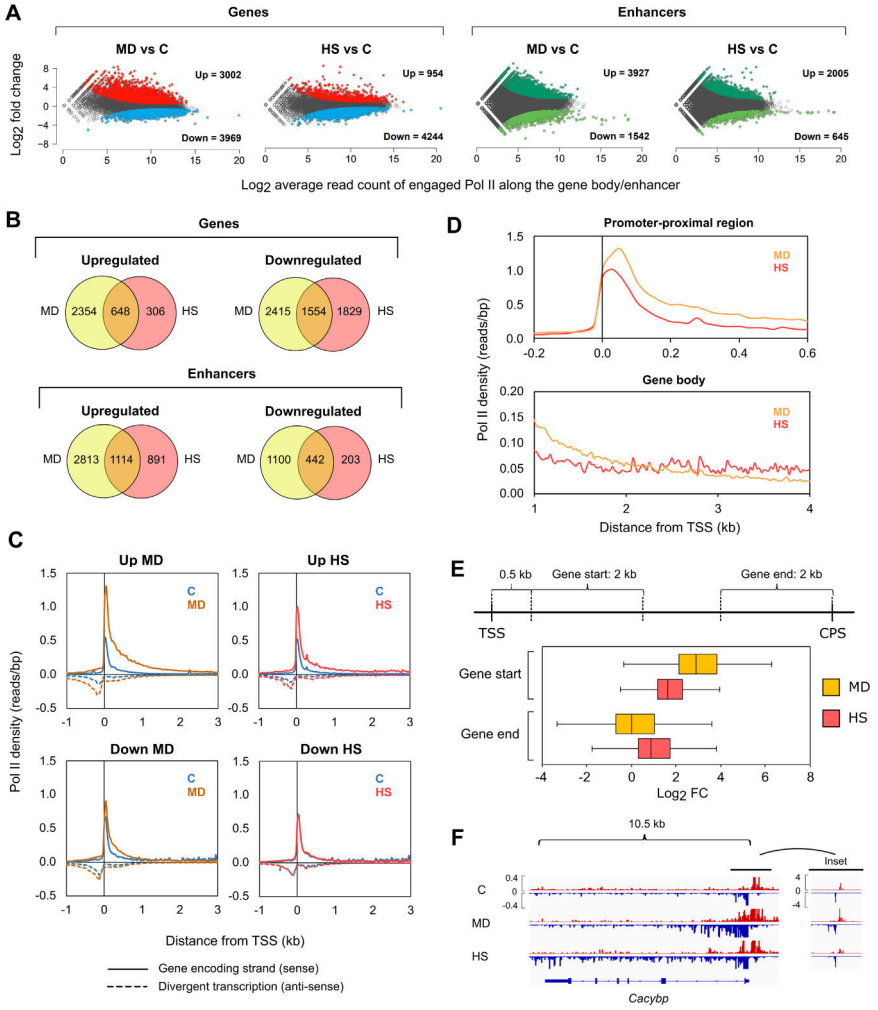

Figure 1. Oxidative stress and heat shock display distinct changes in the transcription of genes and enhancers. PRO-seq was performed in MEFs that were exposed to oxidative stress induced by menadione (MD, 30 μM, 2 h) or to heat shock (HS, 42°C, 1 h). (**A**) The number of upregulated and downregulated genes and enhancers in stressed cells was determined. Threshold for p-value was set to 0.05, and threshold for fold change was set to 1.5 and 0.667 to call statistically significant upregulations and downregulations, respectively. (**B**) Genes and enhancers with altered expression during menadione and heat shock were compared to determine the number of genes and enhancers that were upregulated or downregulated in a stress type-specific manner. (**C**) Average density of Pol II was analyzed upstream and downstream of the TSS in the genes that were upregulated or downregulated by menadione or heat shock. Pol II density was measured separately for the sense (solid line) and antisense (dotted line) strands. (**D**) Pol II densities of upregulated genes in menadione and heat shock samples were overlaid in promoter-proximal region (–0.2–0.6 kb relative to the TSS) and gene body (1–4 kb relative to the TSS). (**E**) Log_2 fold changes (FC) of upregulated genes in cells treated with menadione or heat shock were determined in start and end of the genes. Start of the gene was defined as a 2-kb window starting 0.5 kb downstream from the TSS. End of the gene was defined as a 2-kb window upstream of the CPS. (**F**) PRO-seq profile of calcylin-binding protein (*Cacybp*) gene in cells exposed to menadione and heat shock. C: control.

(Figure 1A). During both stresses, the number of downregulated genes was greater than the number of upregulated genes, whereas enhancers displayed an opposite pattern (Figure 1A). These results show a general reduction of gene transcription in response to stress, accompanied with increased residency of engaged Pol II at enhancers. Comparison of transcriptional changes at individual genes and enhancers, however, revealed a prominent stress-specific reprogramming of transcription (Figure 1B).

Pol II pause-release triggers rapid gene activation in the oxidative stress response

To gain a mechanistic understanding of transcriptional reprogramming, caused by oxidative stress and heat shock, we analyzed the distribution of Pol II along genes and enhancers. Previous studies have shown that upon induction of genes by heat shock, the paused Pol II is released from promoter-proximal regions into elongation simultaneously with the recruitment of new Pol II molecules to the promoters (6,8,44). In contrast, repression of gene transcription by heat shock occurs by reducing the pause-release, which causes accumulation of Pol II within promoter-proximal regions (6). Our results show that the distribution of Pol II in the upregulated and downregulated genes follows the same pattern at the promoter-proximal pause region upon menadione treatment and heat shock, indicating that the induction and repression of transcription is regulated at the level of Pol II pause-release during both types of stress (Figure 1C). These results demonstrate that cells activate and repress stress-specific sets of genes through universal mechanisms.

Engaged Pol II accumulates at enhancers upon oxidative stress and heat shock

The enhancers that were induced upon stress, showed an absence of Pol II under normal growth conditions (Supplementary Figure S5A). Consequently, the critical step in the upregulation of enhancers, upon both oxidative stress and heat shock, was the recruitment of Pol II, which is different from the stress-mediated activation of genes (Supplementary Figure S5A). Downregulated enhancers, in turn, displayed Pol II occupancy already under normal growth conditions, and the occupancy decreased in response to both stresses (Supplementary Figure S5A). Intriguingly, the profiles of downregulated enhancers, showed several Pol II peaks, which implies that transcriptionally active enhancer clusters, also known as super-enhancers (45), lose engaged Pol II under stress conditions.

Increased Pol II density at early gene bodies coincides with oxidative DNA damage

A detailed analysis of Pol II distribution along genes revealed that oxidative stress induced a more profound increase in Pol II density at the promoter-proximal region and beginning of the gene body (0–2 kb from TSS) than was detected at heat-activated genes (Figure 1D). In contrast, as Pol II reached more distal parts of the gene body (2–4 kb from TSS), a higher Pol II density was detected in heat-shocked cells (Figure 1D). Since productive elongation requires Pol II to transcribe through the entire gene body and beyond the cleavage and polyadenylation site (CPS), these results suggest a transcriptional hindrance after the release of paused Pol II in the menadione-treated cells. To investigate whether Pol II proceeded to the end of menadione-activated genes, we determined the fold change of engaged Pol II at the start of the gene (0.5–2.5 kb relative to TSS) and the end of the gene (-2–0 kb relative to CPS) (Figure 1E). We selected the 0.5–2.5 kb region to represent the start of the gene to avoid the paused Pol II from interfering with the measurement of the fold change in the gene body. We also discarded short genes (0–5 kb) from the analysis. Interestingly, menadione caused a greater fold change in the start of the genes than heat shock, while the fold change in the end of the genes was higher upon heat shock (Figure 1E). These results are exemplified by the calcylin-binding protein (*Cacybp*) gene, which is upregulated by both stresses, but shows elevated levels of Pol II throughout the gene body only upon heat shock (Figure 1F).

Although the average induction during menadione treatment was observed particularly in the start of the genes, we found that 37% of the menadione-inducible genes included in the analysis, displayed a fold change above 1.5 also in the end of the genes (Supplementary Figure S5B). Genes that showed increased levels of Pol II throughout the gene body in menadione-treated cells include fork head box O4 (*Foxo4*) and heme oxygenase 1 (*Hmox1*) (Supplementary Figure S5C), known to be critical in the oxidative stress response (46,47). The induction that was observed only in the start of several menadione-inducible genes could occur due to oxidative DNA damage, which has been shown to impede the elongation of Pol II (48). This is supported by our finding, which shows that the amount of DNA damage, as measured by levels of phosphorylated H2AX, was increased in response to menadione but not heat shock (Supplementary Figure S6). Furthermore, the DNA damage is likely to affect open regions, such as early gene bodies where histone acetylation increases upon transcriptional activation (6,49).

HSF1 and HSF2 direct the oxidative stress response

HSF1 is a well-known *trans*-activator of protein folding machinery under proteotoxic stress conditions, while the role of HSF2 in the regulation of stress-inducible transcription has remained elusive (17). For determining the specific roles of HSF1 and HSF2 in transcriptional activation of enhancers and genes during oxidative stress and heat shock, we quantified transcription from the PRO-seq data that we produced from WT, HSF1 KO, and HSF2 KO MEFs. To analyze the impact of HSFs on the enhancer transcription, we selected enhancers that were upregulated in WT MEFs and contained one of the two enhancer-associated histone marks, H3K27ac or H3K4me1 (Supplementary Figure S4). Previously, it has been shown that H3K27ac marks active enhancers, whereas H3K4me1 primes poised enhancers for subsequent activation (43,50,51). Similarly to heat shock, menadione treatment resulted in upregulation of hundreds of genes and enhancers in an HSF1- and/or HSF2-dependent manner (Figure 2A and B). We also found

6108 Nucleic Acids Research, 2022, Vol. 50, No. 11

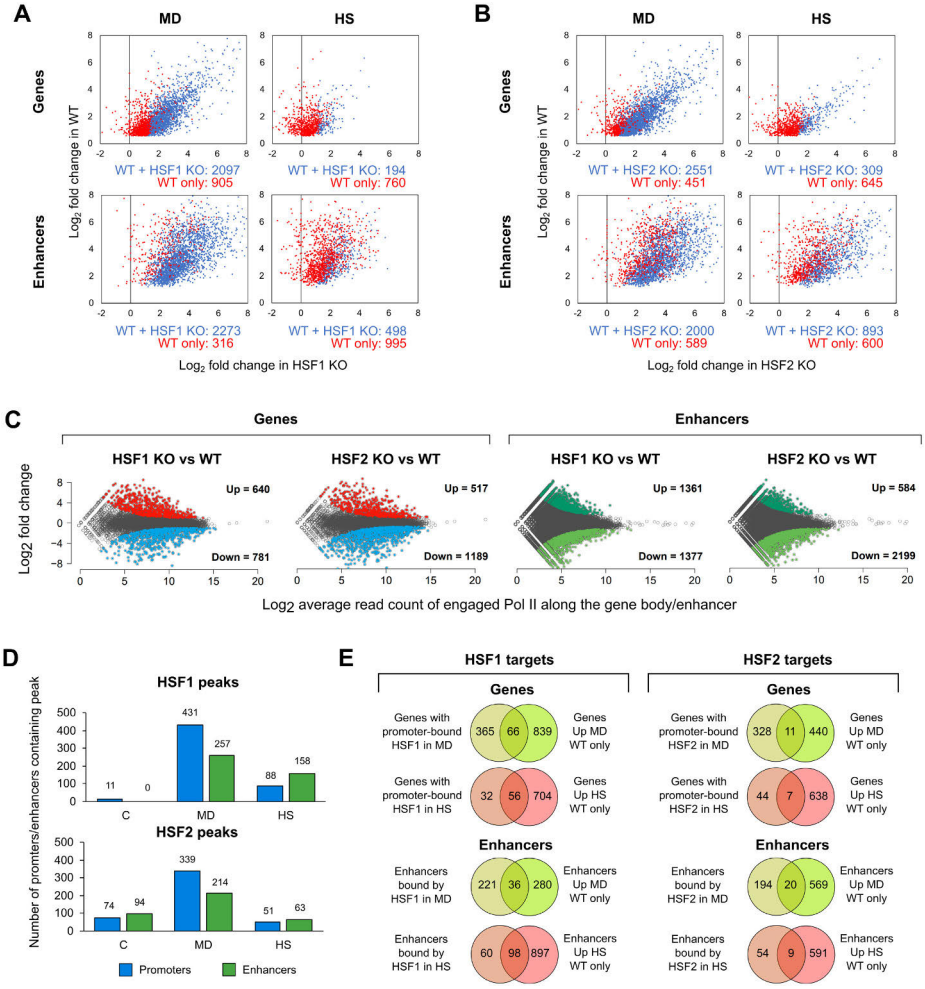

Figure 2. HSF1 and HSF2 reprogram the transcription of genes and enhancers in response to oxidative stress and heat shock. PRO-seq was performed in wild-type (WT), HSF1 knock-out (HSF1 KO) and HSF2 knock-out (HSF2 KO) MEFs that were exposed to oxidative stress induced by menadione (MD, 30 μM, 2 h) or to heat shock (HS, 42°C, 1 h). (**A, B**) Log_2 fold changes are shown for the genes and enhancers that are upregulated either in WT and KO cells (blue dots) or only WT cells (red dots). Some of the HSF-dependent genes and enhancers are likely false positives, since they displayed high fold change in both WT and KO cells (red dots towards the right side of the panels). In these cases, the fold changes in KO cells were not statistically significant and, therefore, these genes and enhancer are upregulated only in WT cells. (**C**) Comparison between KO and WT cells revealed several genes and enhancers that are upregulated or downregulated in HSF1 and HSF2 KO cells under normal growth conditions. (**D**) Antibodies against HSF1 and HSF2 were used to perform ChIP-seq in MEFs that were exposed to menadione or heat shock. The number of promoters and enhancers that contained HSF1 or HSF2 peak was determined in cells exposed to menadione or heat shock. (**E**) Target genes and enhancers regulated through direct binding of HSF1 or HSF2 were identified by comparing the targets bound by HSF1 or HSF2 with the targets that were upregulated only in WT cells. C: control.

Nucleic Acids Research, 2022, Vol. 50, No. 11 **6109**

that the transcriptional program was altered in HSF1 and HSF2 KO MEFs already under normal growth conditions (Figure 2C). This result is in line with the various roles of HSF1 and HSF2 under physiological conditions, including differentiation, development, and cell cycle control as well as in pathological states, such as cancer and neurodegeneration (14,15).

To distinguish the direct targets of HSF1 and HSF2 from the indirect ones, we identified genes and enhancers occupied by HSF1 and HSF2 in stressed cells. We treated WT MEFs with menadione (30 μM, 2 h) or heat shock (42°C, 1 h), and immunoprecipitated HSF1 and HSF2 for the ChIP-seq analysis. A clear correlation was observed between two biological ChIP-seq replicates (Supplementary Figure S7A), and thus, we combined reads from the replicates to perform peak calling. Robustness of the replicates was also evident from the profiles of HSF1 and HSF2 binding at the *Hspa1b* and *Bag3* promoters, both of which are strongly stress-inducible HSF targets (Supplementary Figure S7B). A strong stress-inducible binding of HSF1 to promoters and enhancers was evident during both stresses, and remarkably, the number of HSF1-bound promoters and enhancers was even higher upon menadione treatment than heat shock (Figure 2D). In addition to HSF1, HSF2 displayed a prominent inducible binding to both promoters and enhancers in menadione-treated cells (Figure 2D). Unlike HSF1, HSF2 bound to several targets prior to stress exposures, and the number of HSF2 targets did not increase in response to heat shock (Figure 2D). This observation could be explained by heat-induced degradation of HSF2, which occurs shortly after exposure to heat shock (52). Together, our results indicate distinct kinetics of HSF2-mediated transcription in heat-shocked and ROS-challenged cells.

Next, we identified the direct targets of HSFs whose stress-inducibility was dependent on the binding of HSF1 or HSF2 to the corresponding *cis*-acting elements in the genome. Our analysis revealed a multitude of menadione- and heat-inducible genes and enhancers, which were dependent on HSF1 binding (Figure 2E and Supplementary Table S1). Although menadione-inducible target genes of HSF1 play roles in various biological processes, many of them were related to protein folding (Supplementary Table S1). In line with our previous findings (26), HSF2-dependent heat induction was detected only for seven target genes and nine target enhancers, and HSF2 was not required for stress-inducible upregulation of *HSP* genes (Figure 2E and Supplementary Table S1). Similarly to heat shock, HSF2 was required for induction of only 11 genes and 20 enhancers during oxidative stress, implying that in both stresses, HSF1 functions as a more prominent *trans*-activator than HSF2 (Figure 2E and Supplementary Table S1).

HSF2 cooperates with HSF1 during oxidative stress and heat shock

HSF2 has been primarily described as a modulator of HSF1 activity in the heat shock response (15). In agreement, we found nearly all HSF targets in heat-shocked cells, including ST13 hsp70 interacting protein (*ST13*) gene, to be *trans*-activated in an HSF1-dependent manner (Figure 3B and C, Supplementary Table S1). However, induction of some genes, such as *Adgra3*, was dependent on HSF2, indicating that HSF2 is capable of functioning as a stress-responsive transcription factor (Figure 3B and C, Supplementary Table S1). Next, we sought to understand whether HSF2 plays an HSF1-supportive role in oxidative stress or whether it can *trans*-activate genes and enhancers independently of HSF1. In menadione-treated cells, a majority of HSF-dependent transcriptional induction was triggered by HSF1, as exemplified by an HSF1-specific target gene, solute carrier family 25 member 38 (*Slc25a38*) (Figure 3A and C, Supplementary Table S1). Although three genes and ten enhancers were HSF2-specific targets, most of them displayed equal fold changes in WT and HSF2 KO MEFs exposed to menadione (Figure 3A). Despite the minor effect of HSF2 on stress-induced transcription, HSF2 was found to co-localize to the same sites as HSF1 during both oxidative stress and heat shock, indicating that HSF2 cooperates with HSF1 to orchestrate transcription in response to different types of stress (Figure 3A–C). This is in line with a recent finding demonstrating that HSF2 occupies the same target genes with HSF1 in cancer to drive malignancy (18).

HSFs activate distinct transcription programs through stress-specific binding to chromatin

We found that HSFs regulated unique sets of genes and enhancers in cells treated with menadione or heat shock (Figure 3C and Supplementary Figure S8, Table S1). Next, we asked whether HSFs bind to stress-specific sites in the chromatin to regulate their stress-specific targets. Our results revealed a large group of genes that were occupied and activated by HSF1 only in menadione-treated cells, demonstrating for the first time that HSFs can bind unique sites in response to distinct stress stimuli (Figure 3D, Supplementary Table S1). Interestingly, we found that while heat-inducible HSF1 targets were bound by HSF1 also in response to menadione, a majority of these targets were induced in an HSF1-dependent manner only in heat-shocked cells (Figure 3E, Supplementary Table S1). This implies that HSF1 lack the full *trans*-activation capacity at certain genes during oxidative stress, which could occur either because oxidative stress represses HSF1 or because transcriptional co-activators of HSF1 are not available during oxidative stress.

Differential binding patterns of HSFs between menadione treatment and heat shock could be explained by their preference for distinct target motifs in the DNA. It is known that HSFs bind to their *cis*-acting heat shock elements (HSEs), which were originally defined to contain three inverted nGAAn sequences (53). These motifs are called canonical HSEs, but subsequent studies have identified also non-canonical HSEs, which consist of highly variable sequences (54,55). Therefore, it is plausible that oxidative stress-specific target genes of HSF1 contain primarily non-canonical HSEs that are not recognized by current motif finding algorithms. We found that canonical HSEs were equally prevalent in the menadione- and heat shock-specific target promoters and enhancers of HSF1 (Figure 3F). Taken together, our data indicate that although HSF1 binds to the same HSE motifs in both stresses, it displays

6110 Nucleic Acids Research, 2022, Vol. 50, No. 11

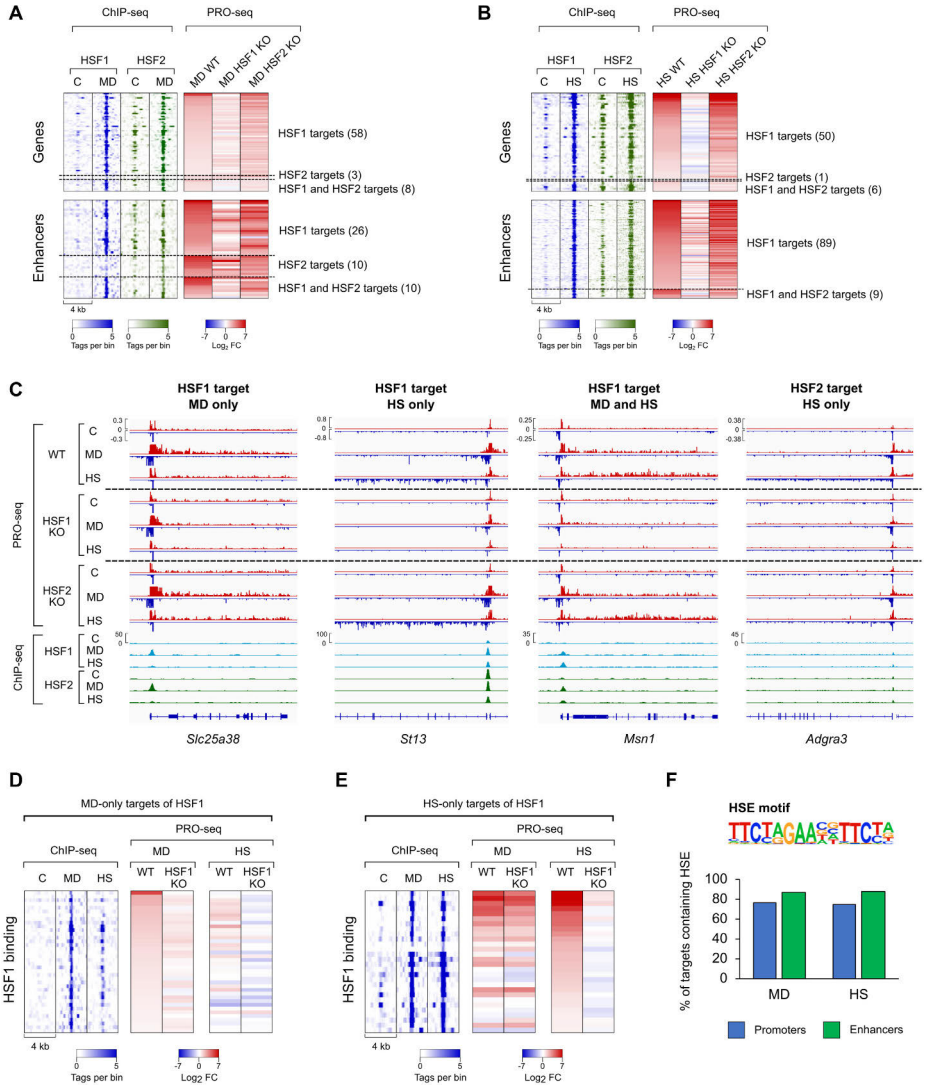

Figure 3. HSF1 and HSF2 drive distinct transcriptional programs upon oxidative stress and heat shock. (**A, B**) Heatmaps were generated from menadione- (MD, 30 μM, 2 h) (A) and heat-treated (HS, 42°C, 1 h) (**B**) MEFs to show genes and enhancers, which are regulated through direct binding of both HSF1 and HSF2 or only one of these factors. (**C**) PRO-seq and ChIP-seq profiles are shown for selected genes that are induced by HSF1 and HSF2 in response to menadione or heat shock. Headings above each of the four panels indicate whether the gene is regulated by HSF1 or HSF2 during menadione, heat shock or both. (**D**, **E**) Heatmaps were generated from menadione- (D) and heat shock (E) -specific target genes of HSF1. (**F**) Motif analysis was performed to determine the percentage of menadione- and heat shock-specific targets of HSF1 that contain canonical HSEs. C: control, *Slc25a38*: solute carrier family 25 member 38, *St13*: Hsp70 interacting protein, *Msn1*: meiosis specific nuclear structural 1, *Adgra3*: adhesion G protein-coupled receptor A3.

stress type-specific binding, which results in the activation of distinct transcription programs.

HSF1 and HSF2 bind enhancers to drive stress-inducible gene transcription

Since a majority of HSF1-dependent genes were not directly regulated by promoter-bound HSF1 (Figure 3E), we hypothesized that these genes could be induced through enhancers. Interestingly, we observed that during heat shock, a prominent number of HSF1-dependent genes resided within 100 kb from the direct enhancer targets of HSF1 (Figure 4A). Furthermore, most of these genes were devoid of promoter-bound HSF1, suggesting that HSF1 regulates a subset of heat-inducible genes through nearby enhancers (Figure 4A). Also, several menadione-induced genes required HSFs for activation and had the closest HSF binding-site at a nearby enhancer (Figure 4A). However, no general correlation was found between the distance of HSF-dependent genes and the enhancers activated in an HSF1-dependent manner upon menadione treatment (Figure 4A).

Since only heat-induced target enhancers and genes of HSF1 were found in the vicinity of each other, we assessed how the HSF1-activated enhancers impact distinct steps of transcription at nearby genes during heat shock. Previous studies have shown that binding of HSF1 to promoters is essential for the heat-inducible pause-release and recruitment of Pol II (56,57). Thus, we analyzed the distribution of Pol II at genes whose heat-induction was indirectly dependent on HSF1 and which were located within 100 kb from direct target enhancers. Our result showed that, similarly to the promoter-bound HSF1, binding of HSF1 to enhancers was required for the pause-release and recruitment of Pol II at nearby genes (Figure 4B). Noteworthy is that the average distribution of Pol II revealed two sites of paused Pol II in the genes that resided in the vicinity of HSF1-bound enhancers, as exemplified by the promoter-proximal region of *B4galt1* gene (Figure 4B and Supplementary Figure S9A). This pausing pattern is in line with previous results showing that certain genes display multiple TSSs (58).

Finally, we addressed whether HSF1 regulates different cellular processes through promoters and enhancers in cells exposed to cytotoxic stress, especially heat shock. For this purpose, we compared GO terms between the direct target genes of HSF1 and the indirect target genes located within 100 kb from its enhancer targets. As expected, the direct HSF1 target genes were related to processes of protein folding, and cellular stress responses (Figure 4C). On the contrary, the indirect target genes residing in the vicinity of enhancer targets were strongly associated with GO terms, such as focal adhesion and transmembrane receptor-linked signaling pathways (Figure 4C). Examples of these targets are filamin b (*Flnb*) and membrane-associated guanylate kinase, WW and PDZ domain containing 1 (*Magi1*) genes, both of which encode proteins localized to the plasma membrane (Figure 4D and Supplementary Figure S9B). Furthermore, certain genes with the highest transcriptional induction, e.g. *Hspb1*, recruited HSF1 both to the promoter and a nearby enhancer (Figure 4D).

Previous studies have shown that besides protein folding, HSFs regulate genes related to many other processes, including cell adhesion (59,60). Moreover, maintenance of cell adhesions was shown to be essential for surviving stress (60). Our results advance these studies by revealing that in contrast to the promoter-bound HSF1, which drives the classical chaperone genes, binding of HSF1 to enhancers activates genes encoding proteins localized at cell junctions and the plasma membrane. We also found that both HSFs are important for the activation of oxidative stress-inducible genes and enhancers, which are different from heat shock-inducible HSF targets. Hereby, we conclude that HSFs function as multi–stress-responsive transcription factors that activate distinct sets of genes and enhancers depending on the type of stress experienced by cells.

DISCUSSION

Mechanisms of transcriptional reprogramming in response to cellular stresses, especially acute heat shock, are well characterized, but they have remained poorly understood under other stress conditions. Here, we provide the first comprehensive study, in which we combined PRO-seq and ChIP-seq to determine the roles of HSF1 and HSF2 in the regulation of nascent transcription in cells exposed to two different types of cytotoxic stress, i.e. oxidative stress and heat shock. As illustrated in our model (Figure 5), these two stresses cause clearly stress type-specific changes to the transcription of genes and enhancers. Although the transcriptional programs differ between oxidative stress and heat shock, our results reveal that during both stresses, genes are regulated at the level of Pol II pause-release, while enhancers are regulated *via* recruitment of Pol II. Unlike heat-inducible genes, a large fraction of oxidative stress-inducible genes displayed elongating Pol II only within the early gene body (0–2 kb from TSS). This could be due to oxidative DNA damage, which has been shown to cause stalling of elongating Pol II (48). Other possible explanations are a slower movement speed of Pol II and a failure in the chromatin remodeling in front of elongating Pol II during oxidative stress.

Transcriptional regulation in oxidative stress responses has been largely devoted to nuclear factor erythroid 2-related factor 2 (Nrf2) and members of the Foxo family (46,61). Here, we expand the repertoire of transcription factors in oxidative stress by identifying HSF1 and HSF2 as new regulators of genes and enhancers in cells exposed to elevated ROS production (Figure 5). This is an important finding, since HSFs have been considered as master regulators of proteotoxic stress responses, especially the heat shock response, and they also play vital roles in cancer progression. While HSF1 triggered genome-wide changes in gene and enhancer transcription, HSF2 was found dispensable for genome-wide stress inducibility. However, HSF2 co-occupied the same promoters and enhancers with HSF1, implying that HSF1 and HSF2 cooperate to drive transcription under distinct types of stress. We also show that HSFs bind and regulate largely different targets upon oxidative stress and heat shock (Figure 5). Intriguingly, HSFs bound to the canonical HSEs in response to both stresses, suggesting that these transcription factors are recruited to their stress type-specific sites through mechanisms that are independent of the target site sequence. It is likely that HSFs

6112 Nucleic Acids Research, 2022, Vol. 50, No. 11

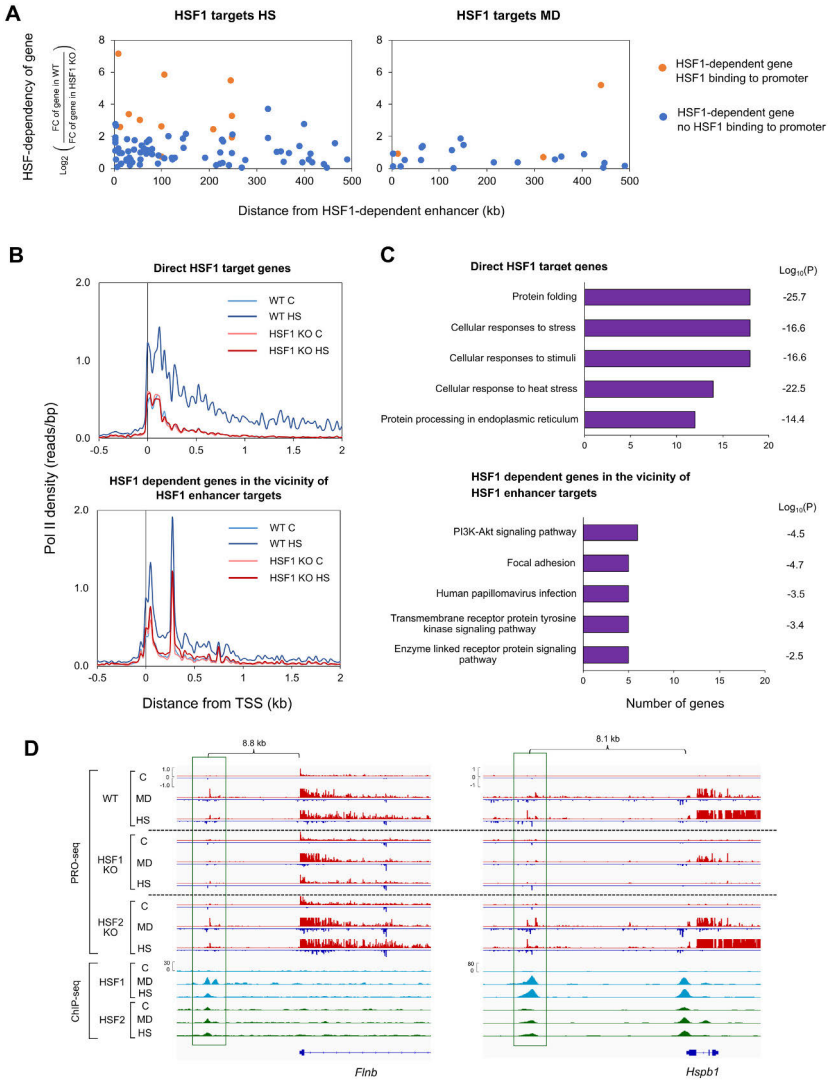

Figure 4. HSF1-dependent genes are located in the vicinity of HSF1-bound enhancers. (**A**) Distances from the target enhancers of HSF1 to the HSF1-dependent genes were measured in cells exposed to menadione (MD, 30 μM, 2 h) and heat shock (HS, 42°C, 1 h). Distances were calculated between the summit of an enhancer and the TSS of a gene. Genes were divided into two groups depending on whether their promoters were bound by HSF1 (orange dots) or not (blue dots). (**B**) Average Pol II density was analyzed in the direct HSF1 target genes and HSF1 dependent genes located within 100 kb of direct enhancer targets of HSF1. Pol II densities are shown in wild-type (WT) and HSF1 knock-out (HSF1 KO) MEFs. (**C**) GO terms of two different heat-inducible gene groups were analyzed: direct HSF1 targets and indirect HSF1 targets that were located within 100 kb of direct enhancer targets of HSF1. GO terms were ranked in descending order based on the number of genes associated with each term. (**D**) PRO-seq and ChIP-seq profiles of selected target enhancers and genes of HSF1 that were found in the vicinity of each other. Enhancers are framed with green rectangles. All the enhancers and *Hspb1* gene are regulated through direct binding of HSF1, while *Flnb* gene is devoid of promoter-bound HSF1. C: control, *Flnb*: filamin b, *B4galt1*: beta-1,4-galactosyltransferase.

Nucleic Acids Research, 2022, Vol. 50, No. 11 **6113**

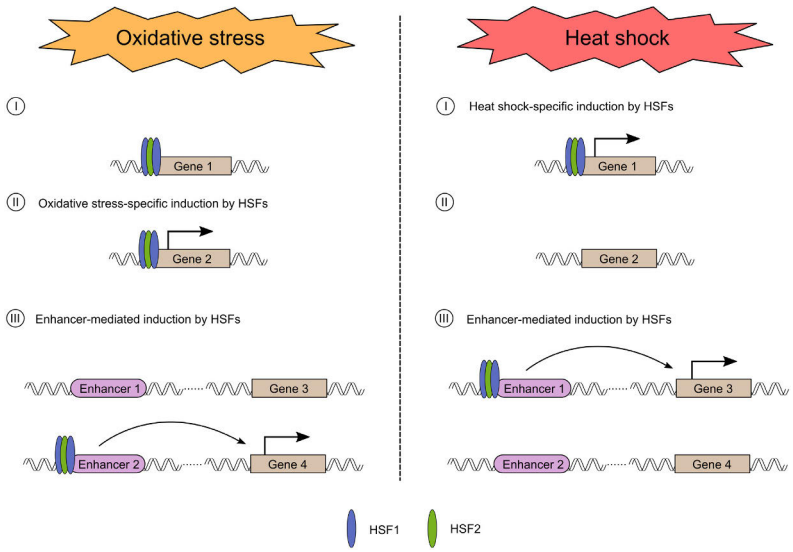

Figure 5. Schematic model of how HSF1 and HSF2 drive stress-specific transcriptional programs through activation of genes and enhancers. (I) HSF1 and HSF2 co-occupy several gene promoters during oxidative stress and heat shock. However, many of these HSF1 and HSF2 -bound genes are only induced in response to heat shock, in an HSF1-dependent manner. (II) Increased levels of ROS trigger HSF1 and HSF2 to bind to their oxidative stress-specific target genes. (III) HSF1 and HSF2 bind stress-inducibly to a large number of enhancers. The HSF-bound enhancers differ in heat shock *versus* oxidative stress, but during both conditions HSFs can trigger the release of paused Pol II from the promoter-proximal region of a nearby gene. Please note, in this model co-occupancy of HSF1 and HSF2 is drawn as a heterotrimer.

bind to their oxidative stress-specific targets by interacting with cofactors that are activated by changes in the cellular redox status. Formation of these interactions, in turn, could involve stress-specific protein modifications, since HSFs are known to undergo extensive post-translational modifications, including the oxidation of two redox-sensitive cysteines within the DNA-binding domain of HSF1 (17,19). In addition, chromatin environment likely undergoes different changes upon oxidative stress and heat shock, which could allow HSFs to access unique sites depending on the type of stress.

Our data uncover a new regulatory level of stress-inducible transcription that is mediated through enhancers, which in turn are activated by HSFs (Figure 5). We found that unlike promoter-bound HSF1, which activates classical chaperone genes, enhancer-bound HSF1 was required for the transcriptional induction of cell type-specific genes, including genes that encode proteins localized in the plasma membrane and cell junctions. Enhancer-mediated induction of genes by HSFs is likely not restricted to stress, since HSFs are important transcription factors in a wide variety of physiological processes, including development, differentiation, and metabolism, as well as pathologies, especially cancer and neurodegeneration (14,15). Furthermore, enhancers play key roles in determining cell fate during development and differentiation, while cancer cells hijack oncogenic enhancers to promote malignancy (62). In future studies, it will be fundamental to determine the functional relevance of HSF-activated enhancers in physiology and pathology.

DATA AVAILABILITY

Collection of PRO-seq and ChIP-seq raw data has been deposited to Gene Expression Omnibus (GEO) database with accession number GSE183245. In addition to raw data, accession contains bedgraph files that are used for the visualization of the data.

SUPPLEMENTARY DATA

Supplementary Data are available at NAR Online.

ACKNOWLEDGEMENTS

We thank all the members of Sistonen laboratory for constructive discussions during the preparation of the manuscript. The Finnish Functional Genomics Centre (Turku Bioscience, University of Turku, Åbo Akademi University and Biocenter Finland) is acknowledged for services, instrumentation and expertise.

FUNDING

Academy of Finland [to A.V., L.S.]; Sigrid Jusélius Foundation [to A.V., L.S.]; Åbo Akademi University [to L.S.]; Can-

cer Foundation Finland [to L.S.]; Magnus Ehrnrooth Foundation [to L.S]; Finnish Cultural Foundation [to S.V.H.]; Alfred Kordelin Foundation [to S.V.H.]; Swedish Cultural Foundation, Finland [to M.C.P.]; Science for Life Laboratory, Sweden [to A.V.]; Joe, Tor and Pentti Borg Foundation [to A.V.]; Svenska Tekniska Vetenskapsakademien i Finland [to A.V.]; South-West Finland's Cancer Foundation [to A.V.]. Funding for open access charge: Sigrid Juselius Foundation.

Conflict of interest statement. None declared.

REFERENCES

1. Sies,H., Berndt,C. and Jones,D.P. (2017) Oxidative stress. *Annu. Rev. Biochem.*, **86**, 715–748.
2. Mogk,A., Bukau,B. and Kampinga,H.H. (2018) Cellular handling of protein aggregates by disaggregation machines. *Mol. Cell*, **69**, 214–226.
3. Forman,H.J. and Zhang,H. (2021) Targeting oxidative stress in disease: promise and limitations of antioxidant therapy. *Nat. Rev. Drug Discov.*, **20**, 689–709.
4. Himanen,S.V. and Sistonen,L. (2019) New insights into transcriptional reprogramming during cellular stress. *J. Cell Sci.*, **132**, jcs238402.
5. Dukler,N., Booth,G.T., Huang,Y., Tippens,N., Danko,C.G., Lis,T. and Siepel,A. (2017) Nascent RNA sequencing reveals a dynamic global transcriptional response at genes and enhancers to the natural medicinal compound celastrol. *Genome Res.*, **27**, 1816–1829.
6. Vihervaara,A., Mahat,D.B., Guertin,M.J., Chu,T., Danko,C.G., Lis,J.T. and Sistonen,L. (2017) Transcriptional response to stress is pre-wired by promoter and enhancer architecture. *Nat. Commun.*, **8**, 255.
7. Nilson,K.A., Lawson,C.K., Mullen,N.J., Ball,C.B., Spector,B.M., Meier,J.L. and Price,D.H. (2017) Oxidative stress rapidly stabilizes promoter-proximal paused pol II across the human genome. *Nucleic Acids Res.*, **45**, 11088–11105.
8. Ray,J., Munn,P.R., Vihervaara,A., Lewis,J.J., Ozer,A., Danko,C.G. and Lis,J.T. (2019) Chromatin conformation remains stable upon extensive transcriptional changes driven by heat shock. *Proc. Natl. Acad. Sci. U.S.A.*, **116**, 19431–19439.
9. Vihervaara,A., Mahat,D.B., Himanen,S.V., Blom,M.A.H., Lis,J.T. and Sistonen,L. (2021) Stress-induced transcriptional memory accelerates promoter-proximal pause release and decelerates termination over mitotic divisions. *Mol. Cell*, **81**, 1715–1731.
10. Hou,T.Y. and Kraus,W.L. (2021) Spirits in the material world: enhancer RNAs in transcriptional regulation. *Trends Biochem. Sci.*, **46**, 138–153.
11. Kwak,H., Fuda,N.J., Core,L.J. and Lis,J.T. (2013) Precise maps of RNA polymerase reveal how promoters direct initiation and pausing. *Science*, **339**, 950–953.
12. Core,L.J., Martins,A.L., Danko,C.G., Waters,C.T., Siepel,A. and Lis,J.T. (2014) Analysis of nascent RNA identifies a unified architecture of initiation regions at mammalian promoters and enhancers. *Nat. Genet.*, **46**, 1311–1320.
13. Wang,Z., Chu,T., Choate,L.A. and Danko,C.G. (2019) Identification of regulatory elements from nascent transcription using dREG. *Genome Res.***29**, 293–303.
14. Gomez-Pastor,R., Burchfiel,E.T. and Thiele,D.J. (2018) Regulation of heat shock transcription factors and their roles in physiology and disease. *Nat. Rev. Mol. Cell Biol.*, **19**, 4–19.
15. Joutsen,J. and Sistonen,L. (2019) Tailoring of proteostasis networks with heat shock factors. *Cold Spring Harb. Perspect. Biol.*, **11**, a034066.
16. Liu,X.D., Liu,P.C.C., Santoro,N. and Thiele,D.J. (1997) Conservation of a stress response: human heat shock transcription factors functionally substitute for yeast HSF. *EMBO J.*, **16**, 6466–6477.
17. Roos-Mattjus,P. and Sistonen,L. (2021) Interplay between mammalian heat shock factors 1 and 2 in physiology and pathology. *FEBS J.*, https://doi.org/10.1111/febs.16178.
18. Smith,R.S., Takagishi,S.R., Amici,D.R., Metz,K., Gayatri,S., Alasady,M.J., Wu,Y., Brockway,S., Taiberg,S.L., Khalatyan,N. *et al.* (2022) HSF2 cooperates with HSF1 to drive a transcriptional program critical for the malignant state. *Sci. Adv.***8**, eabj6526.
19. Ahn,S.G. and Thiele,D.J. (2003) Redox regulation of mammalian heat shock factor 1 is essential for hsp gene activation and protection from stress. *Genes Dev.*, **17**, 516–528.
20. Yan,L., Christians,E.S., Liu,L., Xiao,X., Sohal,R.S. and Benjamin,I.J. (2002) Mouse heat shock transcription factor 1 deficiency alters cardiac redox homeostasis and increases mitochondrial oxidative damage. *EMBO J.*, **21**, 5164–5172.
21. Grossi,V., Forte,G., Sanese,P., Peserico,A., Tezil,T., Signorile,M.L., Fasano,C., Lovaglio,R., Bagnulo,R., Loconte,D.C. *et al.* (2018) The longevity SNP rs2802292 uncovered: HSF1 activates stress-dependent expression of FOXO3 through an intronic enhancer. *Nucleic Acids Res.*, **46**, 5587–5600.
22. Rabenius,A., Chandrakumaran,S., Sistonen,L. and Vihervaara,A. (2022) Quantifying RNA synthesis at rate-limiting steps of transcription using nascent RNA-sequencing data. *STAR Protoc.*, **3**, 101036.
23. McMillan,D.R., Xiao,X., Shao,L., Graves,K. and Benjamin,I.J. (1998) Targeted disruption of heat shock transcription factor 1 abolishes thermotolerance and protection against heat-inducible apoptosis. *J. Biol. Chem.*, **273**, 7523–7528.
24. Kallio,M., Chang,Y., Manuel,M., Alastalo,T.P., Rallu,M., Gitton,Y., Pirkkala,L., Loones,M.T., Paslaru,L., Larney,S. *et al.* (2002) Brain abnormalities, defective meiotic chromosome synapsis and female subfertility in HSF2 null mice. *EMBO J.*, **21**, 2591–2601.
25. Mahat,D.B., Kwak,H., Booth,G.T., Jonkers,I.H., Danko,C.G., Patel,R.K., Waters,C.T., Munson,K., Core,L.J. and Lis,J.T. (2016) Base-pair-resolution genome-wide mapping of active RNA polymerases using precision nuclear run-on (PRO-seq). *Nat. Protoc.*, **11**, 1455–1476.
26. Östling,P., Björk,J.K., Roos-Mattjus,P., Mezger,V. and Sistonen,L. (2007) Heat shock factor 2 (HSF2) contributes to inducible expression of hsp genes through interplay with HSF1. *J. Biol. Chem.*, **282**, 7077–7086.
27. Martin,M. (2011) Cutadapt removes adapter sequences from high-throughput sequencing reads. *EMBnet. J.*, **17**, 10–12.
28. Langmead,B. and Salzberg,S.L. (2012) Fast gapped-read alignment with bowtie 2. *Nat. Methods*, **9**, 357–359.
29. Ball,C.B., Nilson,K.A. and Price,D.H. (2019) Use of the nuclear walk-on methodology to determine sites of RNA polymerase II initiation and pausing and quantify nascent RNAs in cells. *Methods*, **159–160**, 165–176.
30. Mahat,D.B., Salamanca,H.H., Duarte,F.M., Danko,C.G. and Lis,J.T. (2016) Mammalian heat shock response and mechanisms underlying its genome-wide transcriptional regulation. *Mol. Cell*, **62**, 63–78.
31. Duarte,F.M., Fuda,N.J., Mahat,D.B., Core,L.J., Guertin,M.J. and Lis,J.T. (2016) Transcription factors GAF and HSF act at distinct regulatory steps to modulate stress-induced gene activation. *Genes Dev.*, **30**, 1731–1746.
32. Tettey,T.T., Gao,X., Shao,W., Li,H., Story,B.A., Chitsazan,A.D., Glaser,R.L., Goode,Z.H., Seidel,C.W., Conaway,R.C. *et al.* (2019) A role for FACT in RNA polymerase II promoter-proximal pausing. *Cell Rep.*, **27**, 3770–3779.
33. Reimer,K.A., Mimoso,C.A., Adelman,K. and Neugebauer,K.M. (2021) Co-transcriptional splicing regulates 3′ end cleavage during mammalian erythropoiesis. *Mol. Cell*, **81**, 998–1012.
34. Judd,J., Duarte,F.M. and Lis,J.T. (2021) Pioneer-like factor GAF cooperates with PBAP (SWI/SNF) and NURF (ISWI) to regulate transcription. *Genes Dev.*, **35**, 147–156.
35. Danko,C.G., Hah,N., Luo,X., Martins,A.L., Core,L., Lis,J.T., Siepel,A. and Kraus,W.L. (2013) Signaling pathways differentially affect RNA polymerase II initiation, pausing, and elongation rate in cells. *Mol. Cell*, **50**, 212–222.
36. Jonkers,I., Kwak,H. and Lis,J.T. (2014) Genome-wide dynamics of pol II elongation and its interplay with promoter proximal pausing, chromatin, and exons. *eLife*, **3**, e02407.
37. Henriques,T., Scruggs,B.S., Inouye,M.O., Muse,G.W., Williams,L.H., Burkholder,A.B., Lavender,C.A., Fargo,D.C. and Adelman,K. (2018) Widespread transcriptional pausing and elongation control at enhancers. *Genes Dev.*, **32**, 26–41.
38. Love,M.I., Huber,W. and Anders,S. (2014) Moderated estimation of fold change and dispersion for RNA-seq data with DESeq2. *Genome Biol.*, **15**, 550.

39. Heinz,S., Benner,C., Spann,N., Bertolino,E., Lin,Y.C., Laslo,P., Cheng,J.X., Murre,C., Singh,H. and Glass,C.K. (2010) Simple combinations of lineage-determining transcription factors prime cis-regulatory elements required for macrophage and b cell identities. *Mol. Cell*, **38**, 576–589.
40. Zhou,Y., Zhou,B., Pache,L., Chang,M., Khodabakhshi,A.H., Tanaseichuk,O., Benner,C. and Chanda,S.K. (2019) Metascape provides a biologist-oriented resource for the analysis of systems-level datasets. *Nat. Commun.*, **10**, 1523.
41. Klotz,L.O., Hou,X. and Jacob,C. (2014) 1,4-naphthoquinones: From oxidative damage to cellular and inter-cellular signaling. *Molecules*, **19**, 14902–14918.
42. Heintzman,N.D., Stuart,R.K., Hon,G., Fu,Y., Ching,C.W., Hawkins,R.D., Barrera,L.O., van Calcar,S., Qu,C., Ching,K.A. *et al.* (2007) Distinct and predictive chromatin signatures of transcriptional promoters and enhancers in the human genome. *Nat. Genet.*, **39**, 311–318.
43. Creyghton,M.P., Cheng,A.W., Welstead,G.G., Kooistra,T., Carey,B.W., Steine,E.J., Hanna,J., Lodato,M.A., Frampton,G.M., Sharp,P.A. *et al.* (2010) Histone H3K27ac separates active from poised enhancers and predicts developmental state. *Proc. Natl. Acad. Sci. U.S.A.*, **107**, 21931–21936.
44. Gressel,S., Schwalb,B. and Cramer,P. (2019) The pause-initiation limit restricts transcription activation in human cells. *Nat. Commun.*, **10**, 3603.
45. Hnisz,D., Abraham,B.J., Lee,T.I., Lau,A., Saint-André,V., Sigova,A.A., Hoke,H.A. and Young,R.A. (2013) Super-enhancers in the control of cell identity and disease. *Cell*, **155**, 934–947.
46. Tothova,Z., Kollipara,R., Huntly,B.J., Lee,B.H., Castrillon,D.H., Cullen,D.E., McDowell,E.P., Lazo-Kallanian,S., Williams,I.R., Sears,C. *et al.* (2007) FoxOs are critical mediators of hematopoietic stem cell resistance to physiologic oxidative stress. *Cell*, **128**, 325–339.
47. Loboda,A., Damulewicz,M., Pyza,E., Jozkowicz,A. and Dulak,J. (2016) Role of Nrf2/HO-1 system in development, oxidative stress response and diseases: an evolutionarily conserved mechanism. *Cell. Mol. Life Sci.*, **73**, 3221–3247.
48. Oh,J., Fleming,A.M., Xu,J., Chong,J., Burrows,C.J. and Wang,D. (2020) RNA polymerase II stalls on oxidative DNA damage via a torsion-latch mechanism involving lone pair–π and CH–π interactions. *Proc. Natl. Acad. Sci. U.S.A.*, **117**, 9338–9348.
49. Mueller,B., Mieczkowski,J., Kundu,S., Wang,P., Sadreyev,R., Tolstorukov,M.Y. and Kingston,R.E. (2017) Widespread changes in nucleosome accessibility without changes in nucleosome occupancy during a rapid transcriptional induction. *Genes Dev.*, **31**, 451–462.
50. Bonn,S., Zinzen,R.P., Girardot,C., Gustafson,E.H., Perez-Gonzalez,A., Delhomme,N., Ghavi-Helm,Y., Wilczyński,B., Riddell,A. and Furlong,E.E.M. (2012) Tissue-specific analysis of chromatin state identifies temporal signatures of enhancer activity during embryonic development. *Nat. Genet.*, **44**, 148–156.
51. Wang,C., Lee,J.E., Lai,B., Macfarlan,T.S., Xu,S., Zhuang,L., Liu,C., Peng,W. and Ge,K. (2016) Enhancer priming by H3K4 methyltransferase MLL4 controls cell fate transition. *Proc. Nat. Acad. Sci. U.S.A.*, **113**, 11871–11876.
52. Ahlskog,J.K., Björk,J.K., Elsing,A.N., Aspelin,C., Kallio,M., Roos-Mattjus,P. and Sistonen,L. (2010) Anaphase-promoting complex/cyclosome participates in the acute response to protein-damaging stress. *Mol. Cell. Biol.*, **30**, 5608–5620.
53. Amin,J., Ananthan,J. and Voellmy,R. (1988) Key features of heat shock regulatory elements. *Mol. Cell. Biol.*, **8**, 3761–3769.
54. Jaeger,A.M., Makley,L.N., Gestwicki,J.E. and Thiele,D.J. (2014) Genomic heat shock element sequences drive cooperative human heat shock factor 1 DNA binding and selectivity. *J. Biol. Chem.*, **289**, 30459–30469.
55. Li,J., Chauve,L., Phelps,G., Brielmann,R.M. and Morimoto,R.I. (2016) E2F coregulates an essential HSF developmental program that is distinct from the heat-shock response. *Genes Dev.*, **30**, 2062–2075.
56. Lis,J.T., Mason,P., Peng,J., Price,D.H. and Werner,J. (2000) P-TEFb kinase recruitment and function at heat shock loci. *Genes Dev.*, **14**, 792–803.
57. Takii,R., Fujimoto,M., Matsumoto,M., Srivastava,P., Katiyar,A., Nakayama,K.I. and Nakai,A. (2019) The pericentromeric protein shugoshin 2 cooperates with HSF1 in heat shock response and RNA pol II recruitment. *EMBO J.*, **38**, e102566.
58. Carninci,P., Sandelin,A., Lenhard,B., Katayama,S., Shimokawa,K., Ponjavic,J., Semple,C.A.M., Taylor,M.S., Engström,P.G., Frith,M.C. *et al.* (2006) Genome-wide analysis of mammalian promoter architecture and evolution. *Nat. Genet.*, **38**, 626–635.
59. Mendillo,M.L., Santagata,S., Koeva,M., Bell,G.W., Hu,R., Tamimi,R.M., Fraenkel,E., Ince,T.A., Whitesell,L. and Lindquist,S. (2012) HSF1 drives a transcriptional program distinct from heat shock to support highly malignant human cancers. *Cell*, **150**, 549–562.
60. Joutsen,J., da Silva,A.J., Luoto,J.C., Budzynski,M.A., Nylund,A.S., de Thonel,A., Concordet,J.P., Mezger,V., Sabéran-Djoneidi,D., Henriksson,E. *et al.* (2020) Heat shock factor 2 protects against proteotoxicity by maintaining cell-cell adhesion. *Cell Rep.*, **30**, 583–597.
61. Malhotra,D., Portales-Casamar,E., Singh,A., Srivastava,S., Arenillas,D., Happel,C., Shyr,C., Wakabayashi,N., Kensler,T.W., Wasserman,W.W. *et al.* (2010) Global mapping of binding sites for Nrf2 identifies novel targets in cell survival response through chip-seq profiling and network analysis. *Nucleic Acids Res.*, **38**, 5718–5734.
62. Ko,J.Y., Oh,S. and Yoo,K.H. (2017) Functional enhancers as master regulators of tissue-specific gene regulation and cancer development. *Mol. Cells*, **40**, 169–177.

Supplementary Materials for

HSFs drive transcription of distinct genes and enhancers during oxidative stress and heat shock

Samu V Himanen[1,2], Mikael C Puustinen[1,2], Alejandro J Da Silva[1,2], Anniina Vihervaara[3], Lea Sistonen[1,2*]

Correspondence to: lea.sistonen@abo.fi

This PDF file includes:

Figs. S1 to S9

Table S1

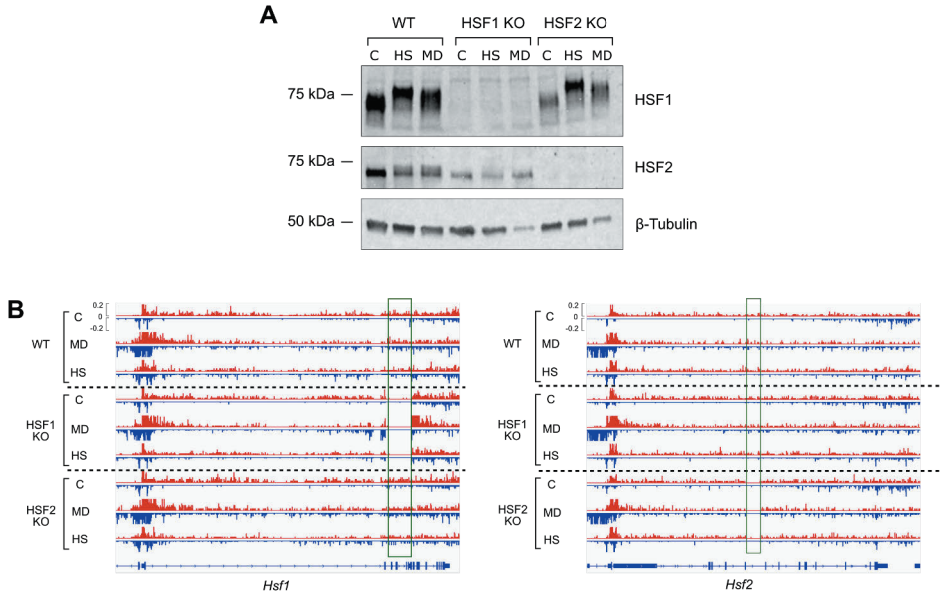

Figure S1. Validation of HSF1 and HSF2 knock out MEFs. (**A**) Western blot was used to determine the levels of HSF1 and HSF2 in wild-type (WT), HSF1 knock-out (HSF1 KO) and HSF2 knock-out (HSF2 KO) MEFs that were exposed to menadione (MD, 30 μM, 2 h) or to heat shock (HS, 42°C, 1 h). β-tubulin was used as a loading control. (**B**) PRO-seq profiles of *Hsf1* and *Hsf2* genes in WT, HSF1 KO and HSF2 KO MEFs that were exposed to menadione or heat shock. Green rectangles indicate regions of HSF1 and HSF2 genes that were deleted to create KO mice, from which the cell lines used in this study have been derived. C: control.

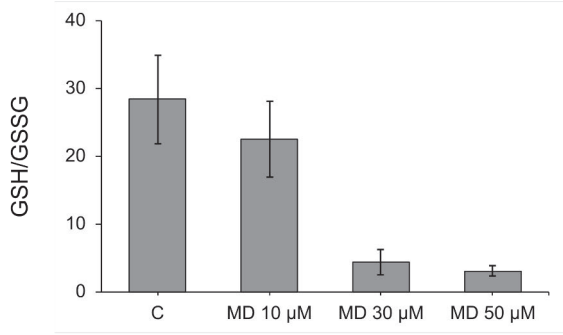

Figure S2. Measurement of GSH/GSSG ratio in menadione-treated cells. MEFs were treated with different concentration of menadione for 2 h to induce oxidative stress. Next, the level of oxidative stress was assessed by measuring the ratio between reduced and oxidized glutathione (GSH/GSSG).

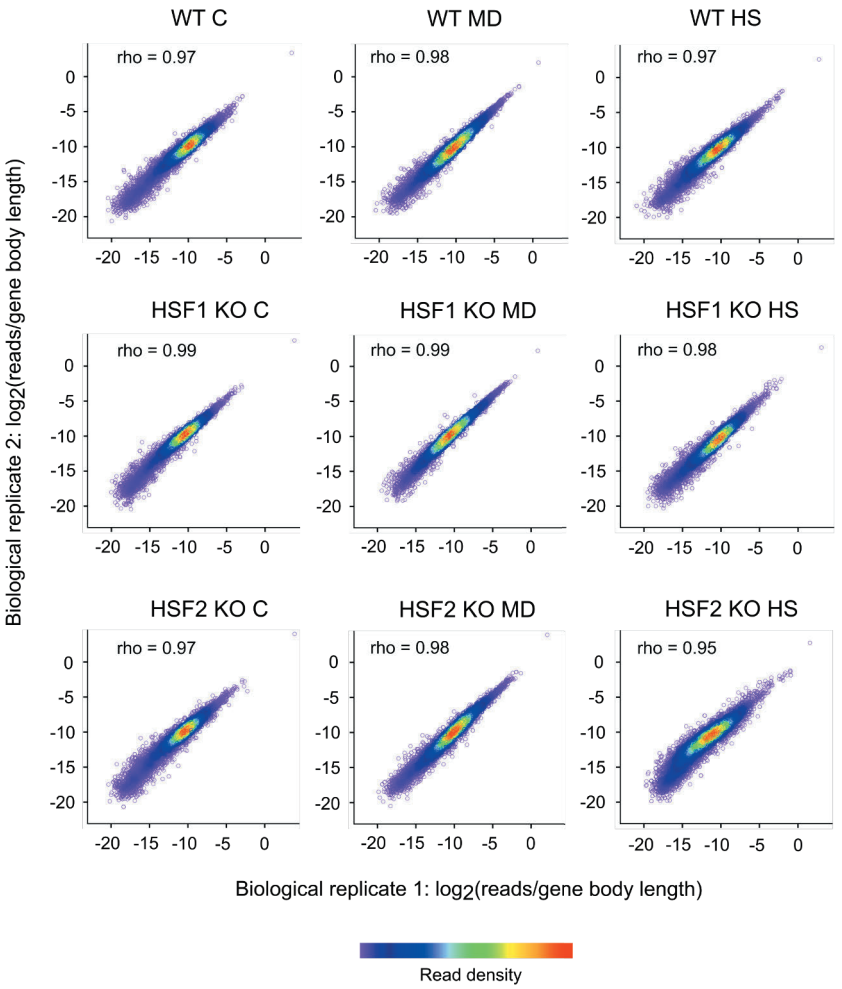

Figure S3. Correlation between biological PRO-seq replicates. PRO-seq was performed in wild-type (WT), HSF1 knock-out (HSF1 KO) and HSF2 knock-out (HSF2 KO) MEFs that were exposed to oxidative stress induced by menadione (MD, 30 μM, 2 h) or to heat shock (HS, 42°C, 1 h). Correlation plots of gene body transcription are shown between two biological PRO-seq replicates. Rho indicates Spearman rank correlation.

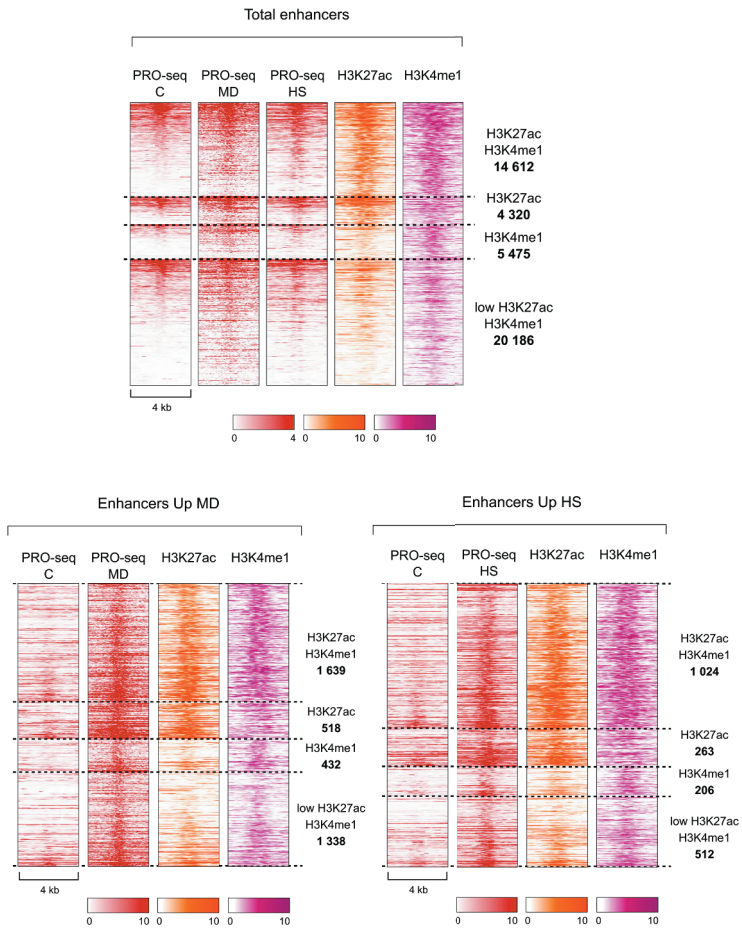

Figure S4. Enhancers detected by PRO-seq contain enhancer-associated histone marks, H3K27ac and H3K4me1. PRO-seq was used to identify transcriptionally active enhancers in MEFs treated with menadione (MD, 30 μM, 2 h) or heat shock (HS, 42°C, 1 h). Enhancers were analyzed for their content of histone marks H3K27ac and H3K4me1, both of which are known to be enriched in enhancers (42, 43). Histone marks were analyzed separately from total enhancers and upregulated enhancers. Intensity of the signal in the heatmaps indicates the number of tags per bin. Bin size was set to 50 bp. C: control.

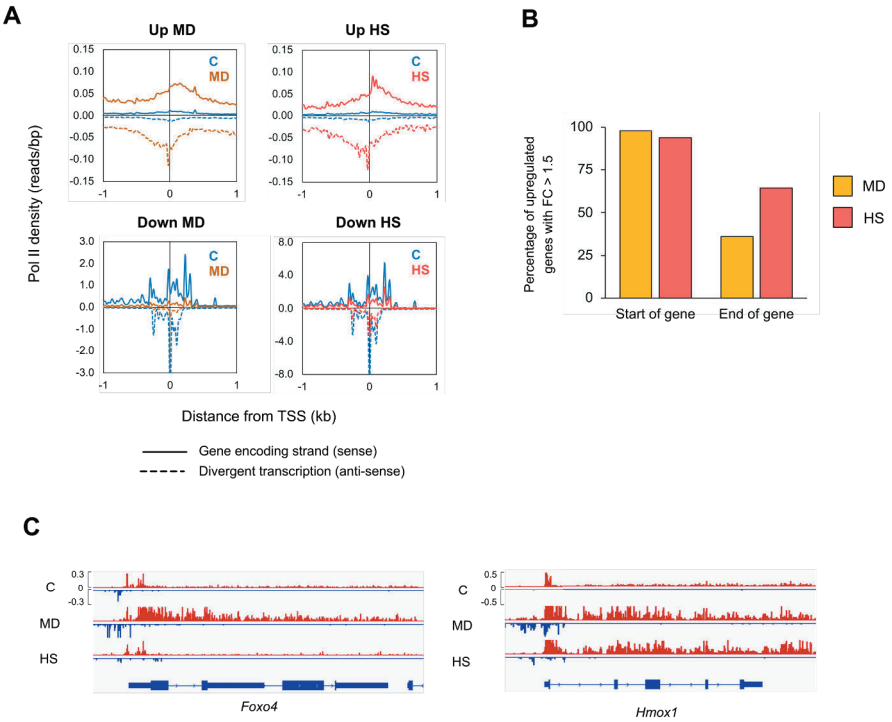

Figure S5. Profiles of Pol II are similar in enhancers but different in genes between oxidative stress- and heat-treated cells. (**A**) PRO-seq was performed in MEFs that were exposed to oxidative stress induced by menadione (MD, 30 μM, 2 h) or to heat shock (HS, 42°C, 1 h). Average density of Pol II was analyzed within enhancers that were upregulated or downregulated by menadione or heat shock. Pol II density was measured separately for plus (solid line) and minus (dotted line) strands. (**B**) Fold changes (FC) of upregulated genes in menadione- and heat-treated cells were determined in start and end of the genes. After this, the percentage of genes that displayed FC over 1.5 in gene start or end were calculated. Start of the gene was defined as a 2 kb window starting 0.5 kb downstream from TSS. End of the gene was defined as a 2kb window upstream of CPS. (**C**) PRO-seq profiles of *Foxo4* and *Hmox1* genes in cells exposed to menadione and heat shock. C: control, *Foxo4*: fork head box O4, *Hmox1*: and heme oxygenase 1.

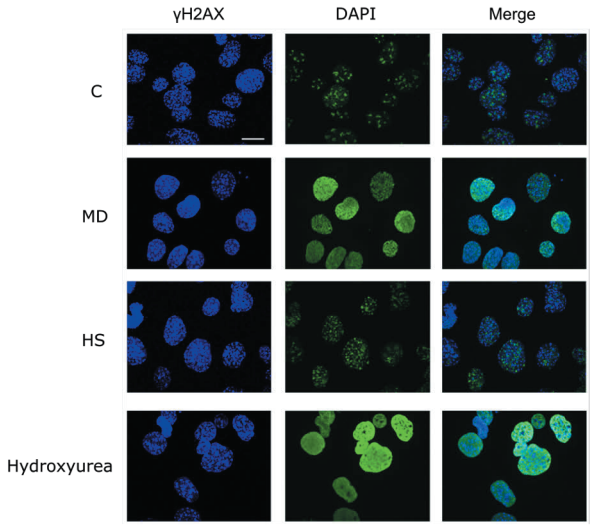

Figure S6. Oxidative stress induced by menadione causes DNA damage. MEFs were exposed to oxidative stress induced by menadione (MD, 30 µM, 2 h) or to heat shock (HS, 42°C, 1 h). The amount of DNA damage was determined by immunofluorescence staining of the phosphorylated H2AX (γH2AX). Hydroxyurea (2 mM, 17 h) was used as a positive control to induce DNA damage. DAPI was used to stain DNA. All images correspond to maximum intensity projections. Scalebar: 20 µm. C: control.

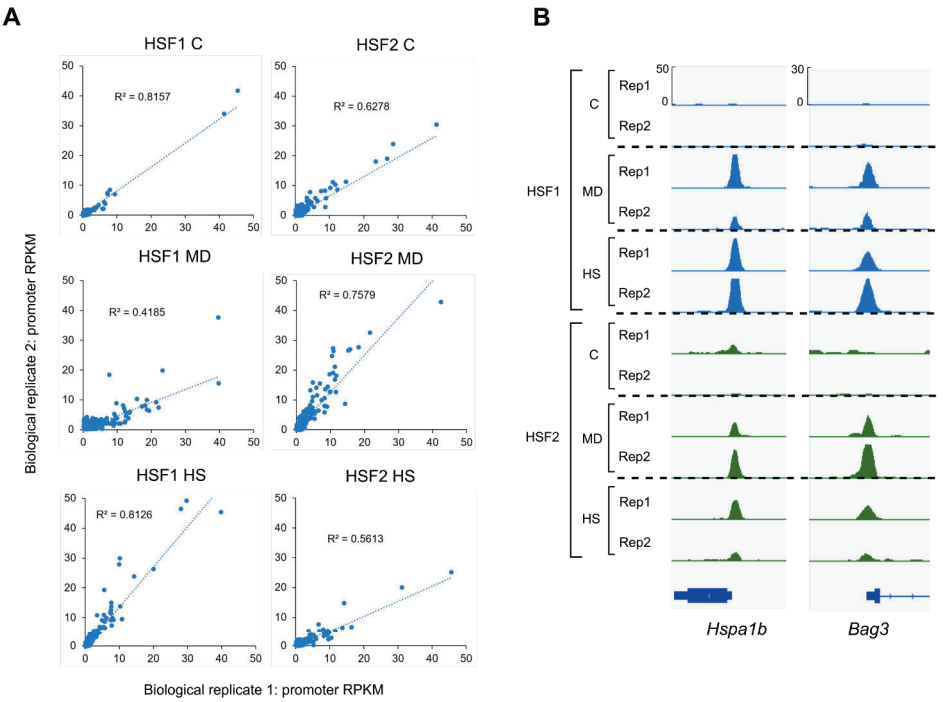

Figure S7. Correlation between biological ChIP-seq replicates. Antibodies against HSF1 and HSF2 were used to perform ChIP-seq in MEFs that were exposed to menadione (MD, 30 µM, 2 h) or to heat shock (HS, 42°C, 1 h). (**A**) Correlation plots of RPKM values at promoters are shown between two biological ChIP-seq replicates. Promoters were defined as 0.5 kb windows centered around TSSs. (**B**) HSF1 and HSF2 occupancies at the *Hspa1b* and *Bag3* promoters are shown in two biological replicates. HSF1 and HSF2 signals in the profiles were normalized to total read counts.

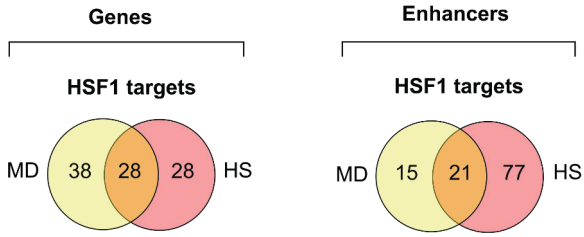

Figure S8. HSF1 regulates stress-specific sets of genes and enhancers. Comparison between menadione- and heat-inducible targets of HSF1 revealed genes and enhancers that are regulated by HSF1 in a stress type-specific manner.

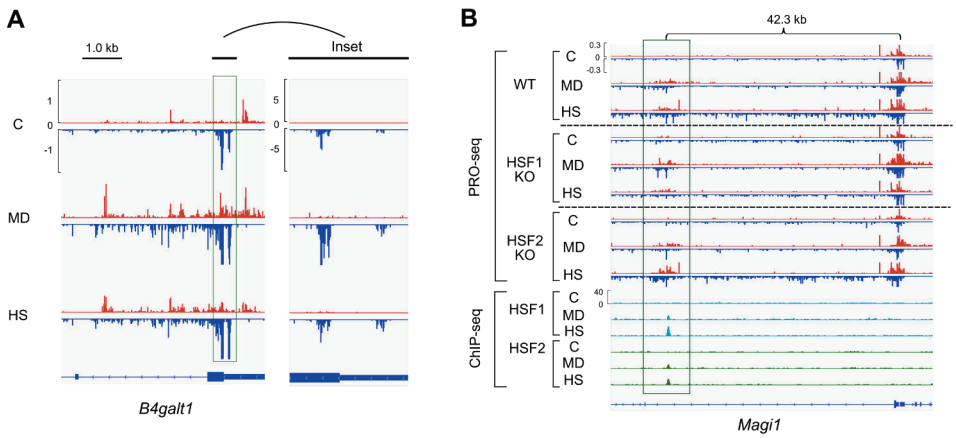

Figure S9. Direct target enhancer of HSF1 is located in the vicinity of the HSF1-dependent gene, *Magi1*. (**A**) PRO-seq profile of *B4galt1* gene showing two distinct TSSs. (**B**) PRO-seq and ChIP-seq profiles of *Magi1* gene and its downstream enhancer. Enhancer is framed with green rectangle. Enhancer is regulated by direct binding of HSF1, while *Magi1* gene is devoid of promoter-bound HSF1. C: control; MD: menadione, 30 μM, 2 h; HS: heat shock, 42°C, 1 h; *B4galt*1: beta-1,4-galactosyltransferase 1; *Magi1*: membrane associated guanylate kinase, WW and PDZ domain containing 1.

Table S1. List of oxidative stress- and heat shock-inducible target genes of HSF1 and HSF2. Combination of PRO-seq and ChIP-seq was used to identify genes in MEFs that are regulated through direct binding of HSF1 and HSF2 during oxidative stress induced by menadione (MD, 30 μM, 2 h) or heat shock (HS, 42°C, 1 h). Genes in the list are ranked in the descending order according to their fold change (FC) in wild-type MEFs.

HSF1 target genes in HS		**HSF1 target genes in MD**		**HSF2 target genes in HS**		**HSF2 target genes in MD**	
Gene name	FC in WT	Gene name	FC in WT	Gene name	FC in WT	Gene name	FC in WT
Hspa1a	308.8	Hspa1l	47.7	Adgra3	2.9	Bst2	3.7
Hspb1	266.3	Mest	37.1	Slc35e2	2.1	Txnip	2.0
Hspa1b	112.0	Lrrc61	7.6	Ints2	2.0	Mcoln1	1.9
Hsph1	76.4	Hsph1	6.8	Xpnpep3	1.8	Cnpy4	1.9
Dnaja4	48.9	Hikeshi	5.3	Abcc5	1.8	Commd3	1.8
Hspa1l	23.7	Rbm42	5.2	Ptges3	1.7	Ube2g2	1.8
Dnajb1	20.7	Mns1	4.9	Vipas39	1.6	Aox1	1.8
Hsp90aa1	18.9	Slc25a38	4.9			Aptx	1.8
Hspe1	18.3	Nfkbid	4.7			Dnajb5	1.7
Hspa4l	14.8	Bst2	3.7			Atg3	1.6
Bag3	13.5	Gm10069	3.7			Hsp90b1	1.5
Mns1	13.0	Zscan29	3.7				
Dnaja1	9.2	Gm13830	3.6				
Swt1	8.9	Kctd18	3.4				
Hspd1	6.6	Saraf	3.4				
Serpinh1	6.3	Gm6297	3.3				
Gm10069	6.3	Rras	3.2				
Hspb8	5.7	Cacybp	3.2				
Stip1	5.6	Gcnt2	3.0				
Uspl1	4.6	Tmem33	2.9				
Hspa8	4.5	B4galt2	2.9				
Lman2l	3.9	Arl6ip4	2.7				
Kctd18	3.9	Plin2	2.7				
Ahsa1	3.9	Hspa4l	2.6				
P4ha1	3.8	Hsp90ab1	2.5				
Hsp90ab1	3.8	Nr1h2	2.5				
Hikeshi	3.8	Ube2b	2.4				
Cacybp	3.7	Stip1	2.4				
Fkbp4	3.7	Hspd1	2.3				
Chordc1	3.6	Chordc1	2.3				
Mrfap1	3.6	Abcc5	2.2				
St13	3.4	Dbndd2	2.2				
Tmem33	3.4	Rnf34	2.2				
Ubqln1	3.2	Atp6v1a	2.2				
Adgra3	2.9	Actr5	2.2				
Trmt1l	2.8	Cct7	2.1				
Ube2g2	2.6	Slc35e2	2.0				
Chchd2	2.6	Chrac1	2.0				
Gm6297	2.6	Fkbp4	2.0				
Azi2	2.4	Ppid	2.0				
Slc35e2	2.1	Mcoln1	1.9				
Pradc1	2.1	Cnpy4	1.9				
Snx3	2.1	Swt1	1.9				
Rab32	2.0	Serpinh1	1.9				
Ints2	2.0	Azi2	1.9				
Lrrc61	2.0	P4ha1	1.8				
Particl	2.0	Zfp46	1.8				
Serpinb6a	1.9	4833417C18Rik	1.8				
Xpnpep3	1.8	Vipas39	1.8				
Abcc5	1.8	Ube2g2	1.8				
Fbxl14	1.8	Aox1	1.8				
Trim65	1.7	Aptx	1.8				
Prss23	1.7	Esco2	1.7				
Vipas39	1.6	Ddx59	1.7				
Ubb	1.6	Dnajb5	1.7				
Dennd1b	1.6	Rpa2	1.6				
		Sars	1.6				
		Ints2	1.6				
		Serpinb6a	1.6				
		Tcp1	1.6				
		Ppwd1	1.6				
		Xpnpep3	1.6				
		Snx3	1.5				
		Atp5j	1.5				
		Sec62	1.5				
		Hsp90b1	1.5				

Proteomic profiling identifies a direct interaction between HSF2 and the focal adhesion adaptor talin1

Authors:

Alejandro J. Da Silva[1,2], Jens C. Luoto[1,2+], Hendrik S. E. Hästbacka[1,2+], Leila S. Coelho-Rato[1,2], Leena M. Laitala[1,2], Benjamin T. Goult[4], Susumu Y. Imanishi[3], Lea Sistonen[1,2], Eva Henriksson[1,2*]

Affiliations:

[1]Faculty of Science and Engineering, Cell Biology, Åbo Akademi University, 20520 Turku, Finland.

[2]Turku Bioscience Centre, University of Turku and Åbo Akademi University, 20520 Turku, Finland.

[3]Faculty of Pharmacy, Meijo University, Nagoya, Japan.

[4]School of Biosciences, University of Kent, Canterbury CT2 7NJ, Kent, UK.

[+]Equal contribution

*Corresponding author. Email: Eva.Henriksson@abo.fi

Abstract

Heat shock factor 2 (HSF2) is a versatile transcription factor, which regulates gene expression under stress conditions, development, and disease. Despite recent advances in identifying HSF2-dependent target genes, little is known about the protein networks that are associated with this transcription factor. Here, we performed a mass spectrometry analysis to characterize the HSF2 interactome in mouse testis, where HSF2 is required for normal sperm development. Of the HSF2-binding partners, we validated the interaction between HSF2 and the mechanosensitive focal adhesion protein talin1 (TLN1) and expanded the analyses to mouse and human cell lines. We found a TLN1-binding motif in the HSF2 C-terminus that binds directly to multiple regions of TLN1 *in vitro*. Importantly, this TLN1-binding motif is not present in the C-terminus of a closely related HSF family member HSF1, and consistently HSF1 was not found in complex with TLN1. Taken together, our data unveils the HSF2 interactome in a physiologically relevant context and validates TLN1 as the first adhesion-related HSF2-specific protein partner.

Key words: HSF1, HSF2, interactome, LC-MS/MS, LD motif, PLA, spermatogenesis, TLN1

Introduction

All living organisms must respond effectively to environmental insults that challenge the homeostasis of their proteome. For this purpose, every kingdom of life possesses a stress response mechanism known as the heat shock response, which involves the expression of molecular chaperones called heat shock proteins (HSPs) (Kmiecik & Mayer, 2022). The expression of HSPs is regulated by a family of transcription factors known as heat shock factors (HSFs), of which HSF1 and HSF2 are the most studied members in mammals (Joutsen & Sistonen, 2019). While HSF1 is indispensable under acute proteotoxic stress, HSF2 cooperates with HSF1 to drive gene expression under adverse conditions (Himanen et al., 2022; Mahat et al., 2016; Vihervaara et al., 2013). Intriguingly, HSF2 is essential for cell survival during chronic accumulation of misfolded proteins, which shows the independent role of this transcription factor in stress responses (Joutsen et al., 2020; Lecomte et al., 2010; Shinkawa et al., 2011).

In addition to stress, HSF1 and HSF2 play important roles in physiological processes, such as embryogenesis, corticogenesis and spermatogenesis (Abane & Mezger, 2010; Joutsen & Sistonen, 2019). Among adult tissues, testes possess the highest protein levels of HSF2 (Fiorenza et al., 1995; Sarge et al., 1994). Interestingly, mice lacking HSF2 are characterized by reduced testes size, a disorganized structure of seminiferous tubules, pronounced apoptosis in the pachytene spermatocytes, and defects in the quality and number of sperm (Åkerfelt et al., 2008; Kallio et al., 2002; Wang et al., 2003). Moreover, mice lacking both HSF1 and HSF2 suffer from a severe disruption of spermatogenesis leading to male infertility (Wang et al., 2004). Thus, there is accumulating evidence that HSF1 and HSF2 act synergistically during spermatogenesis, which is congruent with ChIP-chip and ChIP-seq experiments showing co-occupancy of genomic loci of these HSFs in mouse testes (Åkerfelt et al., 2008, 2010; Korfanty et al., 2014).

In contrast to the knowledge of downstream targets of HSF1 and HSF2 in stress and development (Abane & Mezger, 2010; Joutsen & Sistonen, 2019), little is known about the protein networks that are associated with these HSFs in different biological contexts. A recent study approached this gap in knowledge by screening for HSF1-binding partners under control conditions, in comparison to responses to either acute (heat shock) or chronic (Huntington's disease) proteotoxic stress (Burchfiel et al., 2021). However, no similar unbiased investigations have been reported for HSF2. Currently, the best characterized HSF2-binding partner is HSF1, since a wealth of studies have provided deep understanding of the HSF1-HSF2 protein complex (Alastalo et al., 2003; He et al., 2003; Jaeger et al., 2016; Sandqvist et al., 2009). HSF1 and HSF2 form homo- and heterotrimers through their highly homologous oligomerization domains, which are composed of two leucine-zipper like heptad repeats (HR-

A and HR-B) (Roos-Mattjus & Sistonen, 2022). Apart from HSF1, only a handful of HSF2-interacting partners have been previously reported and validated, including the molecular chaperone HSP90 (Pesonen et al., 2021), members of the E3 ubiquitin ligase anaphase/cyclosome protein complex (Ahlskog et al., 2010), a subunit of a cullin-RING E3 ubiquitin ligase cullin 3 (Xing et al., 2010), small ubiquitin-related modifier 1 (Goodson et al., 2001), and the acetyltransferase CBP/EP300 (de Thonel et al., 2022).

In this study, we investigate the interactome of endogenous HSF2 in mouse testes. Our data shows that HSF2 associates with proteins associated with gene ontology (GO) terms, such as cell adhesion molecule binding and unfolded protein binding. Of these proteins, we focus on talin 1 (TLN1), which is a mechanosensitive protein that plays a fundamental role in the formation of cell-matrix adhesion by connecting integrin transmembrane receptors to the actin cytoskeleton at complexes known as focal adhesions (Gough & Goult, 2018; Klapholz & Brown, 2017). TLN1 functions as an adaptor protein and several TLN1-binding motifs have been well characterized in different proteins (Goult et al., 2021). Excitingly, we found a TLN1-binding motif at the end of the C-terminus of HSF2, but not in HSF1. By performing a fluorescent polarization assay, we demonstrate that the TLN1-binding motif in HSF2 binds directly with multiple regions of TLN1. We also show that the HSF2-TLN1 interaction is conserved from mouse to human. In summary, we provide the first HSF2 interactome in physiological context and validate TLN1 as the first adhesion-related HSF2-binding partner.

Results

Identification of HSF2-binding partners in mouse testes

To identify proteins interacting with endogenous HSF2 in the context of tissues, we performed an HSF2 co-immunoprecipitation (co-IP) coupled with liquid chromatography tandem-mass spectrometry (LC-MS/MS) from mouse testes (Fig 1A). Mouse testes were used, because we and others have shown that the protein levels of HSF2 are exceptionally high in this tissue, and lack of HSF2 disrupts the process of spermatogenesis (Åkerfelt et al., 2008; Kallio et al., 2002; Sarge et al., 1994). The endogenous HSF2 protein was immunoprecipitated with an HSF2-specific antibody and IgG was used as a negative control. Immunoblotting of the HSF2 co-IP sample showed that HSF2 was efficiently enriched as compared to the IgG control and input (Fig 1B). Additionally, we validated that HSF1 was present in the HSF2 co-IP sample, since these proteins have been shown to associate in mouse testes (Sandqvist et al., 2009). Once the quality of the co-IP samples was verified, the HSF2 interactome was determined through LC-MS/MS. This MS analysis identified 464 proteins in the HSF2 co-IP sample, and 306 in the IgG control (Fig 1C) (Supplemental table 1). Of these, we chose only high confidence HSF2-binding partners (proteins with at least two peptide spectrum matches [PSMs] and a ratio of HSF2 PSMs/IgG PSMs > 3), which led to the identification of 105 HSF2 partners. Interestingly, the MS analysis identified proteins involved in sperm morphogenesis (MAP7, NPHP1), sperm-egg recognition (ACRBP, HSPA2) and meiosis (GOGA3, Nek1, SYCP1), which is congruent with the role of HSF2 in spermatogenesis.

To gain more insights into the type of proteins that were enriched among the 105 HSF2-binding partners, we performed a gene ontology (GO) term analysis with the online tool ShinyGO (Ge et al., 2020) (Fig 1D). The unfolded protein binding GO term was highly enriched, wherein several proteins belonging to the HSP70 and HSP90 chaperone families were found (Fig 1E). This is in agreement with a recent report showing an interaction between HSF2 and HSP90 (Pesonen et al., 2021). Surprisingly, cell adhesion molecule binding was the most enriched GO term (Fig 1D). This is particularly interesting because previous studies have shown that lack of HSF2 alters the expression of cell adhesion-related genes, even though no proteins involved in cell adhesion have been validated as HSF2-binding partners (Björk et al., 2016; Joutsen et al., 2020). Within the cell adhesion molecule binding GO term, we found several adaptor proteins that connect the actin cytoskeleton with transmembrane adhesion receptors. These adaptor proteins were zonula occludens 1 and 2 (ZO1 and ZO2), catenin delta 1 (CTNND1), and talin1 (TLN1), of which we focused on TLN1 (Fig 1E).

The interaction between HSF2 and TLN1 is conserved from mouse to human

TLN1 is an adaptor protein that connects the integrin transmembrane receptors with the actin cytoskeleton at the focal adhesions that are cell-matrix adhesion protein complexes (Gough & Goult, 2018). To validate the HSF2-TLN1 interaction, we performed co-IP of HSF2 in mouse teratocarcinoma F9 cells, in which the levels of HSF2 are considerably high compared to other murine cell lines (Murphy et al., 1994) (Fig 2A). Immunoblotting of the HSF2 co-IP sample showed the enrichment of HSF2, the formation of HSF2 and HSF1 heterotrimers, and the association between HSF2 and TLN1. This finding prompted us to ask whether the HSF2-TLN1 interaction is conserved from mouse to human. Therefore, we immunoprecipitated HSF2 from RWPE-1 (prostate epithelial) and PC-3 (prostate carcinoma) cells (Fig 2B). To exclude an unspecific immunoprecipitation of TLN1 by our HSF2 antibody, we also performed the reciprocal co-IP experiment where TLN1 was immunoprecipitated. These experiments revealed that HSF2 and TLN1 form protein complexes in both human cell lines, confirming that the HSF2-TLN1 interaction is indeed conserved from mouse to human. In contrast, HSF1 and TLN1 were not found in the same protein complex, demonstrating that HSF1-HSF2 heterotrimers do not bind to TLN1 (Fig 2B). This result thus suggests that hetero- and homooligomers of HSF2 exhibit distinct properties.

Next, we utilized indirect immunofluorescent labeling and proximity ligation assay (PLA) to complement the biochemical data on the HSF2-TLN1 interaction. While immunofluorescent labeling of HSF2 showed a predominantly nuclear localization, TLN1 displayed a strong localization in the vicinity of the plasma membrane. Additionally, TLN1 showed a modest nuclear localization, which is supported by the findings of nuclear TLN1 reported in our recent preprint article (Da Silva et al., 2022). Both proteins also exhibited a clear cytoplasmic localization (Fig 2C). In accordance with the co-IP data, the PLA assay showed that HSF2 and TLN1 are in close proximity (≤40 nm) to each other, indicating that these proteins are found in the same complex (Fig 2D). Importantly, the negative control composed of two GFP antibodies showed a dramatic reduction in the corresponding signal, confirming the specificity of the PLA assay. To determine the subcellular localization of the HSF2-TLN1 interaction, we visualized the PLA assay images using an orthogonal projection (Fig 2E). Surprisingly, we observed that most of the PLA signal was localized within the nucleus, suggesting that the HSF2-TLN1 complex resides predominantly in this subcellular compartment (Fig 2F).

The C-terminus of HSF2 binds directly to TLN1

Since the co-IP assays showed that only HSF2 binds to TLN1, we evaluated the similarities in the domain structure of HSF1 and HSF2. Both HSFs are composed of a DNA-binding domain (DBD), an oligomerization domain containing hydrophobic-leucine-zipper-like heptad

repeats (HR-A/B), a C-terminal heptad repeat domain (HR-C), regulatory domains (RD), and transactivation domains (AD) (Fig 3A). Beyond the DBD, HSF1 and HSF2 share approximately 35% identity, which indicates that these proteins are considerably different from each other (Roos-Mattjus & Sistonen, 2022). Hence, we compared the amino acid sequences of these HSFs in different species to identify HSF2-specific regions that could potentially bind to TLN1. A sequence alignment of HSF1 and HSF2 in *Homo sapiens*, *Mus musculus*, *Bos taurus*, *Sus scrofa, Gallus gallus* and *Danio rerio* unveiled that the longest conserved HSF2-specific sequence is located in its C-terminus (Fig 3B). Prompted by this finding, we searched for a TLN1-binding motif in the C-terminus of HSF2. Among the best characterized TLN1-binding motifs is the LD motif, a leucine-rich sequence following the consensus LDXLLXXL (Tumbarello et al., 2002; Zacharchenko et al., 2016). Comparison between the HSF2-specific sequence and five known TLN1-interacting proteins with an LD motif (DLC1, RIAM, PXN, KANK1, and KANK2), revealed that the C-terminus of HSF2 indeed contains an LD motif (Fig 3C).

TLN1 is composed of an N-terminal FERM domain (also known as the head domain) and a C-terminal flexible rod domain, and they are connected through a linker (Gough & Goult, 2018). The head domain of TLN1 consists of four subdomains (F0-F3), whereas the rod domain consists of 13 helical bundles (R1-R13) and a dimerization domain (DD) arranged sequentially like beads on a string (Goult et al., 2021). Importantly, the TLN1-interacting proteins DLC1, RIAM, PXN, KANK1, and KANK2 bind to either the R7 or R8 helical bundle with their LD domain (Fig 3D). Detailed structural work on the interaction between the Rho GAP protein DLC1 and TLN1 has provided a mechanistic understanding of how proteins containing an LD domain bind to TLN1 (Zacharchenko et al., 2016). The LD motif of DLC1 forms a helix that docks in between the second and third helices of the R8 helical bundle in the TLN1 rod domain. This type of binding mechanism is known as helix addition, and it requires the presence of key hydrophobic residues in the LD motif. Consequently, it is plausible that the LD domain also binds to the helical bundles of the TLN1 rod domain. To test this hypothesis, we performed a fluorescent polarization assay with a peptide containing the HSF2 LD motif and three different regions of the rod domain of TLN1 (R4-R8, R9-R12, R13-DD), and the LD motif in KANK1 was used as a positive control (Bouchet et al., 2016) (Fig 3E). Our results show that the C-terminus of HSF2 indeed binds to both R4-R8 and R9-R12 TLN1 fragments. Therefore, we conclude that the C-terminus of HSF2 has multiple binding sites in TLN1.

Discussion

The protein networks associated with HSF2 have been largely unexplored. Here we provide the first proteomic profiling of HSF2 partners in a physiologically relevant context. We performed an LC-MS/MS analysis to identify binding proteins of endogenous HSF2 in mouse testes, a tissue where HSF2 is required for proper formation of haploid spermatozoa during spermatogenesis (Åkerfelt et al., 2008; Kallio et al., 2002; Sarge et al., 1994). Our results show that HSF2 interacts with proteins of different molecular functions, among which cell adhesion-related proteins were the most enriched. This is particularly interesting because increasing evidence shows that there is a functional link between HSF2 and cell adhesion. Lack of HSF2 disrupts the expression of a wide variety of cadherin superfamily members, which are cell-cell adhesion receptors crucial for maintaining tissue integrity (Joutsen et al., 2020; de Thonel et al., 2021). Moreover, downregulation of HSF2 in 3D organotypic cell cultures impairs the expression of cell-matrix adhesion proteins (e.g. integrins), extracellular matrix proteins (e.g. collagens), and regulators of cytoskeletal organization (e.g. members of the Rho family of GTPases) (Björk et al., 2016). Intriguingly, we observed that HSF2 interacts with several adaptor proteins, belonging to major cell adhesion protein complexes in the vicinity of the plasma membrane, such as ZO1 and ZO2, CTNND1 and TLN1 (Goult et al., 2018; Mège & Ishiyama, 2017; Zihni et al., 2016). All of these adaptor proteins have been shown to also reside in the nucleus (Da Silva et al., 2022; Daniel, 2007; Zihni et al., 2016), suggesting that HSF2 might cooperate with them to drive the expression of specific cell adhesion genes during spermatogenesis. In support of this idea, ChIP-seq data from spermatocytes in control conditions shows that HSF2 binds to gene loci corresponding to several families of adhesion proteins, such as ADAMs, cadherins, catenins, claudins, integrins, and protocadherins (Korfanty et al., 2014).

Among the adhesion adaptor proteins identified in our LC-MS/MS analysis, we validated the interaction between HSF2 and TLN1 in mouse and human cells. The analysis of subcellular localization of this interaction, using PLA assay, showed that the HSF2-TLN1 complex resides predominantly in the nucleus. In a recent preprint article, we investigated the nuclear localization of TLN1, and found that TLN1 is strongly associated with the chromatin and regulates gene expression (Da Silva et al., 2022). The molecular mechanisms mediating TLN1 nuclear translocation are currently undefined, but HSF2 could conceivably be involved in the process. Likewise, it is plausible that HSF2 and TLN1 cooperate to bind specific genomic loci and regulate gene expression.

Remarkably, HSF1 was not found in complex with TLN1, indicating that HSF1-HSF2 heterotrimers do not bind to TLN1. This finding is particularly important, because it demonstrates that although HSF1 and HSF2 share certain domains, their protein sequences are largely different. Moreover, it also highlights that HSF2 hetero- and homooligomers have distinct protein partners. Congruently, when we explored the differences in protein sequences between HSF1 and HSF2 in *Homo sapiens*, *Mus musculus*, *Bos taurus*, *Sus scrofa, Gallus gallus* and *Danio rerio*, we found a conserved region at the end of the HSF2 C-terminus that is absent from HSF1. The HSF2-specific sequence contained an LD TLN1-binding motif, which binds directly to two regions of the TLN1 rod domain (R4-R8 and R9-R12). Interestingly, this is different from other known LD-containing TLN1-binding partners, which only bind to individual helical bundles of TLN1 (Gough et al., 2021; Zacharchenko et al., 2016). Hence, this atypical binding mechanism warrants more detailed structural analysis in forthcoming studies.

In this study, we identify TLN1 as the first adhesion-related HSF2-interacting partner and expand HSF2's role beyond the regulation of cell adhesion genes. Interestingly, HSF1 was not found in complex with TLN1 demonstrating distinct partner specificity of HSF1 and HSF2. This finding is particularly important since it establishes a new layer of functional complexity for HSFs. Indeed, specific protein networks could orchestrate the activation, localization, and function of HSF1 and HSF2 in different biological milieus. Therefore, our findings establish a new direction for exploring the unique functions of HSF1 and HSF2.

Materials and Methods

Mice

Male hybrid mice of the B6129SF2/J strain were used for co-immunoprecipitation assays. The pathogen-free mice were housed under controlled environmental conditions at the Animal Core Facility of University of Turku and were provided with food and tap water. The mice were handled according to the institutional animal care policies of Åbo Akademi University (Turku, Finland). Adult (60–80 days old) mice were sacrificed by CO_2 asphyxiation and cervical dislocation, followed by the isolation of testes.

Cell culture

All cells were maintained at 37°C in a humidified 5% CO_2 atmosphere. Mouse teratocarcinoma F9 cells were cultured in suspension with DMEM (Dulbecco's Modified Eagle's media, D6171, Sigma-Aldrich) supplemented with 10% fetal calf serum, 2 mM L-glutamine, and 100 µg/ml penicillin-streptomycin. Human prostate epithelial RWPE-1 cells were cultured in Keratinocyte SFM media (Gibco, 17005042) supplemented with 25 mg of bovine pituitary extract, 2.5 µg of human recombinant EGF, and 100 µg/ml penicillin-streptomycin. Human prostate cancer PC-3 cells were cultured in RPMI (Roswell Park Memorial Institute, 1640, Sigma-Aldrich) supplemented with 10% fetal calf serum, 2 mM L-glutamine, and 100 µg/ml penicillin-streptomycin.

Preparation of cell lysates from mouse testes and cells

Mouse testes were lysed in lysis buffer (25 mM HEPES, pH 8.0, 100 mM NaCl, 5 mM EDTA pH 8.0, 0.5% Triton X-100, 20 mM β-glycerophosphate, 20 mM PNPP, 100 µM Na_3VO_4, 0.5 mM DTT, 0.5 mM PMSF, and 1 x protease Inhibitor Cocktail [04693159001, Roche Diagnostics]). First, the tissue was suspended in lysis buffer and homogenized using an ultra turrax T8 homogenizer (IKA Labortechnik). The resulting lysate was incubated on ice for 15 min and centrifugated at 20,000 rcf for 15 min at 4°C. The supernatant was collected and the protein concentration was measured with the Bradford reagent.

For lysis of cell lines, the corresponding cells were collected in PBS (L0615, BioWest) and lysed in the same lysis buffer used to lyse mouse testes for at least 30 min at 4°C with rotation. Subsequently, the suspension was centrifuged at 20,000 rcf for 10 min at 4°C, the supernatant was collected, and the protein concentration was determined by BCA assay (23225, Thermo Scientific).

Co-immunoprecipitation from cell lines

Cell lysate containing 750 µg total protein was used for each pull-down, and all centrifugation steps were at 2,000 rcf for 2 min at 4°C unless otherwise specified. Lysates were first pre-cleared with 30 µl protein G sepharose beads (50% slurry, GE Healthcare) by 30 min incubation with rotation at 4°C. After centrifugation, the supernatants were transferred to 1.5 ml microcentrifuge tubes and antibodies were added. Following antibodies were used: 5 µl of anti-HSF2 58f (Östling et al., 2007), 5 µg anti-TLN1 8D4 (T3287, Sigma-Aldrich), 5 µg normal rabbit IgG (12-370, Millipore), 5 µg normal mouse IgG (12-371, Millipore). Samples were incubated with rotation over night at 4°C. Next, 30 µl of 50% protein G sepharose bead slurry was added, and the samples were incubated an additional 4 h (at 4°C, with rotation). Following centrifugation, the supernatant was aspirated, the beads washed four times using 1 ml wash buffer (20 mM Tris-HCl pH 7.5, 1 mM EDTA, 10% Glycerol, 150-300 mM NaCl, 0.1% Triton X-100), and 45 µl of 3x laemmli sample buffer was added to each sample. Input samples were prepared by adding laemmli sample buffer to 15 µg whole-cell lysate. All samples were boiled for 5 min and centrifuged for 10 min at max speed (21,800 rcf) at room temperature prior to gel loading.

Immunoblotting

Equal amounts of total protein were resolved on 4–20% or 7.5% Mini-PROTEAN® TGX precast gels (Bio-Rad). The proteins were transferred to a nitrocellulose membrane (0.2 µm pore size), which was blocked in 5% milk-PBS with 0.3% Tween 20 for 1 h at room temperature. The primary antibodies were diluted in 0.5% BSA-PBS-0.02% NaN_3. The following primary antibodies were used: 1:1,000 anti-HSF2 (MAB88079, Millipore), 1:1,000 anti-HSF2 (HPA031455, Sigma-Aldrich), 1:1,000 anti-HSF1 (RT-629-P1, Neomarkers), and 1:1,000 anti-TLN1 8D4 (T3287, Sigma-Aldrich). The nitrocellulose membranes were incubated with the primary antibodies overnight at 4°C. Secondary HRP-conjugated antibodies were purchased from Promega or GE Healthcare (anti-mouse Cat. No. W4021, Promega; anti-rabbit Cat. No. W4011, Promega; anti-rat Cat. No. NA935V, GE Healthcare). All secondary antibodies were diluted in 5% milk-PBS with 0.3% Tween 20. The nitrocellulose membranes were incubated with the secondary antibodies at least 1 h at room temperature, and then incubated with enhanced chemiluminescence reagent (28980926, GE Healthcare; 34579, Thermo Scientific; 34094; Thermo Scientific). Images were acquired with an iBright imaging system (Thermo Scientific).

Mass spectrometry

For sample preparation, 8 mg of protein from the mouse testes lysates were used for co-immunoprecipitation. All centrifugation steps were 2,000 rcf for 2 min at 4°C, unless specified. Protein lysates were first pre-cleared with 100 µl protein G sepharose beads (50% slurry, GE Healthcare) by 30 min incubation with rotation at 4°C. After centrifugation, the supernatants were transferred to 1.5 ml microcentrifuge tubes and antibodies were added. The following antibodies were used: 50 µl of anti-HSF2 58f (Östling et al., 2007) and 150 µl normal rabbit IgG (SC-2027, Santa Cruz Laboratories). Samples were incubated with the corresponding antibody in rotation at room temperature for 30 min. Next, 130 µl of 50% protein G sepharose bead slurry was added, and the samples were incubated an additional 2-3 h (at 4°C, in rotation). Following centrifugation, the supernatant was aspirated, the beads washed four times using 1 ml wash buffer (20 mM Tris-HCl pH 7.5, 1 mM EDTA, 10% Glycerol, 150-300 mM NaCl, 0.1% Triton X-100), and 200 µl laemmli sample buffer was added to each sample. Input samples were prepared by adding laemmli sample buffer to 30 µg whole-cell lysate. All samples were boiled for 5 min and centrifuged for 10 min at max speed (21,800 rcf) at room temperature prior to gel loading.

The supernatants obtained from co-immunoprecipitations were loaded into a 8% polyacrylamide gel. After the proteins were resolved, the gel was treated with fixation solution (30% ethanol, 10% acetic acid) for 18 h, followed by washes with 20% ethanol and water on a platform shaker. The gel was exposed to 1.2 mM sodium thiosulfate pentahydrate for exactly 1.5 min and rinsed with water for 20 s. Subsequently, 11.7 mM silver nitrate was used to stain the gel for 30 min on a platform shaker. After the staining step, development solution (0.217 M potassium carbonate, 6.04 $x10^{-5}$ M sodium thiosulfate pentahydrate, 0.07% formaldehyde) was added. When the bands of the gel had reached the desired intensity, the stop solution (2.5% acetic acid, 418.8 mM sodium thiosulfate pentahydrate) was used. The developed gel was washed with water and stored at 4°C.

Silver-stained protein bands that were present in the HSF2 co-IP and absent from the IgG negative control were subjected to reduction, alkylation, and in-gel tryptic digestion as described previously (Imanishi et al., 2007). The digests were analyzed by nanoflow liquid chromatography-tandem mass spectrometry (LC-MS/MS) using a Q Exactive mass spectrometer coupled to an EASY-nLC 1,000 liquid chromatograph (Thermo Scientific). Database search was performed against the Swiss-Prot (*Mus musculus*) using Mascot 2.4 (Matrix Science) via Proteome Discoverer 1.3 (Thermo Scientific). After applying the cut-off criteria (peptide-spectrum matches (PSMs) >2 and a ratio of HSF2 PSMs/IgG PSMs > 3), a total of 105 HSF2-binding partners were identified.

Gene ontology (GO) term analysis

GO term analyses were performed with the online application ShinyGO (Ge et al., 2020). For analysis performed with ShinyGO v.0.76.1 the following parameters were used: species: mouse, false discovery rate (FDR) cut-off: 0.05, number of top pathways to show: 20, and pathway size min: 2 and max: 2000.

Confocal microscopy

For confocal microscopy analyses, 8×10^4 PC-3 cells were plated on MatTek plates (P35GC-1.5-14-C MatTek corporation) 48 h before imaging. Cells were fixed with 4% paraformaldehyde for 10 min, permeabilized with 0.5% Triton X-100 and 3 mM EDTA in 1x PBS and washed three times with PBS. Cells were blocked with 10% FBS-PBS for at least 1 h at room temperature, and then incubated with the corresponding primary antibody dilution overnight at 4°C. The following primary antibodies were diluted in 10% FBS-PBS: 1:100 anti-TLN1 8D4 (T3287, Sigma-Aldrich), and 1:100 anti-HSF2 (HPA031455, Sigma-Aldrich). After primary antibody incubation the samples were washed three times in PBS and incubated with the corresponding secondary antibody at room temperature for 1 h. The following secondary antibodies were diluted 1:500 in 10% FBS-PBS and used: goat anti-rabbit Alexa Fluor 488 (A11008, Life Technologies), and donkey anti-mouse Alexa Fluor 555 (A31570, Life Technologies). After secondary antibody incubation, cells were washed in PBS, incubated with 300 nM DAPI diluted in PBS for 5 min, washed again with PBS, and covered with VECTASHIELD (H-1000, Vector Laboratories) mounting medium. Images were captured with a 3i CSU-W1 spinning disc confocal microscope (Intelligent Imaging Innovations).

Proximity ligation assay (DUOLINK)

Proximity ligation assay (PLA) by DUOLINK was performed according to the manufacturer's recommendation with a few modifications. In brief, PC-3 cells seeded on cover slips were fixed with 3% PFA for 20 min at room temperature followed by blocking and permeabilization with 0.3% Triton X-100, 10% FBS in PBS for 15 min. The coverslips were washed with PBS and incubated overnight at 4℃ with 5 ug/ml of the primary antibodies anti-TLN1 8D4 (T3287, Sigma-Aldrich), anti-HSF2 (HPA031455, Sigma-Aldrich), anti-GFP mouse (ab1218, Abcam), and anti-GFP rabbit (A-11122, Thermo Scientific), diluted in 10% FBS in PBS. The probes (DUO92002, DUO92004, Sigma-Aldrich), ligation, and amplification (DUO92008, Sigma-Aldrich) reactions were performed according to the manufacturer's recommendations. During the amplification step, 1:500 Alexa Fluor™ 647 Phalloidin (A22287, Thermo Scientific) was also added. The samples were mounted in Mowiol with DABCO and kept in darkness until imaging with a Zeiss LSM510 confocal microscope with a 40x objective and a slice distance

of 0.7 µm. At least three stacked images were taken per field and over 100 cells were analyzed per PLA reaction pair.

The PLA confocal images were pre-processed, segmented, and analyzed using the CellProfiler software (Carpenter et al., 2006) to count the amount of PLA signals per cell. In brief, maximum intensity projections of the PLA confocal images were pre-processed by removing background noise and segmented using OTSU thresholding. The segmented PLA signals were analyzed by a Mann-Whitney t-test using GraphPad Prism 7. The data are presented as mean values of over 100 cells analyzed from across multiple experiments + SEM. ****$p < 0.0001$.

Fluorescence polarization assay

Fluorescence Polarization was carried out on an HSF2 peptide (C-ELAPAPLDSDMPLLDS) with an N-terminal cysteine. Peptide stock solution was composed of PBS, 100 mg/ml TCEP and 0.05% Triton X-100. The Thiol reactive BIODIPY TMR dye (Invitrogen) was coupled to the terminal cysteine in the HSF2 peptide. Gel filtration with a PD-10 column (GE Healthcare) was used to remove uncoupled dye. The labeled peptide was concentrated to a final concentration of 1 mM using a centricon with 3K molecular weight cut off (Millipore). The Fluorescence Polarization assay was performed on a black 96 well plate (Nunc). Titrations were performed in triplicate using a fixed 0.5 mM concentration of peptide and an increasing concentration of talin R4-R8, R9-R12, and R13-DD protein within a final volume of 100 ml of PBS. Fluorescence Polarization measurements were aquired on a BMGLabTech CLARIOstar plate reader at room temperature and analyzed using GraphPad Prism 6.07. Kd values were calculated with a nonlinear curve fitting using a one site total and non-specific binding model.

Acknowledgments

We thank all the members of Sistonen laboratory for expert support during the preparation of the manuscript. Imaging was performed at the Cell Imaging Core, Turku Bioscience Centre, University of Turku and Åbo Akademi University. The instruments used in this project belong to the infrastructure of Turku Bioscience Centre. We thank Markku Saari and Jouko Sandholm from the Cell Imaging Core of Turku Bioscience Centre for technical assistance and advice. Mass spectrometry analyses were performed in the proteomic core facility of Turku Bioscience Centre (Turku, Finland).

This work has been founded by the Academy of Finland (L.S.); Centre for International Mobility (A.J.D.S., E.H); Finish cultural foundation (A.J.D.S); K. Albin Johansson Foundation (A.J.D.S., E.H); Magnus Ehrnrooth's Foundation (A.J.D.S., E.H); Medicinska

understödsföreningen liv och hälsa r.f. (A.J.D.S., E.H); Otto A. Malm foundation (A.J.D.S.); Sigrid Juselius Foundation (L.S.).

Author contributions

A.J.D.S., E.H. and L.S. designed the research. A.J.D.S., J.C.L., H.S.E.H., J.C.P., L. M. L., and B.T.G performed experiments. S.Y.I. and L.S.C. performed the LC-MS/MS analysis. A.J.D.S., H.S.E.H., J.C.L., B.T.G., E.H., and L.S. interpreted the data. A.J.D.S., E.H. and L.S. wrote the manuscript with the contribution of all the authors.

Conflict of interest

Authors declare that they do not have competing interests.

References

Abane, R., & Mezger, V. (2010). Roles of heat shock factors in gametogenesis and development. *FEBS Journal*, *277*(20), 4150–4172. https://doi.org/10.1111/j.1742-4658.2010.07830.x

Ahlskog, J. K., Björk, J. K., Elsing, A. N., Aspelin, C., Kallio, M., Roos-Mattjus, P., & Sistonen, L. (2010). Anaphase-Promoting Complex/Cyclosome Participates in the Acute Response to Protein-Damaging Stress. *Molecular and Cellular Biology*, *30*(24), 5608–5620. https://doi.org/10.1128/mcb.01506-09

Åkerfelt, M., Henriksson, E., Laiho, A., Vihervaara, A., Rautoma, K., Kotaja, N., & Sistonen, L. (2008). Promoter ChIP-chip analysis in mouse testis reveals Y chromosome occupancy by HSF2. *Proceedings of the National Academy of Sciences of the United States of America*, *105*(32), 11224–11229. https://doi.org/10.1073/pnas.0800620105

Åkerfelt, M., Vihervaara, A., Laiho, A., Conter, A., Christians, E. S., Sistonen, L., & Henriksson, E. (2010). Heat shock transcription factor 1 localizes to sex chromatin during meiotic repression. *Journal of Biological Chemistry*, *285*(45), 34469–34476. https://doi.org/10.1074/jbc.M110.157552

Alastalo, T., Hellesuo, M., Sandqvist, A., Hietakangas, V., Kallio, M., & Sistonen, L. (2003). Formation of nuclear stress granules involves HSF2 and coincides with the nucleolar localization of Hsp70. *Journal of Cell Science*, *116*(17), 3557–3570. https://doi.org/10.1242/jcs.00671

Björk, J. K., Åkerfelt, M., Joutsen, J., Puustinen, M. C., Cheng, F., Sistonen, L., & Nees, M. (2016). Heat-shock factor 2 is a suppressor of prostate cancer invasion. *Oncogene*, *35*(14), 1770–1784. https://doi.org/10.1038/onc.2015.241

Bouchet, B. P., Gough, R. E., Ammon, Y., van de Willige, D., Post, H., Jacquemet, G., Altelaar, A. M., Heck, A. J., Goult, B. T., & Akhmanova, A. (2016). Talin-KANK1 interaction controls the recruitment of cortical microtubule stabilizing complexes to focal adhesions. *ELife*, *5*, 1–23. https://doi.org/10.7554/eLife.18124

Burchfiel, E. T., Vihervaara, A., Guertin, M. J., Gomez-Pastor, R., & Thiele, D. J. (2021). Comparative interactomes of HSF1 in stress and disease reveal a role for CTCF in HSF1-mediated gene regulation. *Journal of Biological Chemistry*, *296*(34), 100097. https://doi.org/10.1074/jbc.RA120.015452

Carpenter, A. E., Jones, T. R., Lamprecht, M. R., Clarke, C., Kang, I. H., Friman, O., Guertin, D. A., Chang, J. H., Lindquist, R. A., Moffat, J., Golland, P., & Sabatini, D. M. (2006). CellProfiler : image analysis software for identifying and quantifying cell phenotypes. *Genome Biology*, *7*(10). https://doi.org/10.1186/gb-2006-7-10-r100

Da Silva, A. J., Hästbacka, H. S. E., Puustinen, M. C., Pessa, J. C., Goult, B. T., Jacquemet, G., Henriksson, E., & Sistonen, L. (2022). A subpopulation of Talin 1 resides in the nucleus and regulates gene expression. *BioRxiv Preprint*. https://doi.org/https://doi.org/10.1101/2022.03.15.484419

Daniel, J. M. (2007). Dancing in and out of the nucleus: p120ctn and the transcription factor Kaiso. *Biochimica et Biophysica Acta (BBA) - Molecular Cell Research*, *1773*(1), 59–68. https://doi.org/10.1016/j.bbamcr.2006.08.052

Fiorenza, M. T., Farkas, T., Dissing, M., Kolding, D., & Zimarino, V. (1995). Complex expression of murine heat shock transcription factors. *Nucleic Acids Research*, *23*(3), 467–474. https://doi.org/10.1093/nar/23.3.467

Ge, S. X., Jung, D., Jung, D., & Yao, R. (2020). ShinyGO: A graphical gene-set enrichment tool for animals and plants. *Bioinformatics*, *36*(8), 2628–2629. https://doi.org/10.1093/bioinformatics/btz931

Goodson, M. L., Hong, Y., Rogers, R., Matunis, M. J., Park-Sargell, O. K., & Sarge, K. D. (2001). SUMO-1 Modification Regulates the DNA Binding Activity of Heat Shock Transcription Factor 2, a Promyelocytic Leukemia Nuclear Body Associated Transcription Factor. *Journal of Biological Chemistry*, *276*(21), 18513–18518. https://doi.org/10.1074/jbc.M008066200

Gough, R. E., & Goult, B. T. (2018). The tale of two talins – two isoforms to fine-tune integrin signalling. *FEBS Letters*, *592*(12), 2108–2125. https://doi.org/10.1002/1873-3468.13081

Goult, B. T., Brown, N. H., & Schwartz, M. A. (2021). Talin in mechanotransduction and mechanomemory at a glance. *Journal of Cell Science*, *134*(20), 1–7. https://doi.org/10.1242/jcs.258749

Goult, B. T., Yan, J., & Schwartz, M. A. (2018). Talin as a mechanosensitive signaling hub. *Journal of Cell Biology*, *217*(11), 3776–3784. https://doi.org/10.1083/jcb.201808061

He, H., Soncin, F., Grammatikakis, N., Li, Y., Siganou, A., Gong, J., Brown, S. A., Kingston, R. E., & Calderwood, S. K. (2003). Elevated Expression of Heat Shock Factor (HSF) 2A Stimulates HSF1-induced Transcription during Stress *. *Journal of Biological Chemistry*, *278*(37), 35465–35475. https://doi.org/10.1074/jbc.M304663200

Himanen, S. V, Puustinen, M. C., Da Silva, A. J., Vihervaara, A., & Sistonen, L. (2022). HSFs drive transcription of distinct genes and enhancers during oxidative stress and heat shock. *Nucleic Acids Research*, *50*(11), 6102–6115. https://doi.org/10.1093/nar/gkac493

Imanishi, S. Y., Kochin, V., Ferraris, S. E., de Thonel, A., Pallari, H. M., Corthals, G. L., & Eriksson, J. E. (2007). Reference-facilitated phosphoproteomics: Fast and reliable phosphopeptide validation by μLC-ESI-Q -TOF MS/MS. *Molecular and Cellular Proteomics*, *6*(8), 1380–1391. https://doi.org/10.1074/mcp.M600480-MCP200

Jaeger, A. M., Pemble, C. W., Sistonen, L., & Thiele, D. J. (2016). Structures of HSF2 reveal mechanisms for differential regulation of human heat-shock factors. *Nature Structural & Molecular Biology*, *23*(2), 147–154. https://doi.org/10.1038/nsmb.3150

Joutsen, J., Da Silva, A. J., Luoto, J. C., Budzynski, M. A., Nylund, A. S., de Thonel, A., Concordet, J. P., Mezger, V., Sabéran-Djoneidi, D., Henriksson, E., & Sistonen, L. (2020). Heat Shock Factor 2 Protects against Proteotoxicity by Maintaining Cell-Cell Adhesion. *Cell Reports*. https://doi.org/10.1016/j.celrep.2019.12.037

Joutsen, J., & Sistonen, L. (2019). Tailoring of proteostasis networks with heat shock factors. *Cold Spring Harbor Perspectives in Biology*, *11*(4), 1–18. https://doi.org/10.1101/cshperspect.a034066

Kallio, M., Chang, Y., Manuel, M., Alastalo, T. P., Rallu, M., Gitton, Y., Pirkkala, L., Loones, M. T., Paslaru, L., Larney, S., Hiard, S., Morange, M., Sistonen, L., & Mezger, V. (2002). Brain abnormalities, defective meiotic chromosome synapsis and female subfertility in HSF2 null mice. *EMBO Journal*, *21*(11), 2591–2601. https://doi.org/10.1093/emboj/21.11.2591

Klapholz, B., & Brown, N. H. (2017). Talin – the master of integrin adhesions. *Journal of Cell Science*, jcs.190991. https://doi.org/10.1242/jcs.190991

Kmiecik, S. W., & Mayer, M. P. (2022). Molecular mechanisms of heat shock factor 1 regulation. *Trends in Biochemical Sciences*, *47*(3), 218–234. https://doi.org/10.1016/j.tibs.2021.10.004

Korfanty, J., Stokowy, T., Widlak, P., Gogler-Piglowska, A., Handschuh, L., Podkowiński, J., Vydra, N., Naumowicz, A., Toma-Jonik, A., & Widlak, W. (2014). Crosstalk between HSF1 and HSF2 during the heat shock response in mouse testes. *International Journal of Biochemistry and Cell Biology*, *57*, 76–83. https://doi.org/10.1016/j.biocel.2014.10.006

Lecomte, S., Desmots, F., Le Masson, F., Le Goff, P., Michel, D., Christians, E. S., & Le Dréan, Y. (2010). Roles of heat shock factor 1 and 2 in response to proteasome inhibition: Consequence on p53 stability. *Oncogene*, *29*(29), 4216–4224. https://doi.org/10.1038/onc.2010.171

Mahat, D. B., Salamanca, H. H., Duarte, F. M., Danko, C. G., & Lis, J. T. (2016). Mammalian Heat Shock Response and Mechanisms Underlying Its Genome-wide Transcriptional Regulation. *Molecular Cell*, *62*(1), 63–78. https://doi.org/10.1016/j.molcel.2016.02.025

Mège, R. M., & Ishiyama, N. (2017). Integration of cadherin adhesion and cytoskeleton at adherens junctions. *Cold Spring Harbor Perspectives in Biology*, *9*(5). https://doi.org/10.1101/cshperspect.a028738

Murphy, S. P., Gorzowski, J. J., Sarge, K. D., & Phillips, B. (1994). Characterization of constitutive HSF2 DNA-binding activity in mouse embryonal carcinoma cells. *Molecular and Cellular Biology*, *14*(8), 5309–5317.

https://doi.org/10.1128/mcb.14.8.5309-5317.1994

Östling, P., Björk, J. K., Roos-Mattjus, P., Mezger, V., & Sistonen, L. (2007). Heat Shock Factor 2 (HSF2) contributes to inducible expression of hsp genes through interplay with HSF1. *Journal of Biological Chemistry*, *282*(10), 7077–7086. https://doi.org/10.1074/jbc.M607556200

Pesonen, L., Svartsjö, S., Bäck, V., de Thonel, A., Mezger, V., Sabéran-Djoneidi, D., & Roos-Mattjus, P. (2021). Gambogic acid and gambogenic acid induce a thiol-dependent heat shock response and disrupt the interaction between HSP90 and HSF1 or HSF2. *Cell Stress and Chaperones*, *26*(5), 819–833. https://doi.org/10.1007/s12192-021-01222-4

Roos-Mattjus, P., & Sistonen, L. (2021). Interplay between mammalian heat shock factors 1 and 2 in physiology and pathology. *FEBS Journal*, *289*, 7710–7725. https://doi.org/10.1111/febs.16178

Sandqvist, A., Björk, J. K., Åkerfelt, M., Chitikova, Z., Grichine, A., Vourc'h, C., Jolly, C., Salminen, T. A., Nymalm, Y., & Sistonen, L. (2009). Heterotrimerization of Heat-Shock Factors 1 and 2 Provides a Transcriptional Switch in Response to Distinct Stimuli. *Molecular Biology of the Cell*, *20*(5), 1340–1347. https://doi.org/10.1091/mbc.e08-08-0864

Sarge, K. D., Park-Sarge, O.-K., Kirby, J. D., Mayo, K. E., & Morimoto, R. I. (1994). Expression of Heat Shock Factor 2 in Mouse Testis: Potential Role as a Regulator of Heat-Shock Protein Gene Expression during Spermatogenesis1. *Biology of Reproduction*, *50*(6), 1334–1343. https://doi.org/10.1095/biolreprod50.6.1334

Shinkawa, T., Tan, K., Fujimoto, M., Hayashida, N., Yamamoto, K., Takaki, E., Takii, R., Prakasam, R., Inouye, S., Mezger, V., & Nakai, A. (2011). Heat shock factor 2 is required for maintaining proteostasis against febrile-range thermal stress and polyglutamine aggregation. *Molecular Biology of the Cell*, *22*(19), 3571–3583. https://doi.org/10.1091/mbc.E11-04-0330

Tumbarello, D. A., Brown, M. C., & Turner, C. E. (2002). The paxillin LD motifs. *FEBS Letters*, *513*(1), 114–118. https://doi.org/10.1016/S0014-5793(01)03244-6

Vihervaara, A., Sergelius, C., Vasara, J., Blom, M. A. H., Elsing, A. N., Roos-Mattjus, P., & Sistonen, L. (2013). Transcriptional response to stress in the dynamic chromatin environment of cycling and mitotic cells. *Proceedings of the National Academy of Sciences of the United States of America*, *110*(36). https://doi.org/10.1073/pnas.1305275110

Wang, G., Ying, Z., Jin, X., Tu, N., Zhang, Y., Phillips, M., Moskophidis, D., & Mivechi, N. F. (2004). Essential Requirement for Both hsf1 and hsf2 Transcriptional Activity in Spermatogenesis and Male Fertility. *Genesis*, *38*(2), 66–80. https://doi.org/10.1002/gene.20005

Wang, G., Zhang, J., Moskophidis, D., & Mivechi, N. F. (2003). Targeted disruption of the heat shock transcription factor (hsf)-2 gene results in increased embryonic

lethality, neuronal defects, and reduced spermatogenesis. *Genesis*, *36*(1), 48–61. https://doi.org/10.1002/gene.10200

Xing, H., Hong, Y., & Sarge, K. D. (2010). *PEST sequences mediate heat shock factor 2 turnover by interacting with the Cul3 subunit of the Cul3-RING ubiquitin ligase*. 301–308. https://doi.org/10.1007/s12192-009-0144-7

Zacharchenko, T., Qian, X., Goult, B. T., Jethwa, D., Almeida, T. B., Ballestrem, C., Critchley, D. R., Lowy, D. R., & Barsukov, I. L. (2016). LD Motif Recognition by Talin: Structure of the Talin-DLC1 Complex. *Structure*, *24*(7), 1130–1141. https://doi.org/10.1016/j.str.2016.04.016

Zihni, C., Mills, C., Matter, K., & Balda, M. S. (2016). Tight junctions: from simple barriers to multifunctional molecular gates. *Nature Reviews Molecular Cell Biology*, *17*(9), 564–580. https://doi.org/10.1038/nrm.2016.80

FIGURE 1

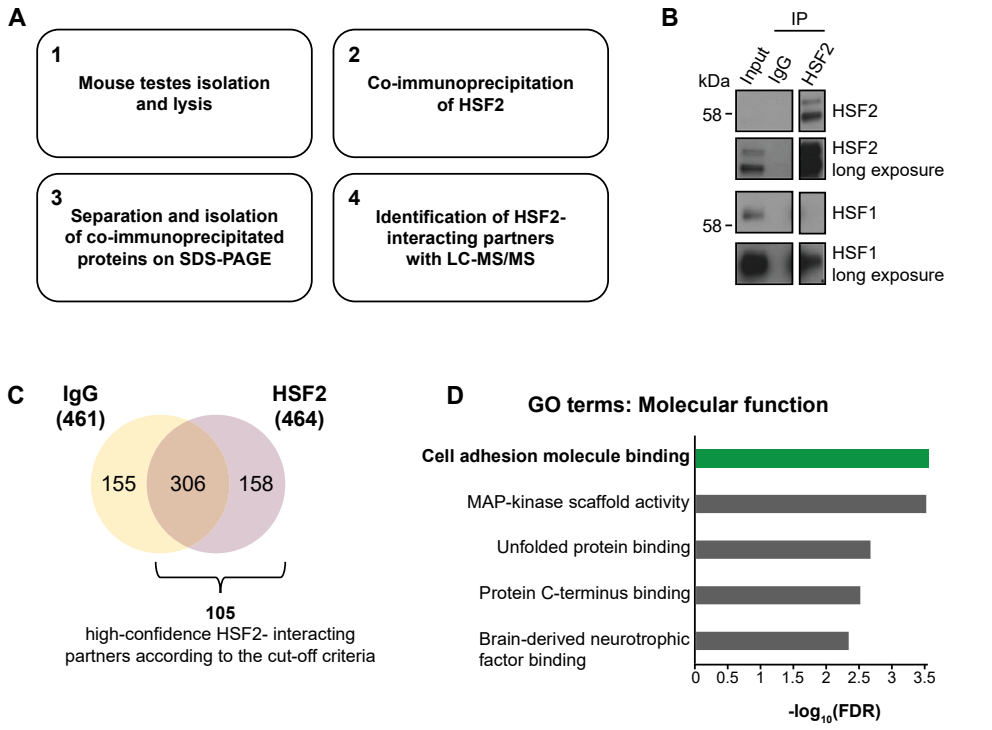
A
1
Mouse testes isolation and lysis
2
Co-immunoprecipitation of HSF2
3
Separation and isolation of co-immunoprecipitated proteins on SDS-PAGE
4
Identification of HSF2-interacting partners with LC-MS/MS
B
IP
Input
IgG
HSF2
kDa
58
HSF2
HSF2 long exposure
58
HSF1
HSF1 long exposure
C
IgG (461)
HSF2 (464)
155
306
158
105
high-confidence HSF2- interacting partners according to the cut-off criteria
D
GO terms: Molecular function
Cell adhesion molecule binding
MAP-kinase scaffold activity
Unfolded protein binding
Protein C-terminus binding
Brain-derived neurotrophic factor binding
0
0.5
1
1.5
2
2.5
3
3.5
-log10(FDR)
E
Unfolded protein binding
HSPA1L
HSPA2
HSPA9
HSP90B1
UBE4B
HSF2
Cell adhesion molecule binding
CTNND1
FBLN5
FN1
LCP1
MYH9
SHTN1
TLN1
ZO1
ZO2

Figure 1. Identification of the HSF2 interactome in mouse testes. (A) A schematic figure of the workflow. Mouse testes were isolated and lysed. The endogenous HSF2 protein was immunoprecipitated with an antibody specific for HSF2 and IgG was used as negative control. The proteins that co-precipitated with HSF2 were separated and isolated by SDS-PAGE. HSF2-binding partners were identified by liquid chromatography tandem-mass spectrometry (LC-MS/MS). **(B)** Immunoblot of co-immunoprecipitation (co-IP) of HSF2 and a negative control IgG in mouse testes. The efficacy of the immunoprecipitation was evaluated by immunoblotting with antibodies specific for HSF2 and HSF1. The immunoblot is a representative figure of three biological replicates. **(C)** Venn diagram showing shared and distinct proteins identified by LC-MS/MS in the HSF2 co-IP sample and the IgG negative control. After applying our cut-off criteria (peptide-spectrum matches (PSMs) > 2 and a ratio of HSF2 PSMs/IgG PSMs > 3) a total of 105 proteins were identified. **(D)** Gene ontology (GO) terms associated with the 105 HSF2-binding partners that met our cut-off criteria were analyzed with ShinyGO (Ge et al., 2020). The molecular function GO terms were ranked according to their false discovery rate (FDR) and the redundant terms were withdrawn. Top 5 GO term categories are shown **(E)** HSF2-binding partners within the top three categories shown in D.

FIGURE 2

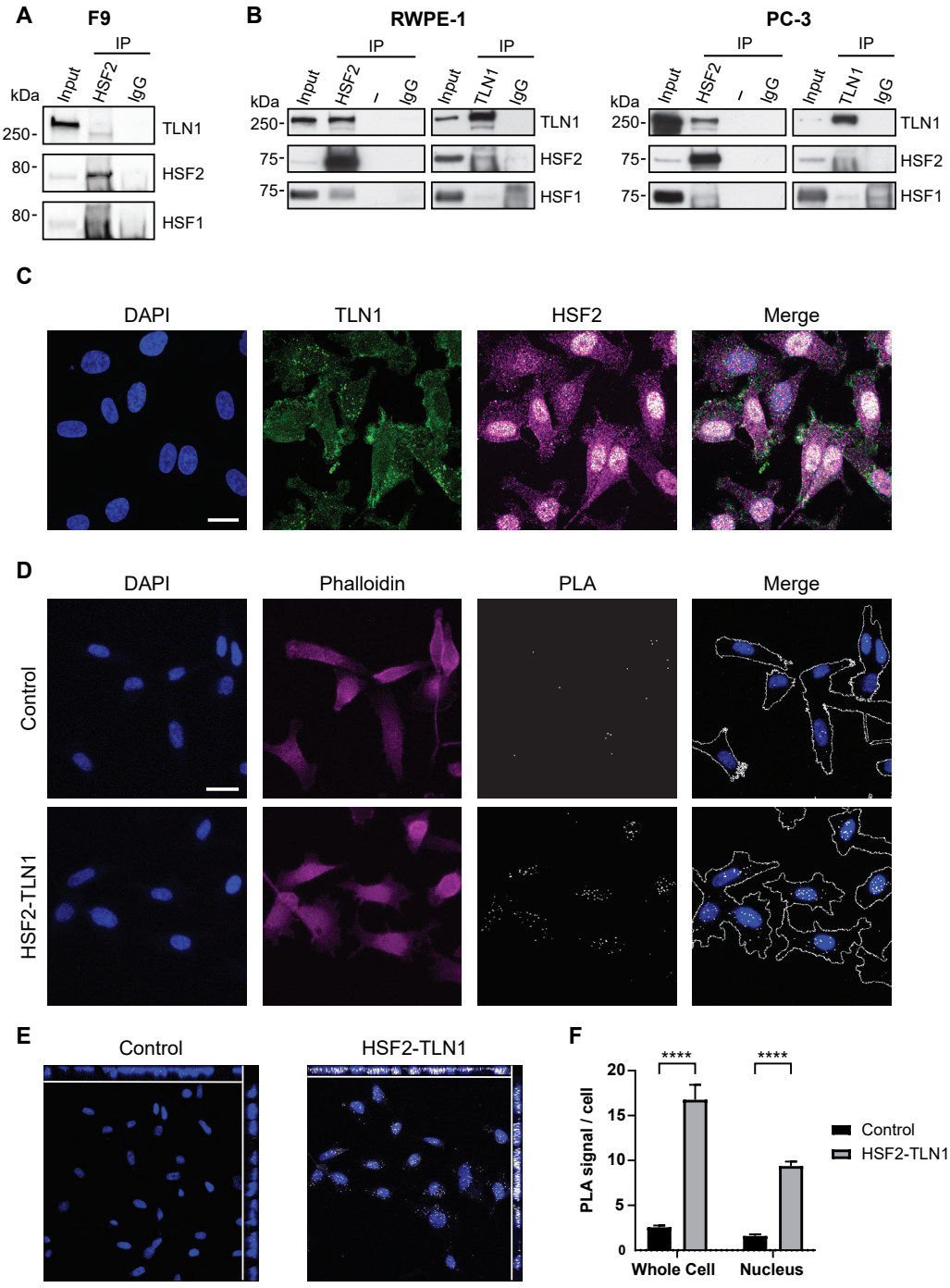
A
F9
IP
kDa
Input
HSF2
IgG
250-
80-
80-
TLN1
HSF2
HSF1
B
RWPE-1
PC-3
IP
kDa
Input
HSF2
-
IgG
TLN1
75-
HSF2
HSF1
C
DAPI
TLN1
HSF2
Merge
D
DAPI
Phalloidin
PLA
Merge
Control
HSF2-TLN1
E
Control
HSF2-TLN1
F
PLA signal / cell
20
15
10
5
0
****
Whole Cell
Nucleus
Control
HSF2-TLN1

Figure 2. The HSF2 and TLN1 interaction is conserved from mouse to human. **(A)** co-IP of HSF2 and a negative control IgG in the mouse cell line F9. HSF2, TLN1 and HSF1 were examined by immunoblotting in the co-IP samples. The immunoblot is a representative figure of three biological replicates. **(B)** co-IP of HSF2, TLN1 and a negative control IgG in human RWPE-1 and PC-3 cells. TLN1, HSF2 and HSF1 were examined by immunoblotting in the co-IP samples. All images are representatives of three biological replicates. **(C)** Confocal microscopy images of immunofluorescent staining of PC-3 cells showing nuclei (DAPI, blue), TLN1 (green), HSF2 (magenta), and a merged image of the three channels. Images are shown as maximum intensity projections and they are representative of three biological replicates. Scale bar 20 µm. **(D)** Proximity ligation assay (PLA) with antibodies specific for HSF2 and TLN1 in PC-3 cells. As negative controls, antibodies against a non-specific target (GFP) were used. Phalloidin staining (magenta) was used to visualize the borders of the cells, which were marked with white lines in the merge image. The PLA signals appear as white dots indicating close proximity (≤40 nm) of the antibodies. Images are shown as maximum intensity projections and they are representative of over 100 cells analyzed per staining. Scale bar 20 µm. **(E)** Orthogonal projection of PLA images, the PLA signal appears as white dots and nuclei was stained with DAPI **(F)** Quantification of the PLA signals in the whole cell and nucleus. A Mann-Whitney t-test was performed using GraphPad Prism 7. The data are presented as mean values of over 100 cells analyzed from across multiple experiments + SEM. ****$p < 0.0001$.

FIGURE 3

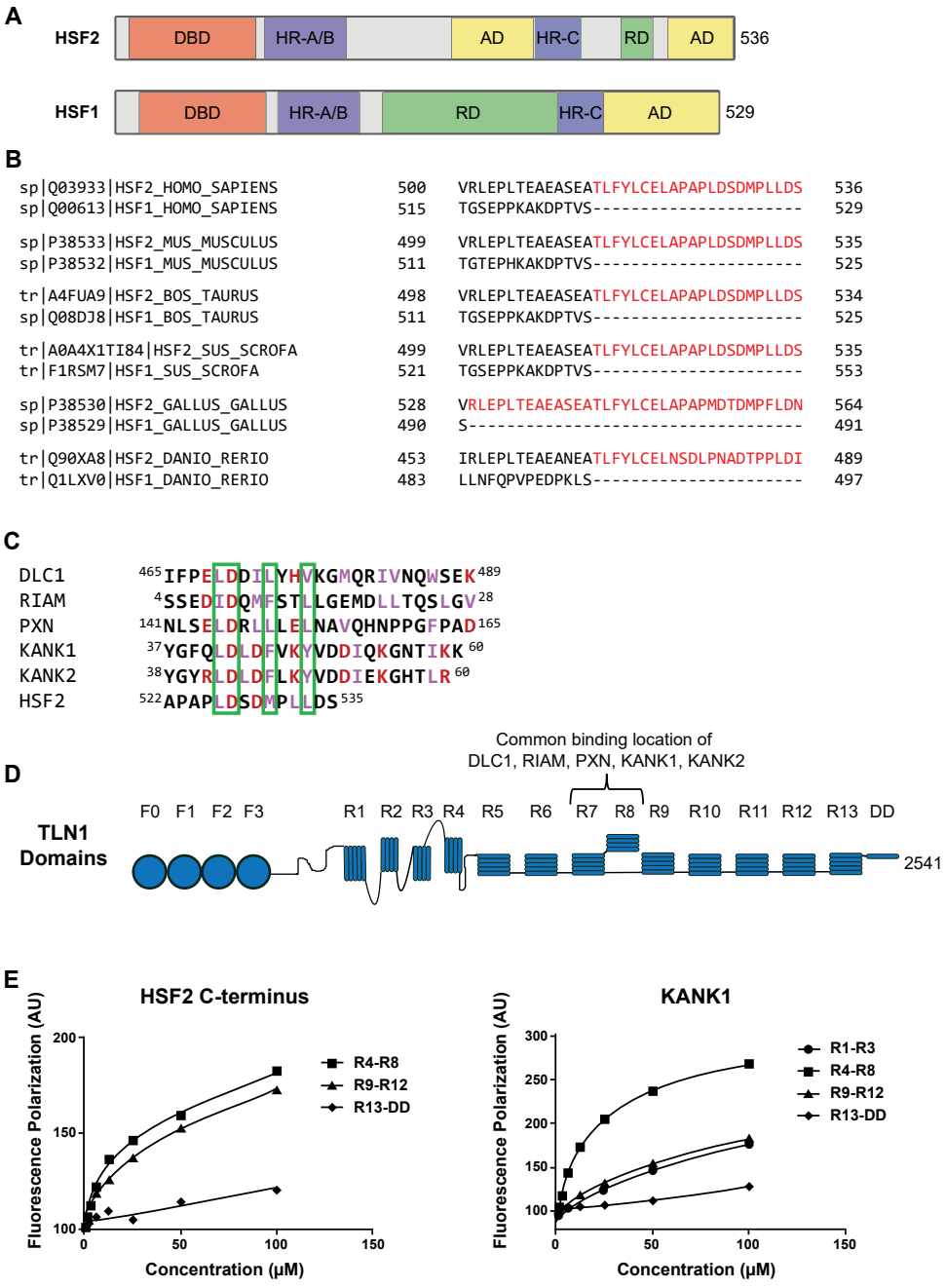
A
HSF2
DBD
HR-A/B
AD
HR-C
RD
AD
536
HSF1
DBD
HR-A/B
RD
HR-C
AD
529
B
sp|Q03933|HSF2_HOMO_SAPIENS 500 VRLEPLTEAEASEATLFYLCELAPAPLDSDMPLLDS 536
sp|Q00613|HSF1_HOMO_SAPIENS 515 TGSEPPKAKDPTVS---------- 529
sp|P38533|HSF2_MUS_MUSCULUS 499 VRLEPLTEAEASEATLFYLCELAPAPLDSDMPLLDS 535
sp|P38532|HSF1_MUS_MUSCULUS 511 TGTEPHKAKDPTVS---------- 525
tr|A4FUA9|HSF2_BOS_TAURUS 498 VRLEPLTEAEASEATLFYLCELAPAPLDSDMPLLDS 534
sp|Q08DJ8|HSF1_BOS_TAURUS 511 TGSEPPKAKDPTVS---------- 525
tr|A0A4X1TI84|HSF2_SUS_SCROFA 499 VRLEPLTEAEASEATLFYLCELAPAPLDSDMPLLDS 535
tr|F1RSM7|HSF1_SUS_SCROFA 521 TGSEPPKAKDPTVS---------- 553
sp|P38530|HSF2_GALLUS_GALLUS 528 VRLEPLTEAEASEATLFYLCELAPAPMDTDMPFLDN 564
sp|P38529|HSF1_GALLUS_GALLUS 490 S---------- 491
tr|Q90XA8|HSF2_DANIO_RERIO 453 IRLEPLTEAEANEATLFYLCELNSDLPNADTPPLDI 489
tr|Q1LXV0|HSF1_DANIO_RERIO 483 LLNFQPVPEDPKLS---------- 497
C
DLC1 465IFPELDDILYHVKGMQRIVNQWSEK489
RIAM 4SSEDIDQMFSTLLGEMDLLTQSLGV28
PXN 141NLSELDRLLLELNAVQHNPPGFPAD165
KANK1 37YGFQLDLDFVKYVDDIQKGNTIKK 60
KANK2 38YGYRLDLDFLKYVDDIEKGHTLR 60
HSF2 522APAPLDSDMPLLDS535
D
Common binding location of
DLC1, RIAM, PXN, KANK1, KANK2
TLN1
Domains
F0 F1 F2 F3 R1 R2 R3 R4 R5 R6 R7 R8 R9 R10 R11 R12 R13 DD
2541
E
HSF2 C-terminus
Fluorescence Polarization (AU)
Concentration (μM)
R4-R8
R9-R12
R13-DD
KANK1
Fluorescence Polarization (AU)
Concentration (μM)
R1-R3
R4-R8
R9-R12
R13-DD

Figure 3. The C-terminus of HSF2 binds directly to TLN1. **(A)** Schematic figure of HSF1 and HSF2 domains, modified from (Roos-Mattjus & Sistonen, 2022). HSF1 and HSF2 share a highly conserved (70% identity) DNA binding domain (DBD), while the rest of their protein sequences exhibits approximately 35% identity. Both HSFs contain an oligomerization domain composed of hydrophobic-leucine-zipper-like heptad repeats (HR-A/B), and C-terminal heptad repeat domain (HR-C), regulatory domains (RD), and transactivation domains (AD). **(B)** Sequence alignment of HSF2 and HSF1 amino acid sequences in *Homo sapiens*, *Mus musculus*, *Bos taurus*, *Sus scrofa, Gallus gallus*, *and Danio reiro*. HSF2-specific amino acid sequences are depicted in red **(C)** Multiple sequence alignment of the LD TLN1-binding motif in known TLN1-binding partners (DLC1, RIAM, PAX-LD2, KANK1, KANK2) and HSF2. The key amino acids of the LD motif are aligned across the different proteins in green. Hydrophobic residues are depicted in purple whereas polar hydrophilic residues are in red. **(D)** Schematic figure of TLN1 domains, modified from (Gough & Goult, 2018). TLN1 is composed of 18 domains including an N-terminal head domain with four subdomains (F0-F3), a flexible linker, and a C-terminal rod domain composed of 13 alpha helical bundles (R1-R13) and a dimerization domain (DD). **(E)** *In vitro* fluorescent polarization assay between a short peptide of HSF2 containing amino acids 519-535 and three regions of TLN1 (R4-R8, R9-R12, R13-DD). The LD motif of KANK1 was used as positive control (R1-R3, R4-R8, R9-R12, R13-DD).

A subpopulation of Talin 1 resides in the nucleus and regulates gene expression

Authors:

Alejandro J. Da Silva[1,2], Hendrik S. E. Hästbacka[1,2], Mikael C. Puustinen[1,2], Jenny C. Pessa[1,2], Benjamin T. Goult[4], Guillaume Jacquemet[1,2,3], Eva Henriksson[1,2], Lea Sistonen[1,2,*].

Affiliations:

[1]Faculty of Science and Engineering, Cell Biology, Åbo Akademi University, 20520 Turku, Finland.

[2]Turku Bioscience Centre, University of Turku and Åbo Akademi University, 20520 Turku, Finland.

[3]Turku Bioimaging University of Turku and Åbo Akademi University, 20520 Turku, Finland.

[4]School of Biosciences, University of Kent, Canterbury CT2 7NJ, Kent, UK.

*Corresponding author. Email: lea.sistonen@abo.fi

Running title:

Nuclear TLN1 regulates gene expression

Abstract

Talin 1 (TLN1) is best known for its role at focal adhesions, where it activates β-integrin receptors and transmits mechanical stimuli to the actin cytoskeleton. Interestingly, the localization of TLN1 is not restricted to the focal adhesions, but its function in other cellular compartments remains poorly understood. By utilizing both biochemical and confocal microscopy analyses, we show that TLN1 localizes to the nucleus and that it strongly interacts with the chromatin. Importantly, depletion of endogenous TLN1 results in extensive changes in the gene expression profile of human breast epithelial cells. To determine the impact of nuclear TLN1 on gene regulation, we expressed a TLN1 fusion protein containing a nuclear localization signal. Our results revealed that nuclear TLN1 regulates a specific subset of the TLN1-dependent genes. Taken together, we show that apart from localizing at the plasma membrane and cytoplasm, TLN1 also resides in the nucleus where it functions in the regulation of gene expression.

Key words:

Chromatin / gene expression / nucleus / talin 1 / TLN1

Introduction

Accumulating evidence indicates active communication between the cell cortex and the nucleus by nuclear translocation of proteins (Zheng & Jiang, 2022). Many of these proteins are associated with transmembrane adhesion receptors, which connect the extracellular matrix (ECM) and surface proteins of neighboring cells to the cytoskeleton (Hintermann & Christen, 2019; Zheng & Jiang, 2022). These cell-ECM and cell-cell junctions provide cells with structural and mechanical stability, and both types of junctions act as signaling platforms that collect information from the extracellular space. Therefore, identifying proteins that mediate the communication between the cell cortex and the nucleus is fundamental to understand how cells respond to their surroundings. In a recent preprint article Byron and collaborators performed proteomic analyses and found that a considerable number of adhesion complex-associated proteins also reside in the nucleus (preprint: Byron *et al*, 2021). However, the functions of most adhesion-associated proteins inside the nucleus remain poorly understood.

Talin 1 (TLN1) is a 270 kDa adaptor protein that is best known for its role in focal adhesion (FA) assembly (Gough & Goult, 2018). FAs are structures characterized by proteins that crosslink actin filaments to the integrin transmembrane receptors (Case & Waterman, 2015). To achieve its function at the FAs, TLN1 has a particular domain structure that is composed of an N-terminal FERM (4.1 protein, ezrin, radixin, moesin) domain, known as the head domain, which is coupled to a flexible rod domain comprised of 13 helical bundles (Goult *et al*, 2013b). The head domain interacts with the cytoplasmic tails of β-integrin subunits, whereas the rod domain binds to actin filaments and acts as a mechanosensitive signaling hub (Goult *et al*, 2021) (Fig 1A, left panel). Dysregulation of TLN1 is associated with different diseases, such as cancer, cardiovascular malfunction, and hematologic disorders, which makes TLN1 a relevant protein in the context of therapeutics and diagnostics (Azizi *et al*, 2021; Li *et al*, 2021; Haining *et al*, 2016). Interestingly, TLN1 is not confined to the FA complexes indicating that this protein has other roles apart from the FA assembly. For example, TLN1 is localized at invadopodia, which are actin-rich protrusions that mediate cancer cell invasion and metastasis, where it acts as a scaffold to recruit the sodium/hydrogen exchanger 1 protein (Beaty *et al*, 2014). Moreover, TLN1 can also reside in the cytoplasm where it adopts a conformation that is unable to mediate the connection between integrins and the actin cytoskeleton, and therefore might have a role in other signaling pathways (Haage *et al*, 2018; Goult *et al*, 2013a). Consequently, characterizing the subcellular localization and function of TLN1 is fundamental for understanding its role in physiological processes and pathological states.

In this study, we investigated the subcellular localization of TLN1. Biochemical and confocal microscopy analyses showed, to our surprise, that TLN1 can also localize to the nuclei of human epithelial cells, where it strongly interacts with the chromatin. Moreover, depletion of TLN1 resulted in extensive changes in the gene expression profile of breast epithelial cells, causing upregulation and downregulation of approximately 300 and 400 genes, respectively. To determine the importance of nuclear TLN1 in gene regulation, we generated a fusion protein composed of the full-length human TLN1 coupled to GFP and a nuclear localization signal (NLS). By ectopically expressing the TLN1-NLS fusion protein, we demonstrate that enriching TLN1 in the nucleus impacts the expression of a specific subset of genes. Taken together, this study identifies TLN1 as a nuclear protein that regulates gene expression.

Results

TLN1 is localized in the nucleus where it strongly interacts with the chromatin

To initiate the study on the subcellular localization of talin 1 (TLN1), we examined the gene ontology (GO) terms associated with 1304 TLN1-interacting proteins, that were identified in a recently published mass spectrometry screen (Gough ***et al***, 2021) (Fig 1A, right panel). Gough and collaborators determined the probability of *bona fide* protein-protein interactions by calculating the Significance Analysis of INTeractome (SAINT) score, and a total of 72 TLN1-interacting partners, which had a SAINT score ≥ 0.7, were chosen for our GO term analysis. Interestingly, the analysis revealed that a majority, i.e. 37, of these 72 proteins are nuclear, and 32 proteins are involved in nucleic acid binding (Fig 1B) (Table1). This unexpected result prompted us to investigate whether TLN1 is localized in the nucleus of transformed (HS578T, MDA-MB-231) and non-transformed (MCF10A) human breast epithelial cells, as well as transformed human prostate epithelial cells (PC3). To achieve fractions of high purity, we utilized a protocol based on stepwise cell lysis where the cytoplasm is separated from the intact nucleus, which in turn is lysed separately to extract proteins located either in the nucleoplasm or in the chromatin. To assess the purity of the subcellular fractions, we monitored the localization of proteins that are known to reside in the following compartments: plasma membrane (β1 integrin), cytoplasm (α tubulin), nucleus (lamin A/C), and chromatin (histone H4) (Herrmann *et al*, 2017; Abdrabou *et al*, 2020; Alanko *et al*, 2015). The results showed that the control proteins were clearly enriched in their corresponding fractions, demonstrating the efficacy of the subcellular fractionation protocol (Fig 1C). In accordance with the mass spectrometry data analysis, we found that TLN1 co-purifies with the nuclear and chromatin-associated fractions of all the cell lines tested.

Next, we evaluated the strength of the TLN1-chromatin interaction by differential salt fractionations. The pellet, which remained after collecting the nuclear fraction, was incubated with increasing concentrations of NaCl (0.3, 0.45, 0.6, 0.8, and 1.2 M) to release proteins bound to the chromatin. Proteins weakly bound to chromatin (e.g. transcription factors) are soluble in low concentrations of NaCl, while proteins tightly bound to chromatin (e.g. histones) are only displaced at high concentrations of NaCl (Herrmann *et al*, 2017). In MCF10A and MDA-MB-231 cells, TLN1 co-eluted with histone H4 at the highest concentrations of the NaCl, whereas in HS578T cells, TLN1 co-eluted with lamin A/C throughout the NaCl gradient (Fig 1D) indicating a weaker interaction with the chromatin. These data indicate that the strength of the TLN1-chromatin interaction varies among cell lines, which may be due to differences in the identity of TLN1-interacting partners in these cells. Taken together, our results clearly

demonstrate that TLN1 is localized in the nucleus, where it strongly interacts with the chromatin.

TLN1 concentrates in specific areas within the nucleus

To investigate the nuclear distribution of TLN1, we performed indirect immunofluorescence staining of TLN1 in HS578T and MDA-MB-231 cells. For this purpose, we used three different antibodies against distinct epitopes of TLN1, one antibody recognizing the head domain and two antibodies recognizing the rod domain, to be able to validate the specificity of the TLN1 fluorescent signal (Fig 2A). The expected localization of TLN1 in the FAs was observed at the bottom plane of the cells, while visualizing the middle plane of the cells displayed nuclear TLN1 signal irrespective of the antibody and the cell line used (Fig 2B-E). Interestingly, a strong nuclear foci pattern was detected in a subset of cells. These foci co-localized with the dark areas of the DAPI staining, which typically correspond to the presence of nucleoli (Di Tomaso *et al*, 2013). Therefore, we co-stained HS578T and MDA-MB-231 cells with an antibody specific for nucleolin (NCL), a well-known nucleolar protein (Jia *et al*, 2017). As anticipated, the immunofluorescent signals corresponding to TLN1 and NCL clearly co-localized, indicating that TLN1 is present in the nucleoli of these cells (Fig 2E). The nucleolar localization of TLN1 is also supported by our mass spectrometry data analysis, which showed 14 nucleolar-associated TLN1-interacting partners with a high confidence score (≥ 0.7 SAINT score) (Fig 1B, left panel) (Table 1).

Nuclear TLN1 regulates gene expression

The nuclear localization of TLN1 and its strong interaction with the chromatin prompted us to investigate whether TLN1 affects gene expression. We depleted TLN1 in HS578T cells by transfecting them with a combination of two small interfering RNAs (siRNAs) specific for TLN1 (siTLN1) and used scramble siRNAs as a control (Scr). The efficacy of the TLN1 downregulation was assessed by immunoblot analysis (Fig 3A-B). Since a prominent reduction in the TLN1 protein levels was detected, we proceeded with analyzing the global gene expression profiles with RNA-seq. Differentially expressed (DE) genes between the Scr and siTLN1 transfected cells were determined with the Bioconductor R package edgeR (Robinson *et al*, 2009), using a $\log_2$ fold change of at least ± 0.5 and a false discovery rate (FDR) < 0.05 from two biological replicates. Depletion of TLN1 caused extensive changes in the gene expression profile of HS578T cells, resulting in the upregulation of 318 genes and the downregulation of 419 genes (Fig 3C) (Table 2). Notably, TLN1 was the most significantly downregulated gene in our RNA-seq screen, thereby confirming the efficacy of the silencing method (Fig 3C, right panel). Normalized gene expression data was used to generate heatmaps from the top 25 upregulated and 25 downregulated DE genes (Fig 3D). Based on

the well-known function of TLN1 as a mechanosensitive adaptor protein in FAs, it is plausible that its depletion affected the expression of genes related to cell adhesion. Accordingly, we found several TLN1-dependent genes that are involved in cell adhesion (Fig 3E). Since we found that TLN1 is also present in the nucleus, we searched for genes related to nuclear functions. Among the DE genes, we identified those encoding nuclear structural proteins (NEMP1, H2BC4), chromatin remodelers (BCL7B, MORF4L1), and transcription factors (NFATC2) (Fig 3F).

These results are, to the best of our knowledge, the first report of a TLN1-dependent gene expression profile. Due to the key role of TLN1 in the FA complexes, it is possible that part of the changes in gene expression upon TLN1 depletion are caused by the disruption of cell-ECM junctions. For instance, it has been shown that the focal adhesion kinase (FAK), a well-established marker of integrin activation, translocates from the cell cortex to the nucleus, where it binds to the chromatin and regulates gene expression (Griffith *et al*, 2021). In addition, the integrity of the FA sites is critical for transforming mechanical stimuli into biochemical signals that eventually affect the expression of different genes (Janota *et al*, 2020). Therefore, it is crucial to distinguish the impact of nuclear TLN1 from the impact of cytoplasmic TLN1 on gene expression.

For interrogating the role of nuclear TLN1 in the regulation of gene expression, we enriched the amount of nuclear TLN1 and determined the mRNA levels of five TLN1-dependent genes: SEMA7A, NFATC2, ACTG1, BCL7B, and SEC23A (Figs 3D and 4B). To specifically increase the level of TLN1 in the nucleus, we constructed a fusion protein consisting of the full-length human TLN1 coupled with GFP and a nuclear localization signal (TLN1-NLS). HS578T cells were transfected with the TLN1-NLS construct, and GFP was used as the corresponding mock control. Analysis with confocal microscopy confirmed that the TLN1-NLS fusion protein was confined inside the nucleus, whereas the GFP control was dispersed in the whole cell (Fig 4A). Next, the mRNA levels of the five TLN1-dependent genes were examined in the mock and TLN1-NLS transfected cells with qRT-PCR (Fig 4B). In line with our RNA-seq data, enriching TLN1 in the nucleus shifted the expression of SEMA7A, NFATC2 and ACTG1 in an opposite pattern to that observed upon TLN1 depletion (Figs 3D and 4B). In contrast, the expression of BCL7B and SEC23A remained unchanged irrespective of the amount of nuclear TLN1, showing that not all TLN1-dependent genes are responsive to nuclear TLN1 (Fig 4B). Taken together, these results demonstrate that nuclear TLN1 regulates the expression of a specific subset of genes.

Discussion

The function of TLN1 as a mechanosensitive adaptor protein in integrin adhesion complexes is extensively characterized and continues to be the major focus in the field of TLN1 research. Nevertheless, roles of TLN1 in other cellular compartments have remained enigmatic, which prompted us to investigate the subcellular localization of TLN1. To our surprise, both biochemical and confocal microscopy analyses showed that TLN1 also resides in the nucleus and strongly interacts with the chromatin. RNA-seq analysis revealed that depletion of TLN1 results in extensive changes in the gene expression profile of human breast epithelial cells, which to the best of our knowledge is the first report of gene regulation in a TLN1-dependent manner. Finally, by enriching TLN1 in the nucleus, we demonstrate that TLN1 impacts the expression of a specific subset of the TLN1-dependent genes (Fig 4C).

Active communication between the cell cortex and the nucleus is important to ensure a coordinated transcriptional response upon extracellular stimuli (Zheng & Jiang, 2022). Among the proteins that participate in the FAs, zyxin, paxillin and FAK have been shown to translocate to the nucleus and regulate gene expression (Wang & Gilmore, 2003; Lim *et al*, 2008). Interestingly, studies centered on FAK have led to the hypothesis that FERM domain-containing proteins act as information mediators between the plasma membrane and the nucleus (Frame *et al*, 2010). Our results support this idea and suggest that TLN1 translocate from the cortex to the nucleus to regulate gene expression in response to extracellular stimuli. However, further studies are required to determine the mechanisms mediating TLN1 nuclear translocation.

In the light of our results, it is interesting to address a question how nuclear TLN1 is able to regulate gene expression. Previous studies have shown that nuclear FAK controls chromatin accessibility to allow the binding of transcription factors to specific genomic loci (Griffith *et al*, 2021). In addition, nuclear actin and nuclear myosin-1C, which were initially thought to be strictly cytoplasmic proteins, alter chromatin landscape and also cooperate to maintain active RNA polymerase II at gene promoters (Klages-Mundt *et al*, 2018; Almuzzaini *et al*, 2015). Our results demonstrate that TLN1 strongly interacts with the chromatin of human epithelial cells, suggesting that it could function in a similar manner as nuclear actin, nuclear myosin-1C and/or nuclear FAK. The finding that TLN1 is present in the nucleolus also offers an entry point to exploit the mechanisms by which TLN1 contributes to gene regulation. To this end, it is tempting to speculate that TLN1 plays a role in rRNA maturation, since proteins that are required for the synthesis (e.g. POLR2E, POLR2H, and POLR1C) and maturation (e.g. NIP7 and NOP16) of the polycistronic rRNA precursors were found among the previously identified TLN1-interacting proteins (Tafforeau *et al*, 2013; Goodfellow & Zomerdijk, 2013) (Table 1).

Due to the mechanosensitive role of TLN1 in FA complexes, it is important to consider whether nuclear TLN1 might also respond to mechanical stimuli. Over the last years, it has been recognized that the nucleus reacts to mechanical forces from the extracellular space and the cytoskeleton (Janota *et al*, 2020). Among the best characterized mechanisms of nuclear mechanosensitivity is the protein machinery known as linker of nucleoskeleton and cytoskeleton (LINC) complex (Jahed & Mofrad, 2019). The LINC complex connects the nuclear envelope with the contractile cytoskeleton, and this physical connection mediates the transmission of force to proteins in the inner periphery of the nuclear envelope including nuclear lamins (Miroshnikova *et al*, 2019; Khilan *et al*, 2021). Curiously, the rod domain of TLN1 is composed of 13 α-helical bundles that function as mechanosensitive switches, which change their conformation to expose binding sites for different interacting partners (Goult *et al*, 2021). Thus, one can hypothesize that TLN1 acts as a nuclear mechanosensitive signaling hub. In support of this view, our mass spectrometry data analysis revealed that TLN1 interacts with nine proteins associated with the nuclear envelope, of which emerin mediates changes in nuclear stiffness upon stimulation of the LINC complex (Janota *et al*, 2020). Taken together, we report an unprecedented property of TLN1 by showing that in addition to its association to the plasma membrane and cytoplasm, TLN1 also resides in the nucleus where it interacts with the chromatin and regulates gene expression. These results provide a paradigm shift in the field of TLN1 research, thereby expanding the canonical view of TLN1 subcellular localization and function.

Materials and methods

Cell culture

All cells were maintained at 37°C in a humidified 5% CO_2 atmosphere. MCF10A cells were cultured in DMEM/F12 (Dulbecco's Modified Eagle's media, 11330-032, Gibco) medium supplemented with 10 µg/ml cholera toxin, 4% horse serum, 10 µg/ml insulin, 10 µg/ml EGF, 0.5 mg/ml hydrocortisone, and 100 µg/ml penicillin-streptomycin. HS578T cells were cultured in DMEM (Dulbecco's Modified Eagle's media, D6171, Sigma-Aldrich) supplemented with 10% fetal calf serum, 2 mM L-glutamine, 100 µg/ml penicillin-streptomycin, and 10 µg/ml insulin. MDA-MB-231 cells were cultured in DMEM (Dulbecco's Modified Eagle's media, D6171, Sigma-Aldrich) supplemented with 10% fetal calf serum, 2 mM L-glutamine, and 100 µg/ml penicillin-streptomycin. PC3 cells were cultured in RPMI (Roswell Park Memorial Institute, 1640, Sigma) supplemented with 10% fetal calf serum, 2 mM L-glutamine, and 100 µg/ml penicillin-streptomycin.

Transfections and gene silencing

All transfections were performed using the NEON Transfection System (MPK5000, Thermo Fisher Scientific) according to the manufacturer's instructions. Briefly, 2.2×10^6 HS578T cells were suspended in 100 µl of resuspension buffer, mixed with either 13 µg of DNA or 1.6 µM of RNA, and electroporated using 3×20ms 1050V pulses. To silence TLN1 an equal mixture (1:1) of two siRNAs was used, the siRNAs were purchased from Dharmacon: Cat. No. J-012949-06-0010 and Cat. No. J-012949-07-0010. As a control the ON-TARGETplus Non-targeting control pool from Dharmacon was used (Cat. No. D-001810-10-20). All RNAs were used with a final concentration of 1.6 µM.

Plasmid construction

The TLN1-NLS plasmid was generated by cloning full-length human TLN1 from PC3 cells. Total RNA was isolated with RNeasy mini kit (74106, QIAGEN) and the complementary DNA was synthetized using random hexamer primers (SO142, Thermo Fisher Scientific). The full-length TLN1 was inserted into a pEGFP-N2 vector using the In-Fusion HD cloning kit (Takara Bio USA). Silent mutations on TLN1 were generated with the QuikChange site-directed mutagenesis kit (Agilent Technologies) to make our construct resistant against the previously described siRNA specific for TLN1 (Cat. No. J-012949-06-0010 and Cat. No. J-012949-07-0010, Dharmacon). Finally, a gene strand containing a Strep-tag II and the NLS of c-myc (Dang & Lee, 1988) was purchased from Eurofins Genomics and inserted in the C-termini of GFP with the In-Fusion HD cloning kit (Takara Bio USA). All primers used for the plasmid construction are listed in Table 3.

Gene Ontology (GO) term analysis

GO term analyses were performed with the online applications ShinyGO (Ge *et al*, 2020). For analysis performed with ShinyGO v.0.66 the following parameters were used: species: human, p-value cutoff: 0.05, and number of top pathways to show: 30.

Immunoblotting

Cells were washed and collected in PBS (L0615, BioWest). After collection, the cells were lysed in lysis buffer (10% glycerol, 1 mM EDTA, pH 7.4, 150 mM NaCl, 2 mM $MgCl_2$, 1% Triton X-100, 50 mM HEPES pH 7.4, 1 x Protease Inhibitor Cocktail [04693159001, Roche Diagnostics], 50 mM NaF, 0.2 mM Na_3VO_4). The protein concentration was determined by BCA assay (23225, Thermo Fischer Scientific). Equal amounts of total protein were resolved on 4–20% Mini-PROTEAN® TGX precast gels (Bio-Rad). The proteins were transferred to a nitrocellulose membrane, which was blocked in 5% milk-PBS with 0.3% Tween 20 for 1 h at room temperature. The primary antibodies were diluted in 0.5% BSA-PBS-0.02% NaN_3. The following primary antibodies were used: anti-α tubulin (AB 1157911, Developmental Studies Hybridoma Bank), anti-β_1 integrin (610468, BD Biosciences), anti-histone H4 (05-858, Millipore), anti-HSC70 (ADI-SPA-815, Enzo Life Sciences), anti-lamin A/C (ab26300, Abcam), anti-TLN1 205 (ab78291, Abcam), and anti-TLN1 8D4 (T3287, Sigma Aldrich). The nitrocellulose membranes were incubated with the primary antibodies overnight at 4°C. Secondary HRP-conjugated antibodies were purchased from Promega or GE Healthcare (anti-mouse Cat. No. W4021, Promega; anti-rabbit Cat. No. W4011, Promega; anti-rat Cat. No. NA935V, GE Healthcare). All secondary antibodies were diluted in 5% milk-PBS with 0.3% Tween 20. The nitrocellulose membranes were incubated with the secondary antibodies at least 1 h at room temperature, and then incubated with enhanced chemiluminescence reagent (28980926, GE Healthcare; 34579, Thermo Fisher; 34094; Thermo Fisher). Images were acquired with an iBright imaging system (Thermo Fisher). Unless indicated, all immunoblotting experiments were performed three times.

Confocal microscopy

For confocal microscopy analyses, 8×10^4 HS578T or MDA-MB-231 cells were plated on MatTek plates (P35GC-1.5-14-C MatTek corporation) 48 h before imagining. Cells were fixed with 4% paraformaldehyde for 10 min, permeabilized with 0.5% Triton X-100 and 3 mM EDTA in 1x PBS and washed three times with PBS. The cells were blocked with 10% FBS-PBS for at least 1 h at room temperature, and then incubated with the corresponding primary antibody dilution overnight at 4°C. The following primary antibodies were diluted in 10% FBS-PBS: 1:220 anti-lamin A/C (ab26300, Abcam), 1:100 anti-nucleolin ZN004 (39-6400, Thermo Fischer Scientific), 1:100 anti-TLN1 205 (ab78291, Abcam), 1:100 anti-TLN1 8D4 (T3287,

Sigma Aldrich), and 1:100 anti-TLN1 (HPA004748, Sigma Aldrich). After primary antibody incubation the samples were washed three times in PBS and incubated with the corresponding secondary antibody at room temperature for 1 h. The following secondary antibodies were diluted 1:500 in 10% FBS-PBS and used: goat anti-rabbit Alexa Fluor 488 (A11008, Life Technologies), donkey anti-mouse Alexa Fluor 555 (A31570, Life Technologies), goat anti-rabbit Alexa Fluor 546 (A11010, Life Technologies), and goat anti-mouse Alexa Fluor 488 (A11001, Life Technologies). After secondary antibody incubation, the cells were washed in PBS, incubated with 300 nM DAPI diluted in PBS for 5 min, washed again with PBS, and covered with VECTASHIELD (H-1000, Vector Laboratories) mounting medium. Images were captured with a 3i CSU-W1 spinning disc confocal microscope (Intelligent Imaging Innovations).

Subcellular fractionations

Cells (MCF10A, MDA-MB-231, HS578T, and PC3) were treated with trypsin, collected in culture media, washed with PBS and counted. The 13% of the cell suspension was set apart for preparation of the whole cell lysate using lysis buffer (10% glycerol, 1 mM EDTA, pH 7.4, 150 mM NaCl, 2 mM $MgCl_2$, 1% Triton X-100, 50 mM HEPES pH 7.4, 1 × Protease Inhibitor Cocktail [04693159001, Roche Diagnostics], 50 mM NaF, 0.2 mM Na_3VO_4). The remaining (87%) cell suspension was used for subcellular fractionation. Cytoplasmic, nuclear, and chromatin fractions were prepared using NE-PER Nuclear and Cytoplasmic Extraction Reagents (78833, Thermo Fisher Scientific) according to manufacturer's instructions. Briefly, the wet volume of the cell pellet was estimated by considering that 2×10^6 is equal to 20 µl of wet volume. The cell pellet was suspended in cytoplasmic extraction reagent I, vortexed 15 s, and incubated on ice (see Table 4 for incubation and vortex times per cell line). After incubation, the cytoplasmic extraction reagent II was added. The suspension was incubated on ice and centrifuged (20,000×g, 5 min). The supernatant was collected (cytoplasmic fraction), and the pellet was washed three times with cold PBS. After the washes, the pellet was resuspended in 100 µl of nuclear extraction reagent, incubated on ice and centrifuged (20,000×g, 10 min). The supernatant (nuclear fraction) was collected, and the pellet was washed three times with cold PBS. Following the washes with PBS, the pellet was resuspended in nuclear extraction reagent, supplemented with 1×10^3 micrococcal nucleases (M02475, New England Biolabs), 5 mM CaCl, and 1 × Protease Inhibitor Cocktail (04693159001, Roche Diagnostics), and incubated at 37°C for 5 min. After incubation the suspension was centrifuged (20,000×g, 10 min) and the supernatant was stored as the chromatin fraction. The protein concentrations of the fractions were determined by BCA assay (23225, Thermo Fischer Scientific).

Differential salt fractionation

Once the nuclear fraction was collected, the pellet was incubated for 30 min at room temperature with the corresponding dilution of NaCl. NaCl was diluted in water and the following concentrations were used: 0.3, 0.45, 0.6, 0.8, and 1.2 M. After incubation in the first fraction of the NaCl gradient, the suspension was centrifuged (20,000×g, 10 min), the supernatant was collected, and the pellet was incubated in the second fraction. This procedure was repeated consecutively until the pellet was exposed to all the concentrations of NaCl.

RNA-sequencing

HS578T cells were transfected with either Scr or a combination of two siRNAs specific for TLN1 (Cat. No. J-012949-06-0010 and Cat. No. J-012949-07-0010, Dharmacon). After 48 h the cells were collected, and total RNA was purified with AllPrep DNA/RNA/miRNA Universal Kit (80224, QIAGEN) according to manufacturer's instructions. The RNA library was prepared according to Illumina stranded RNA preparation guide (1000000124518). Briefly, poly-A containing RNA molecules were purified with poly-T oligo magnetic beads and fragmented with divalent cations under elevated temperatures. For first-strand cDNA synthesis, RNA fragments were copied using reverse transcriptase and random primers. In a second-strand cDNA synthesis, dUTP replaces dTTP to achieve strand specificity. Unique dual indexing adapters were ligated to each sample. The quality and concentration of cDNA samples were analyzed with Advanced Analytical Fragment Analyzer and Bioanalyzer 2100 (Agilent, Santa Clara, CA, USA) and Qubit Fluorometric Quantitation (Life Technologies). Samples were sequenced with NovaSeq 6000 S1 v1.5. All the experimental steps after the RNA extraction were conducted in the Finnish Microarray and Sequencing Center, Turku, Finland. RNA-sequencing was performed from two independent sample series.

FastQC v0.11.9 was used to confirm the quality of the raw reads. The paired-end reads were aligned to the human genome (primary assembly GRCh38, GENCODE) with STAR version 2.7.9a (Dobin *et al*, 2013), using the default settings. The number of read pairs mapped to each genomic feature in release 33 of the GENCODE annotation was determined by featureCounts from subread v2.0.1 (Liao *et al*, 2014). Only read pairs where both ends aligned were counted. Differential gene expression analysis was performed using the Bioconductor R package edgeR v3.34.1. Weakly expressed genes were filtered using filterByExpr defaults, and samples were normalized using the trimmed mean of M-values (TMM) method. The threshold for differentially expressed genes was set to $\log_2$ fold change of at least ± 0.5 and a false discovery rate (FDR) < 0.05 from two biological replicates. The gene expression data was visualized as an MA-plot, produced by the Bioconductor R package Glimma v2.2.0 (Su *et al*, 2017). Z score transformed log2CPM values were used by the CRAN R package

pheatmap v1.0.12 to perform K-Means clustering of the differentially expressed genes and to produce the heat map.

Quantitative RT-PCR (qRT-PCR)

RNA was isolated using a RNeasy mini kit (74106, QIAGEN) according to the manufacturer's instructions. For each sample, 1 µg of RNA was reverse transcribed with an iScript cDNA Synthesis Kit (#1708891, Bio-Rad). The SensiFAST SYBR® Hi-ROX kit (Bioline) was used for qRT-PCR that was performed with the QuantStudio 3 Real-Time PCR system (Applied Biosystems, Thermo Fisher Scientific). The mRNA expression levels were normalized against the respective GAPDH expression in each sample. All reactions were run in triplicates from samples derived from three biological replicates. Statistical analyses were performed with GraphPad Prism 7 Software (GraphPad Prism Software, La Jolla California USA, https://www.graphpad.com). The statistical significance was analyzed with paired two-tailed student's t-test. See Table 5 for primers used in the amplification step.

Data availability

The original data are available at Gene Expression Omnibus (GEO) database under accession number GSE198191.

Acknowledgments

We thank all the members of Sistonen laboratory for expert support during the preparation of the manuscript. Imaging was performed at the Cell Imaging Core, Turku Bioscience Centre, University of Turku and Åbo Akademi University. The instruments used in this project belong to the infrastructure of Turku Bioscience Centre. We thank Markku Saari and Jouko Sandholm from the Cell Imaging Core of Turku Bioscience Centre for technical assistance and advice. The Finnish Functional Genomics Centre (Turku Bioscience, University of Turku, Åbo Akademi University and Biocenter Finland) is acknowledged for services, instrumentation, and expertise.

Author contributions

A.J.D.S., E.H. and L.S. designed the research. A.J.D.S., H.S.E.H., M.C.P., J.C.P., and E.H performed experiments. H.S.E.H. analyzed the RNA-seq data. A.J.D.S., H.S.E.H., M.C.P.,

J.C.P., B.T.G., G.J., E.H., and L.S. interpreted the data. A.J.D.S., E.H. and L.S. wrote the manuscript with the contribution of all the authors.

Conflict of interest

Authors declare that they do not have competing interests.

References

Abdrabou A, Brandwein D & Wang Z (2020) Differential subcellular distribution and translocation of seven 14-3-3 isoforms in response to EGF and during the cell cycle. *Int J Mol Sci* 21: 1–24

Alanko J, Mai A, Jacquemet G, Schauer K, Kaukonen R, Saari M, Goud B & Ivaska J (2015) Integrin endosomal signalling suppresses anoikis. *Nat Cell Biol* 17: 1412–1421

Almuzzaini B, Sarshad AA, Farrants AKÖ & Percipalle P (2015) Nuclear myosin 1 contributes to a chromatin landscape compatible with RNA polymerase II transcription activation. *BMC Biol* 13: 1–15

Azizi L, Cowell AR, Mykuliak V V., Goult BT, Turkki P & Hytönen VP (2021) Cancer associated talin point mutations disorganise cell adhesion and migration. *Sci Rep* 11: 1–16

Beaty BT, Wang Y, Bravo-Cordero JJ, Sharma VP, Miskolci V, Hodgson L & Condeelis J (2014) Talin regulates moesin-NHE-1 recruitment to invadopodia and promotes mammary tumor metastasis. *J Cell Biol* 205: 737–751

Byron A, Griffith BGC, Herrero A, Loftus AEP, Emma S, Dawson JC, Kogerman L, Mcgivern N, Culley J & Graeme R (2021) Characterisation of a nucleo-adhesome. doi.org/10.1101/2021.08.31.458428 [Preprint].

Case LB & Waterman CM (2015) Integration of actin dynamics and cell adhesion by a three-dimensional, mechanosensitive molecular clutch. *Nat Cell Biol* 17: 955–963

Dang C V & Lee WM (1988) Identification of the human c-myc protein nuclear translocation signal. *Mol Cell Biol* 8: 4048–4054

Dobin A, Davis CA, Schlesinger F, Drenkow J, Zaleski C, Jha S, Batut P, Chaisson M & Gingeras TR (2013) STAR: Ultrafast universal RNA-seq aligner. *Bioinformatics* 29: 15–21

Frame MC, Patel H, Serrels B, Lietha D & Eck MJ (2010) The FERM domain: Organizing the structure and function of FAK. *Nat Rev Mol Cell Biol* 11: 802–814

Ge SX, Jung D, Jung D & Yao R (2020) ShinyGO: A graphical gene-set enrichment tool for animals and plants. *Bioinformatics* 36: 2628–2629

Goodfellow SJ & Zomerdijk JCBM (2013) Basic Mechanisms in RNA Polymerase I Transcription of the Ribosomal RNA Genes. In *Epigenetics: Development and Disease,*

pp 211–236.

Gough RE & Goult BT (2018) The tale of two talins – two isoforms to fine-tune integrin signalling. *FEBS Lett* 592: 2108–2125

Gough RE, Jones MC, Zacharchenko T, Le S, Yu M, Jacquemet G, Muench SP, Yan J, Humphries JD, Jørgensen C, *et al* (2021) Talin mechanosensitivity is modulated by a direct interaction with cyclin-dependent kinase-1. *J Biol Chem* 297: 1–18

Goult BT, Brown NH & Schwartz MA (2021) Talin in mechanotransduction and mechanomemory at a glance. *J Cell Sci* 134: 1–7

Goult BT, Xu XP, Gingras AR, Swift M, Patel B, Bate N, Kopp PM, Barsukov IL, Critchley DR, Volkmann N, *et al* (2013a) Structural studies on full-length talin1 reveal a compact auto-inhibited dimer: Implications for talin activation. *J Struct Biol* 184: 21–32

Goult BT, Zacharchenko T, Bate N, Tsang R, Hey F, Gingras AR, Elliott PR, Roberts GCK, Ballestrem C, Critchley DR, *et al* (2013b) RIAM and vinculin binding to talin are mutually exclusive and regulate adhesion assembly and turnover. *J Biol Chem* 288: 8238–8249

Griffith BGC, Upstill-Goddard R, Brunton H, Grimes GR, Biankin A V., Serrels B, Byron A & Frame MC (2021) FAK regulates IL-33 expression by controlling chromatin accessibility at c-Jun motifs. *Sci Rep* 11: 1–14

Haage A, Goodwin K, Whitewood A, Camp D, Bogutz A, Turner CT, Granville DJ, Lefebvre L, Plotnikov S, Goult BT, *et al* (2018) Talin Autoinhibition Regulates Cell-ECM Adhesion Dynamics and Wound Healing In Vivo. *Cell Rep* 25: 2401-2416.e5

Haining AWM, Lieberthal TJ & Del Río Hernández A (2016) Talin: A mechanosensitive molecule in health and disease. *FASEB J* 30: 2073–2085

Herrmann C, Avgousti D & Weitzman M (2017) Differential Salt Fractionation of Nuclei to Analyze Chromatin-associated Proteins from Cultured Mammalian Cells. *Bio-Protocol* 7: 1–13

Hintermann & Christen (2019) The Many Roles of Cell Adhesion Molecules in Hepatic Fibrosis. *Cells* 8: 1503

Jahed Z & Mofrad MR (2019) The nucleus feels the force, LINCed in or not! *Curr Opin Cell Biol* 58: 114–119

Janota CS, Calero-Cuenca FJ & Gomes ER (2020) The role of the cell nucleus in mechanotransduction. *Curr Opin Cell Biol* 63: 204–211

Jia W, Yao Z, Zhao J, Guan Q & Gao L (2017) New perspectives of physiological and pathological functions of nucleolin (NCL). *Life Sci* 186: 1–10

Khilan AA, Al-Maslamani NA & Horn HF (2021) Cell stretchers and the LINC complex in mechanotransduction. *Arch Biochem Biophys* 702: 1–7

Klages-Mundt NL, Kumar A, Zhang Y, Kapoor P & Shen X (2018) The Nature of Actin-Family Proteins in Chromatin-Modifying Complexes. *Front Genet* 9: 1–16

Li Y, Gao S, Han Y, Song L, Kong Y, Jiao Y, Huang S, Du J & Li Y (2021) Variants of Focal Adhesion Scaffold Genes Cause Thoracic Aortic Aneurysm. *Circ Res*: 8–23

Liao Y, Smyth GK & Shi W (2014) FeatureCounts: An efficient general purpose program for assigning sequence reads to genomic features. *Bioinformatics* 30: 923–930

Lim S-T, Chen XL, Lim Y, Hanson DA, Vo T-T, Howerton K, Larocque N, Fisher SJ, Schlaepfer DD & Ilic D (2008) Nuclear FAK Promotes Cell Proliferation and Survival through FERM-Enhanced p53 Degradation. *Mol Cell* 29: 9–22

Miroshnikova YA, Cohen I, Ezhkova E & Wickström SA (2019) Epigenetic gene regulation, chromatin structure, and force-induced chromatin remodelling in epidermal development and homeostasis. *Curr Opin Genet Dev* 55: 46–51

Robinson MD, McCarthy DJ & Smyth GK (2009) edgeR: A Bioconductor package for differential expression analysis of digital gene expression data. *Bioinformatics* 26: 139–140

Su S, Law CW, Ah-Cann C, Asselin-Labat ML, Blewitt ME & Ritchie ME (2017) Glimma: Interactive graphics for gene expression analysis. *Bioinformatics* 33: 2050–2052

Tafforeau L, Zorbas C, Langhendries JL, Mullineux ST, Stamatopoulou V, Mullier R, Wacheul L & Lafontaine DLJ (2013) The complexity of human ribosome biogenesis revealed by systematic nucleolar screening of pre-rRNA processing factors. *Mol Cell* 51: 539–551

Di Tomaso MV, Liddle P, Lafon-Hughes L, Laura A & Folle G (2013) Chromatin Damage Patterns Shift According to Eu/ Heterochromatin Replication. In *The Mechanisms of DNA Replication*, Stuart D (ed) pp 351–375. Rijeka: InTech

Wang Y & Gilmore TD (2003) Zyxin and paxillin proteins: Focal adhesion plaque LIM domain proteins go nuclear. *Biochim Biophys Acta - Mol Cell Res* 1593: 115–120

Zheng HC & Jiang HM (2022) Shuttling of cellular proteins between the plasma membrane and nucleus (Review). *Mol Med Rep* 25: 1–12

Table Legends

Table 1: GO term analyses of TLN1 interacting partners with a SAINT score ≥70 performed with ShinyGO

Table 2: Differentially expressed genes between Scr and siTLN1 transfected HS578T cells

Table 3: Primers and custom DNA strands used to construct the TLN1-NLS vector

Table 4: Duration of incubation (4ºC) and vortex steps during subcellular fractionations performed with NE-PER kit (78833, Thermo Fisher Scientific)

Table 5: Primers used in qRT-PCR

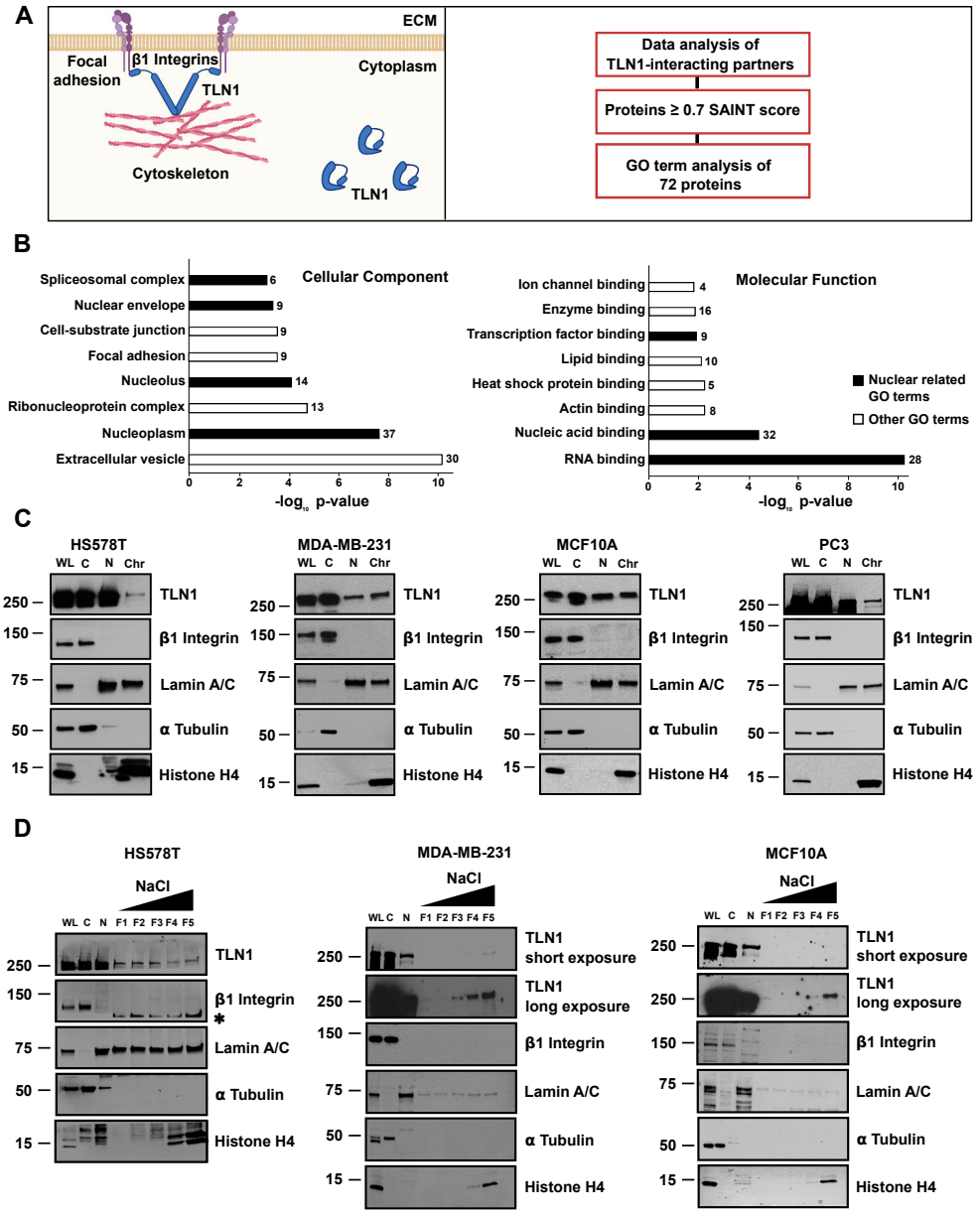
A
ECM
Cytoplasm
Focal adhesion
β1 Integrins
TLN1
Cytoskeleton
TLN1
Data analysis of TLN1-interacting partners
Proteins ≥ 0.7 SAINT score
GO term analysis of 72 proteins
B
Cellular Component
Spliceosomal complex 6
Nuclear envelope 9
Cell-substrate junction 9
Focal adhesion 9
Nucleolus 14
Ribonucleoprotein complex 13
Nucleoplasm 37
Extracellular vesicle 30
-log10 p-value
Molecular Function
Ion channel binding 4
Enzyme binding 16
Transcription factor binding 9
Lipid binding 10
Heat shock protein binding 5
Actin binding 8
Nucleic acid binding 32
RNA binding 28
Nuclear related GO terms
Other GO terms
-log10 p-value
C
HS578T
MDA-MB-231
MCF10A
PC3
WL C N Chr
250
150
75
50
15
TLN1
β1 Integrin
Lamin A/C
α Tubulin
Histone H4
D
HS578T
MDA-MB-231
MCF10A
NaCl
WL C N F1 F2 F3 F4 F5
TLN1
β1 Integrin
Lamin A/C
α Tubulin
Histone H4
TLN1 short exposure
TLN1 long exposure

Figure 1

Figure 1. TLN1 is localized in the nucleus where it strongly interacts with the chromatin. **A)** A schematic overview of the subcellular localization of Talin 1 (TLN1) according to the current literature. TLN1 is localized in the focal adhesions and the cytoplasm (left panel). Analysis of TLN1 interacting partners previously identified by Gough and collaborators (right panel) (Gough *et al*, 2021). Made in BioRender.com **B)** Gene ontology (GO) terms associated with TLN1 interacting partners were analyzed with the online application ShinyGO (Ge *et al*, 2020). The GO terms within the "cellular component" and "molecular function" ontologies were ranked according to their p-values and the redundant terms were withdrawn. The number of proteins associated with each term is indicated, and terms composed of less than four proteins are not shown. GO terms related to the nucleus are highlighted in black. **C)** Immunoblot analysis of TLN1 in subcellular fractionations of HS578T, MDA-MB-231, MCF10A, and PC3 cells. WL: whole cell lysate, C: cytoplasmic fraction, N: nuclear fraction, Chr: chromatin fraction. To monitor the purity of the fractionation protocol the following controls were used: β1 Integrin (plasma membrane), Lamin A/C (nucleus), α Tubulin (cytoplasm), Histone H4 (chromatin). **D)** Immunoblot analysis of TLN1 in differential salt fractionation of HS578T, MDA-MB-231, and MCF10A cells. F1: 0.3, F2: 0.45, F3: 0.6, F4: 0.8, and F5: 1.2 M of NaCl. The fractionation controls were the same as in panel C and remanent signal from a previous LAM A/C immunoblot is indicated with an asterisk (*).

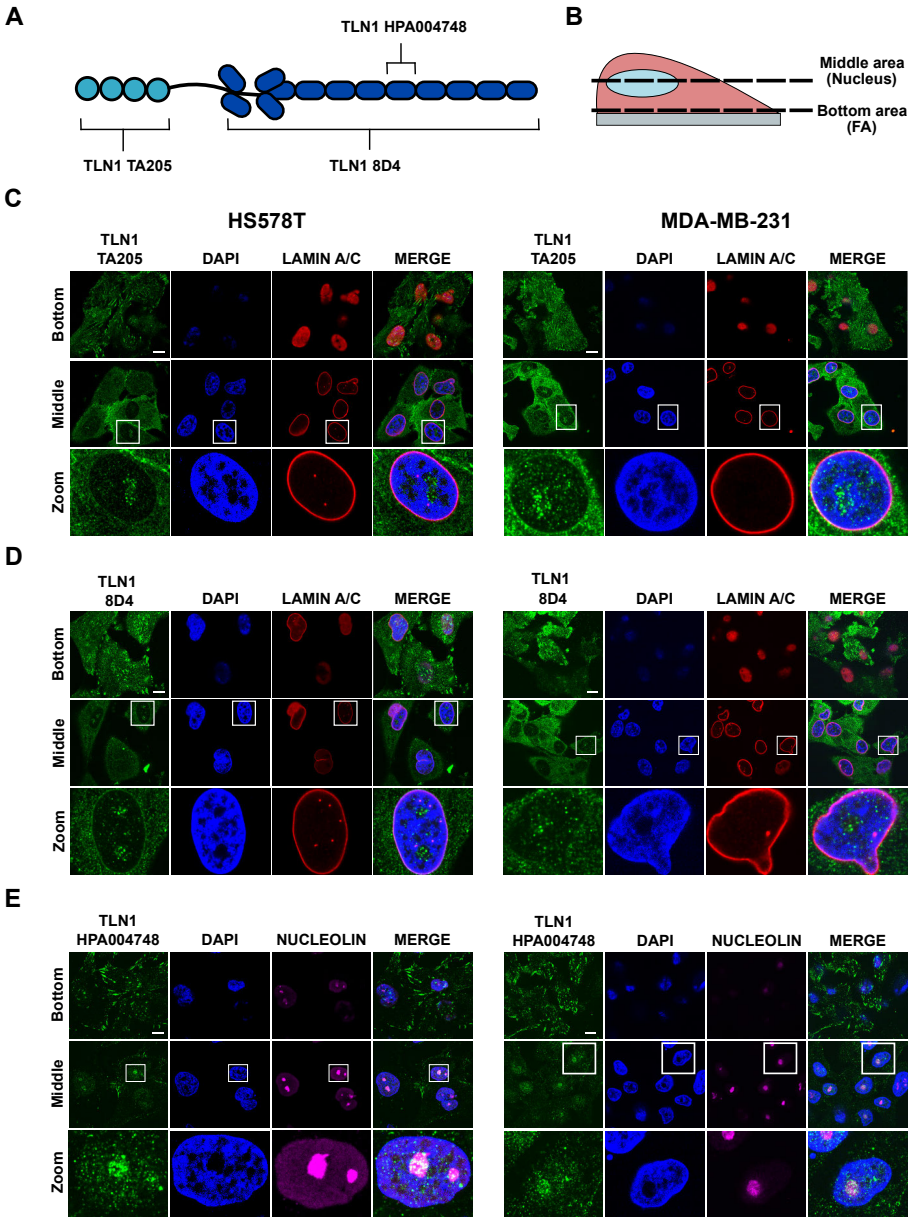
A
TLN1 HPA004748
TLN1 TA205
TLN1 8D4
B
Middle area (Nucleus)
Bottom area (FA)
C
HS578T
MDA-MB-231
TLN1 TA205
DAPI
LAMIN A/C
MERGE
Bottom
Middle
Zoom
D
TLN1 8D4
E
TLN1 HPA004748
NUCLEOLIN

Figure 2

Figure 2. TLN1 concentrates in specific areas within the nucleus. A) A schematic overview of the TLN1 epitopes that are recognized by the antibodies used for immunofluorescent stainings. **B)** A schematic overview of single focal planes shown in C-E. Lamin A/C and DAPI were used as nuclear markers, and nucleolin (NCL) as a nucleolar marker. Scale bar 10 µm. Each figure panel shows a different TLN1 immunofluorescent staining performed with the following antibodies **C)** anti-TLN1 TA205 **D)** anti-TLN1 8D4 **E)** anti-TLN1 HPA004748. All images are representative of three biological replicates.

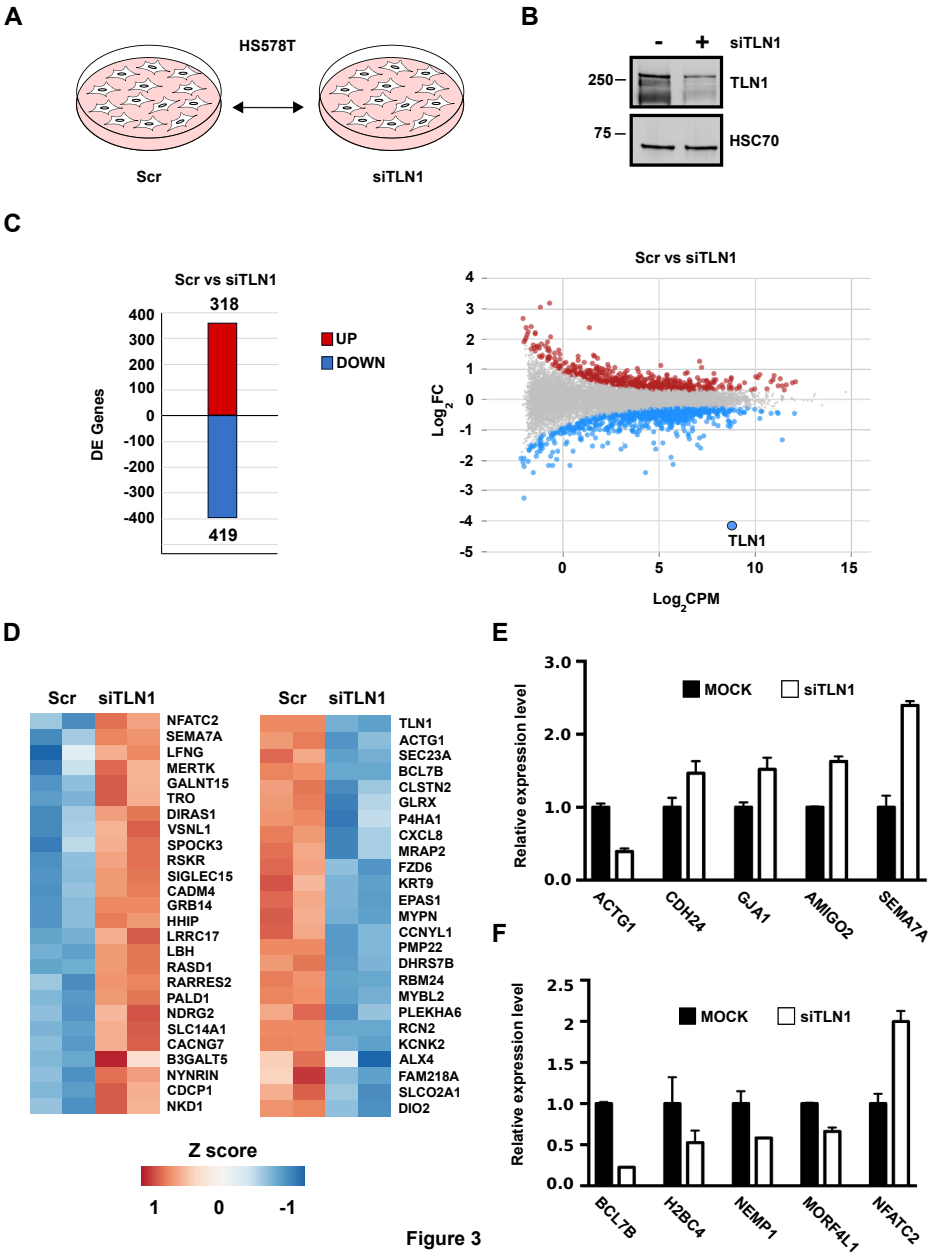
A
HS578T
Scr
siTLN1
B
-
+
siTLN1
250
TLN1
75
HSC70
C
Scr vs siTLN1
318
419
DE Genes
UP
DOWN
Scr vs siTLN1
Log2FC
Log2CPM
TLN1
D
Scr
siTLN1
NFATC2
SEMA7A
LFNG
MERTK
GALNT15
TRO
DIRAS1
VSNL1
SPOCK3
RSKR
SIGLEC15
CADM4
GRB14
HHIP
LRRC17
LBH
RASD1
RARRES2
PALD1
NDRG2
SLC14A1
CACNG7
B3GALT5
NYNRIN
CDCP1
NKD1
TLN1
ACTG1
SEC23A
BCL7B
CLSTN2
GLRX
P4HA1
CXCL8
MRAP2
FZD6
KRT9
EPAS1
MYPN
CCNYL1
PMP22
DHRS7B
RBM24
MYBL2
PLEKHA6
RCN2
KCNK2
ALX4
FAM218A
SLCO2A1
DIO2
Z score
E
MOCK
siTLN1
Relative expression level
ACTG1
CDH24
GJA1
AMIGO2
SEMA7A
F
MOCK
siTLN1
Relative expression level
BCL7B
H2BC4
NEMP1
MORF4L1
NFATC2

Figure 3

Figure 3. Depletion of TLN1 triggers extensive changes in gene expression. A) A schematic overview of the experimental setup for RNA-seq. HS578T cells were transfected with either Scr or siTLN1, and the total RNA from each cell population was extracted and analyzed by RNA-seq. The arrows depict the comparation made for the RNA-seq analysis. **B)** Immunoblot analysis of TLN1 expression in HS578T cells transfected with either Scr or siTLN1. HSP70 was used as a loading control. **C)** Differentially expressed (DE) genes in the Scr vs siTLN1 comparison were determined by Bioconductor R package edgeR (Robinson *et al*, 2009)(Log_2 FC at least ± 0.5; FDR < 0.05). The number of upregulated and downregulated genes are indicated with red and blue bars, respectively (left panel). Individual DE genes between the Scr and siTLN1 samples were visualized in an MA plot. TLN1 is highlighted (right panel). **D)** The top 50 DE genes were used to generate heatmaps with the CRAN R package pheatmap. The top 25 upregulated and downregulated genes are shown in the left and right panels, respectively. **E-F)** Relative expression levels of five DE genes related to cell adhesion (E) and nuclear functions (F). Error bars +SD. Note that these genes were chosen from the list of total DE genes (Table 2).

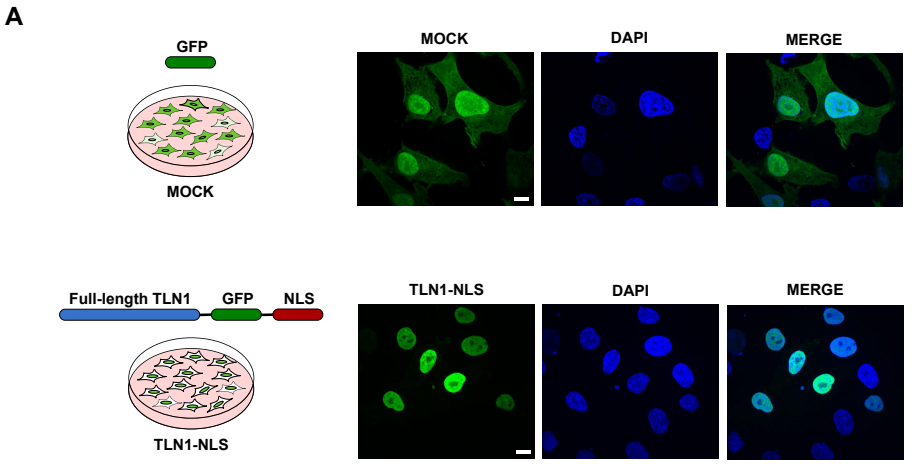
A
GFP
MOCK
MOCK
DAPI
MERGE
Full-length TLN1
GFP
NLS
TLN1-NLS
TLN1-NLS
DAPI
MERGE
B
Relative mRNA Fold Change
1.5
1.0
0.5
0.0
*
*
**
ns
ns
SEMA7A
NFATC2
ACTG1
BCL7B
SEC23A
MOCK
TLN1-NLS
C
ECM
Focal
adhesion
β1 Integrins
TLN1
Cytoskeleton
TLN1
Cytoplasm
Nucleus
Nucleolus

Figure 4

Figure 4. Nuclear TLN1 regulates gene expression. A) A schematic overview of the experimental setup to test the role of nuclear TLN1 for gene expression in HS578T cells (left panels). Confocal microscopy images corresponding to maximum intensity projections of the fluorescent signal emitted by GFP or the TLN1-NLS construct (right panels). **B)** mRNA expression of semaphoring 7A (SEMA7A), nuclear factor of activated T cell 2 (NFATC2), actin gamma 1 (ACTG1), BAF chromatin remodeling complex subunit BCL7B (BCL7B), and SEC23 Homolog A (SEC23A) in HS578T cells. The mRNA levels were quantified with qRT-PCR, and GAPDH was used as housekeeping gene. The data is presented as mean values of three biological replicates +SEM, ns: not significant, *$p < 0.05$, **$p < 0.01$. **C)** A schematic model of the subcellular localization of TLN1. Apart from being present in the periphery of the plasma membrane and cytoplasm, TLN1 is also present in the nucleus (where it interacts with the chromatin) and nucleolus of the cell. Nuclear TLN1 is represented in close conformation, but this does not exclude the possibility of nuclear TLN1 adopting other conformations. Made with BioRender.com.

ISBN 978-952-12-4288-5